UNIVERSITY OF CALIFORNIA, SAN DIEGO

Squeeze and Nonlinear Effects in Trivelpiece-Gould and Electron Acoustic Waves

A dissertation submitted in partial satisfaction of the
requirements for the degree
Doctor of Philosophy

in

Physics

by

Arash Ashourvan

Committee in charge:

Professor Daniel H. E. Dubin, Chair
Professor Charles F. Driscol
Professor Thomas M. O'Neil
Professor George R. Tynan
Professor William R. Young

2014

The dissertation of Arash Ashourvan is approved, and it is acceptable in quality and form for publication on microfilm and electronically:

_____

_____

_____

_____

_____

Chair

University of California, San Diego

2014

DEDICATION

This thesis is dedicated

to the love of my life, Sareh,
to my mother, Homa and my father, Hamid.

TABLE OF CONTENTS

LIST OF FIGURES

LIST OF TABLES

ACKNOWLEDGEMENTS

I would like to thank my advisor, professor Daniel Dubin for giving me the chance to be a part of the nonneutral plasma group. He has been my teacher, mentor and a role model as a professional physicist. I owe the structure, discipline, style and in general the thought process for problem solving that I have developed to him.

I benefited from many stimulating and illuminating conversations with professor Tom O'Neil. His door was always open to me and I have learned so much from him. I will be forever grateful to him.

In every step of my research as a theoretician, Professor Fred Driscol, Dr. Francois Anderegg and fellow PhD student Matt Affolter shared with me the experimentalist's point of view of the problems, which was very useful and I appreciate all the insight they gave me.

Chapter 1, in part, is a reprint of the material as it appears in Physics of Plasmas. Arash Ashourvan and Daniel H.E. Dubin, *Physics of Plasmas* **21**, 052103 (2007). The dissertation author was the primary investigator and author of this paper.

Some of the material in Chapters 2, 3 and 4 are in preparation for publication. The dissertation author was the primary investigator and author of this material.

VITA

2003	B. S. in Physics, Tehran University, Tehran, Iran
2006	M. S. in Physics, Institute for Advanced Studies in Basic Sciences, Zanjan, Iran
2014	Ph. D. in Physics, University of California, San Diego

PUBLICATIONS

Arash Ashourvan, Daniel H. E. Dubin "Collisionless and collisional effects on plasma waves from a partition squeeze", *J. Plasma Physics* (submitted) (2014)

Arash Ashourvan, Daniel H. E. Dubin "Effect of squeeze on electrostatic Trivelpiece-Gould wave damping", *Phys. Plasmas*, 21, 052109 (2014).

Arash Ashourvan, Daniel H. E. Dubin "Effect of squeeze on electrostatic TG wave damping", *Conf. Proc.*, 1521, 7 (2013).

Arash Ashourvan, MirFaez Miri and Ramin Golestanian "Casimir rack and pinion ", *J. Phys.: Conf. Ser.*, 89, 012017 (2007).

Arash Ashourvan, MirFaez Miri and Ramin Golestanian "Rectification of the lateral Casimir force in a vibrating non-contact rack and pinion", *Phys. Rev. E*, 75, 040103(R) (2007).

Arash Ashourvan, MirFaez Miri and Ramin Golestanian, "Non-contact rack and pinion powered by the lateral Casimir force", *Phys. Rev. Lett.*, 98, 140801 (2007)

ABSTRACT OF THE DISSERTATION

Squeeze and Nonlinear Effects in Trivelpiece-Gould and Electron Acoustic Waves

by

Arash Ashourvan

Doctor of Philosophy in Physics

University of California, San Diego, 2014

Professor Daniel H. E. Dubin, Chair

We study the enhanced damping of Trivelpiece-Gould modes in a nonneutral plasma column, due to application of a Debye-shielded cylindrically symmetric squeeze potential φ_1. Damping of these plasma modes is caused by additional Landau resonances at energies E_n for which the particle bounce frequency $\omega_b(E_n)$ and the wave frequency ω satisfy $\omega = n\omega_b(E_n)$. In the first chapter we assume a smooth squeeze of finite width and find that additional resonances induced by the squeeze cause substantial damping, even in the large wave phase velocity compared to thermal velocity regime. For $\omega/k \gg \sqrt{T/m}$ and $\varphi_1 \ll T$, the resonance damping rate has a $|\varphi_1|^2$ dependence. This dependence agrees with the simulations and experimental results.

In chapter 2 a narrow partition-like squeeze is added to an unsqeezed 1D plasma and we evaluate the plasma heating, caused by cylindrically symmetric plasma modes. As in chapter 1, collisionless heating is enhanced by the squeeze, due to additional resonances, even when $\omega/k \gg \sqrt{T/m}$. Adding collisions to the theory broadens these resonances and also creates a boundary layer at the separatrix between trapped and passing particles. This further enhances the heating at $\omega/k v_s < 1$, where v_s is the separatrix velocity.

We study the nonlinear interaction of TG waves in chapter 3. We obtain corrections to the forms and frequencies of weakly nonlinear modes. Futhermore, we study the decay instability between a dominant axial mode $m = 2$ and a small amplitude mode $m = 1$, using both analytical and numerical techniques.

In chapter 4, we study nonlinear interactions of the novel Electron Acoustic Waves in a 1D plasma. Here, we use a weakly nonlinear analysis of a 1D Vlasov-Poisson system, in a modified Maxwellian equilibrium, flattened at the phase velocity of the waves. Using numerical simulation of the 1D Vlasov-Poisson system, we study the unstable collapse of an EAW mode $m = 2$ to an EAW mode $m = 1$ and compare the numerically-obtained exponential growth rates to the analytically obtained results.

Chapter 1

Effect of squeeze on electrostatic Trivelpice-Gould wave damping

1.1 Introduction

Trivelpiece-Gould (TG) modes are electrostatic normal modes of a cylindrical plasma column. For a cold plasma contained in a perfectly conducting cylinder of radius r_w, with uniform plasma density up to the plasma surface at radius $r_p \leq r_w$, the dispersion relation for the TG modes is [40]:

$$\omega \approx \omega_p \frac{k_m}{\sqrt{k_\perp^2 + k_m^2}} \left[1 + \frac{3}{2} \left(\frac{k_m v_T}{\omega} \right)^2 \right]. \tag{1.1}$$

The above equation employs the following notation: mode frequency ω, plasma frequency $\omega_p = \sqrt{4\pi q^2 n_0 / m_q}$, density n_0, particle charge q, particle mass m_q, thermal velocity $v_T = \sqrt{T/m_q}$, perpendicular wave number $k_\perp$ and axial wave number $k_m = \pi m / L$ (L is the length of the plasma). Throughout this chapter we assume that $L \gg r_w$. For such a thin and long plasma, and for cylindrically symmetric modes, to the lowest order in r_w/L the radial wave number is approximated by:

$$k_\perp \approx \frac{1}{r_p} \sqrt{\frac{2}{\log(r_w/r_p)}},$$

for the lowest order radial mode; and for modes with one or more radial nodes, $k_\perp r_p \simeq j_{1n}$ where j_{1n} is the n$^{\text{th}}$ zero of the Bessel function $J_1(x)$. (However, if $r_p = r_w$, $k_\perp r_p = j_{0n}$. [40])

This chapter considers the effect on cylindrically-symmetric Trivelpiece-Gould modes of applying a cylindrically symmetric, axially localized "squeeze" potential $\varphi_{\text{sq}}(r,z)$ to the plasma column. In experiments, a controlled squeeze potential is created by applying a voltage to a conducting ring encircling the plasma column. Uncontrolled axial squeezes, both magnetic and electrostatic, are ubiquitous in many different experiments, and our work is an attempt to quantify their effect on plasma modes. We focus on plasma conditions such that the mode phase velocities are much greater than the thermal velocity of the plasma. In such conditions, Landau damping in the absence of squeeze is expected to be negligibly small. The presence of the squeeze potential modifies the orbits of the particles as well as the spatial form of the mode potential, which results in additional resonances at particle bounce frequencies satisfying $\omega_b(E_n) = \omega/n$, where $\omega_b(E)$ is the frequency of axial bounce motion of particles with energy E. Physically, particles moving in z experience a non-sinusoidal mode potential caused by the squeeze, producing high-frequency harmonics that can resonate with the wave frequency to cause Landau damping, even when the mode phase velocity is large compared to the thermal velocity. We will see that these added resonances cause an enhancement to the mode damping rate that has a $|\varphi_1|^2$ dependence. We also derive a real frequency shift proportional to φ_1. These theory results are verified by computer simulations.

Previous work has examined the effect of an axisymmetric squeeze on θ-dependent ExB drift modes, in theory [19,26] and experiment. [15] Enhanced damping due to squeeze was also observed on these modes, but due mainly to collisional effects, caused by a mode-driven discontinuity in the velocity distribution function at the separatrix between passing particles (those with kinetic energy large enough to pass over the squeeze potential) and particles trapped on either side of the squeeze. While collisional effects can play an important role in TG mode damping, particularly in low temperature multispecies plasmas, we believe collisions are unimportant in determining the enhanced damping due to squeeze compared to the colli-

sionless effects considered here, in the regime where the collision rate is small compared to the bounce frequency. TG mode frequencies are much higher than those for the ExB drift modes considered previously, and this tends to suppress the separatrix discontinuity that enhances collisional damping.

In section 1.2 we present a 1D model theory for squeezed Trivelpiece-Gould modes, which includes a self-consistent treatment of the mode potential in the presence of a 1D squeeze potential. In the analytical solution of this model, we assume that $\varphi_1/T \ll 1$ and treat its effect with perturbation theory. This naturally neglects trapped particle effects on the modes. We evaluate the mode damping rate and frequency shift from our theory and compare these results to computer simulations, which make no assumptions about the size of φ_1/T, finding good agreement when φ_1/T is small.

In section 1.4 we extend our method to a cylindrically symmetric r and z dependent plasma of length L trapped in a Malmberg-Penning trap of the same length and wall radius r_w, assuming flat plasma ends that specularly reflect particles. A squeeze potential φ_{sq} is applied to a conducting cylindrical section of width Δ at the axial center of trap. Similar to the 1D model, since the squeeze potential is Debye shielded from the inner plasma, we assume that the Debye shielded squeeze potential energy inside the plasma is small compared to plasma temperature i.e. $\varphi_1(r,z) \ll T$ and thus, neglect trapped particle effects. Using perturbation theory, corrections due to squeeze potential to the r and z dependent eigenmodes and their related eigenfrequencies and damping rates are obtained.

1.2 1D model

In this section we neglect radial variation for simplicity, we assume the plasma ends are flat, and that particles undergo specular reflection at the ends, $z = \pm L/2$. We also assume that the squeeze potential is symmetric in z with respect to the center of plasma. This is not necessarily the case in the experiments, however this added symmetry simplifies the problem. In this 1D model we will find that Eq. (1.1) still applies, but now $k_\perp$ is an arbitrary parameter. We focus on azimuthally sym-

metric modes in a strong magnetic field and we assume the following ordering for the time scales:

$$\nu_{col} \ll \omega_b \lesssim \omega \lesssim \omega_p \ll \omega_c . \tag{1.2}$$

Here, ν_{col} is the collision frequency and $\omega_c = qB/m_q c$ is the cyclotron frequency. Reading from left to right, the first inequality allows us to use collisionless theory to describe the waves; the second inequality is necessary so that waves are not heavily Landau damped; and the fourth assumes a strong magnetic field. In such a strong magnetic field the distribution of particle guiding centers is described by drift-kinetic equations. Particle motion consists of $\mathbf{E} \times \mathbf{B}$ drift motion across the magnetic field and streaming along the magnetic field in the z direction. Since we assume the plasma consists of one type of particles with charge q, in our calculation we make use of potential energy instead of electrostatic potential, in order to simplify our notation.

In this 1D strong-magnetic-field model, collisionless plasma dynamics is described by the time evolution of the Vlasov particle density $f(z, v, t)$, a solution of the 1D Vlasov equation

$$\frac{\partial f}{\partial t} + v\frac{\partial f}{\partial z} - \frac{1}{m_q}\frac{\partial \varphi}{\partial z}\frac{\partial f}{\partial v} = 0 , \tag{1.3}$$

where $\varphi(z, t)$ is the potential energy of a particle. This potential energy is the sum of a given time-independent applied external squeeze potential $\varphi_{sq}(z)$, and the plasma response $\varphi_p(z, t)$,

$$\varphi(z, t) = \varphi_{sq}(z) + \varphi_p(z, t) \tag{1.4}$$

where the plasma response satisfies Poisson's equation,

$$\frac{\partial^2 \varphi_p}{\partial z^2} - k_\perp^2 \varphi_p = -4\pi q^2 \left(\int dv\, f - n_0 \right). \tag{1.5}$$

Here, n_0 is the density of a uniform neutralizing background charge (provided by rotation at a given frequency through the uniform magnetic field in the actual plasma system.) We also assume here that "radial dependence" of the plasma potential in

our 1D slab model is given by the $k_\perp^2\varphi$ term. In the actual plasma experiments this term is replaced by the radial part of the Laplacian operator–see Sec. II for the model including radial dependence.

For our analysis of linear modes, we linearize Eqs. (1.3) and (1.4) in the wave potential, writing

$$\varphi_p(z,t)=\varphi_{pe}(z)+\delta\varphi(z,t) \tag{1.6}$$

and

$$f(z,v,t)=n_0(\mathrm{F}_0(z,v)+\delta\mathrm{f}(z,v,t)). \tag{1.7}$$

Here, φ_{pe} is the equilibrium plasma potential, $n_0\mathrm{F}_0(z,v)$ is the equilibrium distribution function, and $\delta\varphi$ and δf are the perturbed potential and distribution function respectively due to the TG mode. The equilibrium quantities satisfy the time-independent Vlasov-Poisson system,

$$v\frac{\partial \mathrm{F}_0}{\partial z}-\frac{1}{m_q}\frac{\partial\varphi_1}{\partial z}\frac{\partial \mathrm{F}_0}{\partial v}=0, \tag{1.8}$$

$$\frac{\partial^2\varphi_{pe}}{\partial z^2}-k_\perp^2\varphi_{pe}=-4\pi q^2 n_0\left(\int dv\,\mathrm{F}_0-1\right), \tag{1.9}$$

where

$$\varphi_1(z)=\varphi_{sq}(z)+\varphi_{pe}(z)+C \tag{1.10}$$

is the total equilibrium potential energy, and C is any constant (we may choose to measure potential energy with respect to any convenient zero value). For our purposes we find it convenient to take $C=-\varphi_{sq}(L/2)-\varphi_{pe}(L/2)$, so that (for a symmetric squeeze potential) $\varphi_1(\pm L/2)=0$. In the next section we discuss the solution of this coupled equilibrium system for a given symmetric squeeze potential $\varphi_{sq}(z)$.

To determine the dispersion relation for TG waves in the presence of a squeeze potential, we substitute Eqs. (1.6) and (1.7) into Eqs. (1.3) and (1.5) and linearize in the wave amplitude obtaining the linearized Vlasov-Poisson system,

$$\frac{\partial\delta\mathrm{f}}{\partial t}+v\frac{\partial\delta\mathrm{f}}{\partial z}-\frac{1}{m_q}\frac{\partial\varphi_1}{\partial z}\frac{\partial\delta\mathrm{f}}{\partial v}-\frac{1}{m_q}\frac{\partial\delta\varphi}{\partial z}\frac{\partial \mathrm{F}_0}{\partial v}=0, \tag{1.11}$$

$$\frac{\partial^2 \delta\varphi}{\partial z^2} - k_\perp^2 \delta\varphi = -4\pi q^2 n_0 \int d\,v\,\delta \mathrm{f}. \tag{1.12}$$

We consider solutions of these coupled linearized equations in Sec. 1.2.2.

1.2.1 Squeezed thermal equilibrium

The plasma in this model is a slab of width L running from $-L/2 \le z \le L/2$. In the absence of a squeeze it has uniform density n_0. We assume that the applied squeeze potential $\varphi_{sq}(z)$ is symmetric with respect to the center of plasma. It has a maximum $\varphi_{sq}^{\max} = \varphi_{sq}(0)$ and minima at the plasma ends. Then the solution of Eq. (1.8) for the equilibrium distribution function is $\mathrm{F}_0 = \mathrm{F}_0(H_0(z,v))$, where $H_0(z,v)$ is the Hamiltonian of the plasma equilibrium given by

$$H_0 = m_q v^2/2 + \varphi_1(z). \tag{1.13}$$

For any given function form of $\mathrm{F}_0(H_0)$ Eqs. (1.8)–(1.10) and (1.13) can be solved for the plasma potential energy $\varphi_{pe}(z)$, for given boundary conditions on Eq. (1.9). We assume periodic boundary conditions with period L. The functional form we choose for $\mathrm{F}_0(H_0)$ is the Boltzmann distribution,

$$\mathrm{F}_0(H_0(z,v)) = \frac{e^{-\frac{H_0}{T}}}{\sqrt{2\pi T/m_q}\int_{-L/2}^{L/2} e^{-\frac{\varphi_1(z)}{T}} d(z/L)}, \tag{1.14}$$

normalized so that

$$\int_{-\infty}^{\infty}\int_{-L/2}^{L/2} \mathrm{F}_0\, d\,v\, d\,z = L\,. \tag{1.15}$$

We are particularly interested in a case where the squeeze potential is Debye shielded to the extent that the equilibrium potential energy φ_1 inside the plasma is much smaller than the average kinetic energy; i.e., $\varphi_1/T \ll 1$. In this situation, we can expand Eq. (1.9) to the first order in φ_1/T and get the following relation:

$$(-k_\perp^2 + \partial_z^2)\varphi_{pe} = \lambda_D^{-2}\left(\varphi_1 - \left\langle \varphi_1 \right\rangle\right), \tag{1.16}$$

where $\lambda_D = \sqrt{T/4\pi q^2 n_0}$ is the Debye length, and $\langle\cdot\rangle = \int_{-L/2}^{L/2} dz/L$. For a squeeze potential which is symmetric with respect to the center of the plasma we have the following representations (using the periodic boundary conditions):

$$\varphi_1(z) = \langle\varphi_1\rangle + \sum_{n=1}^{\infty} \varphi_n^1 \cos[\tfrac{2n\pi}{L}(z+\tfrac{L}{2})], \tag{1.17}$$

$$\varphi_{sq}(z) = \langle\varphi_{sq}\rangle + \sum_{n=1}^{\infty} \varphi_{sq}^n \cos[\tfrac{2n\pi}{L}(z+\tfrac{L}{2})]. \tag{1.18}$$

From Eqs. (1.16), (1.17) and (1.10) we can solve for φ_1, the Debye shielded squeeze potential:

$$\begin{aligned} \langle\varphi_1\rangle &= \langle\varphi_{sq}\rangle - \varphi_{pe}(L/2) - \varphi_{sq}(L/2), \\ \varphi_n^1 &= \frac{(k_\perp^2 + k_{2n}^2)\lambda_D^2 \varphi_{sq}^n}{(k_\perp^2 + k_{2n}^2)\lambda_D^2 + 1}, \end{aligned} \tag{1.19}$$

$$\varphi_{pe}(L/2) = -\sum_{n=1}^{\infty} \frac{\varphi_{sq}^n}{(k_\perp^2 + k_{2n}^2)\lambda_D^2 + 1}, \tag{1.20}$$

where $k_n = n\pi/L$.

As a model for numerical work, the applied squeeze potential $\varphi_{sq}(z)$ is taken as a Gaussian function with maximum $\varphi_{sq}^{\max}$ at the center of plasma $z = 0$ and width Δ:

$$\varphi_{sq}(z) = \varphi_{sq}^{\max} e^{-\frac{z^2}{2\Delta^2}}. \tag{1.21}$$

From Eq. (1.19) we can see that the magnitude of the potential inside the plasma is linearly proportional to the magnitude of the squeeze potential in the regime where $\varphi_1 \ll T$. For future reference, we define the maximum of the Debye shielded squeeze potential at $z = 0$ as $\varphi_s \equiv \varphi_1(0)$.

1.2.2 Obtaining the matrix linear dispersion relation

In this section we solve the linearized Vlasov equation (1.11), for the perturbed distribution function $\delta f(z, v)$, and use the linearized Poisson's equation (1.12) to obtain a dispersion relation for the electrostatic potential energy $\delta\varphi$ in the plasma

waves. We define the scaled potential $\overline{\varphi}_1$ and scaled energy variable u as:

$$\overline{\varphi}_1(z) = \varphi_1(z)/T, \tag{1.22}$$

$$u = m_q v^2/2T + \varepsilon\overline{\varphi}_1(z). \tag{1.23}$$

Here, ε is an auxiliary smallness parameter, pertinent for a system where the squeeze is small, $\varphi_1/T \ll 1$. At the end of the calculation ε will be set to 1. We rewrite the equilibrium distribution function in terms of u as

$$\mathrm{F}_0(u) = \frac{e^{-u}}{\sqrt{2\pi T/m_q}\int_{-L/2}^{L/2} e^{-\varepsilon\overline{\varphi}_1(z)} d(z/L)}. \tag{1.24}$$

To solve for δf, we note that particles perform a periodic bounce motion along their orbits in the equilibrium potential $\varphi_1(z)$. Thus, in order to simplify our calculations, we use the canonical action-angle variables of the orbits, ψ and I, which are defined by:

$$\psi = \omega_b \int_{z0}^{z} \frac{dz}{v(z)}, \tag{1.25}$$

$$I = \frac{1}{2\pi}\oint p_z dz.$$

Here, the velocity of a particle with scaled energy u is given by

$$v(z) = v_T\sqrt{2(u-\varepsilon\overline{\varphi}_1(z))}. \tag{1.26}$$

The bounce frequency ω_b is the fundamental frequency of the periodic orbits and can be calculated from

$$\omega_b = 2\pi/\tau, \quad \tau = \oint \frac{dz}{v(z)}, \tag{1.27}$$

where τ is the time period of one cycle of motion for particle of action I. For particles with energy $u > \varepsilon\overline{\varphi}_s$ (where $\overline{\varphi}_s = \overline{\varphi}_1(0)$), which we term "passing particles," this cycle of motion is from $-L/2$ to $L/2$ and back . For particles with energy $u < \varepsilon\overline{\varphi}_s$,

which are trapped on one side of the squeeze, there is a turning point as particles reflect from the squeeze potential. The bounce frequency of the cycle of motion ω_b can also be expressed as

$$\omega_b(I) = T\partial u/\partial I\,. \tag{1.28}$$

Using Eq. (1.25), ψ can be written as a function of z and scaled energy u:

$$\begin{aligned}\psi &= \frac{2\pi}{\oint \frac{dz}{\sqrt{(2(u-\varepsilon\overline{\varphi}_1(z))}}}\int_{z0}^{z}\frac{dz}{v_T\sqrt{2(u-\varepsilon\overline{\varphi}_1(z))}},\\ &= \frac{2\pi}{\oint \frac{dz}{\sqrt{1-\varepsilon\varphi_1(z)/u}}}\int_{z0}^{z}\frac{dz}{\sqrt{1-\varepsilon\overline{\varphi}_1(z)/u}},\\ &= \psi(z,\varepsilon/u).\end{aligned} \tag{1.29}$$

As a result of inverting Eq. (1.29) we have:

$$z = z(\psi,\varepsilon/u), \tag{1.30}$$

where z is a periodic function of ψ. The mode potential $\delta\varphi(z)$ can then be written in terms of action-angle variables. First, we note that for a long thin plasma where $\omega \ll \omega_p$, to the zeroth order in ω/ω_p the boundary condition on the mode potential at the plasma ends is approximately $\partial_z\delta\varphi(\pm L/2)\approx 0$ [34]. Therefore, the standing mode potential can be written as

$$\delta\varphi(z,t) = \sum_{m=1}^{\infty}\left(e^{-i\omega t}\delta\phi_m + e^{i\omega t}\delta\phi_m^*\right)\cos[k_m(z+L/2)], \tag{1.31}$$

where $k_m = m\pi/L$, $\delta\phi_m = \delta\phi_m^r + i\delta\phi_m^i$ is the mth complex Fourier component in the position space and $\omega = \omega_r + i\gamma$ is the complex mode frequency. Alternatively we can write the above equation in terms of strictly real functions as

$$\delta\varphi(z,t) = 2\sum_{m=1}^{\infty}e^{-\gamma t}\left(\delta\phi_m^i\sin(\omega_r t) + \delta\phi_m^r\cos(\omega_r t)\right)\cos[k_m(z+L/2)] \tag{1.32}$$

Next, since z is periodic in ψ, we can write the z-dependence as a Fourier series in ψ:

$$\cos[k_m(z(\psi,\varepsilon/u)+\tfrac{L}{2})] = \sum_{n=-\infty}^{\infty} C_m^n(\varepsilon/u)e^{in\psi} \tag{1.33}$$

where the connection coefficients C_m^n are

$$C_m^n(\varepsilon/u) = \frac{1}{2\pi}\int_0^{2\pi} e^{-in\psi}\cos[k_m(z(\psi,\varepsilon/u)+\tfrac{L}{2})]\,d\psi. \tag{1.34}$$

These coefficients connect Fourier representations in z and ψ. Using these coefficients we can write:

$$\begin{aligned}\delta\varphi(\psi,\varepsilon/u;t) = \sum_{n=-\infty}^{\infty}\sum_{m=1}^{\infty} \quad & \big(\delta\phi_m C_m^n(\varepsilon/u)e^{i(n\psi-\omega t)} \\ & +\delta\phi_m^* C_m^{-n}(\varepsilon/u)e^{-i(n\psi-\omega t)}\big),\end{aligned} \tag{1.35}$$

Since u (or action I) is a constant of the unperturbed motion and $\psi = \omega_b t + \psi(0)$, relation (1.35) expresses the mode potential as experienced by a particle with scaled energy u, as a function of time along its unperturbed orbit.

The form of the mode potentials as a function of z and the mode eigenfrequencies can be obtained by simultaneously solving the linear 1D Vlasov equation (1.11) and the Poisson equation (1.12), where the mode perturbation to the distribution function is of the form

$$\delta \mathrm{f}(z,v_z;t) = \delta f(z,v)e^{-i\omega t} + c.c. \tag{1.36}$$

Substituting for $\delta\varphi$ from Eq. (1.31), multiplying both sides of Eq. (1.12) by

$$\tfrac{2}{L}e^{-i\omega t}\cos[k_m(z+L/2)], \tag{1.37}$$

integrating in time over a period $(2\pi/\omega)$, and in z over the whole length of the plasma,

from $-L/2$ to $L/2$ we have the following series of equations:

$$(k_\perp^2 + k_m^2)\delta\phi_m = 4\pi q^2 n_0 \frac{2}{L}\int_{-L/2}^{L/2}\int_{-\infty}^{\infty}\delta f(z,v)\cos[k_m(z+\tfrac{L}{2})]\,dz\,dv, \tag{1.38}$$

where $m = 1,2,\ldots$. The linear Vlasov equation (1.11) can also be written in terms of canonical action-angle variables:

$$\partial_t \delta \mathrm{f} + \omega_b \partial_\psi \delta \mathrm{f} - \partial_\psi \delta\varphi \partial_I \mathrm{F}_0(I) = 0. \tag{1.39}$$

This can be solved by expressing δf in terms of action-angle variables,

$$\delta \mathrm{f}(\psi, I; t) = \sum_{n=-\infty}^{\infty} \delta f_n(I) e^{i(n\psi - \omega t)} + c.c. \tag{1.40}$$

Substituting from Eqs. (1.35) and (1.40) in Eq. (1.39) and solving for $\delta f_n(I)$ we obtain:

$$\delta f_n(I) = \frac{n\omega_b \sum_{\overline{m}=1}^{\infty} \delta\phi_{\overline{m}} C_{\overline{m}}^n(\varepsilon/u)\mathrm{F}_0(I)/T}{\omega - n\omega_b}. \tag{1.41}$$

On the right hand side of Eq. (1.41) we used

$$\frac{\partial}{\partial I}\mathrm{F}_0(u) \quad = T^{-1}\left(\frac{du}{dI}\right)\frac{\partial}{\partial u}\mathrm{F}_0(u) = -\omega_b \frac{\mathrm{F}_0}{T},$$

where F_0 is given in Eq. (1.24). Since ψ and I are canonical coordinates, $dz\,dp_z = d\psi\,dI$ and we can exchange the integration over (z,v) variables (on the right hand side of Eq. (1.38)) to (ψ, I) variables. Performing the integral in Eq. (1.38) over ψ from 0 to 2π using Eqs. (1.34) and (1.41) we obtain:

$$\delta\phi_m - \frac{\omega_p^2}{K_m^2}\frac{4\pi}{LT}\sum_{n=-\infty}^{\infty}\int_{\mho} dI \frac{n\omega_b \mathrm{F}_0(I)}{\omega - n\omega_b}\sum_{\overline{m}=1}^{\infty}\delta\phi_{\overline{m}} C_{\overline{m}}^n(\varepsilon/u) C_m^{-n}(\varepsilon/u) = 0, \tag{1.42}$$

where $K_n = \sqrt{k_\perp^2 + k_n^2}$ is the total wave number, and $\mho$ denotes integration with respect to I, performed in the complex plane below the pole (using the Landau con-

tour [29]). Due to the symmetry of the squeeze, we have $C_m^n(\varepsilon/u) = C_m^{-n}(\varepsilon/u)$. Furthermore, in Eq. (1.42) we will neglect trapped particles, assuming $\overline{\varphi}_s \ll 1$, and we will only integrate over the energies of the passing particles, i.e. $u > \varepsilon\overline{\varphi}_s$. Thus, Eq. (1.42) becomes

$$\delta\phi_m - \frac{\omega_p^2}{K_m^2}\frac{8}{\sqrt{2\pi}v_T^2\left\langle e^{-\varepsilon\overline{\varphi}_1}\right\rangle}\sum_{n=1}^{\infty}\int_{\varepsilon\overline{\varphi}_s}^{\infty} du\,\frac{\overline{\omega}_b(u,\varepsilon)e^{-u}}{(\overline{\omega}/n)^2-\overline{\omega}_b(u,\varepsilon)^2}\sum_{\overline{m}=1}^{\infty}\delta\phi_{\overline{m}}C_{\overline{m}}^n(\varepsilon/u)C_m^n(\varepsilon/u) = 0, \tag{1.43}$$

where we used $\omega_b = T\,du/dI$ and Eq. (1.24). Also we define the scaled bounce frequency $\overline{\omega}_b(u,\varepsilon)$ as $\overline{\omega}_b(u,\varepsilon) = \omega_b/k_1 v_T$, and the (complex) scaled mode frequency $\overline{\omega} = \omega/k_1 v_T$. Equation (1.43) is a linear, complex, matrix eigenvalue equation which can be written in the simple matix form as:

$$\mathbf{M}(\overline{\omega},\varepsilon).\mathbf{e} = 0, \tag{1.44}$$

where the dispersion matrix $\mathbf{M}$ and eigenvector $\mathbf{e}$ are given by

$$M^{m\overline{m}}(\overline{\omega},\varepsilon) = \delta_{m\overline{m}} - \frac{8(K_m\lambda_D)^{-2}}{\sqrt{2\pi}\left\langle e^{-\varepsilon\overline{\varphi}_1}\right\rangle}\sum_{n=1}^{\infty}\int_{\varepsilon\overline{\varphi}_s}^{\infty} du\,\frac{\overline{\omega}_b(u,\varepsilon)e^{-u}}{(\overline{\omega}/n)^2-\overline{\omega}_b(u,\varepsilon)^2}C_{\overline{m}}^n(\varepsilon/u)C_m^n(\varepsilon/u), \tag{1.45}$$

$$\mathbf{e}^T = (\delta\phi_1, \delta\phi_2, \ldots). \tag{1.46}$$

Equation (1.44) is solved by finding complex frequencies $\overline{\omega}$ such that an eigenvalue of $\mathbf{M}$ equals zero. The corresponding eigenvector in the nullspace of $\mathbf{M}$ provides the Fourier components of $\delta\varphi(z)$. Different Fourier components of the mode (elements of the right hand side of Eq. (1.46)) are coupled through the off-diagonal elements of $\mathbf{M}$, which are generated by the squeeze potential.

1.2.3 Perturbation method for the small φ_1/T regime

In order to obtain the eigenvalues, eigenvectors and the damping rate of the modes, we will use a perturbation approach and expand the dispersion relation in orders of ε as the smallness parameter. We Taylor expand the dispersion matrix $\mathbf{M}$ for small ε in Eq. (1.45):

$$\mathbf{M}(\overline{\omega},\varepsilon)=\mathbf{M}(\overline{\omega},0)+\partial_\varepsilon\mathbf{M}(\overline{\omega},0)\varepsilon+\frac{1}{2}\partial_\varepsilon^2\mathbf{M}(\overline{\omega},0)\varepsilon^2+\ldots \tag{1.47}$$

We have the following series expansions in terms of ε:

$$\mathbf{M} = \mathbf{M}_0+\mathbf{M}_1\varepsilon+\mathbf{M}_2\varepsilon^2+\ldots, \tag{1.48}$$

$$\mathbf{e} = \mathbf{e}_0+\mathbf{e}_1\varepsilon+\mathbf{e}_2\varepsilon^2+\ldots, \tag{1.49}$$

$$\overline{\omega} = \overline{\omega}_0+\overline{\omega}_1\varepsilon+\overline{\omega}_2\varepsilon^2+\ldots, \tag{1.50}$$

where:

$$\mathbf{M}_0=\mathbf{M}(\overline{\omega},0),\quad \mathbf{M}_1=\partial_\varepsilon\mathbf{M}(\overline{\omega},0),\quad \mathbf{M}_2=\frac{1}{2}\partial_\varepsilon^2\mathbf{M}(\overline{\omega},0). \tag{1.51}$$

Details of calculation of $\mathbf{M}_0,\mathbf{M}_1$ and $\mathbf{M}_2$ are given in appendix B. The complex column vectors $\mathbf{e}_0$, $\mathbf{e}_1$, $\mathbf{e}_2$ and complex frequencies $\overline{\omega}_0,\overline{\omega}_1,\overline{\omega}_2$ determine the spatial form and complex frequency of the eigenfunctions in the presence of a small squeeze potential.

Using relations (1.48) through (1.50), we rewrite the dispersion relation (1.44), collect the terms of orders $\varepsilon^0,\varepsilon^1$ and ε^2 and set the dispersion relation at each order to zero separately.

Zeroth order in ε

The zeroth order dispersion relation (for an unsqueezed plasma) is given by

$$\mathbf{M}_0(\overline{\omega}_0^m).\mathbf{e}_0^m=0, \tag{1.52}$$

where $\overline{\omega}_0^m$ is the zeroth order, complex eigenfrequency of mode m. From Eq. (B.9) the matrix $\mathbf{M}_0$ is, in component form,

$$M_0^{\overline{m}m}(\overline{\omega}) = \left(1 + \frac{1}{\lambda_D^2 K_m^2}\,\mathrm{W}(\overline{\omega}/m)\right)\delta_{\overline{m}m}, \tag{1.53}$$

Thus, we obtain the following zeroth order dispersion relation for mode m:

$$1 + \frac{1}{\lambda_D^2 K_m^2}\,\mathrm{W}\left(\overline{\omega}_0^m/m\right) = 0, \tag{1.54}$$

where the function $\mathrm{W}(b)$ is defined as:

$$\mathrm{W}(b) = \frac{1}{\sqrt{2\pi}}\int_{\mho}\frac{x\,e^{-x^2/2}dx}{x-b}. \tag{1.55}$$

Equation (1.52) is the TG mode dispersion relation of an unsqueezed plasma. Since $\mathbf{M}_0$ is a diagonal matrix, each Fourier cosine function in Eq. (1.31) is an eigenmode. Thus, the zeroth order eigenvector for the mode is

$$\left(\mathbf{e}_0^m\right)_l = \Delta_{m,l}\,\delta\phi_m^m. \tag{1.56}$$

The zeroth order eigenfrequency $\overline{\omega}_0^m$ is obtained by solving Eq. (1.54). For weakly damped modes with frequency $\overline{\omega}_0^m = \overline{\omega}_{0r}^m + i\overline{\gamma}_0^m$, scaled frequency and the damping rate are given by:

$$1 + \frac{1}{\lambda_D^2 K_m^2}\mathrm{Re}\,\mathrm{W}\left(\overline{\omega}_{0r}^m/m\right) = 0, \tag{1.57}$$

$$\overline{\gamma}_0^m = -\frac{\pi\overline{\omega}_{0r}^m e^{-\frac{(\overline{\omega}_{0r}^m)^2}{2m^2}}}{\mathrm{P}\int_{-\infty}^{\infty}\frac{v\,e^{-v^2/2}dv}{(\overline{\omega}_{0r}^m/m - v)^2}}. \tag{1.58}$$

Since we are dealing with linear modes, the mode amplitude $\delta\phi_m^m$ in Eq. (1.57) is an arbitrary parameter, which we take to be real. In Eq. (1.58), $\overline{\gamma}_0^m$ is obtained by perturbation, with the assumption that $\overline{\omega}_{0r}^m \gg \overline{\gamma}_0^m$. When $\overline{\omega}_{0r}^m/m \gg 1$, the Landau-damping damping rate $\overline{\gamma}_0^m$ for the unsqueezed plasma is exponentially small.

Both real and imaginary parts of the zeroth-order (unsqueezed) scaled phase

velocity $\overline{\omega}_0/m$ are functions only of a single parameter, $K_m\lambda_D$. In the limit that the plasma is cold, so that $K_m\lambda_D \ll 1$, the solution of Eq. (1.57) is

$$\frac{\overline{\omega}_{0r}^2}{m^2} = \frac{1}{(K_m\lambda_D)^2} + 3 + 6(K_m\lambda_D)^2 + 24(K_m\lambda_D)^4 + 180(K_m\lambda_D)^6 + \ldots \tag{1.59}$$

The first two terms in this asymptotic series are equivalent to Eq. (1.1).

First order in ε

We obtain the first order correction to the mode frequency $\overline{\omega}_1^m = \overline{\omega}_{1r}^m + i\overline{\gamma}_1^m$, and the first order correction to the eigenvector $\mathbf{e}_1^m$ from the first order dispersion relation given by:

$$\mathbf{M}_0(\overline{\omega}_0^m).\mathbf{e}_1^m + \overline{\omega}_1^m \partial_{\overline{\omega}}\mathbf{M}_0(\overline{\omega}_0^m).\mathbf{e}_0^m + \mathbf{M}_1(\overline{\omega}_0^m).\mathbf{e}_0^m = 0\,, \tag{1.60}$$

where from Eq. (B.16) the components of the matrix $\mathbf{M}_1$ are given by the expression

$$M_1^{mn} = -\frac{4}{K_m^2\lambda_D^2}\left(\frac{m^2}{\overline{\omega}^2}[1-\mathrm{W}(\overline{\omega}/m)]\alpha_n^m + \frac{n^2}{\overline{\omega}^2}[1-\mathrm{W}(\overline{\omega}/n)]\alpha_m^n\right), \tag{1.61}$$

where the coefficients α_m^n are first-order in ε corrections to the Fourier connection coefficients C_m^n, given by

$$\alpha_m^n = \begin{cases} \frac{m}{8}\left(\frac{\overline{\varphi}^1_{|m-n|/2}}{m-n} + \frac{\overline{\varphi}^1_{|m-n|/2}}{m+n}\right), & m \neq \pm n \\ \frac{\overline{\varphi}^1_m}{16}, & m = \pm n \end{cases}. \tag{1.62}$$

From Eq. (1.60) we solve for the first order correction to $\mathbf{e}^m$, which is given by the components

$$(\mathbf{e}_1^m)_j = -\frac{M_1^{jm}(\overline{\omega}_0^m)}{M_0^{jj}(\overline{\omega}_0^m)}\delta\phi_m^m, \quad j \neq m. \tag{1.63}$$

and $(\mathbf{e}_1^m)_m = 0$. Using relation (1.32), we can write the squeezed eigenmode m up to

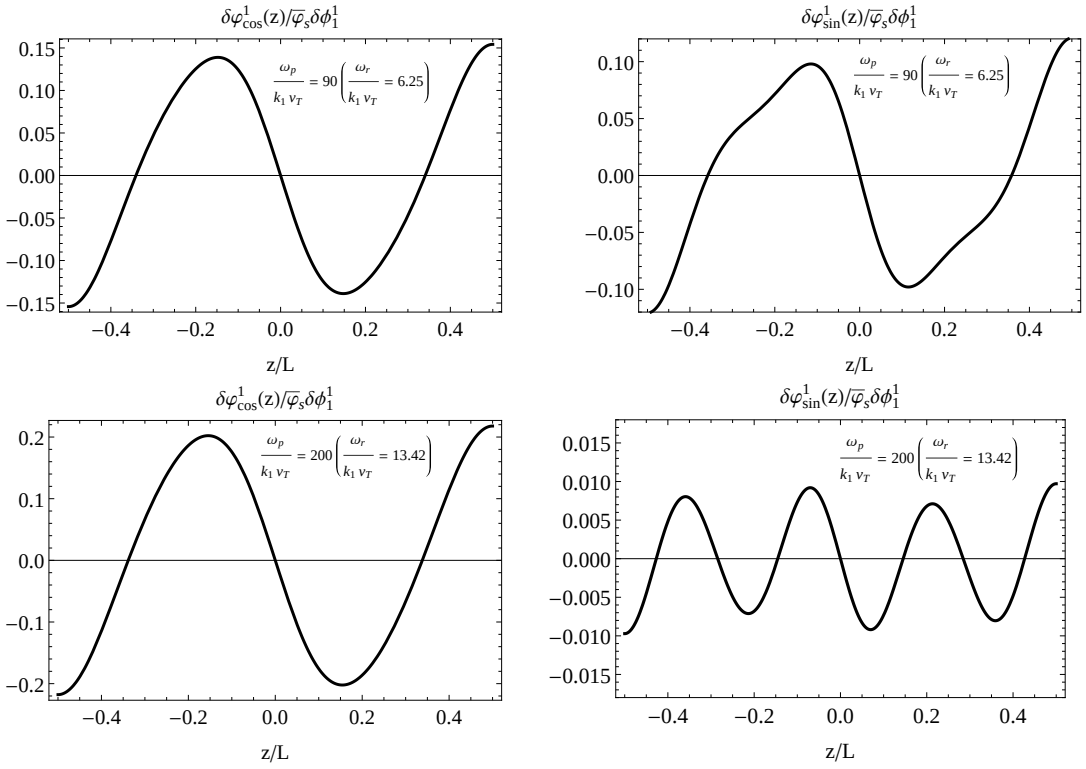

Figure 1.1: The change to the spatial dependence of mode potential for mode $m = 1$, with $\cos(\omega_r t)$ and $\sin(\omega_r t)$ time dependence, in a plasma with $k_\perp L = 15\pi$ and scaled plasma frequencies $\omega_p/k_1 v_T = 90$ and $\omega_p/k_1 v_T = 200$, corresponding to mode phase velocities $\omega_{r_0}/k_1 v_T = 6.25$ and 13.42 respectively.

the first order in ε as:

$$\begin{aligned}\delta\varphi^m(z,t) &= 2\delta\phi^m_m e^{-\gamma t}\cos(\omega_r t)\cos[k_m(z+L/2)] \\ &+ 2\varepsilon\sum_{j\neq m}^{\infty}\mathrm{Im}[\delta\phi^m_j]\cos[k_j(z+L/2)]e^{-\gamma t}\sin(\omega_r t) \\ &+ 2\varepsilon\sum_{j\neq m}^{\infty}\mathrm{Re}[\delta\phi^m_j]\cos[k_j(z+L/2)]e^{-\gamma t}\cos(\omega_r t)\end{aligned} \tag{1.64}$$

where $\delta\varphi^m_j = (\mathbf{e}^m_1)_j$ (see Eqs. (1.46) and (1.63)). Contributions to the mode potential from wave numbers $k_j \neq k_m$ are linearly proportional to the squeeze amplitude φ_s. These terms ($j \neq m$) are also linearly proportional to the amplitude of the unsqueezed mode potential $\delta\phi^m_m$ (as seen from Eq. (1.63)). There are $\sin(\omega_r t)$ dependent as well as $\cos(\omega_r t)$ dependent contributions from the $j \neq m$ terms to the mode potential. Using Eq. (1.63), the spatial dependence of $j \neq m$ terms with $\sin(\omega_r t)$ and $\cos(\omega_r t)$ time dependence are:

$$\delta\phi^m_{\sin}(z) = -2\varepsilon\delta\phi^m_m\sum_{j\neq m}^{\infty}\mathrm{Im}\left[\frac{M_1^{jm}(\overline{\omega}^m_0)}{M_0^{jj}(\overline{\omega}^m_0)}\right]\cos[k_j(z+L/2)] \tag{1.65}$$

$$\delta\phi^m_{\cos}(z) = -2\varepsilon\delta\phi^m_m\sum_{j\neq m}^{\infty}\mathrm{Re}\left[\frac{M_1^{jm}(\overline{\omega}^m_0)}{M_0^{jj}(\overline{\omega}^m_0)}\right]\cos[k_j(z+L/2)] \tag{1.66}$$

Figures (1.1) are plots of $\delta\phi^m_{\sin}/(\overline{\varphi}_s\delta\phi^m_m)$, and $\delta\phi^m_{\cos}/(\overline{\varphi}_s\delta\phi^m_m)$, for mode $m = 1$, with $k_\perp L = 15\pi$ and plasma frequencies $\omega_p/k_1 v_T = 90$ and $\omega_p/k_1 v_T = 200$. We divide out the scaled squeeze potential maximum value $\overline{\varphi}_s$ so that the resulting functions are independent of the size of the squeeze. The $\sin(\omega_r t)$ dependent part of the mode potential becomes smaller for larger values of the phase velocity.

The shift in the frequency of the mode due to the squeeze is found by taking the product of Eq. (1.60) from left with $(\mathbf{e}^m_0)^T$, The first term will result in zero, since $(\mathbf{e}^m_0)^T.\mathbf{M}_0(\omega^m_0) = 0$. Solving for $\overline{\omega}^m_1$ we obtain:

$$\overline{\omega}^m_1 = -\frac{M_1^{mm}(\overline{\omega}^m_0)}{\partial_{\overline{\omega}}M_0^{mm}(\overline{\omega}^m_0)}. \tag{1.67}$$

Substituting from Eq. (1.61) for the numerator and from Eq. (1.53) for the denominator, we write the above equation as:

$$\overline{\omega}_1^m = \frac{\frac{m^2}{2(\overline{\omega}_0^m)^2}\left[1-\mathrm{W}(\overline{\omega}_0^m/m)\right]\overline{\varphi}^1{}_m}{\partial_{\overline{\omega}}\mathrm{W}(\overline{\omega}_0^m/m)}, \tag{1.68}$$

where $\overline{\varphi}^1{}_m \equiv \varphi^1{}_m/T$ is the scaled Fourier component of the squeeze potential [see Eq. (1.17)]. Using the following relation:

$$\partial_b \mathrm{W}(b) \equiv -[1-\mathrm{W}(b)]/b - b\mathrm{W}(b), \tag{1.69}$$

and Eq. (1.54) we can write Eq. (1.68) as:

$$\overline{\omega}_1^m = \frac{m\overline{\varphi}^1{}_m/2}{\frac{\lambda_D^2 K_m^2}{1+\lambda_D^2 K_m^2}(\frac{\overline{\omega}_0^m}{m})^3 - \frac{\overline{\omega}_0^m}{m}}. \tag{1.70}$$

Furthermore, with the assumption that $\overline{\omega}_{0r}^m \gg \overline{\gamma}_0^m$ we can write the real and imaginary part of $\overline{\omega}_1^m = \overline{\omega}_{1r}^m + i\overline{\gamma}_1^m$ as:

$$\overline{\omega}_{1r}^m = -\frac{1+\lambda_D^2 K_m^2}{1-\lambda_D^2 K_m^2\left[(\frac{\overline{\omega}_{0r}^m}{m})^2-1\right]}\frac{m^2}{\overline{\omega}_{0r}^m}\frac{\overline{\varphi}^1{}_m}{2}, \tag{1.71}$$

$$\overline{\gamma}_1^m = -\frac{\overline{\gamma}_0^m}{\overline{\omega}_{0r}^m}(1-\lambda_D^2 K_m^2)\frac{1-\lambda_D^2 K_m^2\left[3(\frac{\overline{\omega}_{0r}^m}{m})^2-1\right]}{\left(1-\lambda_D^2 K_m^2\left[(\frac{\overline{\omega}_{0r}^m}{m})^2-1\right]\right)^2}\frac{m\overline{\varphi}^1{}_m}{2}. \tag{1.72}$$

From Eq. (1.72), we see that when $\overline{\omega}_0^m \gg m$, the first order correction to the damping rate is exponentially small:

$$\overline{\gamma}_1^m \propto \overline{\gamma}_0^m \propto e^{-\frac{(\overline{\omega}_0^m)^2}{2m^2}} \approx 0, \quad \overline{\omega}_{0r}^m \gg m. \tag{1.73}$$

The real frequency shift given by Eq. (1.71) can be rewritten as

$$\overline{\omega}_{1r}^m = \overline{\omega}_{0r}^m \overline{\varphi}^1{}_m g(K_m\lambda_D) \tag{1.74}$$

where the function $g(x)$ is found by substitution of Eq. (1.59) into Eq. (1.71):

$$g(x)=\frac{1}{4}-\frac{7}{8}x^2-\frac{21}{32}x^4-\frac{747}{64}x^6-..., \;\; x\ll 1 \tag{1.75}$$

Equation (1.74) can be expressed in terms of the externally-applied squeeze potential $\varphi_{sq}(z)$using Eq. (1.19):

$$\omega_{1r}^m=\omega_{0r}^m\frac{K_{2m}^2}{1+K_{2m}^2\lambda_D^2}\frac{\varphi_{sq}^m}{m_q\omega_p^2}g(K_m\lambda_D). \tag{1.76}$$

To lowest-order in $K_m\lambda_D$ Eq. (1.76) describes a temperature-independent frequency shift due to the external squeeze potential:

$$\omega_{1r}^m=\omega_{0r}^m K_{2m}^2\frac{\varphi_{sq}^m}{4m_q\omega_p^2}, \quad K_m\lambda_D\rightarrow 0. \tag{1.77}$$

Equation (1.77) shows that, in order for the perturbation theory to be valid, the external squeeze potential need not be small compared to T. Rather, the requirement that perturbation theory be valid is $\varphi_{sq}\ll m_q\omega_p^2/K_{2m}^2$. The right-hand side is typically on the order of the plasma space-charge potential energy. This inequality is consistent with $\varphi_1\ll T$ since Eq. (1.19) implies that $\varphi_m^1\simeq K_{2m}^2\lambda_D^2\varphi_{sq}^m$ at low temperatures where $K_{2m}\lambda_D\ll 1$.

Figure (1.2) is the plot of mode frequency vs. the magnitude of the Debye shielded squeeze potential $\varphi_s\equiv\varphi_1(0)$. Frequencies calculated from the perturbation theory are the sum of the zeroth order frequency calculated from Eq. (1.57), plus the first order correction to mode frequency using the relation (1.71), which is depicted as a solid line. We use the same form for the squeeze as before (Eq. (1.21)). Computer simulations results obtained from the 1D Vlasov-Poisson simulations (described in section 1.3) are depicted with circles. The mode frequency is lowered for positive squeeze potential and raised for negative squeeze potential. This is due to the fact that the density perturbation in the mode, which for $m=1$ is sloshing left and right with its maximum velocity at the center of plasma, has to travel up and down the squeeze, which acts as a kinetic barrier (for positive squeeze). This increases the oscillation time period and hence, lowers the mode frequency. On the

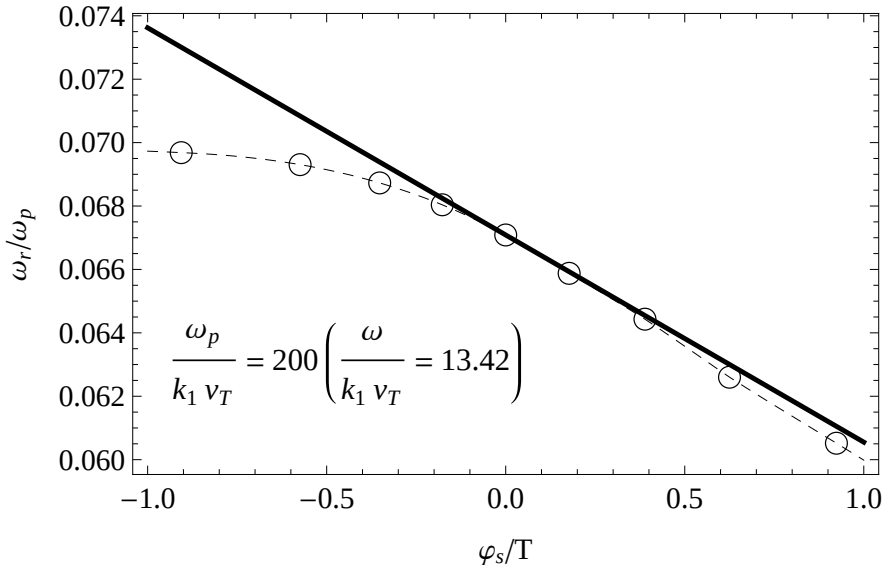

Figure 1.2: The real part of the mode frequency ω_r/ω_p vs. the size of the Debye shielded squeeze potential φ_s/T for mode $m = 1$, where $\varphi_s \equiv \varphi_1(0)$, for $\omega_p/K_1 V_T = 200$ (which implies $\omega_{0r}/K_1 V_T = 13.42$). Analytically calculated results, shown here with a solid line, are up to the first order in φ_s/T using Eq. (1.71); computer simulation results are shown with circles.

other hand for a negative squeeze, the oscillation time period decreases since the density perturbation speeds up as it passes the center of plasma, and as a result mode frequency increases.

Fluid theory for the frequency correction

It is also possible to understand the TG mode frequency shift (but not the damping) caused by applied squeeze using fluid theory rather than kinetic theory. In fluid theory, the equilibrium plasma density varies in z due to the squeeze, and this density variation affects the mode frequency. The density variation is given by the Boltzmann factor ,

$$n_{eq}(z) = n_0 \exp[-\varepsilon \overline{\varphi}_1(z)] / \left\langle \exp[-\varepsilon \overline{\varphi}_1(z)] \right\rangle. \tag{1.78}$$

A fluid theory expression for the wave equation for TG modes in a nonuniform plasma in a strong magnetic field can be found in the literature: [17, 33]

$$\frac{\partial}{\partial z}\alpha(z,\omega)\frac{\partial \delta\phi}{\partial z}+k_{\perp}^{2}\delta\phi=0, \tag{1.79}$$

where

$$\alpha(z,\omega)=\omega_{pz}^{2}(z)/\omega^{2}-1 \tag{1.80}$$

is a dielectric constant for the plasma and $\omega_{pz}(z)$ is the local plasma frequency, given by $\omega_{pz}(z)=\sqrt{4\pi q^{2}n_{eq}(z)/m_{q}}$. A first order correction to the mode due to squeeze can then be obtained by using Eq. (1.78) in Eq. (1.79) and Taylor expanding in ε :

$$\alpha_{0}(\omega)\frac{\partial^{2}\delta\phi}{\partial z^{2}}+\varepsilon[\alpha_{0}(\omega)+1]\frac{\partial}{\partial z}(\langle\overline{\varphi}_{1}\rangle-\overline{\varphi}_{1}(z))\frac{\partial \delta\phi}{\partial z}+k_{\perp}^{2}\delta\phi=0, \tag{1.81}$$

where

$$\alpha_{0}(\omega)=\omega_{p}^{2}/\omega^{2}-1 \tag{1.82}$$

is the z-independent unsqueezed value for α .

To zeroth-order in ε (i.e. for an unsqueezed plasma) the solution of Eq. (1.81) has modes of the form (c.f. Eqs. (1.31), (1.46), and(1.56))

$$\delta\phi_{0}^{m}(z)=\cos[k_{m}(z+L/2)] \tag{1.83}$$

with frequencies satisfying

$$-k_{m}^{2}\alpha_{0}(\omega)+k_{\perp}^{2}=0. \tag{1.84}$$

Equation (1.84) can be solved for ω to yield the cold-fluid TG dispersion relation for unsqueezed frequency for mode m, ω_{0}^{m} :

$$\omega_{0}^{m}=\omega_{p}k_{m}/\sqrt{k_{m}^{2}+k_{\perp}^{2}}. \tag{1.85}$$

The first order correction to ω can be found by applying perturbation theory to Eq. (1.81). Let $\omega = \omega_0^m + \varepsilon\omega_1^m$ where ω_1^m is the first-order correction to the frequency. Also, let $\delta\phi(z) = \delta\phi_0^m(z) + \varepsilon\delta\phi_1^m(z)$ where $\delta\phi_1^m(z)$ is the first ÃŘorder correction to the eigenmode due to squeeze. Substituting these relations in Eq. (1.81) and Taylor expanding to first-order in ε yields, at first order,

$$\omega_1^m \alpha_0{}'(\omega_0^m)\frac{\partial^2\delta\phi_0^m}{\partial z^2} + \alpha_0(\omega_0^m)\frac{\partial^2\delta\phi_1^m}{\partial z^2} + [\alpha_0(\omega_0^m)+1]\frac{\partial}{\partial z}(\langle\overline{\varphi}_1\rangle - \overline{\varphi}_1(z))\frac{\partial\delta\phi_0^m}{\partial z} + k_\perp^2\delta\phi_1^m = 0, \quad (1.86)$$

where the prime on α_0 in the first term denotes differentiation. If we multiply this equation by $\delta\phi_0^m(z)$ and integrate in z over the length of the plasma, we obtain

$$-\frac{L}{2}k_m^2\omega_1^m\alpha_0{}'(\omega_0^m) - k_m^2[\alpha_0(\omega_0^m)+1]\int_{-L/2}^{L/2} dz \sin^2[k_m(z+L/2)](\langle\overline{\varphi}_1\rangle - \overline{\varphi}_1(z)) = 0, \quad (1.87)$$

where we have integrated by parts and substituted for $\delta\phi_0^m(z)$ from Eq. (1.83). Note that on integration by parts the terms involving $\delta\phi_1^m$ vanish. Equation (1.87) can be simplified using the relation $\alpha_0{}'(\omega_0^m) = -2[\alpha_0(\omega_0^m)+1]/\omega_0^m$, which follows from Eq. (1.82). Substituting this into Eq. (1.87) yields the following expression for the first-order frequency shift due to squeeze:

$$\omega_1^m = \omega_0^m \frac{1}{L}\int_{-L/2}^{L/2} dz\, \sin^2[k_m(z+L/2)](\langle\overline{\varphi}_1\rangle - \overline{\varphi}_1(z)). \quad (1.88)$$

This result can be further simplified by substituting the Fourier expansion for $\overline{\varphi}_1(z)$ given in Eq. (1.17), and by using $k_m = m\pi/L$. Then the integral in Eq. (1.88) yields

$$\omega_1^m = \omega_0^m \frac{\varphi_m^1}{4T}, \quad (1.89)$$

where φ_m^1 is the mth Fourier cosine coefficient of the squeeze potential. This expression for the first ÃŘorder frequency shift due to squeeze agrees with the more general result given by Eq. (1.74) when that equation is evaluated in the cold-fluid

regime, $K_m\lambda_D \ll 1$. This provides an independent check of the general result. However, in one sense, Eq. (1.89) is more general than Eq. (1.74): Eq. (1.89) was derived from Eq. (1.88), which is valid for a squeeze of any functional form, not just a symmetric squeeze as was assumed in Eq. (1.74). In fact, Eq. (1.88) shows that only the z-symmetric (cosine) component of the squeeze potential contributes to the first-order frequency shift, since any odd (sine) component to the squeeze potential vanishes upon integration over z.

WKB fluid theory for $m \gg 1$

When the mode number m becomes sufficiently large, the Fourier component of the shielded squeeze potential $\overline{\varphi}^1_m$ becomes exponentially small, assuming that the squeeze is a smooth function of z. In this regime Eq. (1.74) (or Eq. (1.89)) implies that the first order frequency shift due to squeeze is exponentially small, and may therefore be negligible compared to the second-order shift. To find the shift in this regime it is useful to apply WKB theory. For large m, $\delta\phi(z)$ varies rapidly compared to the squeeze, and can be determined using an eikonal approach where we write $\delta\phi(z) = \exp[S(z)]$. From Eq. (1.79) the eikonal $S(z)$ satisfies

$$\alpha[S'' + (S')^2] + S'\alpha' + k_\perp^2 = 0. \tag{1.90}$$

If we assume derivatives of S are of order $m \gg 1$ but the derivative of α is of order unity, the dominant balance in the equation is $\alpha(S')^2 = -k_\perp^2$ with solution

$$S \equiv S_0 = \pm i k_\perp \int^z dz/\sqrt{\alpha(z,\omega)}. \tag{1.91}$$

To next order in $1/m$ we rewrite Eq. (1.90) as

$$S' = \pm i\sqrt{k_\perp^2/\alpha + S'' + S'\alpha'/\alpha}. \tag{1.92}$$

Noting that the last two terms in the square root are small compared to the first, we replace S by S_0 in these two terms in order to obtain the next-order correction to S,

S_1 :

$$\begin{aligned} S_1{}' &= \pm i\sqrt{k_\perp^2/\alpha + S_0{}'' + S_0{}'\alpha'/\alpha} \\ &= \pm i\sqrt{k_\perp^2/\alpha \mp i k_\perp \alpha'/2\alpha^{3/2} \pm i k_\perp \alpha'/\alpha^{3/2}} \\ &\simeq \pm i\frac{k_\perp}{\sqrt{\alpha}}[1 \pm \frac{i\alpha'}{4k_\perp\sqrt{\alpha}}]. \end{aligned} \tag{1.93}$$

where we used Eq. (1.91) in the second step and Taylor-expanded the square root in the last step. Integrating in z, this yields

$$S_1 = S_0 - \frac{1}{4}\ln\alpha. \tag{1.94}$$

Subsituting this eikonal into $\delta\phi(z) = \exp[S(z)]$ implies

$$\delta\phi(z) = [\alpha(z,\omega)]^{-1/4}\exp\left[\pm i k_\perp \int^z dz/\sqrt{\alpha(z,\omega)}\right]. \tag{1.95}$$

These two independent solutions for the mode potential must be combined to match the boundary conditions that the slope of the potential vanishes at both plasma ends, which implies

$$\delta\phi(z) = [\alpha(z,\omega)]^{-1/4}\cos\left[k_\perp \int_{-L/2}^{z} dz/\sqrt{\alpha(z,\omega)}\right], \tag{1.96}$$

where

$$k_\perp \int_{-L/2}^{L/2} dz/\sqrt{\alpha(z,\omega)} = m\pi. \tag{1.97}$$

This is the WKB dispersion relation for a given mode number m. To solve the dispersion relation, we substitute Eqs. (1.80) and (1.78) for α and Taylor expand in ε,

obtaining

$$k_\perp \int_{-L/2}^{L/2} dz \frac{1}{\sqrt{\alpha_0(\omega)}} \left[1 - \frac{\omega_p^2}{2\omega^2} \varepsilon \frac{\langle \overline{\varphi}_1 \rangle - \overline{\varphi}_1}{\alpha_0(\omega)} \right.$$
$$\left. + \frac{\omega_p^2}{8\omega^2 \alpha_0(\omega)} \varepsilon^2 \left(3 \frac{\omega_p^2}{\omega^2} \frac{\left(\langle \overline{\varphi}_1 \rangle - \overline{\varphi}_1 \right)^2}{\alpha_0(\omega)} - 2[\left(\langle \overline{\varphi}_1 \rangle - \overline{\varphi}_1 \right)^2 + \langle \overline{\varphi}_1 \rangle^2 - \langle \overline{\varphi}_1^2 \rangle] \right) \right] = m\pi. \quad (1.98)$$

Upon performing the integration this becomes

$$\frac{k_\perp L}{\sqrt{\alpha_0(\omega)}} \left[1 + \frac{3}{8} \varepsilon^2 \left(\frac{\omega_p^2}{\omega^2 \alpha_0(\omega)} \right)^2 [\langle \overline{\varphi}_1^2 \rangle - \langle \overline{\varphi}_1 \rangle^2] \right] = m\pi. \quad (1.99)$$

Squaring both sides and rearranging yields

$$k_m^2 \alpha_0(\omega) = k_\perp^2 \left[1 + \varepsilon^2 \frac{3}{8} \left(\frac{\omega_p^2}{\omega^2 \alpha_0(\omega)} \right)^2 [\langle \overline{\varphi}_1^2 \rangle - \langle \overline{\varphi}_1 \rangle^2] \right]. \quad (1.100)$$

At $0(\varepsilon^2)$ on the right hand side we can replace $\alpha_0(\omega)$ and ω by their zeroeth ÃŘorder unsqueezed values, given by Eqs. (1.84) and (1.85), obtaining

$$k_m^2 \alpha_0(\omega) = k_\perp^2 \left[1 + \frac{3}{4} \left(1 + \frac{k_m^2}{k_\perp^2} \right)^2 \varepsilon^2 [\langle \overline{\varphi}_1^2 \rangle - \langle \overline{\varphi}_1 \rangle^2] \right]. \quad (1.101)$$

Substituting on the left hand side $\omega = \omega_0^m + \varepsilon^2 \omega_2^m$ and expanding we obtain

$$-2k_m^2 \frac{\omega_p^2}{(\omega_0^m)^3} \omega_2^m = \frac{3}{4} K_m^2 \left(1 + \frac{k_m^2}{k_\perp^2} \right) [\langle \overline{\varphi}_1^2 \rangle - \langle \overline{\varphi}_1 \rangle^2],$$

which implies

$$\omega_2^m = -\frac{3\omega_0^m}{8} \left(1 + \frac{k_m^2}{k_\perp^2} \right) [\langle \overline{\varphi}_1^2 \rangle - \langle \overline{\varphi}_1 \rangle^2]. \quad (1.102)$$

Thus, for the regime $m \gg 1$ where the squeeze potential varies in z slowly compared to the mode wavelength, the frequency shift is always negative, and is second-order in the squeeze potential.

Mode damping at second order in ε

In Eq. (1.73) we observed that TG mode damping due to squeeze is exponentially small at first order in ε when the mode phase velocity is large. We must therefore work to second order in this regime. The second order dispersion relation is given by:

$$\begin{aligned}
&\mathbf{M}_0(\overline{\omega}_0^m).\mathbf{e}_2^m + \overline{\omega}_1^m \partial_{\overline{\omega}} \mathbf{M}_0(\overline{\omega}_0^m).\mathbf{e}_1^m \\
&+\overline{\omega}_2^m \partial_{\overline{\omega}} \mathbf{M}_0(\overline{\omega}_0^m).\mathbf{e}_0^m + \frac{(\overline{\omega}_1^m)^2}{2} \partial_{\overline{\omega}}^2 \mathbf{M}_0(\overline{\omega}_0^m).\mathbf{e}_0^m \\
&+\mathbf{M}_1(\overline{\omega}_0^m).\mathbf{e}_1^m + \overline{\omega}_1^m \partial_{\overline{\omega}} \mathbf{M}_1(\overline{\omega}_0^m).\mathbf{e}_0^m + \mathbf{M}_2(\overline{\omega}_0^m).\mathbf{e}_0^m = 0.
\end{aligned} \tag{1.103}$$

We take the product of $(\mathbf{e}_0^m)^T$ and Eq. (1.103). As a result, the product of the first and second term in Eq. (1.103) are zero and using Eq. (1.57) for $\mathbf{e}_0^m$ and Eq. (1.63) for $\mathbf{e}_1^m$ we have:

$$\begin{aligned}
&-\overline{\omega}_2^m \partial_{\overline{\omega}} M_0^{mm}(\overline{\omega}_0^m) \\
&= \frac{(\overline{\omega}_1^m)^2}{\overline{\omega} 2} \partial_{\overline{\omega}}^2 M_0^{mm}(\overline{\omega}_0^m) + \sum_{j \neq m} M_1^{mj}(\overline{\omega}_0^m).M_1^{jm}(\overline{\omega}_0^m)/M_0^{j,j}(\overline{\omega}_0^m) \\
&+\overline{\omega}_1^m \partial_{\overline{\omega}} M_1^{mm}(\overline{\omega}_0^m) + M_2^{mm}(\overline{\omega}_0^m).
\end{aligned} \tag{1.104}$$

Now we take the imaginary part of above equation assuming that $\overline{\omega}_{0r}^m \gg m$, which implies $\overline{\omega}_0^m \cong \overline{\omega}_{0r}^m, \overline{\omega}_1^m, M_0^{mm}(\overline{\omega}_{0r})$ and $M_1^{mm}(\overline{\omega}_{0r})$ are real. As a result:

$$\begin{aligned}
&-\overline{\gamma}_2^m \partial_{\overline{\omega}} \mathrm{Re} M_0^{mm}(\overline{\omega}_{0r}^m) = \mathrm{Im}\left[M_2^{mm}(\omega_{0r}^m)\right] \\
&+\mathrm{Im}\left[\sum_{j \neq m} M_1^{mj}(\overline{\omega}_{0r}^m) M_1^{jm}(\overline{\omega}_{0r}^m)/M_0^{jj}(\overline{\omega}_{0r}^m)\right].
\end{aligned} \tag{1.105}$$

From Eq. (B.21) the first term on the right hand side of Eq. (1.105), in the limit $\overline{\omega}_0^m \gg m$ is given by:

$$\mathrm{Im}M_2^{mm}(\overline{\omega}_{0r}^m) = \frac{16\pi}{\lambda_D^2 K_m^2 \sqrt{2\pi}} \sum_{n=1}^{\infty} \left(\frac{n}{\overline{\omega}_{0r}^m} \right)^3 e^{-(\overline{\omega}_{0r}^m)^2/2n^2} (\alpha_m^n)^2, \tag{1.106}$$

where α_m^n is defined in Eq. (1.62). Thus, solving for $\overline{\gamma}_2^m$ we obtain:

$$\begin{aligned} \overline{\gamma}_2^m &= -\frac{16m\pi \sum_{n>m}^{\infty} \left(\frac{n}{\overline{\omega}_{0r}^m} \right)^3 e^{-(\overline{\omega}_{0r}^m)^2/2n^2} (\alpha_m^n)^2}{\mathrm{P}\int_{-\infty}^{\infty} \frac{v e^{-v^2/2} dv}{(\overline{\omega}_{0r}^m/m - v)^2}} \\ &+ \frac{\mathrm{Im}\left[\sum_{j \neq m} M_1^{mj}(\overline{\omega}_{0r}^m) M_1^{jm}(\overline{\omega}_{0r}^m) / M_0^{jj}(\overline{\omega}_{0r}^m) \right]}{\partial_{\overline{\omega}} \mathrm{Re} M_0^{mm}(\overline{\omega}_{0r}^m)}. \end{aligned} \tag{1.107}$$

The first term on the right hand side is the contribution to the damping rate due to the mth unsqueezed mode (cosine in position space). Particles slow down as they pass the squeeze and, thus, no longer see this mode as a simple cosine along their bounce orbits, as a function of their angle variables (which is proportional to time). As a result, the mth unsqueezed mode has nonzero Fourier terms in angle variable space. Particles with bounce frequency $\omega_b = \omega/n$ will resonantly interact with the nth Fourier term and, thus, enhance the damping rate of the mode. The lower bound of the sum in the numerator is $n > m$, since all the terms for which $1 \leq n \leq m$ are exponentially small (assuming $\overline{\omega}_{0r}/m \gg 1$).

Moreover, in the presence of a squeeze the spatial form of the eigenmode is affected; see Fig. 1.1. Therefore, the shape of the mode potential is no longer a simple cosine in position space and consists of higher harmonics in z, which are all oscillating at the same frequency ω. The contribution to the damping rate given by the second term on the right hand side of Eq. (1.107), is due to the damping of these higher harmonics.

In Fig. (1.3) we compare the damping rate calculated from our computer simulations to the analytically calculated damping rates. Analytically calculated results, which are depicted as solid black curves, are evaluated from the sum of Eqs. (1.58), (1.72), (1.107), up to second order in ε. The computer simulation results are depicted with squares.

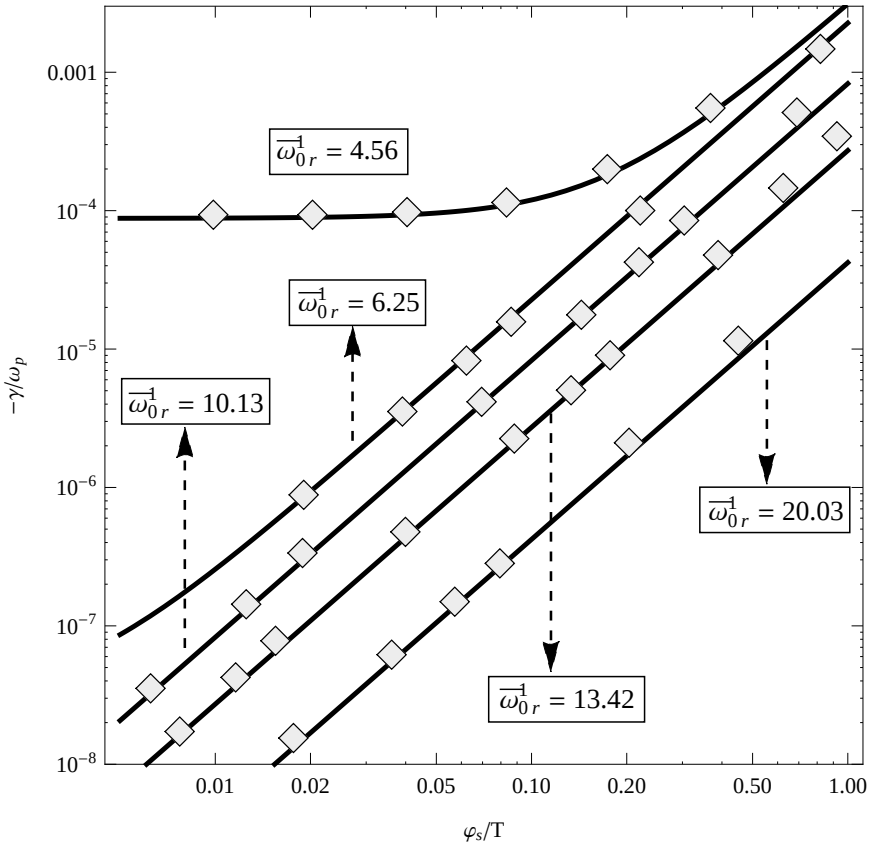

Figure 1.3: Mode damping rate vs. size of the squeeze potential φ_s/T, for phase velocities: $\omega/k_1 v_T = 4.56, 6.25, 10.13, 13.42$ and 20.03 for the mode $m = 1$. Analytically calculated damping rates are shown in solid black lines. Computer simulation results are shown with diamonds.

For the lowest value of $\overline{\omega}^1_{0r} = 4.56$, unsqueezed damping is large and becomes the dominant damping for values of $\varphi_s/T \lesssim 0.25$. However, for $\varphi_s/T \gtrsim 0.25$ squeeze damping with quadratic dependence on φ_s/T becomes larger than the unsqueezed damping rate. For $\overline{\omega}^1_{0r} = 6.25, 10.13, 13.42$ and 20.03, unsqueezed damping is exponentially small. Thus, mode damping is only due to the presence of the squeeze and the damping rate has a quadratic dependence on φ_s/T.

As the amplitude of the squeeze potential φ_s/T approaches 1, the computer simulation results deviate from the analytically calculated damping rates which has a quadratic dependence behavior on $\varphi^{\max}_{sq}$. This is due to the fact that for larger φ_s/T's, terms of order higher than $(\varphi_s/T)^2$ become significant and thus, these higher terms will be needed to more accurately evaluate the corrections to the eigenfrequencies and eigenmodes. Also, for larger φ_s/T's the population of particles trapped in the Debye shielded squeeze potential, which was not accounted for, becomes larger and resonant trapped particle-wave interactions can become significant and further enhance the mode damping rate.

Figure (1.4) depicts the damping rate of the squeezed $m = 1$ mode versus the Debye length. Solid curves are the analytically calculated results using the sum of Eqs. (1.58), (1.72) and (1.107), for squeeze potentials of value $\varphi^{\max}_{sq}/m_q L^2 \omega_p^2 = 8.75 \times 10^{-6}$ and $\varphi^{\max}_{sq}/m_q L^2 \omega_p^2 = 3.5 \times 10^{-5}$, which is 4 times larger than the former. The dashed line is the damping rate of the unsqueezed mode given by Eq. (1.58) and diamonds are the damping rates evaluated using computer simulations. For Debye lengths such that $\overline{\omega}^1_0 \ll 5$, where $\overline{\omega}^1_0 = \omega_r/k_1 v_T$, the two solid curves converge to the unsqueezed (dashed) curve. For Debye lengths for which $\overline{\omega}^1_0 \gtrsim 5$ the unsqueezed damping rate (dashed curve) goes to zero exponentially, whereas the squeezed damping rates (solid curves) are finite. There is an approximately 16 fold difference between the values of the damping rates (solid curves), for Debye lengths at which $\overline{\omega}^1_0 \gtrsim 5$. This shows the quadratic dependence on the applied squeeze potential expected for large $\overline{\omega}^1_0$'s.

At very low values of λ_D/L the damping rate again begins to fall off exponentially as T decreases further. This is because the Debye shielded squeeze potential φ_1 is a smooth function of position and thus, Fourier coefficients of the Debye

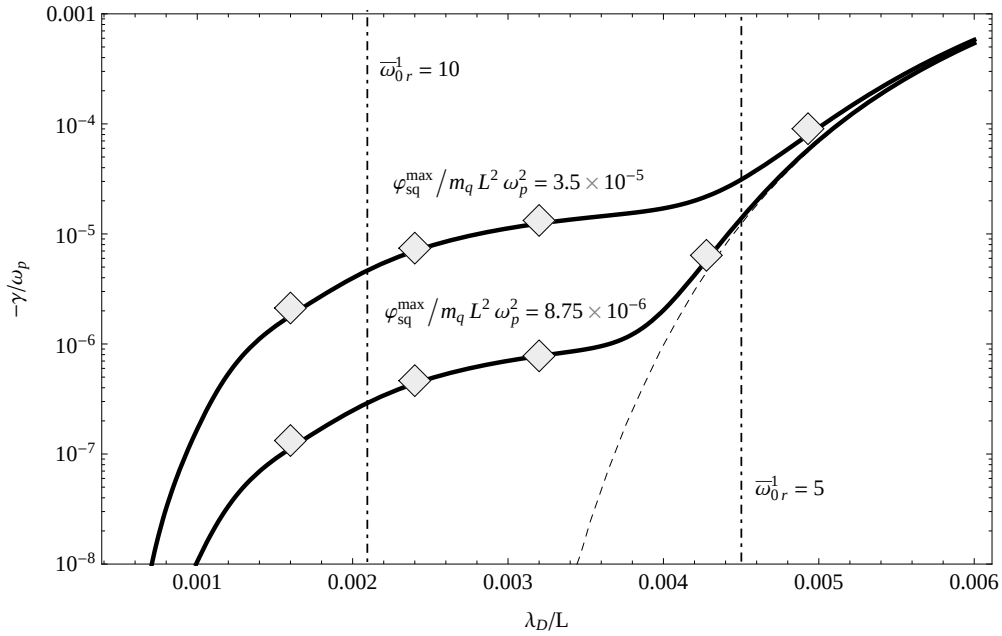

Figure 1.4: Damping rate $(-\gamma/\omega_p)$ of mode $m = 1$ versus Debye length (λ_D/L), depicted for constant squeeze potentials $\varphi_{sq}^{\max}/m_q L^2\omega_p^2 = 3.5\times10^{-5}$ (upper solid curve) and $\varphi_{sq}^{\max}/m_q L^2\omega_p^2 = 8.75\times10^{-6}$ (lower solid curve) in a plasma for which $k_\perp L = 15\pi$. The dashed curve depicts the unsqueezed Landau damping $(\varphi_{sq} = 0)$. The dash-dotted lines depict Debye lengths for which $\overline{\omega}_0^1 = 5$ and $\overline{\omega}_0^1 = 10$, where $\overline{\omega}_0^1 = \omega_r/k_1 v_T$.

shielded squeeze potential i.e. $\overline{\varphi}^1_n$, become exponentially small with growing n. [9] . In the small λ_D/L limit where $\overline{\omega}^1_{0r} \gg 1$, $n \gg 1$ bounce harmonics are necessary in order to satisfy the resonance condition $n\omega_b = \omega^1_{0r}$. The effect of these higher harmonics becomes exponentially small, since these terms depend on $\overline{\varphi}^1_n$'s with $n \gg 1$.

1.3 1D Vlasov-Poisson computer simulations

For our computer simulations we discretized the 2D phase-space (z, v_z) on a 2 dimensional grid (using the method of lines [36]). That is, the distribution is discretized as $f(z_j, v_k, t) = f_{j,k}(t)$ where

$$\begin{aligned} z_j &= j\Delta z - L/2, \qquad j = 0, 1, \ldots, M_z \\ v_k &= (k+1/2)\Delta v, \quad k = -M_v - 1, \ldots, M_v \end{aligned} \tag{1.108}$$

and where $\Delta z = L/M_z$, $\Delta v = V_{\max}/M_v$. The maximum velocity in the simulations is usually taken as $V_{\max} \simeq 8v_T$.

The condition of specular reflection at the plasma ends implies that

$$f(\pm L/2, v, t) = f(\pm L/2, -v, t), \tag{1.109}$$

which translates to the grid as the boundary conditions

$$\begin{aligned} f_{0,k}(t) &= f_{0,-k-1}(t) \\ f_{M_z,k}(t) &= f_{M_z,-k-1}(t). \end{aligned} \tag{1.110}$$

We finite-difference the spatial and velocity derivatives in Eq. (1.3) using the centered difference method, obtaining

$$\begin{aligned} &\frac{\partial}{\partial t} f_{j,k}(t) + v_k \frac{\mathrm{f}_{j+1,k}(t) - \mathrm{f}_{j-1,k}(t)}{2\Delta z} \\ &-\frac{1}{m_q}\left(\frac{\varphi_{j+1}(t) - \varphi_{j-1}(t)}{2\Delta z} + \frac{\partial}{\partial z}\varphi_{sq}(z)\right)\frac{\mathrm{f}_{j,k+1}(t) - \mathrm{f}_{j,k-1}(t)}{2\Delta v} = 0. \end{aligned} \tag{1.111}$$

Poisson's equation, Eq. (1.5), is also finite-differenced and solved at each time-step

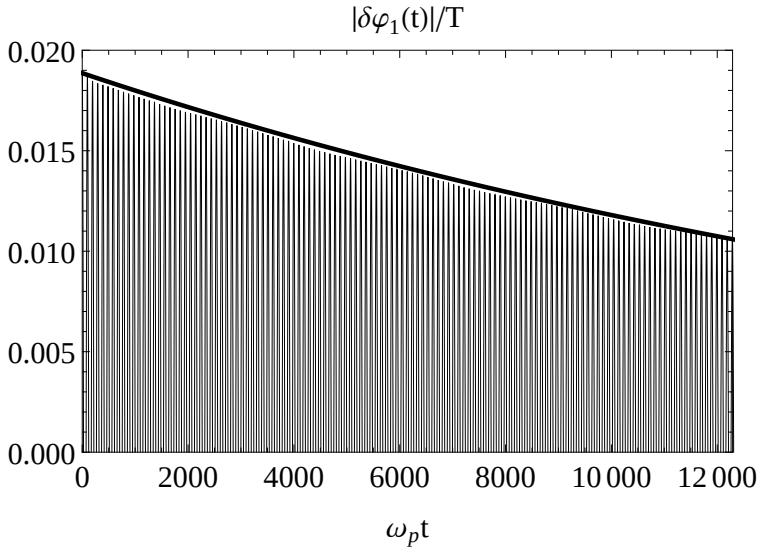

Figure 1.5: The $m_z = 1$ Fourier component $\delta\varphi_1(t)$ of the space-charge potential $\varphi_p(z,t)$ and the exponentially damping amplitude $g(t) = 0.0188\exp[-4.7\times 10^{-5}(\omega_p t)]$ (thick curve), obtained by fitting to $\delta\overline{\varphi}^1(t)$, as functions of time.

using the FFT method. [16]

Time is advanced using the fourth order Runge-Kutta integration and each time step requires four plasma force evaluations.

For simulation of a squeezed plasma, the initial velocity distribution of plasma was Maxwellian. The squeezed equilibrium distribution function was obtained by gradually (adiabatically) turning on the squeeze potential over a time of order of 100 wave periods, in order to avoid launching unwanted modes.

For the initial condition of the squeezed mode damping simulation run, we add a perturbation to the squeezed equilibrium distributions $F_0(z,v)$

$$\mathrm{f}(z,v;t=0) = F_0(z,v)(1+\delta\cos[k_1(z+L/2)]). \tag{1.112}$$

The difference between this initial perturbation from the exact $m = 1$ mode is of the order φ_s/T. The largest contribution to the squeezed mode potential comes from the Fourier term $\cos[k_1(z+L/2)]$. (There are other contributions because our simulation is nonlinear.) We extract the $m_z = 1$ Fourier component, $\delta\varphi_1(t)$, by integrating $\cos(k_z(z+L/2))\varphi_p(z,t)$ over z, where $\varphi_p(z,t)$ is the space charge poten-

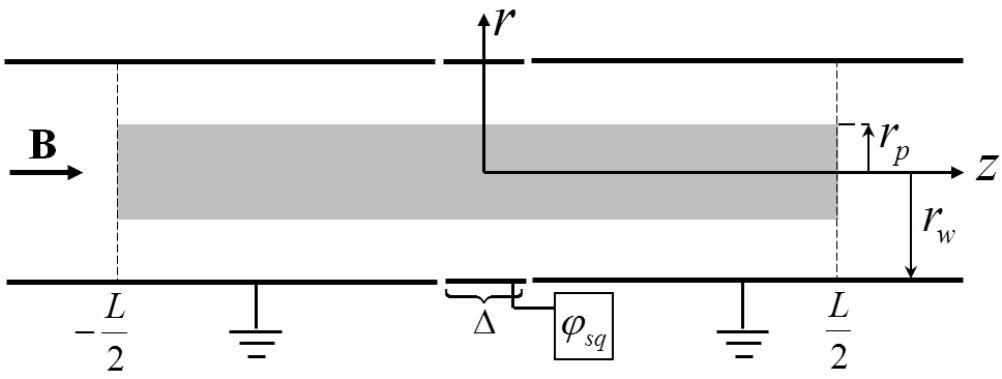

Figure 1.6: Schematic depiction of the trap geometry and squeeze potential φ_{sq} applied to a cylindrical sector of width Δ. Other parts of the trap wall are grounded. Particles are assumed to reflect at the axial ends $z = \pm L/2$.

tial. The damping rate γ and mode frequency ω are obtained by fitting the curve $\delta\varphi_1(t=0)e^{-\gamma t}\cos\omega t$ to $\delta\varphi_1(t)$. A typical result for $\delta\varphi_1(t)$ from our computer simulations is displayed in Fig. (1.5). The thick curve is the amplitude of the fitted function, which is exponentially decaying as a function of time.

1.4 Cylindrically symmetric, r and z dependent system

In order to make quantitative comparison between our theory and experimental results, we extend our 1D theory to a 2D system of axial(z) and radial(r) dependence. Figure 1.6 illustrates the confinement geometry for the rz system. The plasma is confined in a Malmberg-Penning trap consisting of a long conducting cylinder, axially divided into a number of sections. Radial confinement is provided by a strong uniform magnetic field **B** directed along the axis of cylinder. In this section we assume an azimuthally symmetric perfectly conducting cylinder with radius r_w and extending axially from $-L/2$ to $L/2$, with L large compared to r_w. The squeeze potential is applied to a cylindrical section, which is centered at the axial midpoint of the cylinder and has a width Δ. We neglect effects involving the Debye sheath at the plasma ends, and simplify by assuming flat ends on the plasma at $z = \pm L/2$. Particles, which are traveling the length of the plasma along the magnetic field lines, are assumed to reflect specularly from the ends, as in Sec. II. The

boundary conditions for the squeeze potential at the column ends are assumed for later convenience to be homogeneous Neumann conditions. Other homogeneous boundary conditions could have been used with negligible effect on our results, since the squeeze potential is applied at the axial center of a long column (see Fig. 1.6), so the squeeze potential is vanishingly small at the ends due to shielding by the plasma and the conducting walls. Neumann conditions simplify our expressions for the mode damping rate and frequency shift because the axial Fourier expansions for the mode potential and the squeeze potential then have a similar form.

The squeeze potential on the cylinder wall is taken to be

$$\begin{aligned} \varphi(r_w,z) &= 0 \quad -L/2<z<-\Delta/2 \quad \text{or} \quad \Delta/2<z<L/2, \\ \varphi(r_w,z) &= \varphi_{sq} \quad -\Delta/2\le z\le\Delta/2. \end{aligned} \tag{1.113}$$

For a vacuum cylinder we can calculate the potential inside the cylinder, with potential on the conducting walls of the trap given by Eq. (1.113). The vacuum potential φ_T satisfies the Laplace equation:

$$\nabla^2\varphi_T = 0. \tag{1.114}$$

Standard Fourier analysis implies a solution of the form

$$\varphi_T(r,z) = \sum_{n=0}^{\infty} A_{2n} I_0(k_{2n} r)\cos[k_{2n}(z+L/2)] \tag{1.115}$$

where the Fourier coefficients A_{2n} are

$$\begin{aligned} A_{2n} &= \frac{2\varphi_{sq}}{LI_0(k_{2n}r_w)}\int_{-\Delta/2}^{\Delta/2}\cos[k_{2n}(z+L/2)]dz \\ &= \frac{2\varphi_{sq}}{k_{2n}LI_0(k_{2n}r_w)}2\sin[k_{2n}\Delta/2]\cos[k_{2n}L/2], \end{aligned} \tag{1.116}$$

while for $n=0$ term we obtain

$$A_0 = \frac{\varphi_{sq}\Delta}{LI_0(0)}. \tag{1.117}$$

1.4.1 Plasma equilibrium: unsqueezed and squeezed solutions

We assume the equilibrium plasma is a thermal equilibrium described by the Boltzmann distribution

$$\mathrm{F}(\mathbf{r},\mathbf{v}) = \frac{N\exp\left[-(H_0+\omega_r p_\theta)/T\right]}{\int d\mathbf{r}d\mathbf{v}\exp\left[-(H_0+\omega_r p_\theta)/T\right]}, \tag{1.118}$$

where N is the total number of particles, ω_r is the plasma rotation frequency,

$$H_0 = \frac{m_q v^2}{2} + \varphi(\mathbf{r}), \tag{1.119}$$

and the potential $\varphi(\mathbf{r})$ is given by the sum of the vacuum potential $\varphi_T(\mathbf{r})$ and the potential due to plasma and its image on the conducting wall $\varphi_{pe}(\mathbf{r})$:

$$\varphi(\mathbf{r}) = \varphi_T(\mathbf{r}) + \varphi_{pe}(\mathbf{r}). \tag{1.120}$$

The canonical angular momentum is given by

$$p_\theta = m_q v_\theta r + \frac{qB}{2c} r^2. \tag{1.121}$$

Substituting from Eqs. (1.121) and (1.120) in Eq. (1.118) after performing some algebra we get:

$$\mathrm{F}_0(\mathbf{r},\mathbf{v}) = n(r,z)\left(\frac{m_q}{2\pi T}\right)^{3/2}\exp\left[-\frac{m_q}{2T}(\mathbf{v}+\omega_r\hat{\theta})^2\right], \tag{1.122}$$

where the density is given by:

$$n(r,z) = N\frac{\exp\left[-(\varphi_T+\varphi_{pe}+\varphi_c)/T\right]}{\int d\mathbf{r}\exp\left[-(\varphi_T+\varphi_{pe}+\varphi_c)/T\right]}, \tag{1.123}$$

and where $\varphi_c(r)$ is the radial confinement potential due to centrifugal force and magnetic field:

$$\varphi_c(r) = m_q\omega_r(\omega_c-\omega_r)r^2/2. \tag{1.124}$$

In order to calculate the space-charge potential φ_p, we must solve the Poisson equation:

$$\nabla^2\varphi_{pe}(r,z) \;=-\; 4\pi q^2 n(r,z), \tag{1.125}$$

with the boundary condition given by $\varphi_{pe}(r_w,z)=0$. We define the following dimensionless functions:

$$\begin{aligned}\chi(r,z) &= -\varphi_{pe}(r,z)/T, \\ \alpha(r) &= -\varphi_c(r)/T, \\ \beta(r,z) &= -\varphi_T(r,z)/T,\end{aligned} \tag{1.126}$$

and so rewrite Eq. (1.123) as:

$$n(r,z)=N\frac{\exp\left[\chi+\alpha+\beta\right]}{\int d\mathbf{r}\exp\left[\chi+\alpha+\beta\right]}. \tag{1.127}$$

We will use the following averages:

$$\langle\ldots\rangle_z=\int_0^{r_w}\int_{-L/2}^{L/2} dz(\ldots)/L, \tag{1.128}$$

$$\langle\ldots\rangle_r=\int_0^{r_w} 2\pi r\,dr(\ldots)/2\pi r_w^2, \tag{1.129}$$

$$\langle\ldots\rangle_{rz}=\langle\langle\ldots\rangle_r\rangle_z. \tag{1.130}$$

We may then rewrite the Poisson equation (1.125) as:

$$\nabla^2\chi(r,z)=\frac{4\pi q^2 N}{TV}\frac{\exp[\chi+\alpha+\beta]}{\left\langle\exp[\chi+\alpha+\beta]\right\rangle_{rz}}, \tag{1.131}$$

where $V=\pi r_w^2 L$. We expand the solution of Eq. (1.121) to first order in powers of the (scaled) squeeze potential $\beta(r,z)$, introducing the ordering parameter ε as in Sec. II and writing the scaled plasma potential as a sum of the unsqueezed and squeezed

terms,

$$\chi = \chi_0 + \varepsilon\chi_1 . \tag{1.132}$$

We then expand Eq. (1.131) to first order in ε,

$$\begin{aligned} \nabla^2\chi_0(r) + \varepsilon\nabla^2\chi_1(r,z) &= \frac{4\pi q^2 N}{TV}\frac{\exp[\chi_0+\varepsilon\chi_1+\alpha+\varepsilon\beta]}{\left\langle \exp[\chi_0+\varepsilon\chi_1+\alpha+\varepsilon\beta]\right\rangle_{rz}} \\ &\approx \frac{4\pi q^2 N}{TV}\frac{e^{\chi_0+\alpha}}{\left\langle e^{\chi_0+\alpha}\right\rangle_r}\left(1+\varepsilon\chi_1+\varepsilon\beta-\frac{\varepsilon\left\langle(\chi_1+\beta)e^{\chi_0+\alpha}\right\rangle_{rz}}{\left\langle e^{\chi_0+\alpha}\right\rangle_r}\right). \end{aligned} \tag{1.133}$$

Collecting powers of ε implies

$$\nabla^2\chi_0(r) = \frac{4\pi q^2 N}{TV}\frac{e^{\chi_0+\alpha}}{\left\langle e^{\chi_0+\alpha}\right\rangle_r} \tag{1.134}$$

$$\nabla^2\chi_1(r,z) = \frac{4\pi q^2 N}{TV}\frac{e^{\chi_0+\alpha}}{\left\langle e^{\chi_0+\alpha}\right\rangle_r}\left(\chi_1+\beta-\frac{\left\langle(\chi_1+\beta)e^{\chi_0+\alpha}\right\rangle_{rz}}{\left\langle e^{\chi_0+\alpha}\right\rangle_r}\right). \tag{1.135}$$

Solving Eq. (1.134), we obtain the unsqueezed space-charge potential inside the plasma, $\chi_0(r)$. Equation (1.135) provides $\chi_1(r,z)$, the Debye-shielding response to the squeeze potential $\beta(r,z)$, similar to Eq. (1.9).

Unsqueezed equilibrium

The unsqueezed potential and density of a thermal equilibrium plasma was discussed in Ref. 18. The equilibrium Poisson equation (1.125) can be expressed as

$$\left(\frac{1}{\rho}\frac{\partial}{\partial\rho}\rho\frac{\partial}{\partial\rho}\right)\zeta = \exp(\zeta)-\gamma-1, \tag{1.136}$$

where we defined the parameter γ and function ζ as:

$$\gamma = 4\frac{\omega_r}{\omega_p^2}(\omega_c-\omega_r)-1, \tag{1.137}$$

$$\zeta(\rho) = \chi_0(\rho)-\chi_0(0)+\alpha(\rho), \tag{1.138}$$

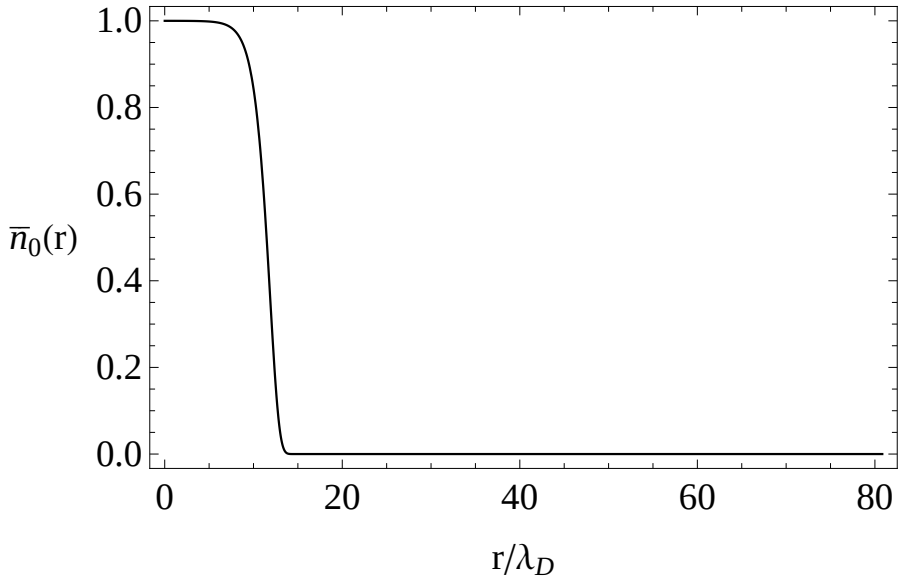

Figure 1.7: Plot of the equilibrium density for a plasma with $T = 50$meV, $L = 10\text{cm}(L/\lambda_D = 282.6)$, $\omega_p = 1.263 \times 10^6$Rad/s, $r_p \approx 0.42$cm $(r_p/\lambda_D \approx 11.87)$, $r_w = 2.86\text{cm}(r_w/\lambda_D = 80.83)$. Maximum density of the plasma at $r = 0$ is normalized to 1.

$\omega_p^2 = 4\pi e^2 n_0(0)/m$, $\rho = r/\lambda_D$, $\lambda_D = v_T/\omega_p$, and the density $n_0(r)$ is

$$n_0(r) = \frac{N}{V}\frac{e^{\chi_{0+\alpha}}}{\langle e^{\chi_{0+\alpha}}\rangle_r}. \tag{1.139}$$

Equation (1.136) is solved with boundary conditions:

$$\zeta(0) = 0, \quad \partial_\rho \zeta|_{\rho=0} \;\; = \;\; 0. \tag{1.140}$$

The first boundary condition follows from Eq. (1.138). We can choose $\chi_0(0)$ so that the boundary condition $\chi_0(r_w) = 0$ is also satisfied. For a plasma with small Debye length compared to plasma radius the plasma density and the potential inside the plasma are constant up to the vicinity of plasma radius where the density drops to zero in a distance of the order of λ_D. We define the plasma radius r_p as the radius where the density falls to $1/e$ of its value at the origin [18]. Figure (1.7) shows an example for an unsqueezed equilibrium, which is obtained from numerically solving Eq. (1.136) with boundary conditions (1.140).

Squeezed equilibrium: a perturbative solution

We rewrite Eq. (1.135) as:

$$\left(\frac{1}{\rho}\frac{\partial}{\partial\rho}\rho\frac{\partial}{\partial\rho}+\frac{\partial^2}{\partial\xi^2}\right)\chi_1(\rho,\xi)=\overline{n}_0(\rho)\left(\chi_1+\beta-\frac{\left\langle\overline{n}_0(\rho)(\chi_1+\beta)\right\rangle_{rz}}{\left\langle\overline{n}_0(\rho)\right\rangle_r}\right), \qquad (1.141)$$

where $\overline{n}_0(\rho)=n_0(\rho)/n_0(0)$ is the scaled unsqueezed density profile, and $\xi=z/\lambda_D$. We will solve for $\chi_1(\rho,\xi)$ using the Galerkin method, as in Sec. I. From Eqs. (1.115) and (1.126) we write β as:

$$\beta(\rho,\xi) = \sum_{n=1}^{\infty}R_n(\rho)\cos[\kappa_{2n}(\xi+\tfrac{\Lambda}{2})], \qquad (1.142)$$

$$R_n(\rho) = -\frac{\varphi_{sq}}{T}\frac{I_0(\kappa_{2n}\rho)}{I_0(\kappa_{2n}\rho_w)}\frac{2(-1)^n}{n\pi}\sin[k_{2n}\Delta/2], \qquad (1.143)$$

where $\rho_w=r_w/\lambda_D$, $\Lambda=L/\lambda_D$, $\kappa_n=\lambda_D k_n$, and we neglect the $n=0$ term in β as the constant term does not affect the solution. We expand χ_1 using a complete series representation in ρ and ξ as follows:

$$\chi_1(\rho,\xi)=\sum_{m=1}^{\infty}\sum_{n=1}^{\infty}A_{mn}\mathrm{J}_0(\tfrac{x_m}{\rho_w}\rho)\cos[\kappa_n(\xi+\tfrac{\Lambda}{2})], \qquad (1.144)$$

where x_m is the m'th zero of J_0. Substituting from Eqs. (1.144) and (1.142) in Eq. (1.141), multiplying by $\cos[\kappa_{2l}(\xi+\Lambda/2)]$ and integrating from $-\Lambda/2$ to $\Lambda/2$ yields

$$\sum_{m=1}^{\infty}A_{m,2l}\left[-\left(\frac{x_m}{\rho_w}\right)^2-\kappa_{2l}^2-\overline{n}_0(\rho)\right]\mathrm{J}_0(\tfrac{x_m}{\rho_w}\rho)=\overline{n}_0(\rho)R_l(\rho). \qquad (1.145)$$

Now we multiply both sides by $\rho\mathrm{J}_0(x_n\rho/\rho_w)$ and integrate from 0 to ρ_w to get:

$$\begin{aligned}&\left[\left(\frac{x_n}{\rho_w}\right)^2+\kappa_{2l}^2\right]\frac{\rho_w^2}{2}\mathrm{J}_1^2(x_n)A_{n,2l}+\sum_m A_{m,2l}\int_0^{\rho_w}\overline{n}_0(\rho)\mathrm{J}_0(\tfrac{x_n}{\rho_w}\rho)\mathrm{J}_0(\tfrac{x_m}{\rho_w}\rho)\rho\,d\rho\\ = &-\int_0^{\rho_w}\overline{n}_0(\rho)R_l(\rho)\mathrm{J}_0(\tfrac{x_n}{\rho_w}\rho)\rho\,d\rho. \qquad (1.146)\end{aligned}$$

This relation can be written in the form of a matrix equation for each axial Fourier

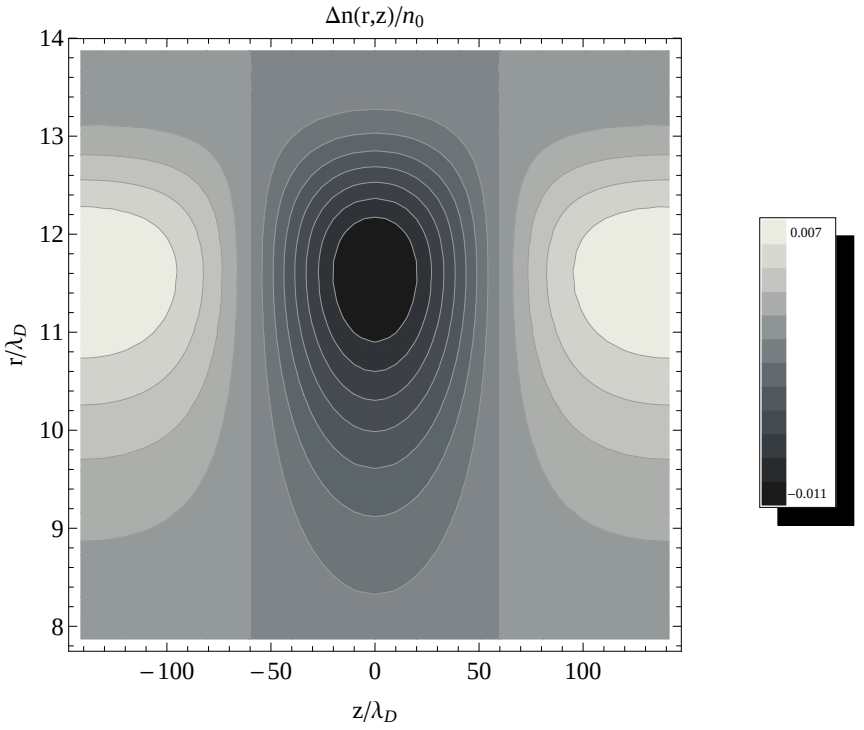

Figure 1.8: Contour plot of the difference between the squeezed equilibrium density and the unsqueezed equilibrium density (the latter is the same as Fig. 1.7) as a function of the radial and axial positions for a plasma, for a squeeze with $\Delta = 2.86$cm and $\varphi_{sq} = 0.1$eV.

number l:

$$\mathbf{N}_l.\mathbf{A}_l = \mathbf{B}_l, \tag{1.147}$$

where:

$$\begin{aligned}
(\mathbf{A}_l)_n &= A_{n,2l}, && (1.148)\\
(\mathbf{B}_l)_n &= -\int_0^{\rho_w} \overline{n}_0(\rho) R_l(\rho) \mathrm{J}_0(\tfrac{x_n}{\rho_w}\rho)\rho\, d\rho, && (1.149)\\
(\mathbf{N}_l)_{n,m} &= \left[\left(\frac{x_n}{\rho_w}\right)^2 + \kappa_{2l}^2\right]\frac{\rho_w^2}{2}\mathrm{J}_1^2(x_n)\delta_{nm} \\
&\quad + \int_0^{\rho_w} \overline{n}_0(\rho)\mathrm{J}_0(\tfrac{x_n}{\rho_w}\rho)\mathrm{J}_0(\tfrac{x_m}{\rho_w}\rho)\rho\, d\rho. && (1.150)
\end{aligned}$$

The solution for $A_{n,2l}$'s is given by:

$$\mathbf{A}_l = (\mathbf{N}_l)^{-1}.\mathbf{B}_l. \tag{1.151}$$

Figure (1.8) is the contour plot of the difference between the squeezed equilibrium density and the unsqueezed equilibrium density as a function of the radial and axial positions for a plasma of $T = 50$meV, $L = 10\text{cm}(L/\lambda_D = 282.6)$, $\omega_p = 1.263 \times 10^6$Rad/s, $r_p \approx 0.42$cm $(r_p/\lambda_D \approx 11.87)$, $r_w = 2.86\text{cm}(r_w/\lambda_D = 80.83)$, for a squeeze with $\Delta = 2.86$cm and $\varphi_{sq} = 0.1$eV. The horizontal range of the plot shows the whole length of the plasma, whereas the vertical (radial) range of the plot covers the vicinity of the plasma surface, since the change in the density due to squeeze potential is maximum close to the surface of plasma and goes exponentially to zero radially, from the surface towards the axis of plasma ($r = 0$). To obtain this solution 200 radial (Bessel) terms and 13 axial Fourier terms were used.

1.4.2 Squeezed linear modes

We now obtain the linear TG modes of the squeezed equilibrium. The method is similar to that used for 1D case, the difference being that there is now radial dependence. The linearized Vlasov equation in the presence of the squeeze is given

by

$$\partial_t \delta \mathrm{f} + v\partial_z \delta \mathrm{f} - \partial_z(\varphi_0 + \varepsilon\varphi_1)/m_q \partial_v \delta \mathrm{f} - \partial_z \delta\varphi/m_q \partial_v \mathrm{F}_0 = 0. \tag{1.152}$$

Here, φ_0 is the unsqueezed equilibrium potential which is the sum of the centrifugal potential and the unsqueezed space-charge potential of the plasma, and φ_1 is the Debye shielded squeeze potential:

$$\varphi_0(r) = -T[\chi_0(r) - \chi_0(0) + \alpha(r)], \tag{1.153}$$

$$\varphi_1(r,z) = -T[\chi_1(r,z) + \beta(r,z)]. \tag{1.154}$$

where α, β, χ_0 and χ_1 were obtained in the last section. The squeezed thermal equilibrium distribution $\mathrm{F}_0(r,z,v)$ is given by Eq. (1.122). Using Eqs. (1.126), (1.131), (1.153) and (1.154) we can write $\mathrm{F}_0(r,z,v)$ as:

$$\mathrm{F}_0(r,z,v) = n_0(0)\left(\frac{m_q}{2\pi T}\right)^{1/2} \frac{\overline{n}_0(r) e^{-\varepsilon\varphi_1/T}}{\langle \overline{n}_0(r) e^{-\varepsilon\varphi_1/T}\rangle_{rz} / \langle \overline{n}_0(r)\rangle_r} \exp\left[-\frac{m_q v^2}{2T}\right], \tag{1.155}$$

where $n_0(0)$ is the unsqueezed density at $r = 0$ and $\overline{n}_0(r) = e^{-\varphi_0(r)/T}$ is the unsqueezed density profile normalized by its maximum value, $n_0(0)$.

As in Sec. II we solve Eq. (1.152) as an expansion in ε, i.e. assuming the height of the Debye shielded squeeze potential is small compared to temperature: $[\varphi_1(r,0) - \varphi_1(r,L/2)]/T \ll 1$. We define the scaled potential function $\overline{\varphi}_1$ and the scaled energy variable u as:

$$\overline{\varphi}_1(r,z) = [\varphi_1(r,z) - \varphi_1(r,L/2)]/T \tag{1.156}$$

$$u = m_q v^2/2T + \varepsilon\overline{\varphi}_1(r,z) \tag{1.157}$$

The reason we defined the function $\overline{\varphi}_1$ is that the bounce frequency and action of an unperturbed orbit of a particle at a radius r are functionals of the difference of the Debye shielded squeeze potential from its absolute minimum at that radius, which is defined by $\overline{\varphi}_1$. At a given radius r inside the plasma, trapped particles and passing particles have scaled energy u such that $0 < u < \varepsilon\overline{\varphi}_1(r,z)$ and $u > \varepsilon\overline{\varphi}_1(r,z)$ respec-

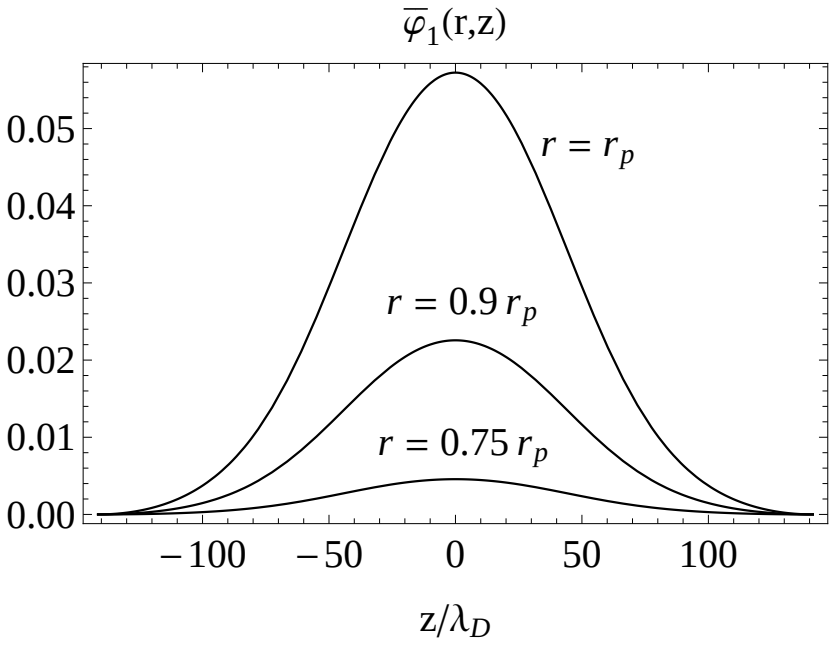

Figure 1.9: Plot of the scaled Debye shielded squeeze potential $\overline{\varphi}_1(r,z)$ as a function of the axial position, at radii $r = r_p, 0.9r_p$ and $0.75r_p$, for a plasma with the same parameters as Fig. 1.7

tively. Figure (1.9) shows the Debye shielded, scaled squeeze potential $\overline{\varphi}_1(r,z)$, as a function of z, for radii $r = r_p$, $r = 0.9r_p$ and $r = 0.75r_p$, for the same parameters as Figs. 1.7 and 1.8. This shows the squeeze potential height dropping exponentially from the plasma surface towards the inner plasma.

The distribution F_0 can be rewritten in terms of u as

$$F_0(r,z,u) = n_0(0)\left(\frac{m_q}{2\pi T}\right)^{1/2} \frac{\overline{n}_0(r)e^{-\varepsilon\varphi_1(r,L/2)/T}}{\langle \overline{n}_0(r)e^{-\varepsilon\varphi_1(r,z)/T}\rangle_{rz} / \langle \overline{n}_0(r)\rangle_r} e^{-u}. \tag{1.158}$$

In order to solve Eq. (1.142) we again introduce action-angle variables for axial particle motion in the equilibrium potential,

$$I(r,u;\varepsilon) = \frac{1}{2\pi}\oint p_z\,dz = \frac{m_q v_T}{2\pi}\oint \sqrt{2[u-\varepsilon\overline{\varphi}_1(r,z)]}\,dz, \tag{1.159}$$

$$\psi(r,z,u;\varepsilon) = \omega_b \int_{z0}^{z} \frac{dz'}{v(r,z',u;\varepsilon)}, \tag{1.160}$$

$$\tau(r,u;\varepsilon)=\frac{2\pi}{\omega_b}=\oint\frac{dz}{v_T\sqrt{2[u-\varepsilon\overline{\varphi}_1(r,z)]}} \tag{1.161}$$

As in Sec. II, the angle variable $\psi(r,z,u;\varepsilon)$ can be shown to have the functional form $\psi=\psi(r,z,\varepsilon/u)$:

$$\begin{aligned}\psi &= \frac{2\pi}{\oint\frac{dz'}{\sqrt{1-\varepsilon\overline{\varphi}_1(r,z')/u}}}\int_{z0}^{z}\frac{dz'}{\sqrt{1-\varepsilon\overline{\varphi}_1(r,z')/u}},\\ &= \psi(r,z,\varepsilon/u),\end{aligned} \tag{1.162}$$

and this equation can be inverted to yield the position versus the angle variable:

$$z=z(r,\psi,\varepsilon/u), \tag{1.163}$$

where z is a periodic function of ψ . We can now write the Vlasov equation in terms of (r,ψ,I) as:

$$\partial_t\delta\mathrm{f}+\omega_b\partial_\psi\mathrm{f}-\partial_\psi\delta\varphi\partial_I\mathrm{F}_0=0. \tag{1.164}$$

We expand the mode potential in a complete series in r and z, using the same Neumann conditions at the plasma ends as in Sec. IIB, assuming $\omega << \omega_p$ [see Eq. (1.31)]:

$$\delta\varphi(r,z,t)=\sum_{l=1}\sum_{m=1}(\delta\phi_{lm}e^{-i\omega t}+\delta\phi^*_{lm}e^{i\omega t})\mathrm{J}_0(\tfrac{x_l}{r_w}r)\cos[k_m(z+L/2)]. \tag{1.165}$$

A particle at radius r and action $I(r,u;\varepsilon)$ follows an unperturbed orbit which is periodic in angle variable ψ. Therefore we can write:

$$\cos[k_m(z(r,\psi,u/\varepsilon)+L/2)]=\sum_{n=-\infty}^{\infty}C_m^n(r,\varepsilon/u)e^{in\psi} \tag{1.166}$$

where the Fourier connection coefficients C_m^n are again given by Eq. (1.26), but are

now functions of r through the action-angle transformation:

$$C_m^n(r,\varepsilon/u)=\int_0^{2\pi}\frac{d\psi}{2\pi}\cos[k_m(z(r,\psi,u/\varepsilon)+L/2)]e^{-in\psi} \tag{1.167}$$

Using Eq. (1.166) we can write Eq. (1.165) as:

$$\delta\varphi(r;\psi,\varepsilon/u)=\sum_{l=1}\sum_{m=1}(\delta\phi_{lm}e^{-i\omega t}+\delta\phi_{lm}^{*}e^{i\omega t})\mathrm{J}_0(\tfrac{x_l}{r_w}r)\sum_{n=-\infty}^{\infty}C_m^n(r,\varepsilon/u)e^{in\psi} \tag{1.168}$$

As in Sec. II, δf and $\delta\varphi$ can be written in terms of Fourier series as:

$$\delta\mathrm{f}(r,\psi,\varepsilon/u)=\sum_{n=-\infty}^{\infty}\delta f_n(r,\varepsilon/u)\exp[i(n\psi-\omega t)]+c.c. \tag{1.169}$$

$$\delta\varphi(r,\psi,\varepsilon/u)=\sum_{n=-\infty}^{\infty}\delta\varphi_n(r,\varepsilon/u)\exp[i(n\psi-\omega t)]+c.c. \tag{1.170}$$

but $\delta\varphi_n(r,\varepsilon/u)$ now has an auxiliary radial expansion in terms of Bessel functions,

$$\delta\varphi_n(r,\varepsilon/u)=\sum_{l=1}\sum_{m=1}\delta\phi_{lm}C_m^n(r,\varepsilon/u)\mathrm{J}_0(\tfrac{x_l}{r_w}r). \tag{1.171}$$

Substituting Eq. (1.169) in Eq. (1.164) we obtain

$$-\omega\delta f_n+n\omega_b\delta f_n+n\omega_b\delta\varphi_n\mathrm{F}_0/T=0, \tag{1.172}$$

where we used $\partial_I\mathrm{F}_0=(du/dI)\partial_u\mathrm{F}_0=-\frac{\omega_b}{T}\mathrm{F}_0$. Solving for δf_n yields

$$\delta f_n(r,\varepsilon/u)=\frac{\omega_b\delta\varphi_n\mathrm{F}_0/T}{\omega/n-\omega_b}. \tag{1.173}$$

The mode potential and mode distribution function satisfy the linearized Poisson equation:

$$\left(\frac{1}{r}\partial_r r\partial_r+\partial_z^2\right)\delta\varphi=-4\pi q^2\int_{-\infty}^{\infty}\delta\mathrm{f}dv. \tag{1.174}$$

Substituting Eq. (1.165) in Eq. (1.174), multiplying both sides by $2\cos[k_{\overline{m}}(z+L/2)]/L$

and integrating over z from $-L/2$ to $L/2$ yields

$$\sum_{l=1}\delta\phi_{l\overline{m}}\left[\left(\frac{x_l}{r_w}\right)^2+k_{\overline{m}}^2\right]\mathrm{J}_0(\tfrac{x_l}{r_w}r)e^{-i\omega t} \tag{1.175}$$
$$=4\pi q^2\frac{2}{L}\int_{-\infty}^{\infty}\int_{-L/2}^{L/2}\delta\mathrm{f}\cos[k_{\overline{m}}(z+L/2)]dz\,dv.$$

As in Sec. II, we can use the canonical variables (ψ, I) instead of (z, v), since $dz\,dp_z = d\psi\,dI = (T/\omega_b)du\,d\psi$. Applying Eq. (1.169),Eq. (1.173) and Eq. (1.171) to Eq. (1.175) we obtain:

$$\sum_{l=1}\delta\phi_{l\overline{m}}\left[\left(\frac{x_l}{r_w}\right)^2+k_{\overline{m}}^2\right]\mathrm{J}_0(\tfrac{x_l}{r_w}r) \tag{1.176}$$
$$=\frac{4\pi q^2}{L}\sum_{l=1}\sum_{m=1}\delta\phi_{lm}\mathrm{J}_0(\tfrac{x_l}{r_w}r)\sum_{n=-\infty}^{\infty}\int_0^{\infty}C_m^n(r,\varepsilon/u)C_{\overline{m}}^{-n}(r,\varepsilon/u)\frac{\mathrm{F}_0}{\omega/n-\omega_b}du.$$

Now we multiply both sides by $r\mathrm{J}_0(\frac{x_{\overline{l}}}{r_w}r)$ and integrate from 0 to r_w. The result is:

$$\delta\phi_{\overline{l}\overline{m}} = \tag{1.177}$$
$$\sum_{l=1}\sum_{m=1}\delta\phi_{lm}\frac{\frac{4\pi q^2}{L}\int_0^{r_w}r\mathrm{J}_0(\frac{x_l}{r_w}r)\mathrm{J}_0(\frac{x_{\overline{l}}}{r_w}r)\sum_{n=-\infty}^{\infty}\int_0^{\infty}C_m^n(r,\varepsilon/u)C_{\overline{m}}^{-n}(r,\varepsilon/u)\frac{\mathrm{F}_0}{\omega/n-\omega_b}du\,dr}{\left[\left(\frac{x_{\overline{l}}}{r_w}\right)^2+k_{\overline{m}}^2\right]\frac{r_w^2}{2}\mathrm{J}_1^2(x_{\overline{l}})}.$$

Equation (1.177) is in the form of a tensor eigenvalue equation:

$$M^{\overline{l}l\overline{m}m}\delta\phi_{lm}=0, \tag{1.178}$$

where

$$M^{\overline{l}l\overline{m}m}=\delta_{\overline{l}l}\delta_{\overline{m}m} \tag{1.179}$$
$$-\frac{\frac{4\pi q^2}{L}\int_0^{r_w}r\mathrm{J}_0(\frac{x_l}{r_w}r)\mathrm{J}_0(\frac{x_{\overline{l}}}{r_w}r)\sum_{n=-\infty}^{\infty}\int_0^{\infty}C_m^n(r,\varepsilon/u)C_{\overline{m}}^{-n}(r,\varepsilon/u)\frac{\mathrm{F}_0}{\omega/n-\omega_b}du\,dr}{\left[\left(\frac{x_{\overline{l}}}{r_w}\right)^2+k_{\overline{m}}^2\right]\frac{r_w^2}{2}\mathrm{J}_1^2(x_{\overline{l}})}.$$

Since we assumed the squeeze to be symmetric with respect to the cylinder we have $C_m^n = C_m^{-n}$. Moreover, we assume the trapped particle population is negligible compared to passing particles, therefore we set the lower limit of the integral on u in

Eq. (1.177) to be the height of the Debye shielded squeeze potential at radius r i.e. $\varepsilon\overline{\varphi}_1(r,0)$. Introducing the scaled bounce frequency $\overline{\omega}_b(r,u)=\omega_b/k_1 v_T$ and using Eq. (1.158) for the thermal equilibrium distribution F_0, we rewrite Eq. (1.179) as

$$M^{\bar{l}l\bar{m}m}=\delta_{\bar{l}l}\delta_{\bar{m}m} \tag{1.180}$$
$$-\frac{\frac{8}{\sqrt{2\pi}\lambda_D^2}\int_0^{r_w} r\,dr\,\mathrm{J}_0(\frac{x_l}{r_w}r)\mathrm{J}_0(\frac{x_{\bar{l}}}{r_w}r)\overline{n}_0(r)e^{-\varepsilon\varphi_1(r,L/2)/T}\sum_{n=1}^{\infty}\int_{\varepsilon\overline{\varphi}_1(r,0)}^{\infty}du\,\frac{\overline{\omega}_b e^{-u}}{(\overline{\omega}/n)^2-\overline{\omega}_b^2}C_m^n(r,\frac{\varepsilon}{u})C_{\overline{m}}^n(r,\frac{\varepsilon}{u})}{\left\langle\frac{\overline{n}_0(r)}{\langle\overline{n}_0(r)\rangle_r}e^{-\varepsilon\varphi_1(r,z)/T}\right\rangle_{rz}\left[\left(\frac{x_{\bar{l}}}{r_w}\right)^2+k_{\overline{m}}^2\right]\frac{r_w^2}{2}\mathrm{J}_1^2(x_{\bar{l}})}.$$

where $\overline{\omega}=\overline{\omega}_r+i\overline{\gamma}$ is the complex eigenfrequency ω scaled to $k_1 v_T$.

1.4.3 Perturbation method

Just as for Sec. I, the linear dispersion relation (1.178) can be writen in matrix form:

$$\mathbf{M}(\overline{\omega}).\mathbf{e}=0, \tag{1.181}$$

where $\mathbf{e}$ is an eigenvector of the nullspace of $\mathbf{M}$ defined as:

$$(\mathbf{e})^{lm}=\delta\phi_{lm} \tag{1.182}$$

and $(\mathbf{M})^{\bar{l}l\bar{m}m}=M^{\bar{l}l\bar{m}m}$ [see Eq. (1.179)].

We again expand the matrix $\mathbf{M}$, the eigenfrequency $\overline{\omega}$ and eigenvector $\mathbf{e}$ in ε as in Eqs. (1.48)-(1.50). The resulting matrices $\mathbf{M}_0$, $\mathbf{M}_1$ and $\mathbf{M}_2$ are derived in Appendix C. For example, the zeroeth-order (unsqueezed) matrix has components

$$M_0^{\bar{l}l\bar{m}m}=\delta_{\bar{m}m}\left(\delta_{\bar{l}l}+2\mathrm{W}(\overline{\omega}/m)\frac{\int_0^{r_w} r\,dr\,\overline{n}(r)\mathrm{J}_0(x_l r/r_w)\mathrm{J}_0(x_l r/r_w)}{\lambda_D^2[x_l^2+k_m^2 r_w^2]\mathrm{J}_1^2(x_l)}\right). \tag{1.183}$$

Zeroth order in ε

The zeroth order dispersion relation for an unsqueezed plasma column is satisfied by mode $\mu=(n_r,m)$, where n_r and m are the radial and the axial mode

numbers respectively. The dispersion relation is given by

$$\mathbf{M}_0(\overline{\omega}_0^\mu)\cdot\mathbf{e}_0^\mu = 0\,, \tag{1.184}$$

From Eq. (1.184) and Eq. (1.183) we obtain the unsqueezed eigenvector ($\mathbf{e}_0^\mu$) and eigenfrequency $\overline{\omega}_0^\mu$. We can write Eq. (1.184) explicitly as:

$$(\mathbf{e}_0^\mu)^{\bar{l}m} = -\sum_{l'=1}^{\infty}(\mathbf{e}_0^\mu)^{l'm}\mathrm{W}(\overline{\omega}_0^\mu/m)\frac{\int_0^{r_w} r\,dr\,\mathrm{J}_0(\frac{x_{l'}}{r_w}r)\mathrm{J}_0(\frac{x_{\bar{l}}}{r_w}r)\overline{n}_0(r)}{\lambda_D^2\left[\left(\frac{x_{\bar{l}}}{r_w}\right)^2+k_m^2\right]\frac{r_w^2}{2}\mathrm{J}_1^2(x_{\bar{l}})}. \tag{1.185}$$

This equation is only dependent on a single axial Fourier index m, while there is coupling between radial Bessel indices related to l' and $\bar{l}$. In other words eigenmode $\mu=(n_r,m)$ is proportional to a single cosine function $\cos[k_m(z+L/2)]$ and a series in Bessel $\mathrm{J}_0(\frac{x_{l'}}{r_w}r)$'s with $l'=1,2,\ldots$:

$$\delta\phi_0^\mu(r,z) = |\delta\phi^\mu|\mathrm{R}_\mu(r)\cos[k_m(z+L/2)] \tag{1.186}$$

where

$$\mathrm{R}_\mu(r) = \sum_{l'=1}^{\infty}\frac{(\mathbf{e}_0^\mu)^{l'm}}{|\delta\phi^\mu|}\mathrm{J}_0(\tfrac{x_{l'}}{r_w}r) \tag{1.187}$$

Here, $|\delta\phi^\mu|$ is the arbitrary linear mode amplitude and $\mathrm{R}_\mu(r)$ are normalized so that $\mathrm{R}_\mu(0)=1$. Eigenfrequencies $\overline{\omega}_0^\mu$ and the radial dependence of the unsqueezed eigenmodes ($(\mathbf{e}_0^\mu)^{l'm}$'s) are obtained by solving Eq. (1.185) as follows. We can rewrite the dispersion relation (1.185) as:

$$\begin{aligned}
&-(\mathrm{W}(\overline{\omega}_0^\mu/m))^{-1}\mathrm{I}.(\mathbf{e}_0^\mu)^m = Q_{mm}.(\mathbf{e}_0^\mu)^m,\\
&(Q_{mm})_{\bar{l}l'} = \frac{\int_0^{r_w} r\,dr\,\mathrm{J}_0(\frac{x_l'}{r_w}r)\mathrm{J}_0(\frac{x_{\bar{l}}}{r_w}r)\overline{n}_0(r)}{\lambda_D^2\left[\left(\frac{x_{\bar{l}}}{r_w}\right)^2+k_m^2\right]\frac{r_w^2}{2}\mathrm{J}_1^2(x_{\bar{l}})},
\end{aligned} \tag{1.188}$$

where I is the unit matrix. Thus, eigenvectors of the matrix Q_{mm} also satisfy the dispersion relation in Eq. (1.185). From the eigenvalue λ_μ of matrix Q_{mm} we obtain

the related eigenfrequency $\overline{\omega}_0^\mu$ via inversion:

$$\overline{\omega}_0^\mu = m\mathrm{W}^{-1}(-\lambda_\mu^{-1}), \tag{1.189}$$

where W^{-1} is the inverse of the function W.

An alternative description of unsqueezed modes can be obtained from Eq. (1.185), (also from Eqs. (1.152) and (1.174) setting $\varphi_1 = 0$): the radial part of the eigenmode μ i.e. $\mathrm{R}_\mu(r)$ satisfies:

$$\left[-\nabla_r^2 + k_m^2 + \lambda_D^{-2}\mathrm{W}(\tfrac{\overline{\omega}_0^\mu}{m})\overline{n}_0(r)\right]\mathrm{R}_\mu(r) = 0, \tag{1.190}$$

where $\nabla_r^2 = \frac{1}{r}\partial_r r\partial_r$. We can show that modes $\mu = (n_r, m)$ and $\mu' = (n_r', m)$, which have the same axial mode number m and different radial mode numbers n_r and n_r', are orthogonal with respect to the inner product $\int_0^{r_w} \overline{n}_0(r) r\,dr(\ldots)$. For the functions R_μ and $\mathrm{R}_{\mu'}$ we can write:

$$\left[-\nabla_r^2 + k_m^2 + \lambda_D^{-2}\mathrm{W}(\tfrac{\overline{\omega}_0^\mu}{m})\overline{n}_0(r)\right]\mathrm{R}_\mu(r) = 0 \tag{1.191}$$

$$\left[-\nabla_r^2 + k_m^2 + \lambda_D^{-2}\mathrm{W}(\tfrac{\overline{\omega}_0^{\mu'}}{m})\overline{n}_0(r)\right]\mathrm{R}_{\mu'}(r) = 0 \tag{1.192}$$

Multiplying Eq. (1.191) by $r\mathrm{R}_{\mu'}(r)$ and Eq. (1.192) by $r\mathrm{R}_\mu(r)$, subtracting Eq. (1.192) from Eq. (1.191) and integrating from 0 to r_w we get:

$$\begin{aligned}&\lambda_D^{-2}\left[\mathrm{W}(\tfrac{\overline{\omega}_0^\mu}{m}) - \mathrm{W}(\tfrac{\overline{\omega}_0^{\mu'}}{m})\right]\int_0^{r_w} \overline{n}_0(r)\mathrm{R}_\mu(r)\mathrm{R}_{\mu'}(r) r\,dr \\ &= \int_0^{r_w} dr\,\partial_r\left(r\mathrm{R}_\mu(r)\partial_r\mathrm{R}_{\mu'}(r) - r\mathrm{R}_\mu(r)\partial_r\mathrm{R}_\mu(r)\right) = 0\end{aligned} \tag{1.193}$$

In the above equation, the right hand side is zero since $\mathrm{R}(r)$'s are zero at the wall. Thus, we arrive at the following orthonormality condition:

$$\int_0^{r_w} \overline{n}_0(r)\mathrm{R}_\mu(r)\mathrm{R}_{\mu'}(r) r\,dr = \delta_{l,l'}\int_0^{r_w} \overline{n}_0(r)[\mathrm{R}_\mu(r)]^2 r\,dr. \tag{1.194}$$

In a similar way we can show $\mathrm{W}(\frac{\overline{\omega}_0^\mu}{m})$ is real. Assuming $\overline{\omega}_0^\mu$ and $\mathrm{R}_\mu(r)$ to be complex,

from Eq. (1.190) we have:

$$\left[-\nabla_r^2 + k_m^2 + \lambda_D^{-2}\mathrm{W}(\tfrac{\overline{\omega}_0^\mu}{m})\overline{n}_0(r)\right]\mathrm{R}_\mu(r) = 0 \tag{1.195}$$

$$\left[-\nabla_r^2 + k_m^2 + \lambda_D^{-2}(\mathrm{W}(\tfrac{\overline{\omega}_0^\mu}{m}))^*\overline{n}_0(r)\right]\mathrm{R}_\mu^*(r) = 0 \tag{1.196}$$

Multiplying Eq. (1.195) by $r\mathrm{R}_\mu^*(r)$ and Eq. (1.196) by $r\mathrm{R}_\mu(r)$, subtracting Eq. (1.196) from Eq. (1.195) and integrating from 0 to r_w we get:

$$\begin{aligned}&\lambda_D^{-2}\left[\mathrm{W}(\tfrac{\overline{\omega}_0^\mu}{m})^* - (\mathrm{W}(\tfrac{\overline{\omega}_0^\mu}{m}))\right]\int_0^{r_w}\overline{n}_0(r)\mathrm{R}_\mu(r)\mathrm{R}_\mu^*(r)r\,dr \\ &= \int_0^{r_w} dr\,\partial_r\left(r\mathrm{R}_\mu(r)\partial_r\mathrm{R}_\mu^*(r) - r\mathrm{R}_\mu^*(r)\partial_r\mathrm{R}_\mu(r)\right) = 0\end{aligned} \tag{1.197}$$

In this equation, the right hand side is zero since $\mathrm{R}_\mu(r_w) = 0$. Also for the integral on the left hand side we can write:

$$\int_0^{r_w}\overline{n}_0(r)\mathrm{R}_\mu(r)\mathrm{R}_\mu^*(r)r\,dr = \int_0^{r_w}\overline{n}_0(r)\left(\mathrm{Re}[\mathrm{R}_\mu(r)]^2 + \mathrm{Im}[\mathrm{R}_\mu(r)]^2\right)r\,dr > 0 \tag{1.198}$$

which implies

$$\mathrm{W}(\tfrac{\overline{\omega}_0^\mu}{m}) = (\mathrm{W}(\tfrac{\overline{\omega}_0^\mu}{m}))^* \tag{1.199}$$

Using Eq. (1.199) in Eq. (1.196) we see that $\mathrm{R}_\mu(r)$ and $\mathrm{R}_\mu^*(r)$ satisfy the same equation. Thus, from the uniqueness of the solution of Poisson equation $\mathrm{R}_\mu(r)$ is also real, and therefore $\mathbf{e}_0^\mu$ is real.

Figure (1.10) shows the first three radial eigenvectors with axial mode number $m = 1$, $\mathrm{R}_{1,1}(r), \mathrm{R}_{2,1}(r)$ and $\mathrm{R}_{3,1}(r)$. We evaluated the eigenfrequencies related to these modes using both the Galerkin method and the shooting method. For the Galerkin method, the matrix eigenvalue equation (1.188) is solved by keeping a finite number of Bessel terms (N_{Gal}), to construct the matrix Q_{11}. For the shooting method, the differential equation (1.190) with initial conditions $\partial_r\mathrm{R}_\mu(0) = 0$ and $\mathrm{R}_\mu(0) = 1$ is solved for an eigenfrequency and its related eigenmode which satisfy the wall boundary condition $\mathrm{R}_\mu(r_p) = 0$. Frequencies obtained from the Galerkin

method $\omega_{\rm Gal}$ and shooting method $\omega_{\rm Sho}$ are compared in table (1.1). In the second column of the table, which gives the mode frequency obtained from Galerkin method with $N_{\rm Gal} = 20$, we see that mode $\mu = (n_r, m)$ with $n_r = 1$ and $m = 1$ is undamped ($\mathrm{Im}[\omega_{\rm Gal}/\omega_p] = -3.84 \times 10^{-35}$). Furthermore the real part of its eigenfrequency is equal to the Trivelpiece-Gould mode frequency for a cold fluid plasma of the same parameters, obtained from Eq. (1.1) (see Table 1.1). The real part of the eigenfrequencies become smaller with increasing radial mode number n_r. Furthermore, modes with higher radial mode number, i.e. $n_r = 2,3$, are heavily damped. The third and fourth column of table (1.1) compare the frequencies obtained from the shooting method to frequencies obtained from Galerkin method with respectively $N_{\rm Gal} = 20$ and $N_{\rm Gal} = 50$ terms. By increasing the number of terms for the Galerkin method, frequencies obtained from the Galerkin method converge to the shooting method frequencies. The fifth column of the table gives the modes frequencies obtained from cold fluid theory with top hat profile, evaluated using Eq. (1.1).

In order to describe the squeezed modes, we find it useful to note that the zeroth order dispersion tensor $\mathbf{M}_0$ has the following form:

$$\mathbf{M}_0 = \begin{pmatrix} \mathbf{M}_0^{11} & 0 & 0 & \dots \\ 0 & \mathbf{M}_0^{22} & 0 & \dots \\ 0 & 0 & \mathbf{M}_0^{33} & \dots \\ \vdots & & & \end{pmatrix}, \tag{1.200}$$

where $(\mathbf{M}_0^{\overline{m}m})^{l\bar{l}} = M_0^{\bar{l}l\overline{m}m}$ and $M_0^{\bar{l}l\overline{m}m}$ is given by Eq. (1.183). The mth unsqueezed eigenvector $(\mathbf{e}_0^{\mu})^m$ satisfies

$$\mathbf{M}_0^{mm}(\overline{\omega}_0^{\mu}).(\mathbf{e}_0^{\mu})^m = 0, \tag{1.201}$$

and has components $((\mathbf{e}_0^{\mu})^m)^l = (\mathbf{e}_0^{\mu})^{ml}$ (see Eqs. (1.184) and (1.185)). The explicit indices (mm) are related to the axial Fourier components, which are not coupled at zeroth order (hence the diagonal form of Eq. (1.200)).

The matrix $\mathbf{M}_0^{mm}$ (for axial mode m) has radial eigenvectors $(\mathbf{e}_0^{\mu})^m$ and eigenfrequencies corresponding to unsqueezed TG modes as shown in Fig. 1.10 (see Eq. (1.187)).

The zeroth order damping rate, which is the Landau damping of the unsqueezed system, follows from the same argument as for our 1D model of Sec. II. Assuming $\overline{\omega}_0^\mu \gg \gamma_0^\mu$ and using the fact that $\mathrm{W}(\overline{\omega}_0^\mu/m)$ is real, a Taylor expansion of $\mathrm{Im}\,\mathrm{W}(\overline{\omega}_0^\mu/m) = 0$ yields

$$\overline{\gamma}_0^\mu = -\frac{\pi \overline{\omega}_{0r}^\mu e^{-\frac{(\overline{\omega}_{0r}^\mu)^2}{2m^2}}}{\mathrm{P}\int_{-\infty}^{\infty} \frac{v e^{-v^2/2} dv}{(\overline{\omega}_{0r}^\mu/m - v)^2}}, \tag{1.202}$$

the same formula as for the 1D model of Sec. II, Eq. (1.60). Since $\overline{\gamma}_0^\mu$ is proportional to $e^{-(\overline{\omega}_0^\mu)^2/2m^2}$, in the regime where $\overline{\omega}_0^\mu \gg m$, the zeroth order damping rate is exponentially small.

We will also be using the left eigenvector $\hat{\mathbf{e}}_0^\mu$ of $\mathbf{M}_0(\overline{\omega}_0^\mu)$. The left eigenvectors differ from the right eigenvectors $\mathbf{e}_0^\mu$ because $\mathbf{M}_0^{mm}$ is not symmetric. The left eigenvectors satisfy

$$\hat{\mathbf{e}}_0^\mu . \mathbf{M}_0(\overline{\omega}_0^\mu) = 0\,. \tag{1.203}$$

Using Eq. (1.183) we can write the above equation explicitly as:

$$(\hat{\mathbf{e}}_0^\mu)^{\bar{l}m} = -\sum_{l'=1}^{\infty} (\hat{\mathbf{e}}_0^\mu)^{l'm} \mathrm{W}(\overline{\omega}_0^\mu/m) \frac{\int_0^{r_w} r\,dr\, \mathrm{J}_0(\frac{x_{l'}}{r_w} r)\mathrm{J}_0(\frac{x_{\bar{l}}}{r_w} r)\overline{n}_0(r)}{\lambda_D^2 \left[\left(\frac{x_{l'}}{r_w}\right)^2 + k_m^2\right] \frac{r_w^2}{2} \mathrm{J}_1^2(x_{l'})}. \tag{1.204}$$

Comparing Eq. (1.185) to Eq. (1.204) we obtain the following relation between $\hat{\mathbf{e}}_0^\mu$ and $\mathbf{e}_0^\mu$:

$$(\hat{\mathbf{e}}_0^\mu)^{\bar{l}m} = \lambda_D^2 \left[\left(\frac{x_{\bar{l}}}{r_w}\right)^2 + k_m^2\right] \frac{r_w^2}{2} \mathrm{J}_1^2(x_{\bar{l}}) (\mathbf{e}_0^\mu)^{\bar{l}m} \tag{1.205}$$

First order in ε

Analysis of the first-order correction to the eigenmodes follows similar steps as for the 1D model of Sec. II, except that the matrix $\mathbf{M}_0^{mm}$ is not symmetric so both

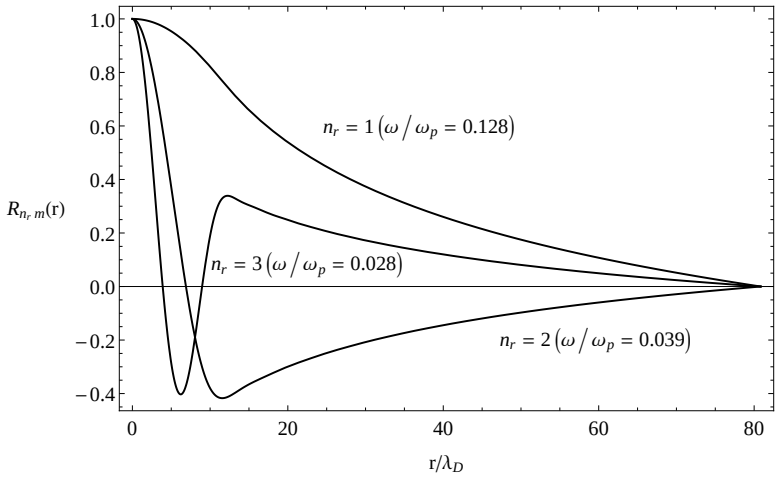

Figure 1.10: Plot of the radial dependence of the modes $\mu = (n_r, m)$, with axial mode number $m = 1$ and three radial mode numbers $n_r = 1, 2, 3$, in an unsqueezed plasma with the same parameters as Fig. 1.7.

Table 1.1: Frequencies of unsqueezed eigenmodes $\mu = (n_r, m)$: $(1,1)$, $(2,1)$ and $(3,1)$, where n_r is the radial and m is the axial mode number, for a plasma with the same parameters as Fig. 1.7. Frequencies were obtained using Galerkin method $\omega_{\rm Gal}$ and shooting method $\omega_{\rm Sho}$. $N_{\rm Gal}$ is the number of Bessel terms used to construct the dispersion matrix $\mathbf{M}_0^{11}$

mode number (n_r, m)	$\omega_{\rm Gal}/\omega_p$ $N_{\rm Gal} = 20$	$(\omega_{\rm Sho} - \omega_{\rm Gal})/\lvert\omega_{\rm Gal}$ $N_{\rm Gal} = 20$	$(\omega_{\rm Sho} - \omega_{\rm Gal})/\lvert\omega_{\rm Gal\rvert}$ $N_{\rm Gal} = 50$	$\omega_{\rm TG}/\omega_p$ (from Eq. (1.1))
(1,1)	0.1285	$(4.1 + i3.7) \times 10^{-3}$	$(2.6 + i2.4) \times 10^{-6}$	0.1285
(2,1)	$0.0388 - i1.08 \times 10^{-3}$	$(5.03 + i1.1) \times 10^{-4}$	$(9.5 + i2.1) \times 10^{-7}$	0.0316
(3,1)	$0.0281 - i5.21 \times 10^{-3}$	2.3×10^{-5}	1.7×10^{-7}	0.0177

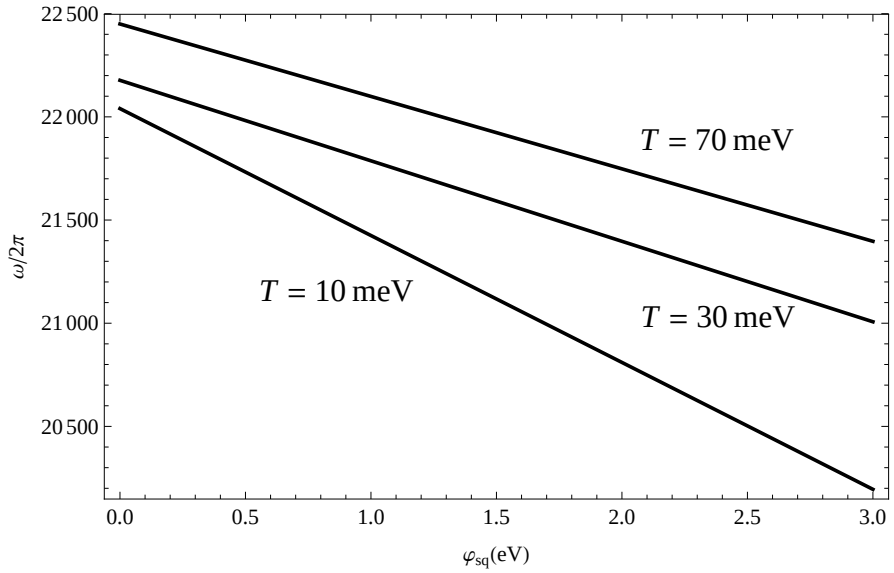

Figure 1.11: Plot of the change in mode frequency for axial mode $m = 1$ versus the applied squeeze potential, in a plasma of $L = 10$cm, $\omega_p = 1.15\times10^6$Rad/s, $r_p \approx 0.4$cm and $r_w = 2.86$cm for temperatures $T = 10$meV, $T = 30$meV and $T = 70$meV.

left and right eigenvectors must be used.

To the first order in ε dispersion relation is given by:

$$\mathbf{M}_0(\overline{\omega}_0^\mu).\mathbf{e}_1^\mu + \overline{\omega}_1^\mu \partial_{\overline{\omega}}\mathbf{M}_0(\overline{\omega}_0^\mu).\mathbf{e}_0^\mu + \mathbf{M}_1(\overline{\omega}_0^\mu).\mathbf{e}_0^\mu = 0\,. \tag{1.206}$$

Taking the product of Eq. (1.206) from the left side with the left eigenvector $\hat{\mathbf{e}}_0^\mu$ and using Eq. (1.203), the first term will be eliminated. We can then solve for $\overline{\omega}_1^\mu$ and obtain:

$$\begin{aligned}\overline{\omega}_1^\mu &= -\frac{\hat{\mathbf{e}}_0^\mu.\mathbf{M}_1(\overline{\omega}_0^\mu).\mathbf{e}_0^\mu}{\hat{\mathbf{e}}_0^\mu.\partial_{\overline{\omega}}\mathbf{M}_0(\overline{\omega}_0^\mu).\mathbf{e}_0^\mu} \\ &= -\frac{(\hat{\mathbf{e}}_0^\mu)^m.\mathbf{M}_1^{mm}(\overline{\omega}_0^\mu).(\mathbf{e}_0^\mu)^m}{(\hat{\mathbf{e}}_0^\mu)^m.\partial_{\overline{\omega}}\mathbf{M}_0^{mm}(\overline{\omega}_0^\mu).(\mathbf{e}_0^\mu)^m}.\end{aligned} \tag{1.207}$$

The real part of $\overline{\omega}_1^\mu$ gives a correction of order ε to the mode frequency and the imaginary part gives an order ε correction to the damping rate. The numerator of Eq. (1.207) can be evaluated using Eqs. (C.1), (C.5), and (1.185). We note that Eqs. (C.1) and (C.5) show that $\mathbf{M}_1^{mm}(\overline{\omega}_0^\mu)$ is a real function of W$(\overline{\omega}_0^\mu/m)$ and $\overline{\omega}_0^\mu$; that is,

$\mathbf{M}_1^{mm}$ is real if $\mathrm{W}(\overline{\omega}_0^\mu/m)$ and $\overline{\omega}_0^\mu$ are real. Furthermore, the denominator of Eq. (1.207) is also a real function of $\mathrm{W}(\overline{\omega}_0^\mu/m)$ and $\overline{\omega}_0^\mu$. This follows from Eq. (1.183) and identity (1.69). Therefore, the right hand side of Eq. (1.207) is a real function of $\mathrm{W}(\overline{\omega}_0^\mu/m)$ and $\overline{\omega}_0^\mu$, which we call $f(\mathrm{W},\overline{\omega}_0^\mu)$. Eq. (1.207) can therefore be written as

$$\overline{\omega}_1^\mu = f(\mathrm{W},\overline{\omega}_0^\mu). \tag{1.208}$$

We can then obtain the first-order correction to the damping rate by taking the imaginary part of this equation, substituting $\overline{\omega}_0^\mu = \overline{\omega}_{0r}^\mu + i\overline{\gamma}_0^\mu$ and Taylor expanding in $\overline{\gamma}_0^\mu$:

$$\overline{\gamma}_1^\mu = \overline{\gamma}_0^\mu \partial_{\overline{\omega}} f(\mathrm{W},\overline{\omega}_0^\mu), \tag{1.209}$$

noting that $\mathrm{W}(\overline{\omega}_0^\mu/m)$ is real. This shows that $\overline{\gamma}_1^\mu$ is directly proportional to the zeroth order damping rate $\overline{\gamma}_0^\mu$. As a result when $\overline{\omega}_0^\mu \gg m$, $\overline{\gamma}_1^\mu$ is also exponentially small.

Figure (1.11) shows the change in mode frequency versus the applied squeeze potential. As in the 1D case, the squeeze causes a decrease in the mode frequency, as the mode's axial sloshing motion is impeded by the squeeze potential.

The first order correction to the eigenmode is obtained from Eq. (1.206) as:

$$(\mathbf{e}_1^\mu)^j \quad = \quad -(\mathbf{M}_0^{jj}(\overline{\omega}_0^\mu))^{-1}.\mathbf{M}_1^{jm}(\overline{\omega}_0^\mu).(\mathbf{e}_0^\mu)^m\,,\; j \neq m\,. \tag{1.210}$$

In the above equation, index j represents the axial Fourier mode number and radial indices are implicit. We also used the fact that the matrix $\mathbf{M}_0$ is block-diagonal in the axial modes (see Eq. (1.200)), which implies that its inverse is also block diagonal, with matrices $(\mathbf{M}_0^{jj})^{-1}$ in each block.

Equation (1.210) applies only for the components $(\mathbf{e}_l^\mu)^j$ with $j \neq m$. The $j = m$ term takes more work. For $j = m$ Eq. (1.206) becomes

$$\mathbf{M}_0^{mm}\cdot(\mathbf{e}_1^\mu)^m + [\overline{\omega}_1^\mu \partial_{\overline{\omega}}\mathbf{M}_0^{mm}(\overline{\omega}_0^\mu) + \mathbf{M}_1^{mm}(\overline{\omega}_0^\mu)]\cdot(\mathbf{e}_0^\mu)^m = 0\,. \tag{1.211}$$

To solve this equation, note that $\mathbf{M}_0^{mm}(\overline{\omega}_0^\mu)$ has a set of right and left eigenvectors $\mathbf{E}^n$ and $\hat{\mathbf{E}}^n$ respectively with nonzero eigenvalues, in addition to the right and left eigenvector $(\mathbf{e}_0^\mu)^m$ and $(\hat{\mathbf{e}}_0^\mu)^m$ whose eigenvalue is zero (see Eqs. (1.201) and

(1.203)). These other eigenvectors satisfy

$$\mathbf{M}_0^{mm}(\overline{\omega}_0^{\mu})\cdot\mathbf{E}^n = \lambda_n \mathbf{E}^n \tag{1.212}$$

and [35]

$$\hat{\mathbf{E}}^n \cdot \mathbf{M}_0^{mm}(\overline{\omega}_0^{\mu}) = \lambda_n \hat{\mathbf{E}}^n. \tag{1.213}$$

We solve Eq. (1.211) by expanding $(\mathbf{e}_1^{\mu})^m$ in the set of right eigenvectors (assuming they form a complete set):

$$(\mathbf{e}_1^{\mu})^m = \sum_n c_n \mathbf{E}^n. \tag{1.214}$$

Note that we neglect the eigenvector with zero eigenvalue in this sum since, by assumption, $(\mathbf{e}_1^{\mu})^m$ is orthogonal to this mode (which is included in the zeroth order). Substituting Eq. (1.214) into Eq. (1.211), and applying a left eigenvector yields the solution,

$$c_n = -\frac{\hat{\mathbf{E}}^n \cdot [\overline{\omega}_1^{\mu}\partial_{\overline{\omega}}\mathbf{M}_0^{mm}(\overline{\omega}_0^{\mu}) + \mathbf{M}_1^{mm}(\overline{\omega}_0^{\mu})]\cdot(\mathbf{e}_0^{\mu})^m}{\lambda_n \hat{\mathbf{E}}^n \cdot \mathbf{E}^n} \tag{1.215}$$

where we have used orthogonality of left and right eigenvectors, $\hat{\mathbf{E}}^{\overline{n}}\cdot\mathbf{E}^n = 0$ [provided $\lambda_{\overline{n}} \neq \lambda_n$]. [35]

Note that the inversion of matrix $\mathbf{M}_0^{jj}$ in Eq. (1.210) can be carried out only when $\mathrm{Det}[\mathbf{M}_0^{jj}] \neq 0$. This condition will not be satisfied in cases where degeneracies exist among the unsqueezed eigenmodes, [4] i.e. when $\overline{\omega}_0^{\mu} = \overline{\omega}_0^{\mu'}$ for unsqueezed modes μ and μ'. Fortunately, for the particular cases studied here, no such degeneracies appear. In Ref. 4, degeneracies occured because ideal cold fluid theory was used; but here Landau-damping of high-order modes breaks the degeneracies.

Using Eq. (1.186) the squeezed eigenmode $\mu = (n_r, m)$ up to the first order in ε is:

$$\begin{aligned} \delta\varphi^{\mu}(r,z,t) &= 2\delta\phi_0^{\mu}(r,z)e^{-\gamma t}\cos(\omega_r t) \\ &+ 2\mathrm{Re}[\delta\phi_1^{\mu}(r,z)]e^{-\gamma t}\cos(\omega_r t) + 2\mathrm{Im}[\delta\phi_1^{\mu}(r,z)]e^{-\gamma t}\sin(\omega_r t), \end{aligned} \tag{1.216}$$

where

$$\delta\phi_1^\mu(r,z)=\varepsilon\sum_{l'\neq l}\sum_{m'\neq m}(\mathbf{e}_1^\mu)^{l'm'}\mathrm{J}_0(\tfrac{x_{l'}}{r_w}r)\cos[k_{m'}(z+L/2)] \tag{1.217}$$

Since elements of $\mathbf{e}_0^\mu$ are linearly proportional to $|\delta\phi^\mu|$ and elements of $\mathbf{e}_1^\mu$ are linear combinations of elements of $\mathbf{e}_0^\mu$, both real and imaginary part of $\delta\phi_1^\mu(r,z)$ are linearly proportional to $|\delta\phi^\mu|$. Figures (1.12a) and (1.12b) respectively depict the contour plots of the $\cos(\omega_r t)$ and $\sin(\omega_r t)$ time dependent part of the change to the $m=1, n_r=1$ eigenmode due to a squeeze potential, which are given respectively by the relations (1.216) and (1.217).

Second order in ε

Evidently, damping from the squeeze is second order in ε, just as in Sec. 1.4. The second order dispersion relation is given by Eq. (1.106),

$$\begin{aligned}&\mathbf{M}_0(\overline{\omega}_0^\mu).\mathbf{e}_2^\mu+\frac{(\overline{\omega}_0^\mu)^2}{2}\partial_{\overline{\omega}}^2\mathbf{M}_0(\overline{\omega}_0^\mu).\mathbf{e}_0^\mu+\overline{\omega}_2^\mu\partial_{\overline{\omega}}\mathbf{M}_0(\overline{\omega}_0^\mu).\mathbf{e}_0^\mu+\overline{\omega}_1^m\partial_{\overline{\omega}}\mathbf{M}_1(\overline{\omega}_0^\mu).\mathbf{e}_0^\mu\\ +\quad&\mathbf{M}_1(\overline{\omega}_0^\mu).\mathbf{e}_1^\mu+\overline{\omega}_1^m\partial_{\overline{\omega}}\mathbf{M}_0(\overline{\omega}_0^\mu).\mathbf{e}_1^\mu+\mathbf{M}_2(\overline{\omega}_0^\mu).\mathbf{e}_0^\mu=0.\end{aligned} \tag{1.218}$$

In order to solve for $\overline{\gamma}_2^\mu$ we take the imaginary part of the product of Eq. (1.218) with $\hat{\mathbf{e}}_0^\mu$. As for the derivations for the 1D case given by Eqs. (1.103) through (1.106), for $\overline{\omega}_0^\mu\gg m$, terms 1,2,4 and 6 are zero. As a result, the second order damping rate is given by:

$$\overline{\gamma}_2^m=-\frac{\mathrm{Im}[\sum_{j=1}^\infty(\hat{\mathbf{e}}_0^\mu)^m.\mathbf{M}_1^{mj}(\overline{\omega}_0^\mu).(\mathbf{e}_1^\mu)^j]+(\hat{\mathbf{e}}_0^\mu)^m.\mathrm{Im}\mathbf{M}_2^{mm}(\overline{\omega}_0^\mu).(\mathbf{e}_0^\mu)^m}{(\hat{\mathbf{e}}_0^\mu)^m.\partial_a\mathrm{Re}\mathbf{M}_0^{mm}(\overline{\omega}_0^\mu).(\mathbf{e}_0^\mu)^m}, \tag{1.219}$$

where $(\mathbf{e}_1^\mu)^j$ is given by Eq. (1.210). Figure (1.13) shows the damping rate versus the applied squeezed potential for various temperatures using relations (1.202), (1.209) and (1.219), for typical confined plasma parameters. The second order damping rate is the result of resonant wave-particle interaction. Thus, lowering the temperature will move the resonances in phase-space to energies where the plasma is less populated i.e higher phase velocities compared to thermal velocity. As a result low-

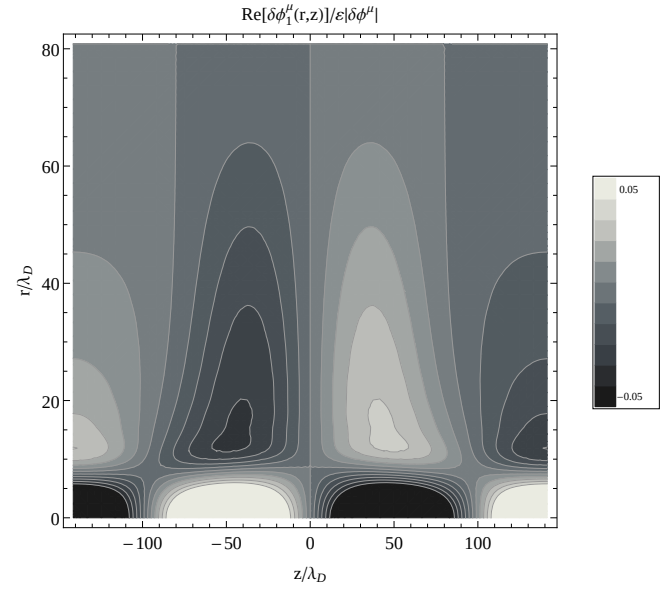

(a)

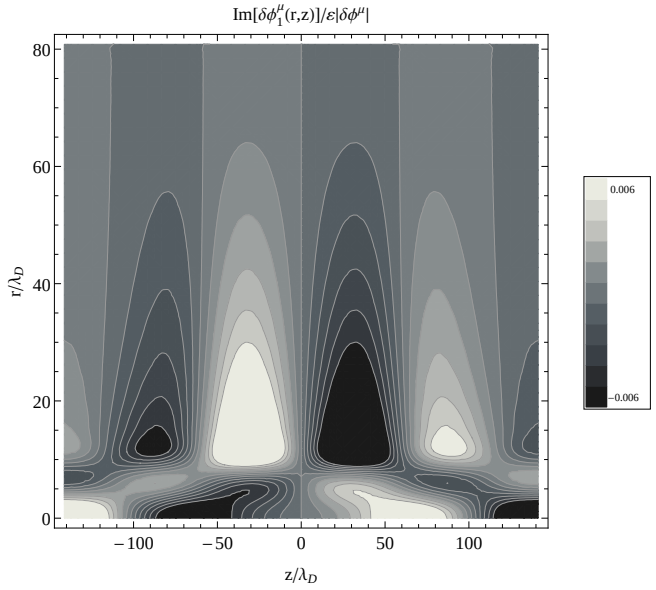

(b)

Figure 1.12: Contour plots of the real and imaginary part of $\delta\phi_1^\mu(r,z)$, the change in the spatial dependence of the eigenmode due to squeeze potential, for the lowest-order mode $\mu=(1,1)$. Re$[\delta\phi_1^\mu(r,z)]$ depicted in (1.12a) has a $\cos(\omega_r t)$ time dependence and Im$[\delta\phi_1^\mu(r,z)]$ depicted in (1.12b) has a $\sin(\omega_r t)$ time dependence. The z axis extends from $-L/2$ to $L/2$ and the r axis extends from 0 to r_w. Plasma parameters are the same as for Fig. 1.7.

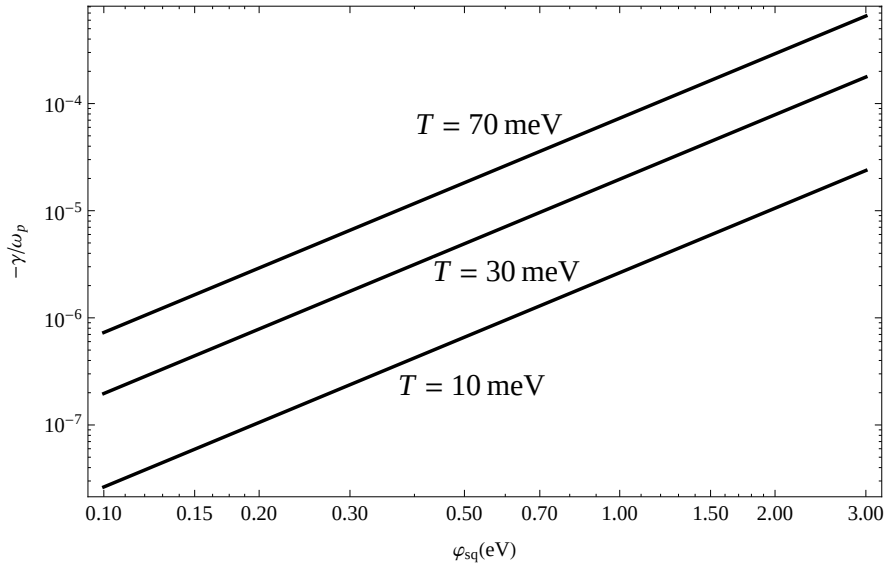

Figure 1.13: Plot of the damping rate of axial mode $m = 1$ versus the applied squeeze potential, in a plasma with same parameters as Fig. 1.11.

ering the temperature results in smaller damping rates.

1.5 Summary

In this chapter we have explored the effect of an applied squeeze potential on the frequency, damping and spatial form of TG modes. The presence of a squeeze potential results in additional resonant wave-particle interactions at the bounce frequencies $\omega_b = \omega/n$, which enhances the mode damping rate. There are two different reasons for these extra resonances to be generated: i) The squeeze potential modifies the unperturbed orbits of the particles in such a way that a single cosine wave in position space is seen by the particles (as a function of time) as perturbed, containing higher harmonics with amplitudes of order φ_s/T. ii) The shape of the mode potential in position space is also modified and contains higher harmonics of amplitudes $\mathcal{O}(\varphi_s/T)$. Our analysis shows that in the regime where $\varphi_s/T \ll 1$ and $\omega/k_m v_T \gg 1$, the mode damping rate has a quadratic dependence on the amplitude of the applied squeeze potential $|\varphi_{sq}|$, while, for low-order TG modes the frequency shift due to squeeze is first-order in the squeeze potential. This behavior is

consistent with experimental results. A detailed comparison to experiments will be presented in future works.

In the theory presented here, we assume that the squeeze is applied slowly so that at every stage the plasma is in a thermal equilibrium state, described by a rigid-rotor Boltzmann distribution. However, in experiments the squeeze may be applied rapidly, so that while the distribution remains Boltzmann along any given field line, the plasma is no-longer a rigid rotor. In following work we will generalize our results to account for effects such as this, where the squeezed plasma is not in a full thermal equilibrium state.

This Chapter, in part, is a reprint of the material as it appears in Physics of Plasmas. Arash Ashourvan and Daniel H.E. Dubin, *Physics of Plasmas* **21**, 052103 (2007). The dissertation author was the primary investigator and author of this paper.

Chapter 2

Effects of a partition type squeeze on a finite length 1D plasma

2.1 Introduction

In this chapter we study the effect on cylindrically-symmetric Trivelpiece-Gould modes of applying a cylindrically symmetric, infinitesimally narrow "squeeze" potential. The squeeze effect was studied in the previous chapter for a smooth squeeze of finite axial extent. Here, the simplification of a narrow squeeze allows the study of collisionless trapped particle heating and the effects of collisions on the heating of a squeezed plasma, effects that were neglected in chapter 1.

The plasma is 1D and of length L, extending from $z = -L/2$ to $z = L/2$. Squeeze potential (energy) φ_s is applied to the center of plasma, at $z = 0$ with a magnitude given by

$$\varphi_s = \frac{1}{2} m_q v_s^2, \tag{2.1}$$

where v_s is the separatix velocity. The separatrix divides the particles into two separate classes:

i) particles with energies $E > \varphi_s$ (velocity $|v| > v_s$) travel the whole length of the plasma. We call these the passing particles. The unperturbed orbit of a passing particle consists of traveling from the left end of plasma at $-L/2$ to the right end of the plasma at $L/2$, bouncing off of the plasma end and traveling back from $L/2$ to $-L/2$.

In the current model, since we assume that the squeeze is infinitesimally narrow, the passing particles do not feel the squeeze as they pass over it, as if the squeeze does not exist for the passing particles. Had the squeeze been a given by a smooth analytic function with a finite width, the passing particles would have gradually slowed down as they were climbing the smooth squeeze and speed up as the were descending from the top of the squeeze, and this would have altered their orbits (see Ref. 5/ chapter 1).

ii) particles with energies $E < \varphi_s$ (velocity $|v| < v_s$) are trapped on one side of the squeeze and cannot pass over to the other side. For a particle trapped on the left side of the squeeze, the unperturbed bounce orbit for a particles consists of traveling from the left end of plasma at $z = -L/2$ to the center at $z = 0$, bouncing off of squeeze and traveling from $z = 0$ to the starting point $z = -L/2$. Particles on the right side of the squeeze travel between the right plasma end at $z = L/2$ and the squeeze at $z = 0$.

In the collisionless theory and in the unperturbed orbits approximation, there is no interchange of particles between trapped and passing population. Adding collisions however can change the velocity stochastically and free the trapped particles(trap the passing particles) by adding a positive(negative) random displacement to a particle's velocity.

We assume a long plasma for which the Debye length λ_D is small: $\lambda_D \ll L$. In such a long plasma we neglect the Debye sheath effect at the plasma ends by assuming that the plasma ends are flat. This assumption is based on the fact that the time a particle spends to turn around at the end Debye sheath is very small compared to the time it spends to travel the whole length of the plasma. as a result, the reflection of the particles from either the plasma ends or the squeeze(trapped particles only) is taken to be specular.

In section 2.2 we introduce our 1D slab geometry plasma model. We apply a small standing sinusoidal (in both space and time) drive potential with angular frequency ω to the plasma and obtain the linear distribution function of a collisionless plasma in response to the drive potential. This drive potential performs positive work on the resonant particles and consequently heats the plasma. We find that the

trapped particles moving in z experience a non-sinusoidal mode potential caused by the squeeze, whereas the passing particles experience the sinusoidal mode potential. As a result, the distribution functions for trapped and passing particles are discontinuous at the separatrix.

In section 2.3 we evaluate the resonant plasma heating. We find that the trapped particles moving in z experience a non-sinusoidal mode potential caused by the squeeze, producing high-frequency harmonics that can resonate with the wave frequency to cause Landau damping and satisfy the condition $\omega_b(E_n) = \omega/n$, where $\omega_b(E)$ is the frequency of axial bounce motion of particles with energy E, even when the mode phase velocity is large compared to the thermal velocity. We will see that these added resonances cause an enhancement to the plasma heating rate has a $|\varphi_s|^2$ dependence.

In section 2.4 we add weak collisions to the system in the form of a Fokker-Planck collision operator. Due to the discontinuities at the separatrix, the velocity derivatives of this collision operator are large in this region. Using the boundary layer method we obtain a local solution to the distribution function at the separatrix which has a width proportional to $\sqrt{D}$ and connects and smooths out the discontinuities present in the collisionless theory. Furthermore we evaluate the heating in the separatrix layer and compare our analytical results to the heating evaluated from the numerical grids method. We find that for small diffusion coefficients D and for an isolated separatrix layer, the heating in this layer also has a $\sqrt{D}$ dependence. We observe that in the limit of small frequency $\omega/k_m v_s < 1$, separatrix heating considerably enhances the plasma heating.

We obtain an analytical solution for the linear distribution of the resonant regions in the weak collisional regime in section 2.5 and verify our results by comparing to the numerical grids method solutions. We find that the width of this resonance region has a $D^{1/3}$ dependence while its peak has a $D^{-1/3}$ dependence. As a result, for a weakly collisional system the resonance region is broadened due to collisions but the change in resonance heating is small.

2.2 1D model

In this section we neglect radial variation for simplicity, we assume the plasma ends are flat, and that particles undergo specular reflection at the ends, $z = \pm L/2$. We also assume that the squeeze potential is symmetric in z with respect to the center of plasma. This is not necessarily the case in the experiments, however this added symmetry simplifies the problem.

We focus on azimuthally symmetric modes in a strong magnetic field and we assume the following ordering for the time scales:

$$\nu_{col} \ll \omega_b \lesssim \omega \lesssim \omega_p \ll \omega_c. \tag{2.2}$$

Here, ν_{col} is the collision frequency and $\omega_c = qB/m_q c$ is the cyclotron frequency. Reading from left to right, the first inequality allows us to use collisionless theory; the second inequality is necessary so that waves are not heavily Landau damped; and the fourth assumes a strong magnetic field. In such a strong magnetic field the distribution of particle guiding centers is described by drift-kinetic equations. Particle motion consists of $\mathbf{E} \times \mathbf{B}$ drift motion across the magnetic field and streaming along the magnetic field in the z direction. Since we assume the plasma consists of one type of particles with charge q, in our calculation we make use of potential energy instead of electrostatic potential, in order to simplify our notation. In this 1D strong-magnetic-field model, collisionless plasma dynamics is described by the time evolution of the 1D Vlasov equation

$$\frac{\partial f}{\partial t} + v\frac{\partial f}{\partial z} - \frac{1}{m_q}\frac{\partial \delta\varphi}{\partial z}\frac{\partial f}{\partial v} = 0, \tag{2.3}$$

where $f(z, v, t)$ is the particle distribution function, $\delta\varphi(z, t)$ is an externally applied drive potential which drives the plasma adiabaticallly from $t = -\infty$. Due to the reflective boundary conditions, the distribution function must satisfy the following

conditions:

$$f(\pm L/2, v) = f(\pm L/2, -v) \quad \text{At the plasma ends,} \tag{2.4}$$

$$f(0, v) = f(0, -v) \quad \text{At squeeze, for trapped particles only.} \tag{2.5}$$

For a long thin palsma to the lowest order in ω_n/ω_p the boundary conditions on the mode potential at the axial ends of plasma are $\partial_z \delta\phi_n(\pm L/2) \approx 0$ [33], where $\delta\phi_n$ is the mode potential, ω_n is the mode frequency and $\omega_n \ll \omega$. Therfore, we take the drive potential $\delta\varphi(z,t)$ to be in the form of a standing wave a s follows

$$\delta\varphi(z,t) = |\delta\overline{\phi}|\cos[k_m(z+L/2)]\cos[\omega t - \alpha_0] \tag{2.6}$$

$$= \delta\phi(z)e^{-i\omega t} + \delta\phi^*(z)e^{i\omega t}, \quad \delta\phi(z) = \tfrac{1}{2}\delta\overline{\phi}\cos[k_m(z+L/2)] \tag{2.7}$$

$$\delta\overline{\phi} = |\delta\overline{\phi}|e^{i\alpha_0} \tag{2.8}$$

Moreover, we neglect the space-charge potential by assuming it to be small in comparison to $\delta\varphi(z,t)$. Particle distribution is given by

$$f(z, v, t) = n_0(\mathrm{F}_0(v) + \delta\mathrm{f}(z, v, t)). \tag{2.9}$$

Here, n_0 is the density of a uniform neutralizing background charge (provided by rotation at a given frequency through the uniform magnetic field in the actual plasma system). $n_0\mathrm{F}_0(z,v)$ is the equilibrium distribution function and δf is the perturbed distribution function due to the presence of the drive potential, which has the following form:

$$\delta\mathrm{f}(z, v, t) = \delta f(z, v)e^{-i\omega t} + \delta f^*(z, v)e^{i\omega t} \tag{2.10}$$

We choose the equilibrium distribution to be of the Boltzmann type:

$$\mathrm{F}_0(v) = \frac{\exp[-m_q v^2/2T]}{L\sqrt{2\pi T/m_q}}, \tag{2.11}$$

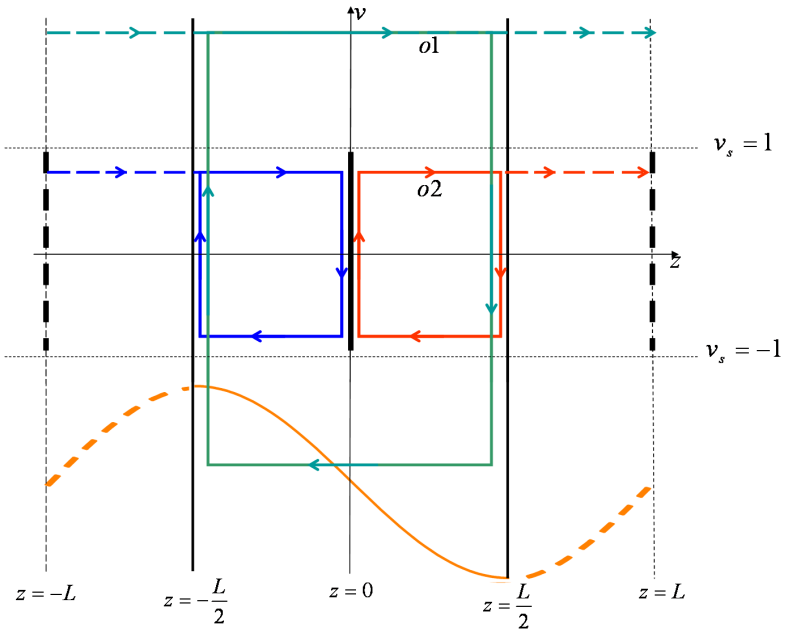

Figure 2.1: A schematic description of extension of the phase-space. Plot in orange is the wave potential, solid part of the plot is inside the original system and the dashed part is inside the extended region.

normalized such that

$$\int_{-\infty}^{\infty}\int_{-L/2}^{L/2} \mathrm{F}_0\, d\,v\, d\,z = 1\,. \tag{2.12}$$

Presence of the squeeze is implicit in the Eq. (2.11): The function does not show a spatial(z) dependence, however the squeeze potential is built into the distribution function and particles with velocities $|v| < v_s$ are trapped and have different unperturbed orbits than the passing particles. Thus δf must be solved separately for trapped and passing particles. For a small amplitude perturbation we linearize the Vlasov equation to obtain:

$$\frac{\partial\,\delta\mathrm{f}}{\partial\,t} + v\frac{\partial\,\delta\mathrm{f}}{\partial\,z} + v\frac{\partial\,\delta\varphi}{\partial\,z}\frac{\mathrm{F}_0}{T} = 0\,, \tag{2.13}$$

where we used $\partial_v \mathrm{F}_0 = -\mathrm{F}_0/T$. We want to use Fourier series expansion to solve for δf, however all the boundaries are of the reflective type.

We can convert these boundary conditions into periodic boundary condi-

tions by even periodic extension of the phase-space. This is done by removing the infinte walls at the end and replacing them with the mirror image of half of the phase-space with respect to that wall. A schematic description of this method is given in Fig. (2.1). An arbitrary passing particle would travel along orbit $o1$ in phase-space, along which it would reflect off of the right wall and instantly go to negative velocity space and then moves in the negative direction. Now with the new boundary conditions, where there are no walls and wave potential has been extended (even periodic) as well as phase-space, that specific passing particle will move to the right side of $z = L/2$ where the right wall used to be, and it will move along until it reaches $z = L$. At this point it will disappear and reappear at $z = -L$. In the extended part of phase-space particle will see the same potential as it would have originally, in the infinite wall case.

A particle in right trap would travel to the right along orbit $o2$, reflect off of the wall at $z = L/2$ and move to left in the negative velocity space until it hits the squeeze and reflects again and moves to right in positive velocity space. Now with the periodic boundary condition, trapped particle moves to the right side of $z = L/2$ until it reaches the image of the squeeze at $z = L$, there it disappears and then reappears at the position of the actual squeeze at $z = 0$ and again moves to the right. Notice that with this type of boundary conditions, a particle's velocity does not change sign and particles keep moving in the same direction. Hence the new boundary conditions are

$$\delta f(z+2L, v) = \delta f(z, v), \text{ passing} \tag{2.14}$$

$$\delta f(z+L, v) = \delta f(z, v), \text{ left trap} \tag{2.15}$$

$$\delta f(z+L, v) = \delta f(z, v), \text{ right trap} \tag{2.16}$$

Similarly, the potential also has periodic extensions. For the passing particles

the potential goes from $-L$ to L and is sinusoidal:

$$\begin{aligned}
\delta\varphi^p(z,t) &= \delta\phi^p(z)e^{-i\omega t}+(\delta\phi^p(z))^* e^{i\omega t} && (2.17)\\
\delta\phi^p(z) &= \tfrac{1}{2}\delta\overline{\phi}\cos[k_m(z+L/2)], \quad -L\le z\le L; \quad \delta\phi^p(z+2L)=\delta\phi^p(z) &&\\
\delta\phi^p(z) &= \delta\phi^p_m e^{ik_m(z+L/2)}+\delta\phi^p_{-m}e^{-ik_m(z+L/2)}, \quad \delta\phi^p_m=\frac{1}{4}\delta\overline{\phi} && (2.18)
\end{aligned}$$

For the left trap the potential is defined over $-L\le z\le 0$ and is periodic over L:

$$\begin{aligned}
\delta\varphi^l(z,t) &= e^{-i\omega t}\delta\phi^l(z)+e^{i\omega t}(\delta\phi^l(z))^* && (2.19)\\
\delta\phi^l(z) &= \tfrac{1}{2}\delta\overline{\phi}\cos[k_m(z+L/2)], \quad -L\le z\le 0; \quad \delta\phi^l(z+L)=\delta\phi^l(z) && (2.20)
\end{aligned}$$

For the right trap the potential is defined over $0\le z\le L$ and is periodic over L:

$$\begin{aligned}
\delta\varphi^r(z,t) &= e^{-i\omega t}\delta\phi^r(z)+e^{i\omega t}(\delta\phi^r(z))^* && (2.21)\\
\delta\phi^r(z) &= \tfrac{1}{2}\delta\overline{\phi}\cos[k_m(z+L/2)], \quad 0\le z\le L; \quad \delta\phi^r(z+L)=\delta\phi^r(z) && (2.22)
\end{aligned}$$

For odd m potential we see that trapped particles experience a non-sinusoidal potential: As a trapped particle moves along its path, it will experience different forcing by the external potential for odd potential modes and this leads to different dynamics. Figures (2.2a) and (2.2b), respectively depict the potential experienced by a left-trapped and a passing particle along their unperturbed orbit. $z(t)$ is the position of a particles as a function of time, moving at a constant velocity v (in their unperturbed orbits). Bounce frequency ω_b is defined as the angular frequency of one cycle of bounce motion of a particle, which for trapped and passing particles is respectively given by $\omega_b = 2\pi|v|/L$ and $\omega_b = \pi|v|/L$. The potential for passing particles is a cosine and the particles' bounce orbiting motion is identical to the motion of a particle moving at a constant velocity, along an extended coordinate, under a periodic cosine potential. For trapped potential this is obviously not the case and potential is not of a cosine form. For even potential modes trapped and passing particles experience the same potential function along their paths and therefore the presence of squeeze potential does not affect an even mode. From here on we take m to be odd. By Fourier expanding the trapped potential in terms of the complete series of

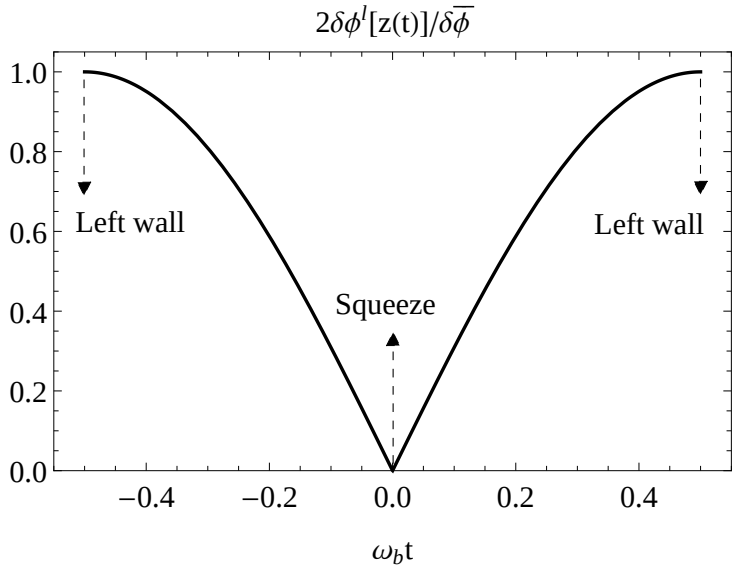

(a)

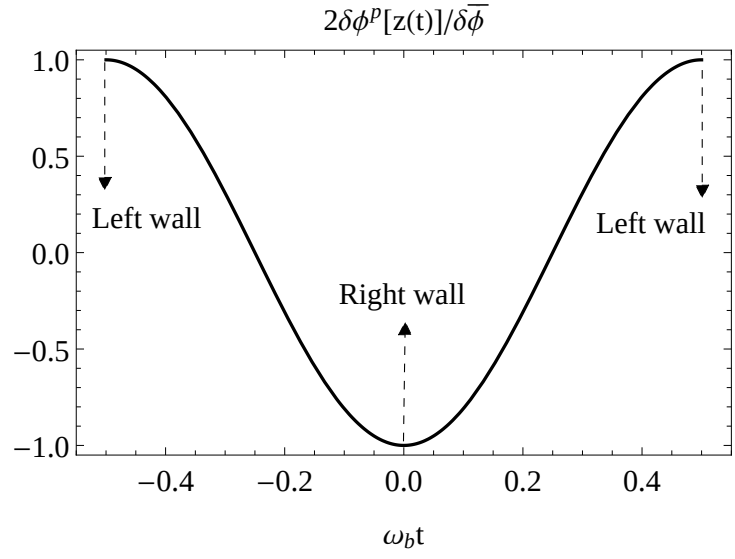

(b)

Figure 2.2: Plots of the potentials experienced by a left-trapped (Fig. (2.2a)) and a passing (Fig. (2.2b)) particle along their unperturbed orbits.

functions $e^{ik_{2n}z}$, which are periodic over L, we obtain an infinite series of harmonics:

$$\delta\phi^l(z) = \sum_{n=-\infty}^{\infty} \delta\phi^l_n e^{ik_{2n}z} \tag{2.23}$$

$$\delta\phi^l_n = \tfrac{1}{2}\delta\overline{\phi}C^l_n, \quad C^l_n = \frac{1}{\delta\overline{\phi}L}\int_{-L/2}^{L/2}\delta\phi^l(z)e^{-ik_{2n}z}dz \tag{2.24}$$

$$\delta\phi^r(z) = -\delta\phi^l(z) \tag{2.25}$$

We evaluate C^l_n and obtain:

$$C^l_n = \frac{2k_m}{k_m^2 - k_{2n}^2}\sin[\tfrac{k_m}{2}] \tag{2.26}$$

$$C^r_n = -C^l_n \tag{2.27}$$

For the passing particles we have the following Vlasov equation:

$$\frac{\partial\delta\mathrm{f}^p}{\partial t} + v\frac{\partial\delta\mathrm{f}^p}{\partial z} + v\frac{\partial\delta\varphi^p}{\partial z}\frac{\mathrm{F}_0}{T} = 0, \tag{2.28}$$

Solution of the above equation is of the form:

$$\delta\mathrm{f}^p(z,v,t) = e^{-i\omega t}\delta f^p(z,v) + c.c. \tag{2.29}$$

$$\delta f^p(z,v) = \delta f^p_m(v)e^{ik_m(z+L/2)} + \delta f^p_{-m}(v)e^{-ik_m(z+L/2)} \tag{2.30}$$

Substituting for passing particles we obtain:

$$-i\omega\delta f^p_m + ivk_m\delta f^p_m + ik_m v\delta\phi^p_m\frac{\mathrm{F}_0}{T} = 0 \tag{2.31}$$

Solving for δf^p_m we obtain:

$$\delta f^p_m = \frac{v\delta\phi^p_m\mathrm{F}_0/T}{\omega/k_m - v} \tag{2.32}$$

The time independent part of the distribution function is the given by:

$$\delta f^{p}(z,v)=\frac{v\delta\phi^{p}_{m}\mathrm{F}_0/T}{\omega/k_m-v}e^{ik_m(z+L/2)}+\frac{v\delta\phi^{p}_{-m}\mathrm{F}_0/T}{-\omega/k_m-v}e^{-ik_m(z+L/2)} \tag{2.33}$$

Solution of the above equation is of the form:

$$\begin{aligned}\delta\mathrm{f}^{l(r)}(z,v,t) &= e^{-i\omega t}\delta f^{l(r)}(z,v)+c.c. &(2.34)\\ \delta f^{l(r)}(z,v) &= \sum_{n=-\infty}^{\infty}\delta f^{l(r)}_{n}(v)e^{ik_{2n}z} &(2.35)\end{aligned}$$

In the above sums the $n=0$ term is excluded, since by adiabatically driving the plasma, the average density in the left trap and right trap does not change. For trapped particles we have the linearized Vlasov equation:

$$\frac{\partial\delta\mathrm{f}^{l}}{\partial t}+v\frac{\partial\delta\mathrm{f}^{l}}{\partial z}+v\frac{\partial\delta\varphi^{l}}{\partial z}\frac{\mathrm{F}_0}{T}=0, \tag{2.36}$$

We substitute for $\delta\mathrm{f}^{l}$ from Eq. (2.34) and solve for δf^{l}_{n} and obtain:

$$\delta f^{l}_{n}=\frac{v\delta\phi^{l}_{n}\mathrm{F}_0/T}{\omega/k_{2n}-v} \tag{2.37}$$

The time independent part of the distribution function is given by:

$$\delta f^{l(r)}(z,v) = \sum_{n=-\infty}^{\infty}\frac{v\delta\phi^{l}_{n}\mathrm{F}_0/T}{\omega/k_{2n}-v}e^{ik_{2n}z} \tag{2.38}$$

Figure (2.3) depicts the time independent part of the perturbed distribution functions of the trapped and passing particles at the separatrix ($v=v_s$), evaluated from Eq. (2.33) and Eq. (2.38) respectively. The plotted function $(\delta f/\delta\phi)/(F_0/T)$ is a function of the dimensionless parameter ω/k_1v_s, which is the phase velocity divided by the separatrix velocity. The distribution function δf is discontinuous at the separatrix and the form of the discontinuity is a function of ω/k_1v_s. Also the velocity derivative of δf is discontinuous at the separatrix velocity, as can be seen from Fig. (2.4). These discontinuities are unphysical and are the artifact of treating the plasma as a collisionless system. Adding collisions to the system will allow the par-

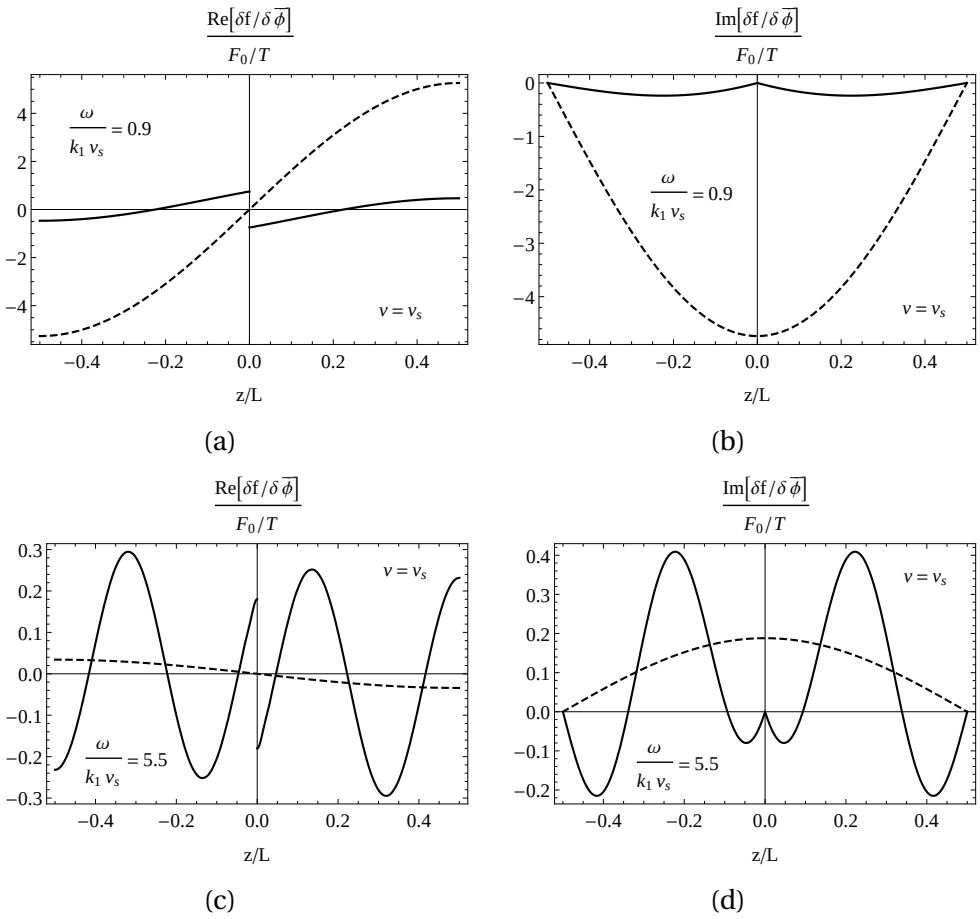

Figure 2.3: Plots of δf as a function of z for the trapped and passing particles at the separatrix ($v = v_s$), using Eq. (2.33) and Eq. (2.38) respectively.

ticle interchange between the trapped and passing regions and as a result, the solutions for δf at the separatrix will connect and smooth out. In the next section we will add a weak collison operator and solve for the distribution function of the collisional system at the separatrix region.

Furthermore, in Fig. (2.4) we can see many singularities present in the trapped region. These singularities are located in velocities $v = \omega/k_{2n}$, in the trapped region of phase-space ($-v_s < v < v_s$), which are the velocities of the particles which are at resonance with the drive potential. Distribution of the resonant particles can be obtained by adding a small collision term to the Vlasov equation($-\nu\delta$f), and applying the Plemelj formula to the relations Eq. (2.32) for passing particles and Eq. (2.37) for the trapped particles:

$$\lim_{\nu\to 0}\delta f_n^l = \mathrm{P}\frac{v\delta\phi_n^l \mathrm{F}_0/T}{\omega/k_{2n}-v} - i\pi\delta(v-\omega/k_{2n})v\delta\phi_n^l \mathrm{F}_0/T \tag{2.39}$$

$$\lim_{\nu\to 0}\delta f_m^p = \mathrm{P}\frac{v\delta\phi_m^p \mathrm{F}_0/T}{\omega/k_m-v} - i\pi\delta(v-\omega/k_m)v\delta\phi_m^p \mathrm{F}_0/T \tag{2.40}$$

This treatment is equivalent to integrating along the Landau contour, i.e. dropping below the poles [40]. In Eqs. (2.39) and (2.40) the first term gives the distribution of the non-resonant particles and "P" represents the principal value of the argument. The imaginary parts give the distribution of the resonant population, which in the collisionless theory has zero width and is given by the Dirac delta function. The drive potential performs work on the resonant particles which will result in the heating of the plasma.

2.3 Collisionless heating

External potential(perturbation) performs work on particles as they move along their (unperturbed)orbits. In case of a self consistent mode, wave potential performs work on the resonant particles and causes the damping of the wave. Time averaged heating of particles over one period of external force is obtained by inte-

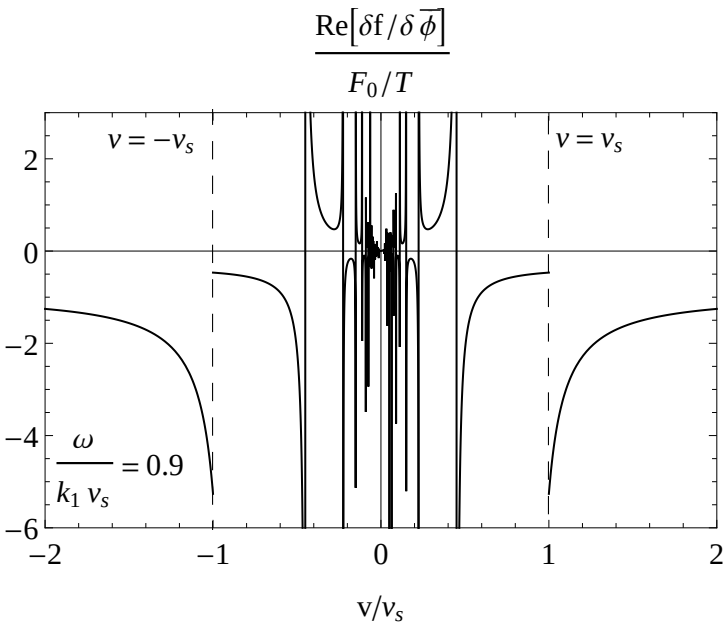

Figure 2.4: Plots of the time independent part of the perturbed distribution functions of the trapped and passing particles at the separatrix ($v = v_s$), using Eq. (2.33) and Eq. (2.38) respectively, for the drive frequencies $\omega/k_1 v_s = 0.9$ and $\omega/k_1 v_s = 5.5$, at the left end of plasma $z = -L/2$.

grating over the whole phase-space accessible to particles which is

$$\begin{aligned}\left\langle \frac{dE}{dt} \right\rangle_t &= n_0 \frac{\omega}{2\pi} \int_0^{2\pi/\omega} \int_{-L/2}^{L/2} \int_{-\infty}^{\infty} dz\, v\, dv\, \delta \mathrm{f}(z, v, t)\left(-\partial_z \delta\varphi(z,t)\right) \qquad (2.41)\\ &= -n_0 \int_{-L/2}^{L/2} \int_{-\infty}^{\infty} dz\, v\, dv \left[\delta f(z,v)\partial_z \left(\delta\phi(z)\right)^* + \delta f^*(z,v)\partial_z \delta\phi(z)\right]\end{aligned}$$

We break the integration over the entire phase-space to integrations over the passing and trapped regions:

$$\begin{aligned}
\left\langle \frac{dE}{dt} \right\rangle_t =& -n_0 \int_{-L/2}^{L/2} \left(\int_{v_s}^{\infty} + \int_{-\infty}^{-v_s} \right) dz\, v\, dv \\
&\times \left[\delta f^p(z,v) \partial_z \left(\delta\phi^p(z) \right)^* + (\delta f^p(z,v))^* \partial_z \delta\phi^p(z) \right] \\
&- n_0 \int_{-L/2}^{0} \int_{-v_s}^{v_s} dz\, v\, dv \left[\delta f^l(z,v) \partial_z \left(\delta\phi^l(z) \right)^* + (\delta f^l(z,v))^* \partial_z \delta\phi^l(z) \right] \\
&- n_0 \int_{0}^{L/2} \int_{-v_s}^{v_s} dz\, v\, dv \left[\delta f^r(z,v) \partial_z \left(\delta\phi^r(z) \right)^* + (\delta f^r(z,v))^* \partial_z \delta\phi^r(z) \right]
\end{aligned}$$

Using Eqs. (2.30), (2.35), (2.23) and (2.18) in Eq. (2.42), only the resonant particles are heated and have a nonzero contribiution to $\left\langle \frac{dE}{dt} \right\rangle_t$ which results in :

$$\begin{aligned}
\left\langle \frac{dE}{dt} \right\rangle_t =& \pi L n_0 \frac{|\delta\overline{\phi}|^2}{T} \left(\frac{k_m}{4} \Theta[\omega/k_m - v_s] v^2 \mathrm{F}_0(v)|_{v=\frac{\omega}{k_m}} \right. \\
&\left. + \sum_{n=n_{\min}}^{\infty} k_{2n} |C_n^m|^2 v^2 \mathrm{F}_0(v)|_{v=\frac{\omega}{k_{2n}}} \right), \quad n_{\min} = \lceil \tfrac{\omega}{k_2 v_s} \rceil
\end{aligned} \tag{2.42}$$

In the above equation $\Theta[x]$ is the step function defined as

$$\begin{aligned}
\Theta[x] &= 1, \quad x > 0, \\
&= 0, \quad x \leq 0.
\end{aligned} \tag{2.43}$$

Furthermore, $\lceil x \rceil$ is the ceiling function, defined as the greater integer between two integers which are the closest to the real number x. In Eq. (2.42), the first term on the right-hand side corresponds to the average work per unit time, performed on the passing particles in resonance with the drive potential. There is only a single resonance related to the passing particles and this resonance only can exist for frequencies $\omega > k_m v_s$.

The second term on the right-hand side of Eq. (2.42) corresponds to the averge work per unit time performed on all the trapped particles. Because of the symmetry of drive potential and the squeeze, left trap and right trap heating have the same average value. The sum is over all the different resonances between the trapped par-

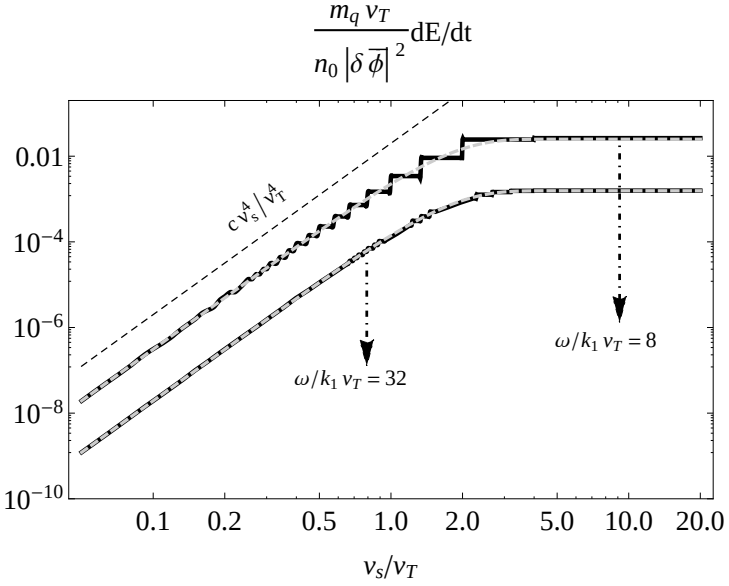

Figure 2.5: Plot of the heating of the collisionless plasma from Eq. (2.42) for large phase velocities $\omega/k_1 v_T = 8$ and $\omega/k_1 v_T = 32$, for drive mode $m = 1$. The dashed line depicts an arbitrary v_s^4/v_T^4 dependence, for comparison.

ticles and the drive potential. The reason for the presence of a series of resonances is that the potential as seen by the particles is non-sinusoidal and contains a series of harmonics which are at resonance with the drive potential at the velocities

$$v_n = \frac{\omega}{k_{2n}}, \quad n = 1, 2, \ldots \tag{2.44}$$

Above equation implies that the higher the number of resonance n, the lower are the velocities of the particles in that resonance. Moreover, the nth resonance can not exist for $v_n > v_s$, which is reflected in the plot of the heating vs v_s/v_T in Fig. (2.5): lowering v_s at a constant ω results in instant, discontinuous drops of heating, which happens each time a trapped resonance disappears at the separatrix. The lower bound of the sum is given by the highest velocity in the trapped region which is in resonance with the drive potential and is located at the velocity

$$v_{n_{\min}} = \frac{\omega}{k_{2n_{\min}}}, \tag{2.45}$$

The upper limit of the sum, which is infinity, is unphysical, since for particles with

small energies, the linear theory and unperturbed orbits approximation are no longer valid: Newton's law gives the change in particle velocity, due to work by the wave potential in one period:

$$m_q \frac{dv}{dt} = -\partial_z \delta\varphi \tag{2.46}$$

The change in the velocity of a particle in one bounce motion is given by $\delta v \approx (dv/dt)/(v/L)$. Thus, substituting $(v/L)\delta v$ for dv/dt and using $\partial_z \delta\varphi \sim k_m \delta\overline{\phi}$ in Eq. (2.46) we obtain:

$$(v/L)\delta v \approx \frac{k_m \delta\overline{\phi}}{m_q} \tag{2.47}$$

Dividing both sides of the RHS relation by v^2 will give:

$$\frac{\delta v}{v} \approx \frac{L k_m \delta\overline{\phi}/m_q}{v^2} = \frac{4\pi}{m}\frac{\omega_{NL}^2}{\omega_B^2} \tag{2.48}$$

$\omega_B = 2\pi v/L$ is the bounce frequency of the unperturbed orbit of the particle, and $\omega_{NL} = \sqrt{k_m^2 \delta\overline{\phi}/m_q}$ is the bounce frequency of a particle in the trough of the wave potential. The following condition must be satisfied for the linear treatment to be valid:

$$\frac{\omega_{NL}^2}{\omega_B^2} \ll 1 \tag{2.49}$$

Above relation states that in order for the nonlinearity to be negligible, ω_{NL} must be much smaller than the unperturbed orbit particle bounce frequency ω_B. For the nth trapped resonance we have $\omega_B = \omega/n$, and the above relation can be written as:

$$\omega_{NL}^2 \ll \omega^2/n^2 \tag{2.50}$$

At low phase velocities such that $v_{ph}/v_T \ll 1$, where v_{ph} is defined as

$$v_{ph} = \omega/k_m v_T, \tag{2.51}$$

in the heating equation (2.42) we will have $F_0 \approx 1$ and as a result, the heating equation will have the following functional form:

$$\left\langle \frac{dE}{dt} \right\rangle_t = \pi L n_0 \frac{|\delta\overline{\phi}|^2}{T} \sum_{n=1}^{\infty} k_{2n} |C_n^m|^2 v^2 F_0(v)|_{v=\frac{\omega}{k_{2n}}}. \quad \omega/k_m v_T \ll 1, \tag{2.52}$$

Therefore, in the small phase velocity limit the collisionless plasma heating is independent of the size of the squeeze (v_s).

In the high phase velocity regime $v_{ph}/v_T \gg 1$, the heating due to the passing resonance becomes exponentially small, because of the F_0 term in (2.42). However, heating of the trapped particles consists of many resonances for which F_0 is not exponentially small. As a result, trapped particle heating is finite at $v_{ph}/v_T \gg 1$. The functional from of the heating due to trapped particles at $v_{ph}/v_T \gg 1$ depends on v_s/v_T. As we can see from the Fig. (2.5) for $v_s/v_T \gg 1$ the plasma heating is independent of v_s/v_T, since plasma is practically cut in half and further raising v_s is not going to change the plasma configuration. On the other hand, in the limit $v_s/v_T \ll 1$, the sum of the large number of resonances results in a v_s^4 dependence for the plasma heating. We have derived these functional forms in appendix D, which yielded the following results:

$$\frac{dE^t}{dt} = \frac{2n_0|\delta\overline{\phi}|^2}{m_q}\sqrt{\frac{2}{\pi}}\frac{v_T}{v_{ph}^2}, \quad \frac{v_{ph}}{v_T} \gg \frac{v_s}{v_T} \gg 1 \tag{2.53}$$

$$= \frac{n_0|\delta\overline{\phi}|^2}{m_q}\sqrt{\frac{2}{\pi}}\frac{v_s^4}{4v_{ph}^2 v_T^3}, \quad \frac{v_{ph}}{v_T} \gg 1 \gg \frac{v_s}{v_T} \tag{2.54}$$

The small squeeze form of the heating in Eq. (2.54) has the same scaling with squeeze potential (proportional to φ_s^2) as in chapter 1. There, the squeeze was not assumed to be infinitesimally narrow and therefore, passing particles were also affected by the squeeze, and in fact provided the largest contribution to the wave damping. Here, we see that trapped particles dominate the heating rate when $v_{ph}/v_T \gg 1$

2.4 Collisional heating at the separatrix

In this section we will add a weak collision effect to the system. Besides our analytical solutions, we use numerical methods to verify our results. We use the grids method to solve the differential equations related to the linearized, collisional Boltzmann equation, details of which are described in section E. In a weakly collisional regime, small-angle scattering has the dominant collisional effect in scattering of particles in velocity space. In this regime the collisional effect is well described by the Fokker-Planck collision operator given by:

$$C(f)=\frac{\partial}{\partial v}\left(D(v)\frac{\partial}{\partial v}f-\frac{v}{T}f\right) \tag{2.55}$$

$D(v)$ is the velocity space diffusion coefficient, which is a function of velocity. Since the Fokker-Planck collision operator contains derivatives of f with respect to v, the effects of collisions are significant in regions where these derivatives are large. The results from the previous section indicate that at the separatrix there is a discontinuity in f and $\partial f/\partial v$. Therefore , in the vicinity of the separatrix, derivitives of f become large and collisions significantly change the distribution function. Other regions in which collisions have significant effect due to large derivatives are the resonant regions. The equilibrium distribution function satisfies the condition $C(\mathrm{F}_0)=0$. Moreover, the linearized Boltzmann equation with the Fokker-Planck collision operator describes the time evoluiton of the system:

$$\frac{\partial \delta \mathrm{f}}{\partial t}+v\frac{\partial \delta \mathrm{f}}{\partial z}-\frac{1}{m_q}\frac{\partial \delta \phi}{\partial z}\frac{\partial \mathrm{F}_0}{\partial v}=C(\delta \mathrm{f}) \tag{2.56}$$

We approximate the collision opertor by its dominant term at the separatrix:

$$C(\delta f)\approx D(v)\partial_v^2\delta f \tag{2.57}$$

Using Eqs. (2.9) and (2.10) in Eq. (2.56), for the time independent part of the linear distribution function and Eq. (2.11) for $\mathrm{F}_0(v)$ we obtain:

$$-i\omega\delta f+v\frac{\partial \delta f}{\partial z}+v\frac{\partial \delta \phi}{\partial z}\frac{\mathrm{F}_0}{T}=D(v)\partial_v^2\delta f \tag{2.58}$$

Considering that $\delta\phi(z)$ has an odd symmetry with respect to the center of plasma, the inherent symmetries of the solution to the above equation are:

$$\delta f(z,v) = -\delta f(-z,-v) \tag{2.59}$$

$$\delta f(z,v) = -\delta f(z+L,v) \tag{2.60}$$

In order to obtain a smooth and connected solution to δf at the separatrix, trapped and passing solutions must match at the separatrix $v = v_s$. We will solve for passing and trapped particles separately and match the solutions across the separatrix. Although the drive potential includes only a single harmonic drive with mode number m(see Eq. (2.6)), due to the collisions, the response of the plasma is not limited to the mth harmonic and has a series form

$$\delta f^p(z,v) = \sum_{\text{odd } m=-\infty}^{\infty} \delta f_m^p(v) e^{ik_m(z+L/2)} \tag{2.61}$$

Substituting from Eq. (2.6) in Eq. (2.58) we obtain

$$i(k_n v-\omega)\delta f_m^p + ik_m v\delta\phi_m^p \frac{\mathrm{F}_0}{T} = D(v)\frac{\partial^2\delta f_m^p}{\partial v^2} \tag{2.62}$$

For the left and right trapped particles we substituting from Eq. (2.34) in Eq. (2.56) and obtain

$$i(k_{2n} v-\omega)\delta f_n^{l,r} + ik_{2n} v\delta\phi_n^{l,r} \frac{\mathrm{F}_0}{T} = D(v)\frac{\partial^2\delta f_n^{l,r}}{\partial v^2} \tag{2.63}$$

The exact solution of these equations involve complex Airy functions and their integrals. We can use the boundary layer approximation method [6] to find local solutions to these equations at the separatrix region. In the narrow separatrix layer the functions $\delta f_n^{l,r}$ and δf_m^p are rapidly varying. whereas all of the other functions of v present in Eqs. (2.62)and (2.63) are slowly varying. We approximate all the slowly varying functions of v to be constants, with their value equal to their given value at

$v = v_s$:

$$\mathrm{F}_0(v) \approx \mathrm{F}_0(v_s) \tag{2.64}$$

$$D(v) \approx D(v_s) \tag{2.65}$$

$$(k_m v - \omega)\delta f_m^p \approx (k_m v_s - \omega)\delta f_m^p \tag{2.66}$$

$$(k_{2n} v - \omega)\delta f_n^{l,r} \approx (k_{2n} v_s - \omega)\delta f_n^{l,r} \tag{2.67}$$

In order for the approximations in Eqs. (2.66) and (2.67) to be correct, i.e. the variation of the functions $(k_m v - \omega)$ and $(k_{2n} v - \omega)$ to be small compared to their value at the separatrix, the resonant regions for which $v_n \approx \omega/k_{2n}$ for trapped, and $v_m \approx \omega/k_m$ for passing region, must be far from the sparatrix layer. Hence, the following condition must be satisfied:

$$\Delta_n^{\mathrm{res}} + \Delta_n^s \ll |v - \omega/k_n| \tag{2.68}$$

where Δ_n^s is the width of the separatrix layer and Δ_n^{res} is the width of nth resonance. In the collisionless theory resonances are singularities in the velocity space and have zero width. However, introducing collisions into the system broadens these resonances and we represent the width of the nth resonance with Δ_n^{res}. Equation (2.68) dictates the condition that the resonance regions and the separatrix layer must not overlap. In other words, regions of rapid variation of the solutions must be isolated. The boundary layer approximated differential equation for the passing region is given by

$$i(k_m v_s - \omega)\delta f_m^p + i k_m v \delta \phi_m^p \frac{F_0(v_s)}{T} = D(v_s)\frac{\partial^2 \delta f_m^p}{\partial v^2} \tag{2.69}$$

This equation has a particular solution which is given by

$$\delta f_m^p = \frac{\delta \phi_m^p v_s \mathrm{F}_0(v_s)/T}{\omega/k_m - v_s} \tag{2.70}$$

This solution corresponds to the collisionless solution (2.32), evaluated at the spara-

trix $v = v_s$. The homogeneous solutions to Eq. (2.69) are given by

$$\delta f_m^p = \delta \phi_m^p \frac{\mathrm{F}_0(v_s)}{T} a_m^{\pm} \exp[\pm i^{3/2} \sqrt{(\omega - k_m v_s)/D}(v - v_s)] \tag{2.71}$$

Since we expect the solutions to stay finite as $v \to +\infty$, the only acceptable solution for the passing region will be the plus sign and we take $a_m^+ = a_m$. Using Eqs. (2.70) and (2.71), the total solution inside the separatrix layer is given by

$$y_{\mathrm{in}}(v) = \frac{\delta \phi_m^p v_s \mathrm{F}_0(v_s)/T}{\omega/k_m - v_s} + \delta \phi_m^p \frac{\mathrm{F}_0(v_s)}{T} a_m \exp[i^{3/2} \sqrt{(\omega - k_m v_s)/D}(v - v_s)], \tag{2.72}$$

which has an undetermined coefficient, a_m. These coefficients, together with all the other undetermined coefficients from the trapped region, will be determined from matching the boundary values at the separatrix. The first term on the right hand-side is the contribution from the collisionless system. The second term on the right-hand side is the perturbation to the collisionless solution, due to the effect of collisions. This solution falls to zero rapidly in a region with a thickness approximately given by

$$\Delta_m^s = \sqrt{2D/(\omega - k_m v_s)}, \tag{2.73}$$

which is the inverse of the coefficient of real part of the exponent in Eq. (2.72).

The boundary layer, which is characterized by the rapid variation of solutions, connects to the outer region. In the outer region, the solution to Eq. (2.62) varies slowly and the derivatives of δf_m^p are small. Since the system is weakly collisional and $D(v)$ is small, we can take $D(v)\partial^2 \delta f / \partial v^2 \approx 0$ in the outer region. As the result of this approximation, the outer region solution to Eq. (2.62) will be:

$$y_{\mathrm{out}}(v) = \frac{\delta \phi_m^p v \mathrm{F}_0(v)/T}{\omega/k_m - v}, \tag{2.74}$$

which is identical to collisionless solution in Eq. (2.32). So far we have the solution for δf_m^p inside the boundary layer given by equation Eq. (2.72), which we called $y_{\mathrm{in}}(v)$, and the solution for the outer region, given by Eq. (2.74), which we called $y_{\mathrm{out}}(v)$. In order to connect these to solutions and obtain a uniform solution over v, we compare the asymptotic form of $y_{\mathrm{in}}(v)$ and $y_{\mathrm{out}}(v)$ to obtain a solution describing

the middle region, i.e. between outer and inner solutions:

$$\lim_{v\to\infty} y_{\text{in}}(v) = \frac{\delta\phi^p_m v_s \mathrm{F}_0(v_s)/T}{\omega/k_m - v_s} \qquad (2.75)$$
$$\lim_{v\to v_s} y_{\text{out}}(v) = \frac{\delta\phi^p_m v_s \mathrm{F}_0(v_s)/T}{\omega/k_m - v_s}$$

Therefore, we take the middle region solution to be:

$$y_{\text{mid}}(v) = \frac{\delta\phi^p_m v_s \mathrm{F}_0(v_s)/T}{\omega/k_m - v_s} \qquad (2.76)$$

We can define a uniform solution as follows:

$$y_{\text{uniform}}(v) = y_{\text{in}}(v) + y_{\text{out}}(v) - y_{\text{mid}}(v) \qquad (2.77)$$

Substituting from Eqs. (2.72), (2.74) and (2.76) into Eq. (2.77), we obtain a uniform solution for δf^p_m:

$$\delta f^p_m(v) = \frac{\delta\phi^p_m v \mathrm{F}_0(v)/T}{\omega/k_m - v} + \delta\phi^p_m \frac{\mathrm{F}_0(v_s)}{T} a_m \exp[i^{3/2}\sqrt{(\omega - k_m v_s)/D}(v - v_s)] \qquad (2.78)$$

As the effect of collisions become weaker, D decreases and the boundary layer shrinks. In the limit where D goes to zero, the boundary layer vanishes and we retrieve the collisionless solution at separatrix from the first term in Eq. (2.78).

Following the steps taken for the passing region, a uniform boundary layer solution to Eq. (2.68) for the left trapped particles is given by

$$\delta f^l_n = \frac{\delta\phi^l_n v \mathrm{F}_0(v)/T}{\omega/k_{2n} - v} + \delta\phi^l_n \frac{\mathrm{F}_0(v_s)}{T} b_n \exp[-i^{3/2}\sqrt{(\omega - k_{2n} v_s)/D}(v - v_s)] \qquad (2.79)$$

The first term on the right hand side is the collisionless solution and the second term is the correction due to collisions and we took the negative sign in order for the solution to stay finite as $v \to 0$. b_n is the undetermined coefficient which must be determined by matching the solutions at the separatrix. Due to symmetry, the right trap solutions are redundant and contain no extra information. Boundary thickness

for the nth trapped Fourier component is defined as

$$\Delta_{2n}^{s} = \sqrt{2D/(\omega - k_{2n} v_s)} \tag{2.80}$$

As was the case for the passing solutions, boundary thickness, which is proportional to $\sqrt{D}$, vanishes as D goes to zero and the collisionless solution will be retrieved. Therefore in the presence of weak collisions, separatrix is surrounded by a layer of width proportional to $\sqrt{D}$ from both above and bellow v_s. In this *separatrix layer* δf rapidly changes from the passing to the trapped side of the separatrix.

2.4.1 Matching the boundary solutions at separatrix

By matching the solutions obtained for trapped and passing distribution functions, we obtain a uniform solution over the whole separatrix region in (z, v) phase-space. Passing distribution has the functional form given by Eq. (2.29) with δf_m^p given by Eq. (2.78). We expand the functions $e^{ik_m(z+L/2)}$ in terms of the complete set of functions $e^{ik_{2n}z}$ which have L periodicity:

$$\begin{aligned} e^{ik_m(z+L/2)} &= \sum_{n=-\infty}^{\infty} l_n^m e^{ik_{2n}z}, \quad l_n^m = \frac{1}{L}\int_{-L}^{0} e^{i(k_m - k_{2n})z} dz \\ l_n^m &= \frac{\sin\frac{m\pi}{2}}{\pi(n - m/2)}, \text{ m odd} \end{aligned} \tag{2.81}$$

As a result, we can rewrite the passing distribution given in Eq. (2.61) as

$$\delta f^p(z, v) = \sum_{n=-\infty}^{\infty} \left(\sum_{\text{odd } m=-\infty}^{\infty} l_n^m \delta f_m^p \right) e^{ik_{2n}z} \tag{2.82}$$

Comparing the above equation to Eq. (2.34), the matching conditions at the separatrix for the left half of the plasma are given by

$$\begin{pmatrix} \delta f_n^l(v_s) \\ \\ \frac{\partial \delta f_n^l(v_s)}{\partial v} \end{pmatrix} = \sum_{\text{odd } m=-\infty}^{\infty} l_n^m \begin{pmatrix} \delta f_m^p(v_s) \\ \\ \frac{\partial \delta f_m^p(v_s)}{\partial v} \end{pmatrix} \tag{2.83}$$

For the right half of plasma we use the symmetry relation Eq. (2.59), instead of matching the solutions, to obtain the uniform solution over the separatrix. We substiture the boundary layer solutions, Eq. (2.79) for δf_n^l and Eq. (2.72) for δf_m^p, in the sets of equations in Eq. (2.83) and solve them to determine the unknown coefficients, a_n's(trapped) and b_m's(passing). a_n's and b_m's are only functions of $\omega/k_m v_s$, since we factored out their dependence on T which was of the form $\mathrm{F}_0(v_s)/T$. For the purpose of practicality we need to truncate the infinite series in order to evaluate the unknown coefficients. For M number of terms kept in the trapped side there are $2M$ equations and we need to keep M terms on the passing side. Keeping more number of terms results in smoother solutions.

Using Mathematica, we solve for the unknown coefficients a_m's and b_n's. Figure (2.6) compares the contour plots of the time independent part of the distribution function δf in the vicinity of the separatrix $v \sim v_s$ over the (z, v) phase-space, for mode $m = 1$ drive potential, with $v_T/v_s = 1.73, \omega/k_1 v_s = 0.8$ and two values of diffusion constant $D_1 L/v_s^3 = 2\times 10^{-4}$ and $D_2 L/v_s^3 = 5\times 10^{-5}$, $(D_1 = 4D_2)$. $M = 101$ terms are kept for trapped particles $(n = -50, -49, \ldots, 49, 50)$ and $M = 101$ for passing $(m = -101, -99, \ldots, 97, 99)$ in the matching Eqs. (2.83). In Fig. (2.7), $\delta f(z, v)$ is plotted near the separatrix, at the left end of plasma $z = -L/2$, for the same parameters as Fig. (2.6). The results from the numerical grids method are plotted in diamonds. The dashed curve shows the δf from the collisionless theroy. Width of the separatrix layer for the plots related to D_2 is approximately 2 times larger than the width of the separatrix layer in the plots related to D_1, which implies the $\sqrt{D}$ dependence of the width of the separatirx layer.

In the collisionless regime $\mathrm{Re}\delta f(z, v)$ at separatrix has an odd symmetry, and so does the drive potential, when resonances are away from separatrix. The drive force, on the other hand, has an even symmetry and is out of phase with $\mathrm{Re}[\delta f/\delta\overline{\phi}]$. Thus, the total work on the particles in the separatrix region is zero, since the forcing and $\mathrm{Re}[\delta f/\delta\overline{\phi}]$ are spatially orthogonal. Because of the collisions, which cause diffusion in velocity space and change the solutions particularly at the separatrix region, $\mathrm{Re}[\delta f/\delta\overline{\phi}]$ in the separatrix layer will develop a term with an even symmetry, which is in phase with the external forcing. This results in a non-zero time-averaged

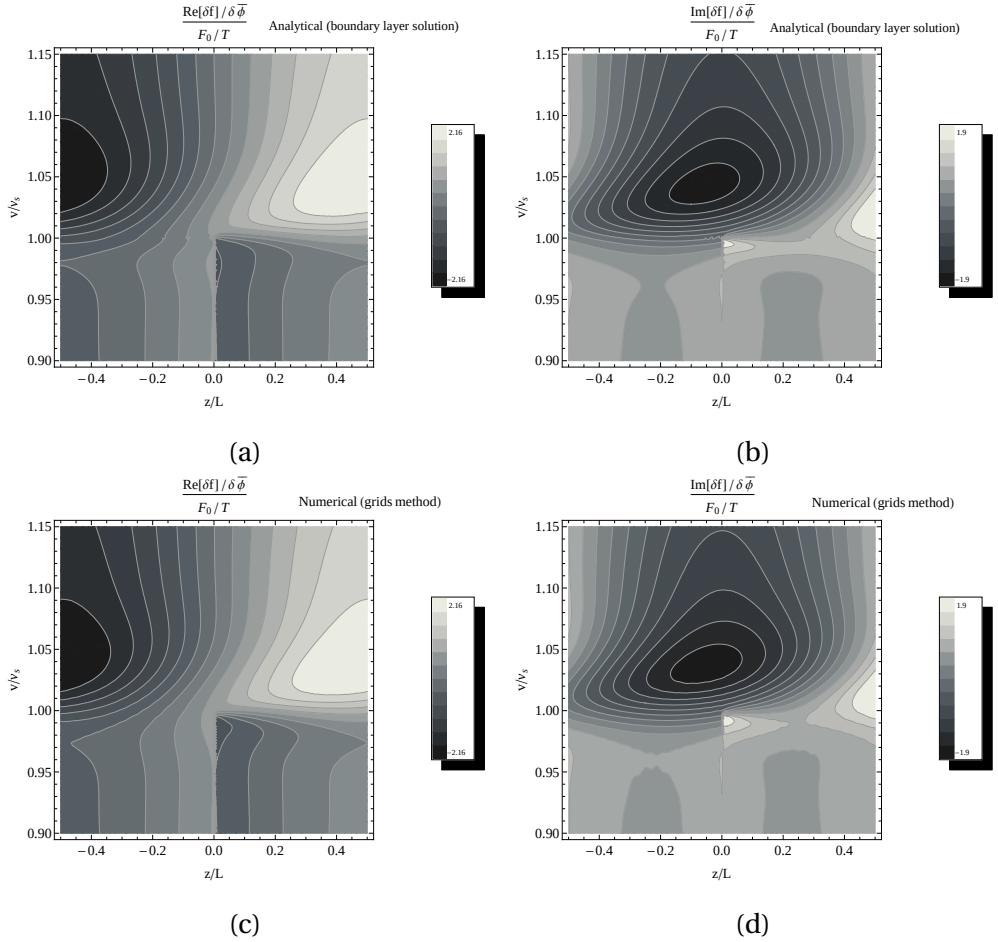

Figure 2.6: Contour plots of the real and imaginary part of δf in the z, v phase-space, near the separatrix ($v/v_s \approx 1$), for $v_T/v_s = 1.73$ and for diffusion coefficient $DL/v_s^3 = 2 \times 10^{-4}$. Plots (2.6a) and (2.6b) are obtained from the analytical boundary layer method and plots (2.6a) and (2.6b) are obtained from the numerical grids method.

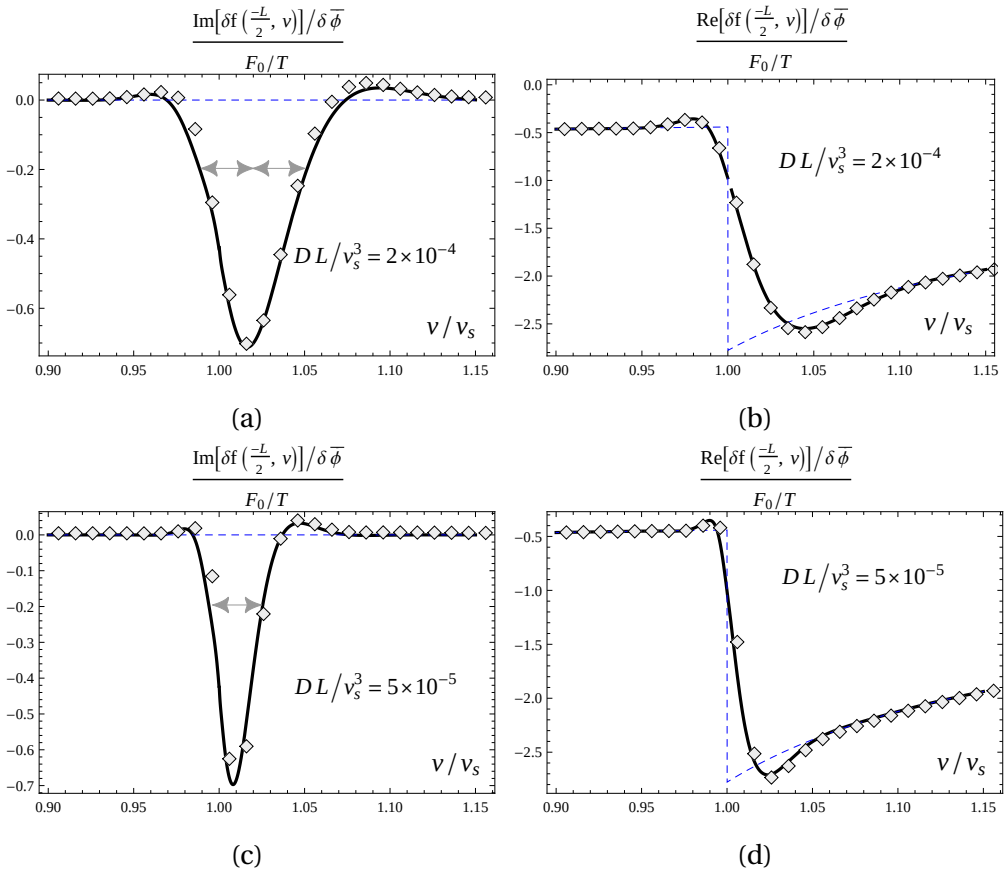

Figure 2.7: Plots of the real and imaginary part of δf as a function of v/v_s near the separatrix ($v/v_s \approx 1$), at the left end od plasma $z = -L/2$, for $v_T/v_s = 1.73$ and for diffusion coefficient given by a)$DL/v_s^3 = 2\times10^{-4}$ and b)$DL/v_s^3 = 5\times10^{-5}$. Solid curves are obtained analytically via the boundary layer method. Dashed lines are the collisionless solutions. Numerical grids method results are depicted in diamonds. Double-headed arrows show the width of separatrix layer.

work on the particles in the separatrix layer.

Now that the undetermined coefficient in Eqs. (2.72) and (2.79) are solved for by matching the boundary conditions, we have obtained the collisional δf_m^p and δf_n^l and we can calculate the heating at separatrix. For small enough D, away from resonances, separatrix layer can be considered as an isolated region in which δf has nontrivial solutions. Heating in separatrix can be calculated independently and added to the resonant heating in other parts of phase-space to get the total heating. We substitute the solved collisional δf_n's in the average heating equation (2.42) and perform the integrals. At $v \approx v_s$, the first term of δf_m^p and δf_n^l, given by Eqs. (2.78) and (2.79) are purely real and give the collisionless solutions. As a result, they do not contribute to heating integrals. The second term which is the collisional correction to δf_m^p and δf_n^l has nonzero value in the integral which is equal to:

$$\frac{dE_{\rm sep}^p}{dt} = n_0 L \sum_{m=-\infty}^{\infty} k_m \mathrm{F}_0(v_s) \frac{|\delta\overline{\phi}|^2}{T} \mathrm{Re}\left(a_m \left[-v_s i^{-1/2} \sqrt{\frac{D}{\omega - k_m v_s}} + i^{-2} \frac{D}{\omega - k_m v_s} \right] \right), \tag{2.84}$$

for the passing side of separatrix layer, and

$$\frac{dE_{\rm sep}^t}{dt} = 2 n_0 L \sum_{n=-\infty}^{\infty} k_{2n} (C_n^l)^2 \mathrm{F}_0(v_s) \frac{|\delta\overline{\phi}|^2}{T} \mathrm{Re}\left(b_n \left[v_s i^{-1/2} \sqrt{\frac{D}{\omega - k_{2n} v_s}} - i^{-2} \frac{D}{\omega - k_{2n} v_s} \right] \right), \tag{2.85}$$

for the trapped side of separatrix, which is written in terms of 2 times the left heating due to symmetry. In evaluation of Eq. (2.85), the limits of integration was from zero to v_s, but the lower limit of integral has been taken to be $-\infty$, since δf falls to zero on the scale of separatrix layer thickness which is much smaller than v_s. The total heating in the separatrix layer is subsequently equal to the sum of the heating in the passing (Eq. (2.84)) and trapped (Eq. (2.85)) side of the separatrix:

$$\frac{dE_{\rm sep}}{dt} = \frac{dE_{\rm sep}^p}{dt} + \frac{dE_{\rm sep}^t}{dt} \tag{2.86}$$

Although weak collisions broaden the resonance regions, the change in resonant heating due to these weak collisions is negligible. As a result the total heating of the plasma is the sum of the separatrix heating and the collisionless resonant heating

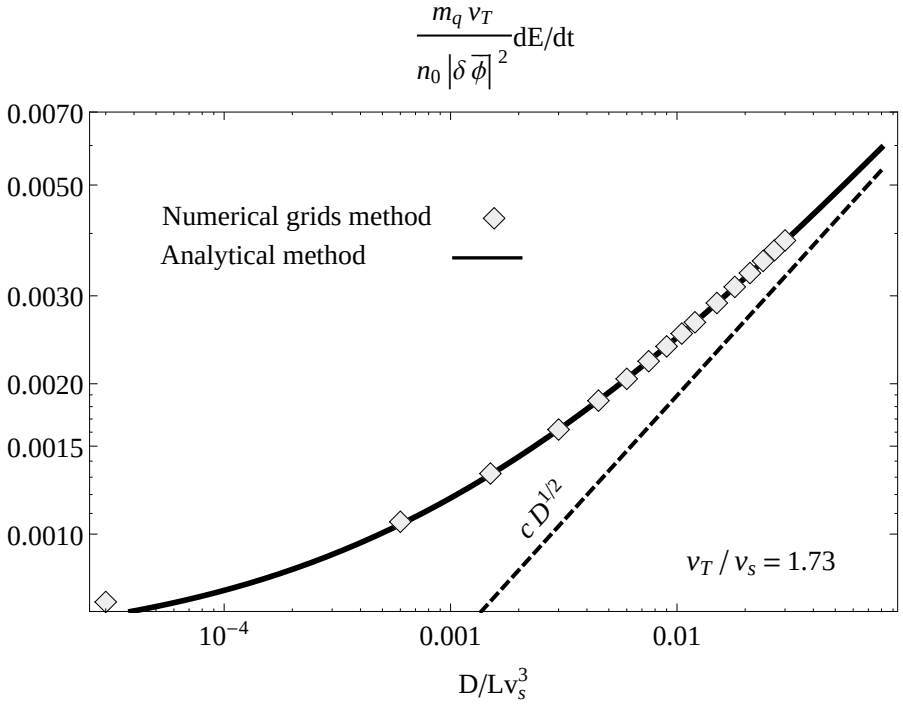

Figure 2.8: Heating per unit time versus the diffusion coefficient D, for $v_T/v_s = 1.73$ and $\omega/k_1 v_s = 0.2$ and for drive mode $m = 1$.

obtained in Eq. (2.42).

In figure (2.8), dE/dt is plotted versus the diffusion coefficient D, for $v_T/v_s = 1.73$ and $\omega/k_1 v_s = 0.2$ and for drive mode $m = 1$. At this frequency the resonances are far from the separatrix and therefore, the separatrix layer is isolated, thus theory is expected to work well. The results obtained from the numerical grids method are depicted in diamonds and the analytically obtained heating is depicted in a solid curve. As $D \to 0$ the value of the dE/dt tends to the collisionless heating obtained from Eq. (2.42). In the limit where $D \to 0$, the separatrix layer vanishes and the heating tends to the collisionless result. Furthermore, as D grows the heating at the separatrix layer dominates which has $\sqrt{D}$ dependence.

Figure (2.9) depicts the heating versus the drive frequency ω. Heating for a collisionles plasma ($D = 0$) is depicted in a dash-dotted and evaluated using Eq. (2.42). The collisional heating result is obtained from the numerical grids method and depicted in a solid curve for $D = 1.5 \times 10^{-3}$, and a dashed curve for $D = 6 \times 10^{-3}$. The collisionless heating is discontinuous for two values of frequency. At $\omega/k_1 v_s = 1$

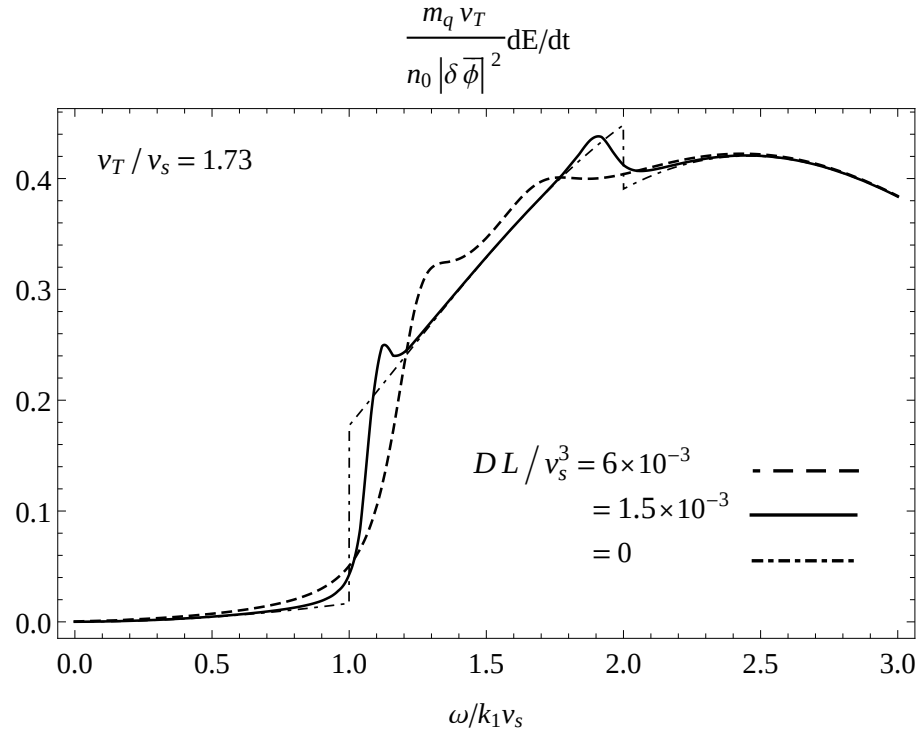

Figure 2.9: Heating per unit time as a function of ω, obtained from numerical grids method for $D = 1.5\times10^{-3}$, and $D = 6\times10^{-3}$, and obtained from Eq. (2.42) for $D = 0$.

the passing resonance appears at the separatrix velocity v_s, which causes a discontinuous jump in the collisionless heating curve. At $\omega/k_1 v_s = 2$ the $n = 1$ trapped resonance disappears at the separatrix and this causes a sudden drop at in the collisionless heating curve. In the presence of collisions, the added heating at the separatrix connects and smooths out these discontinuities, as we can see from the plots related to $D = 1.5\times10^{-3}$ and $D = 6\times10^{-3}$.

In figures (2.10a) and (2.10b) we compare the heating obtained from the analytical boundary layer method and depicted in diamonds, to the numerical grids method results dipcted in solid curves, for the same parameters as Fig. (2.9). For the smaller value of D we have a better agreement between the two methods. Furthermore, we can see that as the frequencies approach resonance, at $\omega/k_1 v_s = 1$ in Fig. (2.10a) and at $\omega/k_1 v_s = 2$ in Fig. (2.10b), the analytical results deviate from the numerical results, since the separatrix layer and resonance regions are overlapping the boundary layer theory is no longer valid.

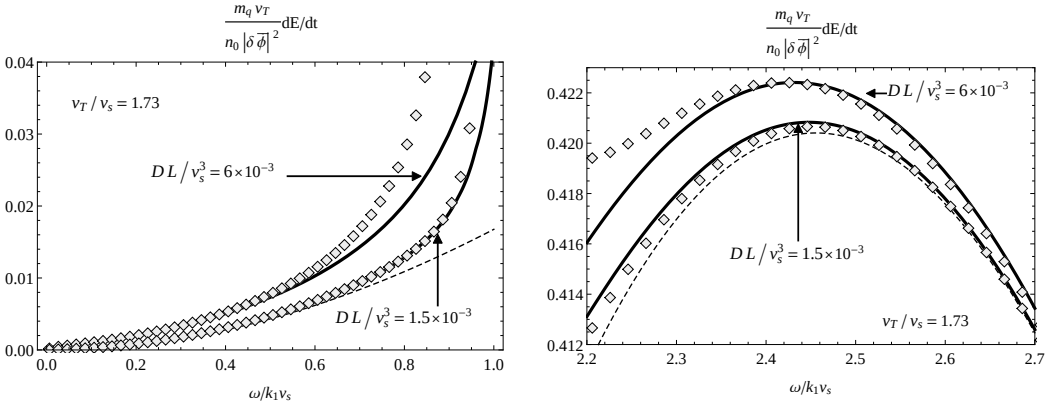

Figure 2.10: Heating per unit time as a function of ω. The results from the analytical boundary layer method are depcted in diamonds. The numerical grids method results are dipcted in solid curves.

Figure (2.11) depicts the heating versus the larger values of the drive frequency ω. At large values of $\omega/k_m v_T$ the discontinuity in the distribution function between the trapped and passing regions becomes small and as a result the collisional heating due to the separatrix is not a large effect. Instead, collisions simply smooth out the steps in the heating rate caused by the disappearance of resonances in the trapped particle distribution as ω increases. For large wave phase velocities, passing and trapped particles near the separatrix energy have nearly the same response to the wave, so the separatrix discontinuity is small and not important to the wave heating. This is as opposed to small wave phase velocities, where there is a large discontinuity in the distribution function at the separatrix and hence a dominant collisional separatrix heating effect.

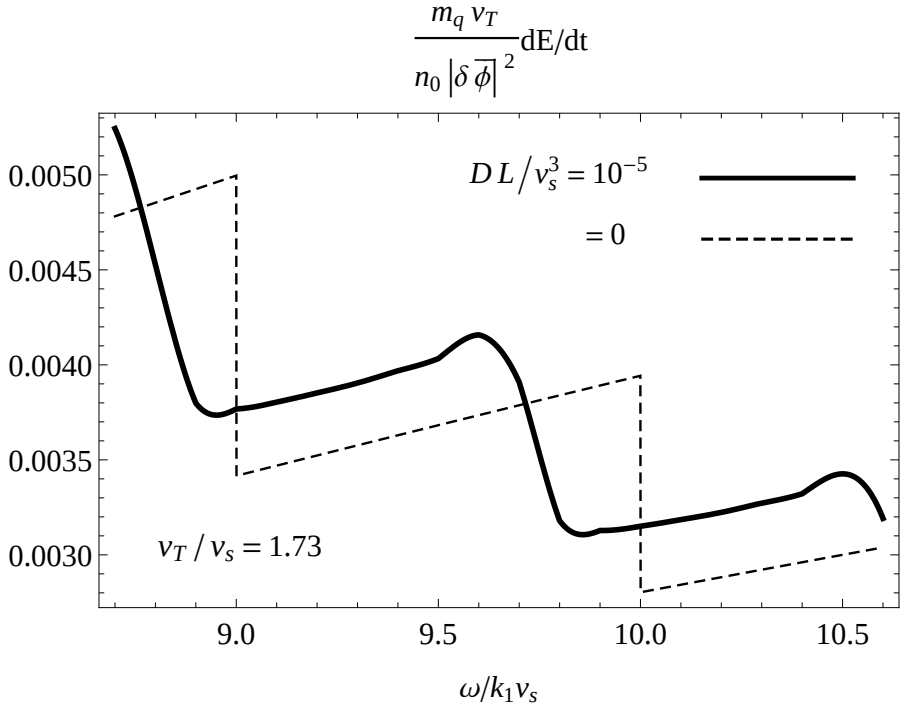

Figure 2.11: Heating per unit time as a function of ω.

2.5 Resonance broadening due to collisions

In this section we study the effect of adding weak collisions, in the form of a Fokker-Planck collision operator, on the plasma distribution function, in the regions of phase-space where are in resonance with the drive potential in the collisionless system. We show that collisions will broaden the resonance regions, which were singularities in the velocity space of the collisionless plasma. Width of these resonance regions has as $D^{1/3}$ dependence, which is the characteristic of Airy functions close to zero of their arguments (also known as the turning points).

We approximate the Fokker-Planck collision operator by its dominant term (see Eq. (2.57)). For the passing region, substituting from Eq. (2.32) in Eq. (2.58), for the nth Fourier component we obtain:

$$i(k_m v-\omega)\delta f_m^p + i k_m \delta\phi_m^p v \frac{\mathrm{F}_0(v)}{T} = D\frac{\partial^2 \delta f_m^p}{\partial v^2} \tag{2.87}$$

We take $\delta f_m^p(v) = \delta\psi_m^p(v) + \delta\chi_m^p(v)$, such that they satisfy the following equations:

$$i(k_m v - \omega)\delta\chi_m^p + i k_m \delta\phi_m^p v \frac{\mathrm{F}_0(v)}{T} = D\frac{\partial^2 \delta\chi_n^p}{\partial v^2} \tag{2.88}$$

$$i(k_m v - \omega)\delta\psi_m^p = D\frac{\partial^2 \delta\psi_n^p}{\partial v^2} \tag{2.89}$$

For the trapped region we substitute from Eq. (2.34) in Eq. (2.61) and we take $\delta f_n^l(v) = \delta\psi_n^l(v) + \delta\chi_n^l(v)$ we obtain

$$i(k_{2n} v - \omega)\delta\chi_n^l + i k_{2n} \delta\phi_n^l v \frac{\mathrm{F}_0(v)}{T} = D\frac{\partial^2 \delta\chi_n^l}{\partial v^2} \tag{2.90}$$

$$i(k_{2n} v - \omega)\delta\psi_n^l = D\frac{\partial^2 \delta\psi_n^l}{\partial v^2} \tag{2.91}$$

$\delta\chi_n^l(v)$ and $\delta\chi_m^p(v)$ are the particular solutions and will take care of the source terms in the differential Eqs. (2.62) and (2.63). $\delta\psi_n^l(v)$ and $\delta\psi_m^p(v)$ are the homogeneous solutions and connect the trapped and passing solutions at the separatrix. The boundary conditions for $\chi_n^l(v)$ and $\chi_m^p(v)$ are such that $\chi_m^p(v)$, $\chi_n^l(v) \to 0$ as $v \to \pm\infty$. The Green's function $g_n^t(v, v_0)$ fo the differential equation in Eq. (2.90) satisfies:

$$i(\omega - k_{2n} v) g_n^t(v, v_0) + D\frac{\partial^2 g_n^t(v, v_0)}{\partial v^2} = \delta(v - v_0) \tag{2.92}$$

with boundary conditions given by

$$\lim_{v \to \pm\infty} g_n^t(v, v_0) \to 0 \tag{2.93}$$

For $v \neq v_0$, the value of the Dirac delta function on the right-hand side of the Eq. (2.92) is equal to zero. Considering the boundary conditions given by Eq. (2.93), the Green's function should be of the form:

$$g_n^t(v, v_0) = \begin{cases} C_+ \mathrm{ai}_{2n}(v) & v > v_0 \\ C_- \mathrm{bi}_{2n}(v) & v < v_0 \end{cases}, \tag{2.94}$$

where the functions $\mathrm{ai}_n(v)$ and $\mathrm{bi}_n(v)$ are defined as

$$\begin{aligned} \mathrm{ai}_n(v) &= \mathrm{Ai}((v-v_n)/\alpha_n) && (2.95)\\ \mathrm{bi}_n(v) &= \mathrm{Ai}\Big(e^{\mathrm{sign}(n)i2\pi/3}(v-v_n)/\alpha_n\Big) && (2.96)\\ \alpha_n &= (D/ik_n)^{1/3} && (2.97)\\ v_n &= \omega/k_{2n} && (2.98) \end{aligned}$$

Constants C_+ and C_- are determined by matching two parts of the piece-wise function Eq. (2.94) at $v = v_0$.

In general, a pair of the Airy function $\mathrm{Ai}(z)$ with any of the Airy functions $\mathrm{Bi}(z)$, $\mathrm{Ai}(ze^{2\pi/3})$ or $\mathrm{Ai}(ze^{-2\pi/3})$ are linearly independent solutions of complex Airy equation [2]. We have constructed the functions $\mathrm{ai}_n(v)$ and $\mathrm{bi}_n(v)$ in such a way that they are linearly independent, $\mathrm{ai}_n(v)$ falls to zero as $v \to +\infty$ and $\mathrm{bi}_n(v)$ falls to zero as $v \to -\infty$. From matching the values of the piecewise form of $g_n^t(v, v_0)$ in Eq. (2.94) at $v = v_0$ we get

$$C_+\mathrm{ai}_{2n}(v_0) = C_-\mathrm{bi}_{2n}(v_0) \tag{2.99}$$

Furthermore, integrating Eq. (2.92) over v, with Green's function replaced by Eq. (2.94) yields

$$D\left(C_+\frac{\partial\,\mathrm{ai}_{2n}(v)}{\partial v}\bigg|_{v_0} - C_-\frac{\partial\,\mathrm{bi}_{2n}(v)}{\partial v}\bigg|_{v_0}\right) = 1 \tag{2.100}$$

From Eqs. (2.99) and (2.100) we determine C_+ and C_-. As a result the Green's function is given by

$$g_n^t(v, v_0) = \begin{cases} \frac{-\mathrm{ai}_{2n}(v)\mathrm{bi}_{2n}(v_0)}{DW_{2n}(v_0)} & v > v_0 \\ -\frac{\mathrm{bi}_{2n}(v)\mathrm{ai}_{2n}(v_0)}{DW_{2n}(v_0)} & v < v_0 \end{cases} \tag{2.101}$$

Wronskian $W_n(v)$ is independent of v and is defined as

$$\begin{aligned} W_n &= \mathrm{ai}_n(v)\mathrm{bi}_n'(v) - \mathrm{ai}_n'(v)\mathrm{bi}_n(v) \\ &= \frac{e^{-i\mathrm{sign}(n)\pi/6}}{2\pi\alpha_n} \end{aligned} \tag{2.102}$$

Finally, we obtain $\delta\chi_n^l$ using the Green's function:

$$\delta\chi_n^l(v) = ik_{2n}\frac{\delta\phi_n^l}{T}\int_{-\infty}^{\infty} g_n^t(v,v_0)v_0\mathrm{F}_0(v_0)dv_0 \tag{2.103}$$

Similarly for passing equations Green's function is:

$$g_m^p(v,v_0) = \begin{cases} \frac{-\mathrm{ai}_m(v)\mathrm{bi}_m(v_0)}{DW_m(v_0)} & v > v_0 \\ -\frac{\mathrm{bi}_m(v)\mathrm{ai}_m(v_0)}{DW_m(v_0)} & v < v_0 \end{cases} \tag{2.104}$$

The particular solution, $\delta\chi_m^p$, is given by:

$$\delta\chi_m^p(v) = ik_m\frac{\delta\phi_m^p}{T}\int_{-\infty}^{\infty} g_m^p(v,v_0)v_0\mathrm{F}_0(v_0)dv_0. \tag{2.105}$$

In the limit where $D\to 0$ the particular solutions $\delta\chi_m^p$ and $\delta\chi_n^l$ will tend to the collisionless linear solutions given by Eqs. (2.32) and (2.37). Therefore, in this limit we expect the imaginary parts of $\delta\chi_m^p/\delta\overline{\phi}$ and $\delta\chi_n^l/\delta\overline{\phi}$ to become proportional to the Dirac delta function, located at the turning points.

Fig. (2.12) depicts the imaginary parts of δf as a function of v/v_s at the $n=1$ trapped resonance region around $v_1=\omega/k_2$, for $v_1/v_s=0.4$, $v_T/v_s=2$, at the left end of the plasma $z=-L/2$, for diffusion coefficients given by $D_1L/v_s^3=5\times10^{-5}$ in Fig (2.12a) and $D_2L/v_s^3=6.25\times10^{-6}$ in Fig. (2.12b), which is 8 times smaller than the diffusion constant of Fig. (2.12a)). The solid curve depicts the analytical result from Eq. (2.103). The width of the δf, which we take to be the width of the function at half of its maximum, is approximately 2 times larger for D_1 than D_2. This behavior is consistent with $D^{1/3}$ dependence of the resonance width. Furthermore, we see that the peak value for Fig. (2.12b) is approximately 2 times larger than that of Fig. (2.12a). Further decreasing the value of D will result in further narrowing and peaking.

The homogeneous solutions ψ_m^p's and ψ_n^l's will connect and smooth out the solutions at the separatrix, by using the matching equations (2.83). The independent homogeneous functions in the passing region ($v>v_s$) are $\mathrm{ai}_n(v)$ and $\mathrm{bi}_n(v)$. Since we want the solutions to remain finite, only $\mathrm{ai}_n(v)$ is permissible for $v>v_s$. Furthermore $\psi_n^p(v)$ should be finite for $v<0$, therefore only $\mathrm{bi}_n(v)$ is acceptable for

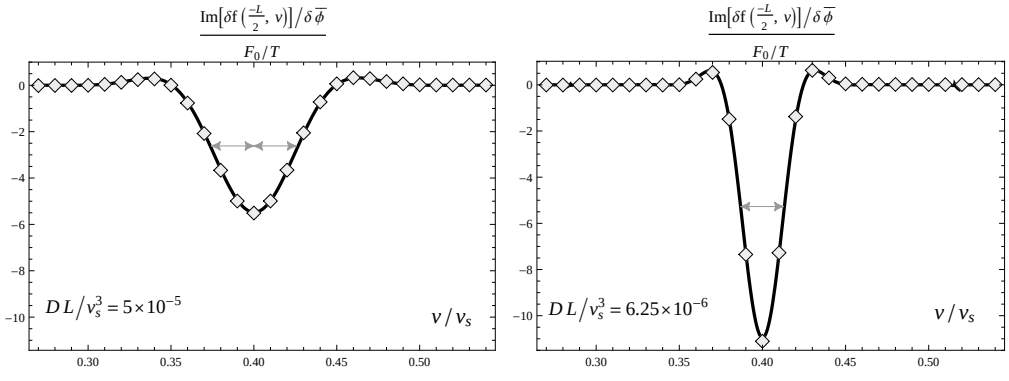

(a) (b)

Figure 2.12: Plots of the imaginary parts of δf as a fuction of v/v_s at the $n=1$ trapped resonance region around $v_1=\omega/k_2$, for $v_1/v_s=0.4$, $v_T/v_s=1.73$, at the left end of the plasma $z=-L/2$, for diffusion coefficients given by $DL/v_s^3=5\times10^{-5}$ in Fig (2.12a) and $DL/v_s^3=6.25\times10^{-6}$ in Fig. (2.12b), which is 8 times smaller than the diffusion constant of Fig. (2.12a)). Solid curves are obtained analytically. Numerical grids method results are depicted in diamonds. Double-headed arrows show the width of the resonance region.

$v<v_s$:

$$\psi_n^p(v)=\begin{cases} a_n \mathrm{ai}_n(v) & v>v_s \\ \\ d_n \mathrm{bi}_n(v) & v<-v_s \end{cases}, \tag{2.106}$$

However, in the left trap we have a combination of ascending and descending solutions:

$$\psi_n^l(v)=b_n \mathrm{bi}_{2n}(v)+c_n \mathrm{ai}_{2n}(v), \quad -v_s<v<v_s. \tag{2.107}$$

From (2.95), The function $\mathrm{ai}_n(v)$ is finite around the zero of Airy function Ai's argument, which is located at $v=\omega/k_n$ and falls to zero on a scale of $|\alpha_n|$. Thus, in the special case where the resonances ($v=\omega/k_{2n}$) are far from separatrix at v_s, i.e. $|v_s-\omega/k_{2n}|>>|\alpha_n|$, at the separatrix we will have $\mathrm{ai}_{2n}(v_s)\approx 0$ and thus, Eq. (2.107) will become:

$$\psi_n^l(v)\approx b_n \mathrm{bi}_{2n}(v);\ v\approx v_s \tag{2.108}$$

For an isolated separatrix layer (where the resonances away from separatrix), we can

use the asymptotic series form of Airy function(with $\xi = 2/3z^{3/2}$):

$$\mathrm{Ai}(z) \sim \frac{e^{-\xi}}{z^4} \tag{2.109}$$

For the passing region, from Eq. (2.95), substituting z with $(ik_n/D)^{1/3}(v-\omega/k_n)$ we see that for large z, since the exponential varies much faster than $z^{-1/4}$, in the separatrix region we approximate:

$$\mathrm{ai}_n(v) = \mathrm{Ai}(z) \sim e^{-\xi}, \quad v \geq v_s \tag{2.110}$$

Now series expanding the exponenet $-\xi$ to the first order in $v - v_s$ we obtain

$$\mathrm{ai}_n(z) \sim e^{i^3/2\sqrt{(\omega k_n - v_s)/D}(v-v_s)}, \quad v \geq v_s \tag{2.111}$$

This solution is equivalent to the approximate solution we obtained in from the boundary layer method. Therefore, away from resonances, the local scaling of the solutions and thickness of separatrix layer is proportional to $\sqrt{D}$.

2.6 Summary

We presented a 1D model of a finite length plasma with its population divided in its equilibrium state in the velocity space, to passing particles $v > v_s$ and trapped particles $v < v_s$ by a squeeze, an infinitesimally narrow kinetic barriers of finite amplitude $\varphi_s = \frac{1}{2}v_s^2$. We apply a standing sinusoidal drive potential of odd symmetry with respect to the center of plasma. Passing and trapped particles experience different potentials along their unperturbed orbits. The response of the trapped particles to the external drive is non-sinusoidal and contains higher harmonics while passing particles are unaffected by the squeeze. Different dynamics for passing and trapped regions has the following results:
i)The drive potential performs non-zero average work on the resonant particles due to the series of higher harmonics in the trapped region at bounce frequencies $\omega_b(E_n) = \omega/n$. In the regime where $v_{ph}/v_T \gg 1$ and the resonant heating in the passing re-

gion is exponentially small, the sum of all of these resonant contributions results in a finite heating in plasma.

ii)Due to different dynamics, passing and trapped distributions are discontinuous at the separatrix ($v = v_s$). Adding a weak collisions in the form of a Fokker-Planck collision operator results in large correctional terms at the separatrix which stem from large velocity derivatives resulting from the discontinuity at $v = v_s$. These corrections connect and smooth out the solutions at the separatrix. Furthermore, the drive potential performs nonzero work in the separatrix layer which can add large contributions to the heating, scaling as $\sqrt{D}$, in the regime where $\omega/k_1 v_s \leq 1$ (where D is the velocity diffusion coefficient). However, when $\omega/k_1 v_s \gg 1$ the discontinuity at the separatrix becomes small and collisionless damping due to Landau resonances caused by the squeeze is the dominant effect.

Moreover, we study the effect of collisions on the resonant regions, which are singularities in the velocity space of the collisionless solutions. We observe that collisions result in broadening these resonances, such that the width of resonance regions has a $D^{1/3}$ dependence, while the heating in the resonances approximately stays constant.p

Some of the material in this Chapter is in preparation for publication. The dissertation author was the primary investigator and author of this material.

Chapter 3

Nonlinear interaction of Trivelpiece-Gould modes

3.1 Introduction

We study the weakly nonlinear wave-wave interactions between cylindrically symmetric Trivelpiece-Gould (TG) waves [40]. Due to nonlinearity, eigenmodes of the system are non-sinusoidal and their forms and eigenfrequencies are functions of the magnitude of nonlinearity. For large wave amplitudes in a long, thin and cold plasma, resonant interaction in TG waves can lead to *decay instability* [20, 31, 37] in which case a pump wave decays into two other modes.

This theory and simulation work is motivated by experiments where nonlinear TG modes in the Malmberg-Penning trap are driven by external potentials applied to the cylindrical sectors of the trap wall. Nonlinear plasma modes (Langmuir modes) have been driven in other experiments using various techniques such as beat-wave excitation (using laser beams) [21], wakefield excitation using electron beams [22] or ion beams [28], laser wakefield excitation [8] and stimulated raman scattering [41]. In the experiments that our theory describes, a strong magnetic field and the conducting cylindrical wall of the trap change the linear dispersion relation for the plasma waves, which greatly affects the nonlinear wave-wave interactions.

Plasma waves can interact with particles and with each other. Waves interact

with resonant particles which are traveling with velocities near the phase velocity $v = \omega/k$, which consequently results in the Landau damping of the TG wave. In a cold plasma for which $v_T \ll \omega/k$, plasma distribution is not populated at the phase velocity $v_{\text{ph}} = \omega/k$. Therefore there are no particles at v_{ph} to interact with the wave. As a result, the waves will be undamped on timescales smaller than the collision time.

In a 1D strong-magnetic-field model and for a cold plasma, the dynamics of the system is well described within the framework of fluid (continuity and momentum equations) and Poisson equations, written respectively in Eqs. (3.2), (3.3) and (3.4). These equations describe the self-consistent evolution of the macroscopic quantities of plasma (density, velocity and plasma potential).

In cases for which the coupling between particles and waves are weak, the dominant effect responsible for the time evolution of the wave amplitudes is the nonlinear coupling to the other waves (wave-wave interaction). For a weakly nonlinear system the strongest wave-wave nonlinearity is the three wave interactions. The condition for a resonant three wave interaction is given by:

$$\omega_3 = \omega_1 + \omega_2, \quad k_3 = k_2 + k_1 \tag{3.1}$$

Matching of the frequencies implies the conservation of wave energy and the matching of wave numbers implies the conservation of wave momentum. Also, similar to the Heisenberg's quantum mechanical uncertainty principle, these matching conditions do not need to be exactly satisfied in order to have resonant interactions between the waves [25], as we will observe later on in sections 3.5.3, 3.5.4 and 3.5.5.

The two factors which determine the behavior of the system in time are nonlinearity and dispersion. In our system of fluid-Poisson equations, nonlinear terms are present in the fluid equations and the wave dispersion arises from the Poisson equation. The effect of nonlinearity is, often, to draw in and peak the pulses (e.g. amplitude growth due to parametric resonance instability), whereas dispersion causes the disturbances to spread, and thus impedes the effect of nonlinearity. The nonlinearity can be measured simply by the size of the normalized wave density perturbation A, and the dispersion can be measured by Δ/ω_1, where $\Delta =$

$\omega_1 + \omega_2 - \omega_3$ is the frequency mismatch, also known as detuning. We are interested in weakly nonlinear regimes for which $A \ll 1$. Generally, for a plasma of finite Length L, Δ/ω_1 is a function of $k_\perp \sim 1/r_p$. For a long and thin plasma for which $r_p \ll L$, linear dispersion relation Eq. (3.105) is near-acoustic and the detuning is small ($\Delta/\omega_1 \ll 1$). However for $k_\perp L \to 0$ (the slab limit) cold plasma modes become degenerate with $\omega \approx \omega_p$. As a result three-wave interaction becomes impossible, since the frequency condition in Eq. (3.1) can not be satisfied. In this regime which has been studied in Refs. 13, 39, 43, nonlinear interaction of plasma modes is of 4-waves type, which is a higher order nonlinear effect (than 3-waves interactions). In this work we will mostly be concerned with the opposite regime $k_\perp L > 1$, where the detuning is fairly small and 3-wave interactions are observed.

Depending on whether the detuning is larger or smaller compared to the nonlinearity, the time evolution of waves behaves differently. Sections 3.2 and 3.3 are in the large detuning regime for which $A \ll \Delta/\omega_1$. In our analysis of this regime, we neglect the possibility of resonant interaction between the waves. We find that in the large detuning regime, the waves in the plasma can be described by the sum of sinusoidal oscillations with constant amplitudes. In parts 3.2.1 and 3.2.2 we obtain the eigenmodes of a weakly nonlinear 1D system, for traveling waves and standing waves respectively. Eigenmodes of the 1D system are periodic non-sinusoidal functions of space and time, with frequency ω and wave number k. Using a weakly nonlinear analysis we obtain the lowest order correction to the linear mode frequency and the lowst order correction to the linear eigenmodes for traveling and standing waves. We observe that as the mode amplitude A approaches Δ/ω_1 the resonant wave-wave interaction is no longer negligible and our perturbation formalism breaks down.

In section 3.3, for a system in the large detuning regime, we present a general, non-resonant, weakly nonlinear analysis for arbitrary number of waves present in the plasma. We obtain corrections to the linear mode frequencies due to nonlinear couplings to all the other modes present in the plasma. Furthermore, using our formalism, we obtain the same nonlinear eigenmode corrections obtained previously in parts 3.2.1 and 3.2.2.

In the small detuning regime for which $A \sim \Delta/\omega_1 \ll 1$, resonant wave-wave interaction is non-negligible. Furthermore in the limit of $A > \Delta/\omega_1$ strong resonant wave-wave coupling can lead to instability and the exponential growth of the mode amplitudes. In section 3.4 we obtain the evolution equations for the slow varying linear mode amplitudes, for the small detuning regime ($A \sim \Delta/\omega_1$) using a weakly nonlinear perturbation method. These series of evolution equations (Eq. (3.148)), together with the linear dispersion relations (Eq. (3.105)) which determine the linear mode frequencies, are the reduced version of evolution equations of the original system of equations given by Eq. (3.84) and Eq. (3.85), since the variables of the system are reduced from $\mathrm{v}_l, \mathrm{n}_l$ to only the variable $n_l^{(1)}(t) = n_l(t)e^{-i\omega_l t}$. Weakly nonlinear analysis based on both macroscopic plasma models, which employ the moment-Maxwell equations [10, 12–14, 23, 27], and microscopic plasma models, which employ the Vlasov-Maxwell equations [1, 3, 11, 24, 27, 42] leads to the similar dynamical equations as Eq. (3.148).

In part 3.4.1 we analyze approximate energy conservation principles for the reduced system of equations Eq. (3.148). We obtain a relation for the time variation of the total energy of the waves in the plasma. The total energy of the waves is of order ε^2, where ε is the size of the amplitude of the perturbations. Our energy conservation relation implies that the energy of a system of small perturbations, in which the resonant wave-wave interactions are negligible, is conserved to the 3rd order in ε ($\delta E \sim \mathcal{O}(\varepsilon^4)$). whereas for a system of larger perturbations at which 4-wave resonance is non-negligible, the total energy of the system is conserved only up to the second order in ε ($\delta E \sim \mathcal{O}(\varepsilon^3)$).

Next, we focus our study on the problem of the interaction between the modes 1 and 2. In section 3.5 we study the system of isolated modes 1 and 2 by keeping only these two modes and their two related evolution equations given by Eqs. (3.187) and (3.188). In part 3.5.1 we develop a phase-space describing the evolution of these two isolated modes. The solutions of these equations are reversible and the equations of motion can be written in terms of a conserved Hamiltonian. We observe that the topology of this phase-space depends on a unitless parameter η which is the measure of the strength of dispersion comparing to nonlinearity. For $\eta = 0$ the

system is at exact resonance. For $0 \leq \eta < 1$ the phase-space contains two saddle points, one of which corresponds to the exponential growth of a small amplitude mode 1 in the presence of a dominant mode 2. The second saddle point is the inverse of the first saddle point, which shows the growth of mode 2 and the decay of mode 1. The value $\eta = 1$ corresponds to the threshold of instability. For $\eta > 1$ the saddle points are absent from the phase-space and the solutions for the mode amplitudes remain near their initial value while performing small amplitude oscillations.

In part 3.5.2, for the isolated system of modes 1 and 2, we obtain the nonlinear eigenmode 1 solution for which linear mode 2 is a harmonic of mode 1. We obtain a correction to the mode frequency and a correction to the mode function, for the limit of small amplitude (non-resonant).

In part 3.5.3, for the isolated system of modes 1 and 2, we study the subharmonic interaction of mode 2 and 1, for which mode 2 is the dominant mode in the system and the amplitude of mode 1 is small. Our discussion follows the same analysis as in Refs. 23, 32 for three wave interactions. In the presence of the dominant mode 2, depending on the magnitude of the amplitude of mode 2, solutions for mode 1 are either oscillatory or unstable. In the oscillatory regime, mode 1 exhibits a beating between two solutions, one with frequency $\overline{\omega}_1$ and one with frequency $\omega_2 - \overline{\omega}_1$. $\overline{\omega}_1$ is the frequency of mode 1 modified due to the nonlinear coupling to mode 2. The beat frequency decreases with increase in the amplitude of mode 2 and reaches minimum at the threshold of instability $A_2^{\mathrm{t,th}}$ for traveling waves ($A_2^{\mathrm{s,th}}$ for standing waves). This threshold depends on the strength of dispersion. Beyond $A_2^{\mathrm{t,th}}$, the system is in the unstable regime in which mode 2 shares its energy with mode 1, and thus mode 1 grows exponentially and decays exponentially, in a reversible way.

In part 3.5.4, we study a system of isolated waves 1, 2 and 3, for an initial condition such that mode 2 is dominant in the plasma and modes 1 and 3 are initially small in comparison to mode 2. We find a general solution for the evolution of modes 1 and 3. Similar to the previous case of isolated modes 1 and 2 only, we find a threshold beyond which the solutions for modes 1 and 3 are unstable and grow ex-

ponentially with the rate Γ. In the oscillatory regime, below the threshold, we show that the response of the plasma to driving mode 1 depends on the way the plasma has been driven. Using a smaller drive potential over a longer drive time will result in exciting only 2 frequencies for mode 1 in the plasma, $\overline{\omega}_1$ and $\omega_2 - \overline{\omega}_1$. We observe that contrary to the previous case of isolated modes 1 and 2, the beat frequency between these two signals given by $\omega_{\text{amp}} = 2\overline{\omega}_1 - \omega_2$ grows with growing amplitude of mode 2.

In part 3.5.5, we study a system of isolated waves 1,2,3 and 4, where a dominant *nonlinear* mode 2 is present in the plasma, which consists of the linear mode 2 oscillating at frequency $\overline{\omega}_2$ and linear mode 4 being the harmonic of linear mode 2 and oscillating at $2\overline{\omega}_2$. Modes 1 and 3 are initially small in comparison to mode 2. By adiabatically driving a small amplitude mode 1 while driving the large amplitude mode 2, the response of plasma for mode 1 contains 2 frequencies $\overline{\omega}_1$ and $\overline{\omega}_2 - \overline{\omega}_1$. The beat frequency between two signals $\omega_{\text{amp}} = 2\overline{\omega}_1 - \overline{\omega}_2$ falls with growing amplitude of mode 2 and goes to zero at the threshold of instability. When the amplitude of mode 2 is larger than the threshold, modes 1 and 3 grow exponentially with the growth rate Γ.

In both the cases of isolated waves 1,2,3 and waves 1,2,3,4, we compare our analytical results obtained from the reduced system of equations (3.148), to the numerically evaluated results obtained for the same isolated modes, evolving in time according to the original system of equations given by Eq. (3.84) and Eq. (3.85).

We extend our numerical evalution by including more waves in plasma evolving according to Eq. (F.2) and Eq. (F.3) (keeping more terms in the truncated sums). In each case we drive a large amplitude mode 2 and a small amplitude mode 1. By increasing the upper limits of the sums M the threshold of instability converges to a finite value independent of M, which for standing waves with $k_\perp = 10k_1$ is $A_2^{\text{s, th}} \approx 0.173$. Furthermore the beat frequency of mode 1 (ω_{amp}) as a function of the amplitude of mode 2 and the growth rate of mode 1 (Γ) versus the amplitude of mode 2 converge to values independent of M. Furthermore we perform Vlasov-Poisson simulations for the same parameters $k_\perp = 10k_1$ in a cold plasma ($\omega_2/k_2 v_T = 12.2$) and compare to the Fluid simulation results. For our Vlasov-Poisson simulations

we used the method of lines, which we described in a previous work Ref. 5. The results from the two methods of simulation are in agreement.

3.2 Nonlinear eigenmodes of the 1D fluid plasma, large detuning

In this section we obtain nonlinear corrections to the forms and frequencies of traveling and standing waves, using a weak nonlinearity perturbation method. We make no assumptions concerning the strength of the dispersion. From examining our results we obtain the conditions for which our derivations are valid: basically, we show that our perturbation method breaks down in the regime where detuning is small, i.e. if the condition given by Eq. (3.36) for traveling waves and the condition given by Eq. (3.75) for standing waves are not satisfied.

3.2.1 Traveling plasma modes, large detuning

We start from 1D equations for a cold fluid system, coupled with Poisson equation:

$$\begin{aligned} \partial_t N + \partial_z (N v) &= 0 \text{(continuity)}, && (3.2)\\ \partial_t v + v \partial_z v &= E \text{ (momentum)}, && (3.3)\\ \left[k_\perp^2 - \partial_z^2\right] E &= -\partial_z N \text{ (Poisson)}, && (3.4) \end{aligned}$$

where $E = -\partial_z \varphi$ is the electric field in the z direction. In the above equations, time is scaled to plasma frequency $\omega_p^2 = 4\pi q^2 N_0 / m_q$, fluid density has been scaled to equilibrium density N_0. The system has periodic boundary conditions over 2 times the length of the plasma.

$$\begin{aligned} N(z+2L) &= N(z),\\ E(z+2L) &= E(z), \qquad (3.5)\\ v(z+2L) &= v(z). \end{aligned}$$

Assuming that the system is in steady state in a frame moving with phase velocity $s > 0$, solutions to the above equations have the following form:

$$N, v, \phi \sim g(\xi), \quad \xi = z - s\,t. \tag{3.6}$$

This implies that

$$\partial_t g = -s\,\partial_\xi g, \tag{3.7}$$

$$\partial_z g = \partial_\xi g. \tag{3.8}$$

Therefore in the steady state frame, Eqs. (3.2) through (3.4) become:

$$-s\,\partial_\xi N + \partial_\xi (N\,v) = 0, \tag{3.9}$$

$$-s\,\partial_\xi v + v\,\partial_\xi v = E, \tag{3.10}$$

$$\left[k_\perp^2 - \partial_\xi^2\right] E = -\partial_\xi N. \tag{3.11}$$

Using perturbation theory we can obtain the nonlinear mode potential which satisfies equations (3.2), (3.3) and, (3.4). We assume the following perturbation expansions:

$$\begin{aligned} N &= 1 + \varepsilon\, n^{(1)} + \varepsilon^2 n^{(2)} + \ldots, \\ v &= \varepsilon\, v^{(1)} + \varepsilon^2 v^{(2)} + \ldots, \\ E &= \varepsilon\, E^{(1)} + \varepsilon^2 E^{(2)} + \ldots, \\ s &= s_0 + \varepsilon\, s_1 + \varepsilon^2 s_2 \ldots . \end{aligned} \tag{3.12}$$

Superscipts for n, v and E represent different functions and are not exponents.The First order of equations (3.9) through (3.11) yields the linear dispersion relation. The equations are given by:

$$-s_0 \partial_\xi n^{(1)} + \partial_\xi v^{(1)} = 0, \tag{3.13}$$

$$-s_0 \partial_\xi v^{(1)} = E^{(1)}, \tag{3.14}$$

$$[k_\perp^2 - \partial_\xi^2] E^{(1)} = -\partial_\xi n^{(1)}. \tag{3.15}$$

From (3.13) and (3.14) we get:

$$\partial_\xi n^{(1)} = -\frac{1}{s_0^2} E^{(1)}. \tag{3.16}$$

From (3.15) and (3.16) we obtain the linear dispersion relation:

$$\left[k_\perp^2 - \partial_\xi^2 - \frac{1}{s_0^2}\right] E^{(1)} = 0. \tag{3.17}$$

The mth eigenmode satisfying Eq. (3.17) together with the periodic boundary conditions Eqs. (3.5) has the form:

$$n^{(1)} = v^{(1)}/s_0 = A_m^t \cos k_m \xi, \quad k_m = m\pi/L, \tag{3.18}$$

$$E^{(1)} = k_m^{-1} s_0^2 A_m^t \sin k_m \xi, \tag{3.19}$$

where A_m^t is the amplitude of density perturbation of the traveling wave. As the result, s_0 for linear mode m is given by:

$$s_0 = \frac{1}{\sqrt{k_\perp^2 + k_m^2}}. \tag{3.20}$$

Second order continuity, momentum and Poisson equations in ε are respectively given by:

$$-s_1 \partial_\xi n^{(1)} - s_0 \partial_\xi n^{(2)} + \partial_\xi v^{(2)} + \partial_\xi (n^{(1)} v^{(1)}) = 0, \tag{3.21}$$

$$-s_1 \partial_\xi v^{(1)} - s_0 \partial_\xi v^{(2)} + v^{(1)} \partial_\xi v^{(1)} = E^{(2)}, \tag{3.22}$$

$$[k_\perp^2 - \partial_\xi^2] E^{(2)} = -\partial_\xi n^{(2)}. \tag{3.23}$$

We eliminate $\partial_\xi v^{(2)}$, solve for $\partial_\xi n^{(2)}$ from Eq. (3.21) and Eq. (3.22), use Eq. (3.20), and substitute the result on the right hand side of (3.23) to obtain:

$$\left[-\partial_\xi^2 - k_m^2\right] E^{(2)} = -\frac{3}{2} \partial_\xi (n^{(1)})^2 + 2 \frac{s_1}{s_0} \partial_\xi n^{(1)}. \tag{3.24}$$

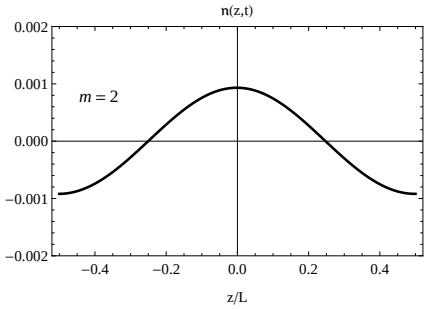

(a)

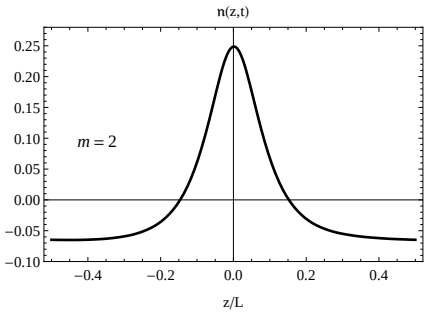

(b)

Figure 3.1: Plots of the density perturbation of the nonlinear traveling mode $m = 2$, for a small amplitude wave in Fig. (3.1a) and a large amplitude wave in Fig. (3.1b), for $k_\perp = 10k_1$, obtained from fluid simulations described in appendix F, with $M = 26$.

The left hand side of above equation is similar to Eq. (3.17) and has homogeneous solutions of the form $\sin[k_m\xi+\alpha]$. In order to have a periodic solution we need to remove the terms from the right hand side of Eq. (3.24) which can be in resonance with the left hand side homogeneous solutions. Thus we set the last term in Eq. (3.24) to zero:

$$2\frac{s_1}{s_0}A_m^t k_m \sin[k_m\xi] = 0. \tag{3.25}$$

As a result we find out that

$$s_1 = 0. \tag{3.26}$$

We substitute for $n^{(1)}$ from (3.18) in (3.24) and solve for the particular solution for

$E^{(2)}$ and obtain:

$$E^{(2)} = \frac{1}{2k_m}(A_m^t)^2 \sin 2k_m\xi. \tag{3.27}$$

Using (3.27) in (3.23), for $n^{(2)}$ we obtain:

$$n^{(2)} = \frac{k_\perp^2 + 4k_m^2}{4k_m^2}(A_m^t)^2 \cos 2k_m\xi. \tag{3.28}$$

Using (3.28) in (3.21) we solve for v^2 to obtain:

$$v^{(2)} = s_0\frac{k_\perp^2 + 2k_m^2}{4k_m^2}(A_m^t)^2 \cos 2k_m\xi. \tag{3.29}$$

Figure (3.1) compares a small amplitude $m = 2$ traveling wave to a large amplitude $m = 2$, nonlinear traveling wave, at the same phase. These plots are obtained from fluid simulations described in appendix F with $M = 26$. In Fig (3.1b) the large amplitude mode is clearly non-sinusoidal.

Third order continuity, momentum and Poisson equations in ε are respectively given by:

$$-s_0\partial_\xi n^{(3)} - s_2\partial_\xi n^{(1)} + \partial_\xi v^{(3)} + \partial_\xi(n^{(2)}v^{(1)} + n^{(1)}v^{(2)}) = 0, \tag{3.30}$$

$$-s_0\partial_\xi v^{(3)} - s_2\partial_\xi v^{(1)} + \partial_\xi(v^{(2)}v^{(1)}) = E^{(3)}, \tag{3.31}$$

$$\left[k_\perp^2 - \partial_\xi^2\right]E^{(3)} = -\partial_\xi n^{(3)}. \tag{3.32}$$

We eliminate $\partial_\xi v^{(3)}$ and solve for $\partial_\xi n^{(3)}$ from (3.30) and (3.31) and substitute the result on the right hand side of (3.32) to obtain:

$$\begin{aligned}\left[-\partial_\xi^2 - k_m^2\right]E^{(3)} &= 2\frac{s_2}{s_0}\partial_\xi n^{(1)} - \frac{1}{s_0}\partial_\xi(n^{(2)}v^{(1)} + 2n^{(1)}v^{(2)}) \\ &= -2\frac{s_2}{s_0}k_m A_m^t \sin k_m\xi - \frac{3k_\perp^2 + 8k_m^2}{8k_m^2}(A_m^t)^3\partial_\xi(\cos 3k_m\xi + \cos k_m\xi)\end{aligned} \tag{3.33}$$

Removing the resonant terms proportional to $\sin k_m\xi$ from the right hand side im-

plies:

$$s_2 = s_0 \frac{3k_\perp^2 + 8k_m^2}{16k_m^2}(A_m^t)^2 \tag{3.34}$$

Thus s_2 ,which is the lowest order correction to the phase velocity of mode m due to nonlinearity, is of the second order in the mode amplitude A_m^t. Combining Eqs. (3.24) and (3.34), the mode frequency up to $\mathcal{O}(\varepsilon^2)$ is given by:

$$\overline{\omega}_m = k_m s = \omega_m \left[1 + \frac{3k_\perp^2 + 8k_m^2}{16k_m^2}(A_m^t)^2\right], \tag{3.35}$$

where $\omega_m = k_m/\sqrt{k_\perp^2 + k_m^2}$ is the linear mode frequency. Hence, to the second order in ε, the mode frequency grows due to nonlinearity quadratically in A_m^t.

However, in the case of a long and thin plasma for which $k_m \ll k_\perp$, Eq. (3.35) is only correct provided:

$$A_m^t \ll k_m^2/k_\perp^2 \approx \Delta_{m,2m}/3\omega_m, \tag{3.36}$$

where $\Delta_{m,2m} = 2\omega_m - \omega_{2m}$ is the detuning between mode m and $2m$. Otherwise, if $A_m^t \sim k_m^2/k_\perp^2$, the frequency correction in Eq. (3.34) will be in fact of the first order in ε. Therefore if $A_m^t \sim k_m^2/k_\perp^2 \sim \varepsilon$, the entire perturbation formalism of ordering used here breaks down. We can see this breakdown of the perturbation from Eq. (3.28) and Eq. (3.29) for the second order perturbations $n^{(2)}$ and $v^{(2)}$, and from Eq. (3.39) and Eq. (3.40) for the third order perturbations $n^{(3)}$ and $v^{(3)}$. All of these higher order perturbations will become of the first order in ε if $k_m^2/k_\perp^2 \sim \varepsilon$. In section 3.4 we will discuss the problem for which the detuning is small, as well as the mode amplitude. Now, for a long and thin plasma, we can expand the frequency correction in Eq. (3.35) in terms of small $k_m/k_\perp$ and to the lowest order we obtain:

$$\omega_m^{(2)} \approx \omega_m \frac{3k_\perp^2}{16k_m^2}(A_m^t)^2 \tag{3.37}$$

Moreover, solving for $E^{(3)}$ we obtain:

$$E^{(3)} = \frac{9k_\perp^2 + 24k_m^2}{64k_m^3}(A_m^t)^3 \sin 3k_m\xi \tag{3.38}$$

For $n^{(3)}$ and $v^{(3)}$ we obtain:

$$n^{(3)} = (3k_\perp^2 + 8k_m^2)(9k_m^2 + k_\perp^2)\frac{(A_m^t)^3}{64k_m^4}\cos 3k_m\xi \tag{3.39}$$

$$v^{(3)} = s_0(3k_\perp^4 + 19k_\perp^2k_m^2 + 24k_m^4)\frac{(A_m^t)^3}{64k_m^4}\cos 3k_m\xi \tag{3.40}$$

We can repeat this process up to an arbitrary order in ε to obtain more accurate nonlinear mode frequencies and eigenmodes.

3.2.2 Standing plasma waves, large detuning

In this section we obtain steady, oscillatory, nonlinear, standing solutions of the equations (3.2)-(3.4) in a plasma of finite length L, assuming boundary conditions at the ends $z = 0, z = L$ to be of Neumann type for mode potential φ and mode density n. This boundary condition is in accordance with Prasad and O'Neil for $\omega \ll \omega_p$ [34]. In order to take advantage of the simplicity of periodic boundary conditions we extend the plasma to a system of length $2L$ and assume periodic boundary conditions with solutions which are periodic over $2L$ and have the forms:

$$N(z,t) = 1 + \sum_{l=1}^{\infty} n_l(t)\cos k_l z, \tag{3.41}$$

$$\varphi(z,t) = \sum_{l=1}^{\infty} \varphi_l(t)\cos k_l z, \tag{3.42}$$

$$v(z,t) = \sum_{l=1}^{\infty} v_l(t)\sin k_l z, \tag{3.43}$$

where $k_l = \pi/L$. These solutions will satisfy the boundary conditions we required for the original system of finite length L. In what follows we find the evolution equations for the time dependent part of the above solutions i.e. $n_l(t)$, $v_l(t)$ and $\varphi_l(t)$. By substituting (3.42) and (3.43) in the Poisson equation (3.4), and taking the integral

product with $\frac{1}{L}\int_0^{2L}\cos k_{\overline{m}}z$ we obtain:

$$\varphi_{\overline{m}}(t)=\frac{n_{\overline{m}}(t)}{k_\perp^2+k_{\overline{m}}^2}. \tag{3.44}$$

Substituting (3.41) and (3.42) in the continuity equation (3.2), and taking the product with $\frac{1}{L}\int_0^{2L}\cos k_{\overline{m}}z\,dz$ yields:

$$k_{\overline{m}}v_{\overline{m}}+\frac{d}{dt}n_{\overline{m}}+\tfrac{1}{L}\int_0^{2L}\cos k_{\overline{m}}z\frac{d}{dz}[(N-1)v]dz=0. \tag{3.45}$$

The last term on the LHS of the above equation will be simplified as follows: using integration by parts we write:

$$\begin{aligned}
&\tfrac{1}{L}\int_0^{2L}\cos k_l z\frac{d}{dz}[(N-1)v]dz\\
&=k_{\overline{m}}\sum_{l=1}^{\infty}\sum_{l'=1}^{\infty}\tfrac{1}{L}\int_0^{2L}n_{l'}v_l\sin k_{\overline{m}}z\sin k_l z\cos k_{l'}z\,dz\\
&=\frac{k_m}{2}\sum_{l=1}^{\infty}\sum_{l'=1}^{\infty}(\delta_{\overline{m},l-l'}+\delta_{\overline{m},l+l'}-\delta_{\overline{m},-l-l'}-\delta_{\overline{m},l'-l})n_{l'}v_l.
\end{aligned}$$

Substituting (3.41), (3.42) and using (3.44) in the momentum equation (3.3), and taking the product with $\frac{1}{L}\int_0^{2L}\sin k_{\overline{m}}z\,dz$ we obtain:

$$\frac{d}{dt}v_{\overline{m}}-\frac{\omega_{\overline{m}}^2}{k_{\overline{m}}}n_{\overline{m}}+\tfrac{1}{L}\int_0^{2L}\sin k_{\overline{m}}z\frac{d}{dz}[\frac{v^2}{2}]dz=0, \tag{3.46}$$

where $\omega_{\overline{m}}$ is given by

$$\omega_{\overline{m}}=\frac{k_{\overline{m}}}{\sqrt{k_\perp^2+k_{\overline{m}}^2}}. \tag{3.47}$$

Using the series in Eq. (3.43) we further expand the last term in Eq. (3.46) as follows:

$$
\begin{aligned}
&\tfrac{1}{L}\int_0^{2L} \sin k_{\overline{m}} z \frac{d}{dz}\left[\frac{v^2}{2}\right] dz \\
&= -k_m \tfrac{1}{2L} \sum_{l=1}^{\infty} \int_0^{2L} \cos k_{\overline{m}} z (\sin k_l z)^2 dz - k_{\overline{m}} \tfrac{1}{L} \sum_{l>l'}^{\infty}\sum_{l'=1}^{\infty} \int_0^{2L} \sin k_{\overline{m}} z \sin k_l z \sin k_{l'} z \, dz \\
&= \frac{k_{\overline{m}}}{4} \sum_{l=1}^{\infty} v_l^2 \delta_{l,\overline{m}/2} - \frac{k_{\overline{m}}}{2} \sum_{l>l'}^{\infty}\sum_{l'=1}^{\infty} \left(\delta_{\overline{m},l-l'} + \delta_{\overline{m},l'-l} - \delta_{\overline{m},-(l'+l)} - \delta_{\overline{m},l'+l}\right) v_l v_{l'} \\
&= \frac{k_{\overline{m}}}{4} \sum_{l=1}^{\infty} v_l^2 \delta_{l,\overline{m}/2} + \frac{k_{\overline{m}}}{2} \sum_{\substack{l\neq\overline{m} \\ l>m/2}}^{\infty} v_l v_{|\overline{m}-l|} \text{sign}(\overline{m}-l). \qquad (3.48)
\end{aligned}
$$

Therefore, we can rewrite the continuity equation (3.45) and the momentum equation (3.46) as:

$$\dot{n}_{\overline{m}} + k_{\overline{m}} v_{\overline{m}} + \frac{k_{\overline{m}}}{2} \sum_{l=1}^{\infty} v_l (n_{|l-\overline{m}|} - n_{l+\overline{m}}) = 0, \qquad (3.49)$$

$$\dot{v}_{\overline{m}} - \frac{\omega_{\overline{m}}^2}{k_{\overline{m}}} n_{\overline{m}} + \frac{k_{\overline{m}}}{4} \sum_{l=1}^{\infty} v_l^2 \delta_{l,\overline{m}/2} + \frac{k_{\overline{m}}}{2} \sum_{\substack{l\neq\overline{m} \\ l>\overline{m}/2}}^{\infty} v_l v_{|\overline{m}-l|} \text{sign}(\overline{m}-l) = 0. \qquad (3.50)$$

In order to carry out perturbation solutions of Eqs. (3.49) and (3.50) it is useful to apply ∂_t to (3.49) and multiply (3.50) by $-k_{\overline{m}}$, then sum the two equations to obtain:

$$
\begin{aligned}
[\partial_t^2 + \omega_{\overline{m}}^2] n_{\overline{m}} &= -\frac{k_{\overline{m}}}{2} \sum_{l=1}^{\infty} \left[\partial_t [v_l (n_{|l-\overline{m}|} - n_{l+\overline{m}})] - \frac{k_{\overline{m}}^2}{4} v_l^2 \delta_{l,\overline{m}/2}\right] \\
&+ \frac{k_{\overline{m}}^2}{2} \sum_{\substack{l\neq\overline{m} \\ l>\overline{m}/2}}^{\infty} v_l v_{|\overline{m}-l|} \text{sign}(\overline{m}-l). \qquad (3.51)
\end{aligned}
$$

In Eqs. (3.49)- (3.51), $n_0 = 0$ since the zeroth Fourier term was extracted from the sum in Eq. (3.41). Also $v_0 = 0$. In the next section where we use the perturbation method, by removing the secular terms from the right hand side of Eq. (3.51) order by order, we obtain the nonlinear oscillatory solution.

3.2.3 Nonlinear standing eigenmodes

In this part we obtain the nonlinear standing eigenmodes satisfying the equations governing the system. These modes are oscillatory in time without damping or growing. However their Fourier amplitudes i.e. the amplitudes of oscillations of n_m's are constant in time. We obtain the nonlinear modes as perturbations to a linear mode m. We will use the multiple time scale analysis using the following series expansions for mode m:

$$\begin{aligned} n_0 &= 0 \\ n_m &= \varepsilon n_m^{(1)} + \varepsilon^2 n_m^{(2)} + \varepsilon^3 n_m^{(3)} + \ldots, \\ v_m &= \varepsilon v_m^{(1)} + \varepsilon^2 v_m^{(2)} + \varepsilon^3 v_m^{(3)} + \ldots, \\ n_l &= \varepsilon^2 n_l^{(2)} + \varepsilon^3 n_l^{(3)} + \ldots, \quad l \neq m \\ v_l &= \varepsilon^2 v_l^{(2)} + \varepsilon^3 v_l^{(3)} + \ldots, \quad l \neq m \end{aligned} \tag{3.52}$$

In the limit $\varepsilon \to 0$, the lowest order solution in ε is the mth linear mode i.e. $n_m^{(1)}, v_m^{(1)}$. We define the following hierarchy of multiplie simescales [30]:

$$t_0 = t,\ t_1 = \varepsilon t,\ t_2 = \varepsilon^2 t, \ldots \tag{3.53}$$

$$\frac{d}{dt} = \partial_{t_0} + \varepsilon \partial_{t_1} + \varepsilon^2 \partial_{t_2} + \ldots \tag{3.54}$$

In the equation Eq. (3.51), the time derivative on the left hand side, up to the third order is given by:

$$\begin{aligned} \partial_t^2 n_m &\approx (\partial_{t_0} + \varepsilon \partial_{t_1} + \varepsilon^2 \partial_{t_2})^2 (\varepsilon n_m^{(1)} + \varepsilon^2 n_m^{(2)} + \varepsilon^3 n_m^{(3)}) \\ &\approx \varepsilon \partial_{t_0}^2 n_m^{(1)} + \varepsilon^2 (\partial_{t_0}^2 n_m^{(2)} + 2\partial_{t_1}\partial_{t_0} n_m^{(1)}) + \varepsilon^3 (\partial_{t_0}^2 n_m^{(3)} + \partial_{t_1}^2 n_m^{(1)} + 2\partial_{t_2}\partial_{t_0} n_m^{(1)} + 2\partial_{t_1}\partial_{t_0} n_m^{(2)}) \\ &= \varepsilon \partial_{t_0}^2 n_m^{(1)} + \varepsilon^2 (\partial_{t_0}^2 n_m^{(2)} - 2k_m \partial_{t_1} v_m^{(1)}) + \varepsilon^3 (\partial_{t_0}^2 n_m^{(3)} + \partial_{t_1}^2 n_m^{(1)} - 2k_m \partial_{t_2} v_m^{(1)} + 2\partial_{t_1}\partial_{t_0} n_m^{(2)}). \end{aligned} \tag{3.55}$$

In the last line of the above equation we used Eq. (3.58). We will substitute from the series introduced in Eq. (3.52), (3.54) and (3.55) in Eq. (3.51) and solve for n_l and then solve for v_l from equation (3.49) at each order of ε and use the results iteratively

in the higher orders in ε. For the lowest order in ε, i.e. the first order, we obtain:

$$[\partial_{t_0}^2 + \omega_m^2] n_m^{(1)} = 0. \tag{3.56}$$

The solution to the above equations is of the general form:

$$n_m^{(1)} = A_m^s(t_1, t_2, \dots)\cos(\omega_m t_0 + \alpha_m(t_1, t_2, \dots)), \tag{3.57}$$

$$v_m^{(1)} = \frac{\omega_m}{k_m} A_m^s(t_1, t_2, \dots)\sin(\omega_m t_0 + \alpha_m(t_1, t_2, \dots)), \tag{3.58}$$

where A_m^s is the amplitude of the density perturbation of the mth standing mode.

Since the right hand side of Eq. (3.51) is of third order and higher in ε for $\overline{m} = m$, the second order equation comes solely from its left hand side. Using Eqs. (3.55) and (3.56) in Eq. (3.51), for the second order in ε we get:

$$\begin{aligned}[\partial_{t_0}^2 + \omega_m^2] n_m^{(2)} &= 2k_m \partial_{t_1} v_m^{(1)} \\ &= 2\omega_m \partial_{t_1} A_m^s \sin(\omega_m t_0 + \alpha_m) + 2\omega_m A_m^s \partial_{t_1} \alpha_m \cos(\omega_m t_0 + \alpha_m),\end{aligned} \tag{3.59}$$

where Eq. (3.58) was used in the second line. Both terms on the RHS are resonant with the homogeneous solutions of the LHS unless:

$$\partial_{t_1} A_m^s = 0 \Rightarrow A_m^s = A_m^s(t_2, t_3, \dots), \tag{3.60}$$

$$\partial_{t_1} \alpha_m = 0 \Rightarrow \alpha_m = \alpha_m(t_2, t_3, \dots). \tag{3.61}$$

Therefore, the lowest order correction to linear frequency ω_m is of the second order in ε. This correction can be obtained from Eq. (3.51) in the third order in ε. In order to obtain this nonlinear frequency correction, we need to evaluate $n_{2m}^{(2)}$ and $v_{2m}^{(2)}$. From Eq. (3.51) for $\overline{m} = 2m$ in the second order in ε we get:

$$\begin{aligned}[\partial_{t_0}^2 + \omega_{2m}^2] n_{2m}^{(2)} &= -k_{2m} \partial_{t_0}(v_m^{(1)} n_m^{(1)}) + (k_m)^2 (v_m^{(1)})^2 \\ &= \frac{\omega_m^2}{2}(A_m^s)^2 - \frac{3}{2}\omega_m^2 (A_m^s)^2 \cos[2(\omega_m t_0 + \alpha_m)],\end{aligned} \tag{3.62}$$

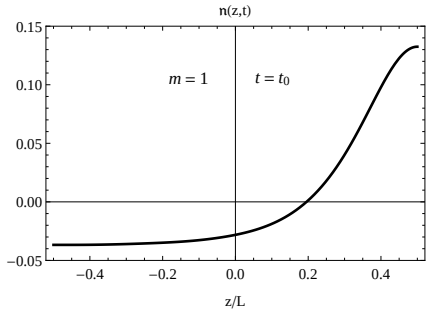

(a)

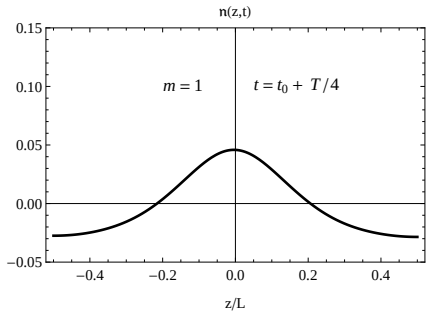

(b)

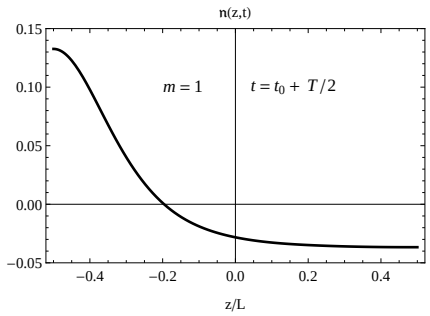

(c)

Figure 3.2: Plots of the density perturbation of a large amplitude nonlinear standing mode $m = 1$, for $k_\perp = 10k_1$, obtained from fluid simulations described in appendix F, with $M = 26$.

where in the second line we used Eqs. (3.57) and (3.58). As a result we obtain:

$$n_{2m}^{(2)} = \frac{\omega_m^2}{2\omega_{2m}^2}(A_m^s)^2 + \frac{k_\perp^2 + 4k_m^2}{8k_m^2}(A_m^s)^2 \cos[2(\omega_m t_0 + \alpha_m)] \\ + C_1 \cos\omega_{2m} t_0 + C_2 \sin\omega_{2m} t_0. \tag{3.63}$$

The functions $C_1 \cos\omega_{2m} t_0$ are $C_2 \sin\omega_{2m} t_0$ are the homogeneous solutions for Eq. (3.62), with C_1 and C_2 determined from the initial conditions. Assuming that only the nonlinear mode m is present in the plasma, the only frequencies present in the plasma must be ω_m and all its harmonics $2\omega_m, 3\omega_m, \ldots$. Therefore in Eq. (3.63) we set C_1 and C_2 to zero to obtain:

$$n_{2m}^{(2)} = \frac{\omega_m^2}{2\omega_{2m}^2}(A_m^s)^2 + \frac{k_\perp^2 + 4k_m^2}{8k_m^2}(A_m^s)^2 \cos[2(\omega_m t_0 + \alpha_m)]. \tag{3.64}$$

We obtain $v_{2m}^{(2)}$ from Eq. (3.49) substituting for $n_{2m}^{(2)}$ from Eq. (3.64):

$$v_{2m}^{(2)} = -\frac{\dot{n}_{2m}^{(2)}}{k_{2m}} - \frac{1}{2} v_{2m}^{(1)} n_m^{(1)} \\ = \left(\frac{\omega_m}{k_m}\right) \frac{k_\perp^2 + 2k_m^2}{8k_m^2}(A_m^s)^2 \sin[2(\omega_m t_0 + \alpha_m)]. \tag{3.65}$$

Figures (3.2) and (3.3) depict the nonlinear standing modes $m = 1$ and $m = 2$ respectively, at times $t = t_0$, $t_0 + T/4$ and $t_0 + T/2$. These plots are obtained from fluid simulations described in appendix F with $M = 26$. We can see that these modes are non-sinusoidal and where mode $m = 2$ has an even symmetry, mode $m = 1$ is a combination of even and odd symmetric terms.

The lowest order correction to mode frequency due to nonlinearity comes from the ε^3 order equations. Using Eq. (3.55) in Eq. (3.51) we get the following third order equation:

$$[\partial_{t_0}^2 + \omega_m^2] n_m^{(3)} = 2k_m \partial_{t_2} v_m^{(1)} - \frac{k_m}{2} \partial_{t_0} (v_{2m}^{(2)} n_m^{(1)} - v_m^{(1)} n_{2m}^{(2)}) - \frac{k_m^2}{2} (v_{2m}^{(2)} v_m^{(1)}). \tag{3.66}$$

Since the first order solutions are independent of t_1, all derivatives with respect to t_1

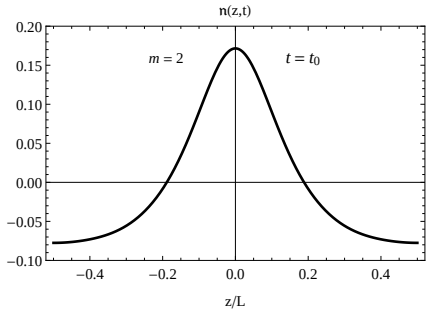

(a)

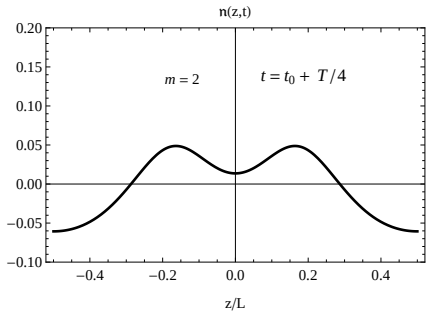

(b)

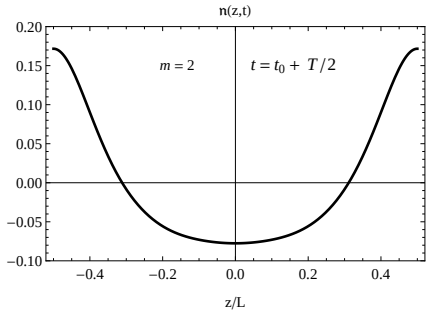

(c)

Figure 3.3: Plots of the density perturbation of a large amplitude nonlinear standing mode $m = 2$, for $k_\perp = 10k_1$, obtained from fluid simulations described in appendix F, with $M = 26$.

resulted in zero. First we simplify the RHS of above equation. Using (3.57) we write:

$$\partial_{t_2} v_m^{(1)} = \frac{\omega_m}{k_m}\partial_{t_2} A_m^s \sin[\omega_m t_0 + \alpha_m] + \frac{\omega_m}{k_m} A_m^s \partial_{t_2}\alpha_m \cos[\omega_m t_0 + \alpha_m]. \tag{3.67}$$

Using (3.57), (3.64) and (3.65) and trigonometrical identities we write:

$$v_{2m}^{(2)} n_m^{(1)} = \left(\frac{\omega_m}{k_m}\right)\frac{k_\perp^2 + 2k_m^2}{16k_m^2}(A_m^s)^3(\sin[3(\omega_m t_0 + \alpha_m)] + \sin[\omega_m t_0 + \alpha_m]), \tag{3.68}$$

$$n_{2m}^{(2)} v_m^{(1)} = \left(\frac{\omega_m}{k_m}\right)\frac{k_\perp^2 + 4k_m^2}{16k_m^2}(A_m^s)^3(\sin[3(\omega_m t_0 + \alpha_m)] - \sin[\omega_m t_0 + \alpha_m])$$
$$+\frac{\omega_m^3}{2k_m\omega_{2m}^2}\sin[\omega_m t_0 + \alpha_m], \tag{3.69}$$

$$v_{2m}^{(2)} v_m^{(1)}$$
$$= \left(\frac{\omega_m}{k_m}\right)^2 \frac{k_\perp^2 + 2k_m^2}{16k_m^2}(A_m^s)^3(\cos[\omega_m t_0 + \alpha_m] - \cos[3(\omega_m t_0 + \alpha_m)]). \tag{3.70}$$

Using Eq. (3.67) through Eq. (3.70) in Eq. (3.66) we obtain:

$$[\partial_{t_0}^2 + \omega_m^2] n_m^{(3)} = \omega_m^2\left(2\omega_m^{-1} A_m^s \partial_{t_2}\alpha_m - \frac{3k_\perp^2 + 8k_m^2}{32k_m^2}(A_m^s)^3 + \frac{\omega_m^2}{2\omega_{2m}^2}(A_m^s)^3\right)\cos[\omega_m t_0 + \alpha_m]$$
$$+2\omega_m \partial_{t_2} A_m^s \sin[\omega_m t_0 + \alpha_m] + \omega_m^2\left(\frac{k_\perp^2}{32k_m^2} + \frac{1}{4}\right)(A_m^s)^3\cos[3(\omega_m t_0 + \alpha_m)]. \tag{3.71}$$

Removing the resonant terms from the RHS of above equation (those with frequency ω_m) we obtain:

$$\partial_{t_2} A_m^s = 0 \Rightarrow A_m^s = A_m^s(t_3, t_4, \ldots). \tag{3.72}$$

Also we obtain

$$\partial_{t_2}\alpha_m = \omega_m \frac{3k_\perp^2(k_\perp^2 + 3k_m^2)}{64k_m^2(k_\perp^2 + k_m^2)}(A_m^s)^2,$$

which implies

$$\alpha_m = \omega_m \frac{3k_\perp^2(k_\perp^2 + 3k_m^2)}{64k_m^2(k_\perp^2 + k_m^2)}(A_m^s)^2 t_2 + \alpha'_m(t_3, \ldots). \tag{3.73}$$

Equation (3.73) gives the lowest order correction to mode frequency ω_m due to nonlinearity. Defining $\overline{\omega}_m$ to be the nonlinear mode frequency and setting $\varepsilon = 1$ so that $t_2 \to t$ we get:

$$\overline{\omega}_m = \omega_m \left(1 + \frac{3k_\perp^2(k_\perp^2 + 3k_m^2)}{64k_m^2(k_\perp^2 + k_m^2)} (A_m^s)^2 + \ldots \right). \tag{3.74}$$

Similar to the traveling wave result, in case of a long and thin plasma for which $k_m^2 \ll k_\perp^2$, the above result is only correct if

$$A_m^s \ll k_m^2/k_\perp^2 \approx \Delta_{m,2m}/3\omega_m, \tag{3.75}$$

where $\Delta_{m,2m} = 2\omega_m - \omega_{2m}$ is the detuning between mode m and $2m$. If $A_m^s \sim k_m^2/k_\perp^2$, the entire perturbation formalism of ordering in terms of small parameter breaks down, since $k_m^2/k_\perp^2$ itself can be small and comparable to wave amplitude A_m^s, which has not been worked into the perturbation formalism above. Now, for a long and thin plasma, we can expand the frequency correction in Eq. (3.35) in terms of small $k_m/k_\perp$ and to the lowest order we obtain:

$$\omega_m^{(2)} \approx \omega_m \frac{3k_\perp^2}{64k_m^2} (A_m^t)^2. \tag{3.76}$$

We can continue the above calculation to the desired order in ε.

3.3 General 1D simplified fluid model, large detuning

In the previous section we focused on the nonlinear corrections to a single traveling mode or standing mode m. For this mode, the mth spatial Fourier is of order ε and all the higher harmonics, which appear in plasma due to mode m being nonlinear, are of order ε^2 and higher.

In this section, an arbitrary number of spatial Fourier terms of order ε are assumed to be present in the plasma and we analyze the weak nonlinear interaction between these terms for both the traveling and the standing waves. We are interested in the nonlinear effects in the regime where the nonlinearity is much weaker than the dispersion. This condition quantitatively is given by the inequality in Eq. (3.107) which compares the size of the plasma density perturbation to the ratio of frequency mismatch(detuning) and mode frequency. Because of the large detuning (strong dispersion), nonlinear resonant wave-wave interaction is absent from the plasma. We start from 1D, fluid equations coupled with Poisson equation:

$$\partial_t N + \partial_z (N v) = 0 \text{(continuity)}, \tag{3.77}$$

$$\partial_t v + v \partial_z v = -\partial_z \phi \text{ (momentum)}, \tag{3.78}$$

$$(-k_\perp^2 + \partial_z^2)\phi = -N \text{ (Poisson)}. \tag{3.79}$$

In the above equations

$$v = v(z,t), \quad N = N(z,t), \quad \phi = \phi(z,t). \tag{3.80}$$

Time is scaled to plasma frequency $\omega_p = \sqrt{4\pi q^2 n_0 / m_q}$ and plasma density has been scaled to the average density n_0. We expand the spatial dependence of the variables

in terms of Fourier series:

$$v(z,t) = \sum_{m=-\infty}^{\infty} \mathrm{v}_m(t) e^{ik_m z}, \tag{3.81}$$
$$N(z,t) = 1 + \sum_{m=-\infty}^{\infty} \mathrm{n}_m(t) e^{ik_m z},$$
$$\phi(z,t) = \sum_{m=-\infty}^{\infty} \phi_m(t) e^{ik_m z}.$$

where all the sums exclude the $m = 0$ term and since $v(z,t), N(z,t)$ and $\phi(z,t)$ are real, we have the following relations:

$$\mathrm{v}_{-m}(t) = \mathrm{v}_m^*(t), \quad n_{-m}(t) = n_m^*(t), \quad \phi_{-m}(t) = \phi_m^*(t). \tag{3.82}$$

We multiply Eq. (3.77) through Eq. (3.79) by $\frac{1}{L} e^{-ik_l z}$ and integrate over the length of the plasma L and use the Fourier expansions given in Eq.'s (3.81). From the Poisson equation Eq. (3.79) we obtain:

$$[k_\perp^2 + k_l^2]\phi_l = \mathrm{n}_l. \tag{3.83}$$

We use the following relation in the continuity equation (3.77):

$$\frac{1}{L}\int_0^L \partial_z[(N(z,t)-1)\mathrm{v}(z,t)]e^{-ik_l z}\,dz$$
$$= ik_l \sum_{m=-\infty}^{\infty}\sum_{m'=-\infty}^{\infty} \frac{1}{L}\int_0^L \mathrm{n}_m \mathrm{v}_{m'} e^{i(k_m + k_{m'} - k_l)z}\,dz = ik_l \sum_{m=-\infty}^{\infty} \mathrm{n}_m \mathrm{v}_{l-m},$$

We use the following relation in the momentum equation (3.78):

$$\frac{1}{L}\int_0^L [\mathrm{v}(z,t)\partial_z \mathrm{v}(z,t)]e^{-ik_l z}\,dz$$
$$= \sum_{m=-\infty}^{\infty}\sum_{m'=-\infty}^{\infty} \frac{1}{L}\int_0^L \mathrm{v}_m e^{ik_m z} ik_m \mathrm{v}_{m'} e^{i(k_m + k_{m'} - k_l)z}\,dz = i\sum_{m=-\infty}^{\infty} k_m \mathrm{v}_m \mathrm{v}_{l-m}$$

As a result we obtain the exact equations

$$\frac{d}{dt}\mathrm{n}_l + ik_l\mathrm{v}_l + ik_l\sum_{m=-\infty}^{\infty}\mathrm{n}_m\mathrm{v}_{l-m} = 0 \tag{3.84}$$

$$\frac{d}{dt}\mathrm{v}_l + i\sum_{m=-\infty}^{\infty}k_m\mathrm{v}_m\mathrm{v}_{l-m} = -i\tfrac{k_l}{k_\perp^2+k_l^2}\mathrm{n}_l, \tag{3.85}$$

where we used Eq. (3.83) on the right hand side of Eq. (3.85). Using multiple time-scale expansion, we assume weak nonlinearity and propose the following solution forms for all m:

$$\begin{aligned}\mathrm{v}_m &= \varepsilon v_m^{(1)} + \varepsilon^2 v_m^{(2)} + \varepsilon^3 v_m^{(3)} + \ldots,\\ \mathrm{n}_m &= \varepsilon n_m^{(1)} + \varepsilon^2 n_m^{(2)} + \varepsilon^3 n_m^{(3)} + \ldots,\end{aligned} \tag{3.86}$$

where based on Eq. (3.82) we have the following relations

$$v_{-m}^{(j)} = (v_m^{(j)})^*, \quad n_{-m}^{(j)} = (n_m^{(j)})^*, \quad j = 1,2,\ldots \tag{3.87}$$

Multiple timescales have the following hierarchy [30]:

$$\tau_0 = t, \quad \tau_1 = \varepsilon t, \quad \tau_2 = \varepsilon^2 t, \ldots \tag{3.88}$$

$$\frac{d}{dt} = \frac{\partial}{\partial\tau_0} + \varepsilon\frac{\partial}{\partial\tau_1} + \varepsilon^2\frac{\partial}{\partial\tau_2} + \ldots \tag{3.89}$$

To the first order in ε, eqn's (3.77) through (3.79) give:

$$\partial_{\tau_0} n_m^{(1)} + ik_m v_m^{(1)} = 0, \tag{3.90}$$

$$\partial_{\tau_0} v_m^{(1)} = -i\tfrac{k_l}{k_\perp^2+k_l^2} n_m^{(1)}. \tag{3.91}$$

Elliminating $v_m^{(1)}$ from Eq. (3.90) and Eq. (3.91) get

$$\left[\partial_{\tau_0}^2 + \frac{k_m^2}{K_m^2}\right] n_m^{(1)} = 0, \tag{3.92}$$

where

$$K_m = \sqrt{k_\perp^2 + k_m^2}. \tag{3.93}$$

For traveling modes, the linear solutions with axial Fourier number m is of the form:

$$n_m^{(1)}(\tau_0, \tau_1) = n_m(\tau_1) e^{-i\omega_m \tau_0}, \tag{3.94}$$

where from Eq. (3.87) n_m's satisfy

$$n_{-m} = n_m^*, \tag{3.95}$$

and with ω_m, the mode frequency to be determined, which satisfies

$$\omega_{-m} = -\omega_m. \tag{3.96}$$

The amplitude of the linear traveling mode $A_m^t(t)$, $(m > 0)$ is defined by:

$$n_m^t(z;t) = A_m^t(t)\cos[k_m z - \omega_m t + \alpha_m(t)] \tag{3.97}$$

$$= \frac{A_m^t(t)}{2}\left[e^{i(k_m z - \omega_m \tau_0 + \alpha_m(t))} + e^{-i(k_m z - \omega_m \tau_0 + \alpha_m(t))}\right],$$

$$= n_m(\tau_1) e^{i(k_m z - \omega_m \tau_0)} + n_m^*(\tau_1) e^{-i(k_m z - \omega_m \tau_0)}, \quad m > 0. \tag{3.98}$$

Thus, for traveling waves we obtain the follwing relation:

$$n_m(t) = \frac{A_m^t(t)}{2} e^{i\alpha_m}, \quad m > 0. \tag{3.99}$$

From Eq. (3.90) and Eq. (3.94) we obtain $v_m^{(1)}$:

$$v_m^{(1)} = v_m(\tau_1) e^{-i\omega_m \tau_0}. \tag{3.100}$$

For standing modes, the linear solutions with axial Fourier number m is of the form:

$$n_m^{(1)}(\tau_0, \tau_1) = n_m(\tau_1) e^{-i\omega_m \tau_0} + n_m^*(\tau_1) e^{i\omega_m \tau_0}, \tag{3.101}$$

with ω_m, the mode frequency to be determined, which satisfies Eq. (3.96) , and since $n_m^{(1)}$'s satisfy Eq. (3.87), n_m's satisfy Eq. (3.95). The amplitude of the linear standing mode $A_m^s(t)$ is defined as:

$$\begin{aligned} n_m^s(z;t) &= A_m^s(t)\cos[\omega_m t - \alpha_m(t)]\cos[k_m z] \\ &= \frac{A_m^s(t)}{4}\left[e^{-i(\omega_m\tau_0-\alpha_m(t))} + e^{i(\omega_m\tau_0-\alpha_m(t))}\right]\left[e^{ik_m z} + e^{-ik_m z}\right] \\ &= \left(n_m(\tau_1)e^{-i\omega_m\tau_0} + n_m^*(\tau_1)e^{i\omega_m\tau_0}\right)\left[e^{ik_m z} + e^{-ik_m z}\right]. \end{aligned} \tag{3.102}$$

Thus we obtain the following relation for the standing waves:

$$n_m(t) = \frac{A_m^s(t)}{4}e^{i\alpha_m}, \quad m > 0.$$

From (3.90) and (3.101) we obtain $v_m^{(1)}$:

$$v_m^{(1)} = \frac{\omega_m}{k_m}n_m(\tau_1)e^{-i\omega_m\tau_0} - \frac{\omega_m}{k_m}n_m^*(\tau_1)e^{i\omega_m\tau_0}, \tag{3.103}$$

which gives:

$$v_m^s(z,t) = v_m^{(1)}e^{ik_m z} + v_{-m}^{(1)}e^{-ik_m z} = A_m^s(t)\sin[\omega_m t - \alpha_m(t)]\sin[k_m z]. \tag{3.104}$$

Since the solutions have similar results for traveling and standing waves, we carry out our derivation for standing waves and explain wherever the results for traveling waves differ. From (3.92) we obtain the dispersion relation:

$$\omega_m = \frac{k_m}{K_m}, \tag{3.105}$$

where K_m is given by Eq. (3.93). We define the frequency mis-match (detuning) $\Delta_{m,l}$ between the three linear waves $l, l-m$ and m as:

$$\Delta_{m,l} = \omega_m + \omega_{l-m} - \omega_l. \tag{3.106}$$

In general, the condition for exact resonance between three linear modes is that $k_m + k_{l-m} - k_l = 0$ and $\Delta_{m,l} = 0$, i.e. exact wavenumber match and frequency match.

In this section we are interested in the large detuning regime for which:

$$|n_l| \ll \Delta_{m,l}/\omega_l. \tag{3.107}$$

For large detuning (strong dispersion), frequency matching between three TG modes and resonant wave-wave interaction is not possible.

Using the perturbation series Eq. (3.86), and multiple time-scale derivative series given in Eq. (3.89), we keep the terms of the second order in ε for Eq. (3.84) and Eq. (3.85):

$$\partial_{\tau_0} n_l^{(2)} + \partial_{\tau_1} n_l^{(1)} + i\,k_l \sum_{m=-\infty}^{\infty} n_m^{(1)} v_{l-m}^{(1)} + i\,k_l\, v_l^{(2)} = 0, \tag{3.108}$$

$$\partial_{\tau_0} v_l^{(2)} + \partial_{\tau_1} v_l^{(1)} + i \sum_{m=-\infty}^{\infty} k_m\, v_m^{(1)} v_{l-m}^{(1)} = -i\frac{\omega_l^2}{k_l} n_l^{(2)}. \tag{3.109}$$

Using Eq. (3.101) and Eq. (3.103), for a standing wave we use the following series in Eq. (3.108):

$$\begin{aligned}
&i\,k_l \sum_{m=-\infty}^{\infty} n_m^{(1)} v_{l-m}^{(1)} \\
&= i\,k_l \sum_{m=-\infty}^{\infty} \frac{\omega_{l-m}}{k_{l-m}} \left(n_m e^{-i\omega_m \tau_0} + n_m^* e^{i\omega_m \tau_0}\right)\left(n_{l-m} e^{-i\omega_{l-m}\tau_0} - n_{l-m}^* e^{i\omega_{l-m}\tau_0}\right) \\
&= i\,k_l \sum_{m=-\infty}^{\infty} \frac{\omega_{l-m}}{k_{l-m}} \left(n_m n_{l-m} e^{-i(\omega_m+\omega_{l-m})\tau_0} + n_m^* n_{l-m} e^{i(\omega_m-\omega_{l-m})\tau_0}\right) + c.c.
\end{aligned}$$

Furthermore, using Eq. (3.103), for a standing wave we use the following series in Eq. (3.109):

$$\begin{aligned}
&i \sum_{m=-\infty}^{\infty} k_m\, v_m^{(1)} v_{l-m}^{(1)} \\
&= i \sum_{m=-\infty}^{\infty} \omega_m \frac{\omega_{l-m}}{k_{l-m}} \left(n_m e^{-i\omega_m \tau_0} - n_m^* e^{i\omega_m \tau_0}\right)\left(n_{l-m} e^{-i\omega_{l-m}\tau_0} - n_{l-m}^* e^{i\omega_{l-m}\tau_0}\right) \\
&= i \sum_{m=-\infty}^{\infty} \omega_m \frac{\omega_{l-m}}{k_{l-m}} \left(n_m n_{l-m} e^{-i(\omega_m+\omega_{l-m})\tau_0} - n_m^* n_{l-m} e^{i(\omega_m-\omega_{l-m})\tau_0} + c.c.\right)
\end{aligned}$$

We operate ∂_{τ_0} on Eq. (3.108), multiply Eq. (3.109) by $-ik_l$ and add the two equations to obtain:

$$[\partial_{\tau_0}^2+\omega_l^2]n_l^{(2)}=2i\omega_l\partial_{\tau_1}n_m(\tau_1)e^{-i\omega_l\tau_0}-k_l\sum_{m=-\infty}^{\infty}\frac{\omega_{l-m}}{k_{l-m}} \tag{3.110}$$
$$\left[(\omega_{l-m}+2\omega_m)n_m n_{l-m}e^{-i(\omega_m+\omega_{l-m})\tau_0}-(2\omega_m-\omega_l)n_m^* n_{l-m}e^{i(\omega_m-\omega_{l-m})\tau_0}\right]+c.c.$$

We operate ∂_{τ_0} on Eq. (3.109), multiply Eq. (3.108) by $-ik_l/K_l^2$ and add the two equations to obtain:

$$\begin{aligned}[\partial_{\tau_0}^2+\omega_l^2]v_l^{(2)}&=2i\frac{\omega_l^2}{k_l}\partial_{\tau_1}n_m(\tau_1)e^{-i\omega_l\tau_0}\\&-\sum_{m=-\infty}^{\infty}\frac{\omega_{l-m}}{k_{l-m}}\Big[(\omega_m^2+\omega_l^2+\omega_m\omega_{l-m})n_m n_{l-m}e^{-i(\omega_m+\omega_{l-m})\tau_0}\\&+(\omega_m^2+\omega_l^2-\omega_m\omega_{l-m})n_m^* n_{l-m}e^{i(\omega_m-\omega_{l-m})\tau_0}\Big]+c.c.\end{aligned} \tag{3.111}$$

The first terms on the right hand side of Eqs. (3.110) and (3.111) are resonant leading to secular growth of the solutions. In order to remove the secular terms on the RHS of equations (3.110) and (3.111) we must have:

$$\partial_{\tau_1}n_l=0, \tag{3.112}$$

Note that by the assumption of large detuning $(\omega_m+\omega_{l-m}-\omega_l)/\omega_l\gg\varepsilon$, there are no other resonant terms. The remaining terms on the right hand side of equations (3.110) and (3.111) contribute to the oscillatory solutions of the the order ε^2. Solving for $n_l^{(2)}$ we obtain:

$$\begin{aligned}n_l^{(2)}&=\sum_{m=-\infty}^{\infty}V_{l,m}[n_m n_{l-m}^*e^{i(\omega_{l-m}-\omega_m)\tau_0}+n_m^* n_{l-m}e^{-i(\omega_{l-m}-\omega_m)\tau_0}]\\&+\sum_{m=-\infty}^{\infty}W_{l,m}[n_m n_{l-m}e^{-i(\omega_{l-m}+\omega_m)\tau_0}+n_m^* n_{l-m}^*e^{i(\omega_{l-m}+\omega_m)\tau_0}],\end{aligned} \tag{3.113}$$

where:

$$
\begin{aligned}
&V_{l,m} = k_l \left(\tfrac{\omega_{l-m}}{k_{l-m}}\right) \tfrac{2\omega_m - \omega_{l-m}}{\omega_l^2 - (\omega_m - \omega_{l-m})^2}, \quad (m, l-m, l) \neq (0,0,0), \\
&V_{l,m} = 0, \quad (m, l-m, l) = (0,0,0), \\
&W_{l,m} = -k_l \left(\tfrac{\omega_{l-m}}{k_{l-m}}\right) \tfrac{2\omega_m + \omega_{l-m}}{\omega_l^2 - (\omega_m + \omega_{l-m})^2}, \quad (m, l-m, l) \neq (0,0,0), \\
&W_{l,m} = 0, \quad (m, l-m, l) = (0,0,0),
\end{aligned} \tag{3.114}
$$

Solving for $v_l^{(2)}$ we obtain:

$$
\begin{aligned}
v_l^{(2)} = &\sum_{m=-\infty}^{\infty} Y_{l,m} \left[n_m n_{l-m} e^{-i(\omega_m + \omega_{l-m})\tau_0} - n_m^* n_{l-m}^* e^{i(\omega_m + \omega_{l-m})\tau_0} \right] \\
&+ Z_{l,m} \left[n_m^* n_{l-m} e^{-i(\omega_{l-m} - \omega_m)\tau_0} - n_m n_{l-m}^* e^{i(\omega_{l-m} - \omega_m)\tau_0} \right],
\end{aligned} \tag{3.115}
$$

where:

$$
\begin{aligned}
&Y_{l,m} = -\left(\tfrac{\omega_{l-m}}{k_{l-m}}\right) \left[\tfrac{\omega_m^2 + \omega_l^2 + \omega_{l-m}\omega_m}{\omega_l^2 - (\omega_m + \omega_{l-m})^2} \right], \quad (m, l-m, l) \neq (0,0,0), \\
&Y_{l,m} = 0, \quad (m, l-m, l) = (0,0,0), \\
&Z_{l,m} = -\left(\tfrac{\omega_{l-m}}{k_{l-m}}\right) \left[\tfrac{\omega_m^2 + \omega_l^2 - \omega_{l-m}\omega_m}{\omega_l^2 - (\omega_m - \omega_{l-m})^2} \right], \quad (m, l-m, l) \neq (0,0,0), \\
&Z_{l,m} = 0, \quad (m, l-m, l) = (0,0,0).
\end{aligned} \tag{3.116}
$$

For traveling waves, we use Eq. (3.94) and Eq. (3.100) in Eq. (3.108) and Eq. (3.109) and following the same steps taken for standing waves we obtain:

$$
n_l^{(2)} = \sum_{m=-\infty}^{\infty} W_{l,m} n_m n_{l-m} e^{-i(\omega_{l-m} + \omega_m)\tau_0}, \tag{3.117}
$$

$$
v_l^{(2)} = \sum_{m=-\infty}^{\infty} Y_{l,m} n_m n_{l-m} e^{-i(\omega_m + \omega_{l-m})\tau_0}, \tag{3.118}
$$

where $W_{l,m}$ and $Y_{l,m}$ are defined in Eq. (3.114) and Eq. (3.116)

We now write the equations in the third order in ε. From Eq. (3.112), Eq. (3.113) and Eq. (3.115) we see that $\partial_{\tau_1} n_l^{(2)} = 0$ and $\partial_{\tau_1} v_l^{(2)} = 0$. Therefore, keeping the terms

of order ε^3 in the equations (3.84) and (3.85) we obtain:

$$\partial_{\tau_0} n_l^{(3)} + \partial_{\tau_2} n_l^{(1)} + [\partial_z (n^{(2)} v^{(1)} + v^{(2)} n^{(1)})]_l + i k_l v^{(3)} = 0, \tag{3.119}$$

$$\partial_{\tau_0} v_l^{(3)} + \partial_{\tau_2} v_l^{(1)} + [\partial_z (v^{(2)} v^{(1)})]_l = -i \frac{\omega_l^2}{k_l} n^{(3)}, \tag{3.120}$$

where the following notation was used:

$$[\dots]_l = \frac{1}{L} \int_0^L (\dots) e^{-i k_l z} dz. \tag{3.121}$$

Operating $-\partial_{\tau_0}$ on Eq. (3.119), multiplying Eq. (3.120) by $i k_l$ and adding the two equations yields:

$$\begin{aligned} &[-\partial_{\tau_0}^2 + \omega_l^2] n_l^{(3)} = i 2 k_l \partial_{\tau_2} v_l^{(1)} \\ &+ i k_l \Big(- \partial_{\tau_0} [n^{(2)} v^{(1)} + v^{(2)} n^{(1)}]_l + i k_l [v^{(2)} v^{(1)}]_l \Big), \end{aligned} \tag{3.122}$$

where we used $-\partial_{\tau_0} \partial_{\tau_2} n_l^{(1)} = i k_l \partial_{\tau_2} v_l^{(1)}$, and also we used:

$$[\partial_z (\dots)]_l = i k_l [\dots]_l. \tag{3.123}$$

By removing the secular terms from the RHS of Eq. (3.122), we obtain a second order mode frequency correction. Details of this calculation are worked out in appendix G. Assuming the functional form:

$$n_l(\tau_2, \tau_3, \dots) = \overline{n}_l(\tau_3, \dots) e^{-i \omega_l^{(2)} \tau_2}, \tag{3.124}$$

we can solve for the nonlinear mode frequency correction $\omega_l^{(2)}$ from Eq. (G.12). Substituting from Eq. (3.124) in Eq. (G.12) we obtain:

$$\begin{aligned} \omega_l^{(2)} = &-\frac{k_l}{2} \sum_m \Big\{ \tfrac{\omega_{l-m}}{k_{l-m}} (V_{m,l} + V_{m,m-l} - W_{m,l} - \overline{\delta}_{m,2l} W_{m,m-l}) + [1 - \tfrac{k_l}{\omega_l} \tfrac{\omega_{l-m}}{k_{l-m}}] (Z_{m,l} - Z_{m,m-l}) \\ &- [1 + \tfrac{k_l}{\omega_l} \tfrac{\omega_{l-m}}{k_{l-m}}] (Y_{m,l} + \overline{\delta}_{m,2l} Y_{m,m-l}) \Big\} |n_{l-m}|^2 \quad \text{(Standing waves)}. \end{aligned} \tag{3.125}$$

where $\overline{\delta}_{m,n}$ is defined in Eq. (G.10). $\omega_l^{(2)}$ is a real correction to the mode frequency. For traveling waves, we can obtain the frequency correction by setting the coefficients V and Z to zero in Eq. (3.125):

$$\omega_l^{(2)} = \frac{k_l}{2}\sum_m \Bigg\{ \frac{\omega_{l-m}}{k_{l-m}}(W_{m,l} + \overline{\delta}_{m,2l}\, W_{m,m-l}) \\ +[1+\tfrac{k_l}{\omega_l}\tfrac{\omega_{l-m}}{k_{l-m}}](Y_{m,l} + \overline{\delta}_{m,2l}\, Y_{m,m-l})\Bigg\}|n_{l-m}|^2 \quad \text{(Traveling waves)}. \tag{3.126}$$

3.3.1 Nonlinear eigenmodes

As a check of these general results, we can retrieve the mode frequency corrections obtained in the previous sections, i.e. Eq. (3.74) for standing waves and for traveling waves Eq. (3.35), from the general nonlinear mode frequency corrections, Eq. (3.125) and Eq. (3.126).

For mode l (standing or traveling) we assume all linear amplitudes except the lth is zero

$$n_j = 0, \quad j \neq \pm l. \tag{3.127}$$

Nonlinear correction to the standing eigenmode is obtained using (3.127) in (3.113):

$$n_{2l}^{(2)} = \frac{4\omega_l^2}{\omega_{2l}^2}|n_l|^2 + \frac{6\omega_l^2}{4\omega_l^2-\omega_{2l}^2}\left[n_l^2 e^{-i2\omega_l\tau_0} + (n_l^*)^2 e^{i2\omega_l\tau_0}\right], \tag{3.128}$$

$$v_{2l}^{(2)} = \left(\frac{\omega_l}{k_l}\right)\frac{\omega_{2l}^2-2\omega_l^2}{\omega_{2l}^2-4\omega_l^2}\left[n_l^2 e^{-i2\omega_l\tau_0} - (n_l^*)^2 e^{i2\omega_l\tau_0}\right]. \tag{3.129}$$

Substituting from Eq. (3.103) for n_l and for ω_l and ω_{2l} from Eq. (3.105) in Eqs. (3.128) and (3.129) we respectively obtain the previously derived results in equations (3.64) and (3.65). Due to the presence of higher spatial Fourier term above, the eigenmode is no longer sinusoidal in space. The correction to lth eigenfequency is obtained from Eq. (3.125), using the $m = 2l$:

$$\omega_l^{(2)} = -\tfrac{k_l}{2}[\tfrac{\omega_l}{k_l}(2V_{2l,l} - W_{2l,l}) - 2Y_{2l,l}]|n_l|^2. \tag{3.130}$$

Using equations (3.105), (3.103), (3.114) and (3.116), $\omega_l^{(2)}$ will have the simple form:

$$\omega_l^{(2)} = \omega_l \frac{3k_\perp^2(k_\perp^2+3k_l^2)}{64k_l^2(k_\perp^2+k_l^2)}|A_l^s|^2, \tag{3.131}$$

which is identical to the result in Eq. (3.74) for standing waves.

We can obtain the frequency shift for traveling waves from Eq. (3.126):

$$\omega_l^{(2)} = -\tfrac{k_l}{2}[\tfrac{\omega_l}{k_l}(-W_{2l,l})-2Y_{2l,l}]|n_l|^2. \tag{3.132}$$

Substituting for $W_{2l,l}$ and $Y_{2l,l}$ and using Eq. (3.99) we obtain:

$$\omega_l^{(2)} = \omega_l \frac{3k_\perp^2+8k_l^2}{16k_l^2}|A_l^t|^2, \tag{3.133}$$

which is identical to the result in Eq. (3.35) for traveling waves.

3.4 Wave-wave interaction in the simplified 1D fluid model, small detuning

In the previous sections we studied the cases for which the detuning was large compared to the size of the mode amplitude (see Eq. (3.107)). In this section we assume the detuning is small, as well as the mode amplitudes:

$$(\omega_m + \omega_{l-m} - \omega_l)/\omega_m \sim |n_l| \ll 1 \tag{3.134}$$

For long, thin plasmas i.e. $L \gg r_p$, which is the area of our interest, detuning is small. Equations (3.77) to (3.105) from the section 3.3 are applicable to this section as well, which include the first order equations in ε and the resulting linear solutions. Moreover, in order to keep track of the smallness of detuning in our perturbation method, we define the detuning $\Delta_{m,l}$ as:

$$\omega_m + \omega_{l-m} - \omega_l = \varepsilon \Delta_{m,l} \tag{3.135}$$

$$\tau_0(\omega_m + \omega_{l-m} - \omega_l) = \varepsilon \tau_0 \Delta_{m,l} = \tau_1 \Delta_{m,l}, \tag{3.136}$$

where we used (3.88) in (3.136) and ε is the same auxiliary smallness parameter that is seen everywhere else.

The second order in ε, continuity and momentum equations are respectively given by (3.108) and (3.109). Using Eq. (3.136), in Eq. (3.108) and Eq. (3.109) we write the exponential terms of the form $e^{-i(\omega_m+\omega_{l-m})\tau_0}$ as $e^{-i\Delta_{m,l}\tau_1 - i\omega_l\tau_0}$. Next, we operate ∂_{τ_0} on Eq. (3.108), multiply Eq. (3.109) by $-ik_l$, and finally add the two equations (3.108) and (3.109) to obtain:

$$[\partial_{\tau_0}^2 + \omega_l^2] n_l^{(2)} = 2i\omega_l \partial_{\tau_1} n_m(\tau_1) e^{-i\omega_l\tau_0} - k_l \sum_{m=-\infty}^{\infty} \frac{\omega_{l-m}}{k_{l-m}} (\omega_l + \omega_m) n_m n_{l-m} e^{-i\Delta_{m,l}\tau_1 - i\omega_l\tau_0}$$
$$+ k_l \sum_{m=-\infty}^{\infty} \frac{\omega_{l-m}}{k_{l-m}} (2\omega_m - \omega_l) n_m^* n_{l-m} e^{i(\omega_m - \omega_{l-m})\tau_0} + c.c. \tag{3.137}$$

We set the resonant terms (terms with $e^{\pm i\omega_l\tau_0}$ time dependence on the RHS) equal

to zero to avoid a secular solution for $n_l^{(2)}$. To this purpose, we set:

$$\partial_{\tau_1} n_l = -i \sum_{m=-\infty}^{\infty} X_{l,m} n_m n_{l-m} e^{-i\Delta_{m,l}\tau_1} \tag{3.138}$$

in Eq. (3.137), where the nonlinear coupling coefficients are defined as following:

$$\begin{aligned} X_{l,m} &= k_l \tfrac{\omega_{l-m}}{2k_{l-m}} \left(1 + \tfrac{\omega_m}{\omega_l}\right), \quad (m, l-m, l) \neq (0,0,0) \\ X_{l,m} &= 0, \quad (m, l-m, l) = (0,0,0) \end{aligned} \tag{3.139}$$

In the next section we investigate the energy conservation for a traveling wave where we will be needing $n_l^{(2)}$ and $v_l^{(2)}$. In order to solve for the second order perturbations $n_l^{(2)}$ and $v_l^{(2)}$, we substitute Eq. (3.138) in Eq. (3.108) to get:

$$\begin{aligned} &\partial_{\tau_0} n_l^{(2)} - i k_l \sum_{m=-\infty}^{\infty} \tfrac{\omega_{l-m}}{2k_{l-m}} \left(1 + \tfrac{\omega_m}{\omega_l}\right) n_m n_{l-m} e^{-i(\omega_m + \omega_{l-m})\tau_0} \\ &+ i k_l \sum_{m=-\infty}^{\infty} \tfrac{\omega_{l-m}}{k_{l-m}} n_m n_{l-m} e^{-i(\omega_m + \omega_{l-m})\tau_0} + i k_l v_l^{(2)} = 0 \end{aligned} \tag{3.140}$$

In deriving Eq. (3.140) from Eq. (3.108) for a traveling wave, we used Eq. (3.94) and Eq. (3.138) which imply:

$$\begin{aligned} \partial_{\tau_1} n_l^{(1)} &= \partial_{\tau_1} n_l(\tau_1) e^{-i\omega_l \tau_0} \\ &= -i \sum_{m=-\infty}^{\infty} X_{l,m} n_m n_{l-m} e^{-i\Delta_{m,l}\tau_1 - i\omega_l \tau_0} \\ &= -i \sum_{m=-\infty}^{\infty} X_{l,m} n_m n_{l-m} e^{-i(\omega_m + \omega_{l-m})\tau_0} \end{aligned} \tag{3.141}$$

In the last line above we used Eq. (3.136).

Equation (3.140) may now be simplified to:

$$\partial_{\tau_0} n_l^{(2)} + i \frac{k_l}{2\omega_l} \sum_{m=-\infty}^{\infty} \tfrac{\omega_{l-m}}{k_{l-m}} (\omega_l - \omega_m) n_m n_{l-m} e^{-i(\omega_m + \omega_{l-m})\tau_0} + i k_l v_l^{(2)} = 0 \tag{3.142}$$

Furthermore, we substitute Eq. (3.138) in Eq. (3.109) and use Eq. (3.100) to obtain

$$\partial_{\tau_0} v_l^{(2)} - i\omega_l \sum_{m=-\infty}^{\infty} \frac{\omega_{l-m}}{2k_{l-m}} \left(1+\frac{\omega_m}{\omega_l}\right) n_m n_{l-m} e^{-i(\omega_m+\omega_{l-m})\tau_0} + i \sum_{m=-\infty}^{\infty} \omega_m \frac{\omega_{l-m}}{k_{l-m}} n_m n_{l-m} e^{-i(\omega_m+\omega_{l-m})\tau_0} + i\frac{\omega_l^2}{k_l} n_l^{(2)} = 0 \tag{3.143}$$

which is simplified to

$$\partial_{\tau_0} v_l^{(2)} - \frac{i}{2} \sum_{m=-\infty}^{\infty} \frac{\omega_{l-m}}{k_{l-m}} (\omega_l - \omega_m) n_m n_{l-m} e^{-i(\omega_m+\omega_{l-m})\tau_0} + i\frac{\omega_l^2}{k_l} n_l^{(2)} = 0 \tag{3.144}$$

Elliminating $v_l^{(2)}$ from Eq. (3.142) and Eq. (3.144) we get:

$$(\partial_{\tau_0}^2 + \omega_l^2) n_l^{(2)} + \frac{k_l}{2\omega_l} \sum_{m=-\infty}^{\infty} (\omega_m + \omega_{l-m} - \omega_l) \frac{\omega_{l-m}}{k_{l-m}} (\omega_l - \omega_m) n_m n_{l-m} e^{-i(\omega_m+\omega_{l-m})\tau_0} = 0 \tag{3.145}$$

Solving for $n_l^{(2)}$ we get:

$$n_l^{(2)} = \sum_{m=-\infty}^{\infty} \frac{k_l}{2\omega_l} \frac{\omega_{l-m}}{k_{l-m}} \frac{\omega_l - \omega_m}{\omega_l + \omega_m + \omega_{l-m}} n_m n_{l-m} e^{-i(\omega_m+\omega_{l-m})\tau_0} \tag{3.146}$$

Substituting from Eq. (3.146) for $n_l^{(2)}$ in Eq. (3.142) and solving for $v_l^{(2)}$ we obtain:

$$v_l^{(2)} = -\sum_{m=-\infty}^{\infty} \frac{\omega_{l-m}}{2k_{l-m}} \frac{\omega_l - \omega_m}{\omega_l + \omega_m + \omega_{l-m}} n_m n_{l-m} e^{-i(\omega_m+\omega_{l-m})\tau_0} \tag{3.147}$$

Equation (3.138) expresses the time evolution of the linear mode amplitudes in both the traveling and standing waves, due to nonlinear coupling between all the possible triads of linear modes (three wave interactions). We drop the multiple time scales perturbation notation and set $\varepsilon = 1$. As a result $\tau_1 = t$ and we obtain the following equations in time t:

$$\frac{dn_l}{dt} = -i \sum_{m=-\infty}^{\infty} X_{l,m} n_m n_{l-m} e^{-i\Delta_{m,l} t}, \tag{3.148}$$

where the nonlinear coupling coefficients are given by Eq. (3.139).

3.4.1 Energy conservation of the small detuning perturbation solution

In the last section we obtained a perturbation solution for the plasma density and velocity to the second order in ε. In this section we want to find out how well these perturbation solutions conserve the energy. Total energy of the plasma is given by:

$$K_E = \int \tfrac{1}{2} N v^2 dz, \tag{3.149}$$

$$V_E = \int \tfrac{1}{2} N \phi dz, \tag{3.150}$$

$$E = V_E + K_E. \tag{3.151}$$

where N, v and ϕ are given by (3.86). Using Eq. (3.81) we expand E, K_E and V_E in terms of spatial Fourier series:

$$K_E = \tfrac{1}{2} \sum_{l=-\infty}^{\infty} \left[\mathrm{v}_l \mathrm{v}_{-l} + \sum_{m=-\infty}^{\infty} \mathrm{n}_l \mathrm{v}_{-m} \mathrm{v}_{m-l} \right], \tag{3.152}$$

$$V_E = \tfrac{1}{2} \sum_{l=-\infty}^{\infty} \tfrac{\omega_l^2}{k_l^2} \mathrm{n}_l \mathrm{n}_{-l}, \tag{3.153}$$

$$E = \tfrac{1}{2} \sum_{l=-\infty}^{\infty} \left[\tfrac{\omega_l^2}{k_l^2} \mathrm{n}_l \mathrm{n}_{-l} + \mathrm{v}_l \mathrm{v}_{-l} + \sum_{m=-\infty}^{\infty} \mathrm{n}_l \mathrm{v}_{-m} \mathrm{v}_{m-l} \right], \tag{3.154}$$

where we used Eq. (3.83) for ϕ_l and we used the following integrals:

$$\int v^2 dz = \int (\sum_{l=-\infty}^{\infty} \mathrm{v}_l e^{ik_l z})(\sum_{l'=-\infty}^{\infty} \mathrm{v}_{l'} e^{ik_{l'} z}) = \sum_{l=-\infty}^{\infty} \mathrm{v}_l \mathrm{v}_{-l}$$

$$\int (v)^2 n dz = \int (\sum_{l=-\infty}^{\infty} \mathrm{n}_l e^{ik_l z})(\sum_{m=-\infty}^{\infty} \mathrm{v}_{-m} e^{ik_{-m} z})(\sum_{l'=-\infty}^{\infty} \mathrm{v}_{l'} e^{ik_{l'} z})$$

$$= \sum_{l=-\infty}^{\infty} \sum_{m=-\infty}^{\infty} \mathrm{n}_{-l} \mathrm{v}_m \mathrm{v}_{l-m}$$

Relations (3.152), (3.153) and (3.154) are for the exact density and velocity of plasma and the energy in (3.154) is conserved exactly. From our computer simulations we

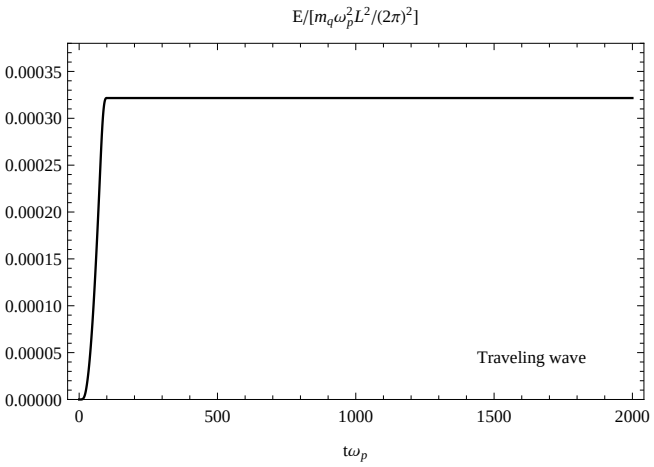

(a)

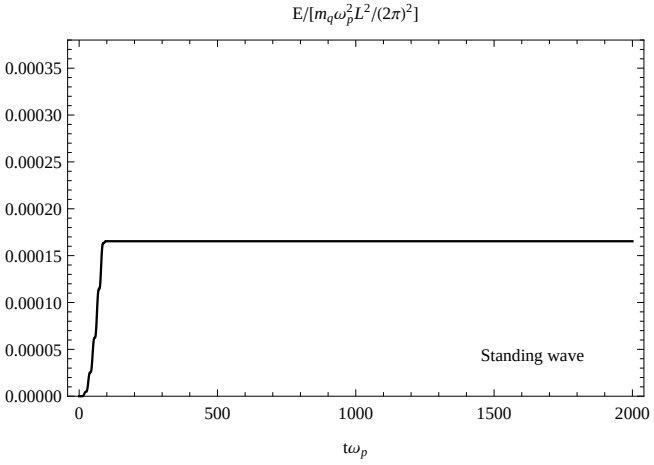

(b)

Figure 3.4: Figure (3.4a) shows the energy of a traveling wave of amplitude $A_2^t = 0.24$ and Fig. (3.4b) shows the energy of a standing wave of amplitude $A_2^s = 0.24$. Forcing time was $T_F\omega_p = 97$ and drive potential was $\overline{V}_2 = 1.8\times10^{-4}[m_q\omega_p^2(L/2\pi)^2]$ and $M =$ 8 Fourier terms were kept, for $k_\perp = 10k_1$.

can see that this is true, for both traveling and standing waves, for any number M of spatial Fourier terms kept M, and energy is conserved as we can see in Fig. (3.4a) for traveling and Fig. (3.4b) for standing waves, where we depicted the energy of the plasma for the amplitudes $A_2^t = A_2^s = 0.24$ and $M = 8$. Now we substitute our perturbation solutions for the exact density and velocity to obtain the perturbation solution for energy:

$$\mathrm{n}_l(t) \approx \varepsilon n_l^{(1)}(t) + \varepsilon^2 n_l^{(2)} \tag{3.155}$$

$$\mathrm{v}_l(t) \approx \varepsilon v_l^{(1)}(t) + \varepsilon^2 v_l^{(2)} \tag{3.156}$$

We use Eq. (3.155) in K_E and V_E given by Eq. (3.152) and Eq. (3.153), and keep the terms up to the third order in ε:

$$K_E = \tfrac{1}{2} \sum_{l=-\infty}^{\infty} \left[\varepsilon^2 v_l^{(1)} v_{-l}^{(1)} + \varepsilon^3 2 v_{-l}^{(1)} v_l^{(2)} + \varepsilon^3 \sum_{m=-\infty}^{\infty} n_{-l}^{(1)} v_{l-m}^{(1)} v_m^{(1)} \right] \tag{3.157}$$

$$V_E = \tfrac{1}{2} \sum_{l=-\infty}^{\infty} \tfrac{1}{K_l^2} \left[\varepsilon^2 n_{-l}^{(1)} n_l^{(1)} + \varepsilon^3 2 n_l^{(2)} n_{-l}^{(1)} \right] \tag{3.158}$$

For a traveling wave $n_l^{(1)}$ is given by (3.94) and $v_l^{(1)}$ is given by (3.100):

$$n_l^{(1)} = n_l(\tau_1) e^{-i\omega_l \tau_0}, \quad v_l^{(1)} = v_l(\tau_1) e^{-i\omega_l \tau_0} \tag{3.159}$$

where $v_l = \frac{\omega_l}{k_l} n_l(\tau_1)$ and the time evolution of $n_l(\tau_1)$ is given by Eq. (3.138). $n_l^{(2)}$ and $v_l^{(2)}$ are given by (3.146) and (3.147). From Eq. (3.157) and Eq. (3.158) the total energy up tp ε^3 is given by:

$$\begin{aligned} E &= K_E + V_E \qquad (3.160) \\ &= \tfrac{1}{2} \sum_{l=-\infty}^{\infty} \left[\varepsilon^2 v_l^{(1)} v_{-l}^{(1)} + \varepsilon^2 \tfrac{\omega_l^2}{k_l^2} n_{-l}^{(1)} n_l^{(1)} + \varepsilon^3 2 v_{-l}^{(1)} v_l^{(2)} + \varepsilon^3 2 n_l^{(2)} n_{-l}^{(1)} + \varepsilon^3 \sum_{m=-\infty}^{\infty} n_{-l}^{(1)} v_{l-m}^{(1)} v_m^{(1)} \right] \end{aligned}$$

Using Eq. (3.146) and (3.147), we obtain:

$$\sum_{l=-\infty}^{\infty} v_l^{(2)} v_{-l}^{(1)}$$
$$= -\frac{1}{2}\frac{\omega_l}{k_l}\sum_{m=-\infty}^{\infty}\frac{\omega_{l-m}}{k_{l-m}}\frac{\omega_l-\omega_m}{\omega_l+\omega_m+\omega_{l-m}} n_l^* n_m n_{l-m} e^{-i(\omega_m+\omega_{l-m}-\omega_l)\tau_0} \quad (3.161)$$
$$\sum_{l=-\infty}^{\infty} \frac{\omega_l^2}{k_l^2} n_l^{(2)} n_{-l}^{(1)}$$
$$= \frac{1}{2}\frac{\omega_l}{k_l}\sum_{m=-\infty}^{\infty}\frac{\omega_{l-m}}{k_{l-m}}\frac{\omega_l-\omega_m}{\omega_l+\omega_m+\omega_{l-m}} n_l^* n_m n_{l-m} e^{-i(\omega_m+\omega_{l-m}-\omega_l)\tau_0} \quad (3.162)$$

As a result, the terms 3 and 4 of the sum in Eq. (3.160) will add to zero:

$$\varepsilon^3 \sum_{l=-\infty}^{\infty} v_l^{(2)} v_{-l}^{(1)} + \varepsilon^3 \sum_{l=-\infty}^{\infty} \frac{\omega_l^2}{k_l^2} n_l^{(2)} n_{-l}^{(1)} = 0 \quad (3.163)$$

For the first two terms of the sum in Eq. (3.160), which makes up the total wave energy as given by the classic linear theory:

$$\tfrac{1}{2}\sum_{l=-\infty}^{\infty} v_l^{(1)} v_{-l}^{(1)} = \tfrac{1}{2}\sum_{l=-\infty}^{\infty} (v_l v_l^*) \quad (3.164)$$
$$\tfrac{1}{2}\sum_{l=-\infty}^{\infty} \tfrac{1}{K_l^2} n_l^{(1)} n_{-l}^{(1)} = \tfrac{1}{2}\sum_{l=-\infty}^{\infty} \tfrac{\omega_l^2}{k_l^2}(n_l n_l^*), \quad (3.165)$$

Since $v_l = \frac{\omega_l}{k_l} n_l$, from adding the equations (3.164) and (3.165) we get:

$$\tfrac{1}{2}\sum_{l=-\infty}^{\infty} (v_l^{(1)} v_{-l}^{(1)} + \tfrac{\omega_l^2}{k_l^2} n_l^{(1)} n_{-l}^{(1)}) = \sum_{l=-\infty}^{\infty} v_l v_l^* \quad (3.166)$$

The last term in Eq. (3.160) can be written as:

$$\tfrac{1}{2}\sum_{l=-\infty}^{\infty}\sum_{m=-\infty}^{\infty} n_{-l}^{(1)} v_{l-m}^{(1)} v_m^{(1)} = \tfrac{1}{2}\sum_{l=-\infty}^{\infty}\sum_{m=-\infty}^{\infty} K_l v_l^* v_{l-m} v_m e^{-i\Delta_{m,l}\tau_1}, \quad (3.167)$$

where we used $n_l^* = K_l v_l^*$. As a result, the total energy up to the order ε^3 after setting $\varepsilon = 1$ is given by:

$$\begin{aligned} E(t) &= K_E + V_E \\ &= \sum_{l=-\infty}^{\infty} \left[v_l v_{-l} + \tfrac{1}{2} \sum_{m=-\infty}^{\infty} K_l v_{-l} v_{l-m} v_m e^{-i\Delta_{m,l} t} \right] \end{aligned} \tag{3.168}$$

We will evaluate the time derivative of energy E given by Eq. (3.168):

$$\frac{d}{dt} E(t) = \sum_{l=-\infty}^{\infty} \left[\frac{d}{dt}(v_l v_{-l}) + \tfrac{1}{2} \frac{d}{dt} \sum_{m=-\infty}^{\infty} K_l v_{-l} v_{l-m} v_m e^{-i\Delta_{m,l} t} \right] \tag{3.169}$$

First we calculate the first term of the above sum. We symmetrize the coupling coefficients in Eq. (3.138) (with $\varepsilon = 1$) as follows:

$$\frac{d}{dt} n_l = -i \frac{1}{2} \left[\sum_{m=-\infty}^{\infty} X_{l,m} n_m n_{l-m} e^{-i\Delta_{m,l} t} + \sum_{m=-\infty}^{\infty} X_{l,m} n_m n_{l-m} e^{-i\Delta_{m,l} t} \right] \tag{3.170}$$

We change the dummy variable on the second sum to $m' = l - m$

$$\frac{d}{dt} n_l = -i \frac{1}{2} \left[\sum_{m=-\infty}^{\infty} X_{l,m} n_m n_{l-m} e^{-i\Delta_{m,l} t} + \sum_{m'=-\infty}^{\infty} X_{l,l-m'} n_{m'} n_{l-m'} e^{-i\Delta_{l,l-m'} t} \right], \tag{3.171}$$

We change the dummy variable on the second sum to $m' = m$, and since we have $\Delta_{m,l} = \Delta_{l-m,l}$ we can write:

$$\frac{d}{dt} n_l = -\frac{i}{2} \sum_{m=-\infty}^{\infty} (X_{l,m} + X_{l,l-m}) n_m n_{l-m} e^{-i\Delta_{m,l} t} \tag{3.172}$$

Since $v_m = n_m / K_m$, we rewrite Eq. (3.172) in terms of v_m's

$$\frac{d}{dt} v_l = -\frac{i}{2} \sum_{m=-\infty}^{\infty} \overline{X}_{l,m} v_m v_{l-m} e^{-i\Delta_{m,l} t} \tag{3.173}$$

$$\tag{3.174}$$

where

$$\begin{aligned}\overline{X}_{l,m} &= \tfrac{\omega_l}{k_l}\tfrac{k_m}{\omega_m}\tfrac{k_{l-m}}{\omega_{l-m}}(X_{l,m}+X_{l,l-m}) \\ &= \tfrac{\omega_l}{2}(K_l+K_m+K_{l-m}), \quad l\neq 2m \qquad (3.175)\\ &= \tfrac{\omega_m}{2}(K_{2m}+2K_m) \quad l=2m \qquad (3.176)\end{aligned}$$

Now we multiply (3.173) by v_{-l} and sum over l to get

$$\sum_{l=-\infty}^{\infty} v_{-l}\frac{d}{dt}v_l = -\frac{i}{2}\sum_{l=-\infty}^{\infty}\sum_{m=-\infty}^{\infty}\overline{X}_{l,m}v_{-l}v_m v_{l-m}e^{-i\Delta_{m,l}t} \qquad (3.177)$$

In the double sum on the RHS of Eq. (3.177), for an arbitrary trio of $-\bar{l},\bar{l}-\overline{m},\overline{m}$ we have the following:

$$\begin{aligned}&-\tfrac{i}{2}\overline{X}_{\bar{l},\overline{m}}v_{-\bar{l}}v_{\overline{m}}v_{\bar{l}-\overline{m}}e^{-i\Delta_{\overline{m},\bar{l}}t} - \tfrac{i}{2}\overline{X}_{-(\bar{l}-\overline{m}),-\bar{l}}v_{-\bar{l}}v_{\overline{m}}v_{\bar{l}-\overline{m}}e^{-i\Delta_{\overline{m},\bar{l}}t}\\ &-\tfrac{i}{2}\overline{X}_{-\overline{m},\bar{l}-\overline{m}}v_{-\bar{l}}v_{\overline{m}}v_{\bar{l}-\overline{m}}e^{-i\Delta_{\overline{m},\bar{l}}t} = -\tfrac{i}{2}(\overline{X}_{\bar{l},\overline{m}}+\overline{X}_{\overline{m}-\bar{l},-\bar{l}}+\overline{X}_{-\overline{m},\bar{l}-\overline{m}})v_{-\bar{l}}v_{\overline{m}}v_{\bar{l}-\overline{m}}e^{-i\Delta_{\overline{m},\bar{l}}t}\\ &=-\tfrac{i}{4}(\omega_{\bar{l}}+\omega_{\overline{m}-\bar{l}}+\omega_{-\overline{m}})(K_{\bar{l}}+K_{\overline{m}}+K_{\bar{l}-\overline{m}})v_{-\bar{l}}v_{\overline{m}}v_{\bar{l}-\overline{m}}e^{-i\Delta_{\overline{m},\bar{l}}t}\\ &=\tfrac{i}{4}\Delta_{\overline{m},\bar{l}}(K_{\bar{l}}+K_{\overline{m}}+K_{\bar{l}-\overline{m}})v_{-\bar{l}}v_{\overline{m}}v_{\bar{l}-\overline{m}}e^{-i\Delta_{\overline{m},\bar{l}}t}, \qquad (3.178)\end{aligned}$$

where we used $\Delta_{\overline{m},\bar{l}} = \omega_{-\bar{l}}+\omega_{\bar{l}-\overline{m}}+\omega_{\overline{m}}$ in the last line above. As a result the first term in Eq. (3.169) is given by:

$$\begin{aligned}&\sum_{l=-\infty}^{\infty}\frac{d}{dt}(v_l v_{-l}) = \sum_{l=-\infty}^{\infty}(\frac{d}{dt}v_{-l})v_l + \sum_{l=-\infty}^{\infty}(\frac{d}{dt}v_l)v_{-l} = 2\sum_{l=-\infty}^{\infty}(\frac{d}{dt}v_l)v_{-l}\\ &= i\sum_{m=-\infty}^{\infty}\sum_{l=-\infty}^{\infty}\frac{\Delta_{m,l}}{6}(K_l+K_m+K_{l-m})v_l^* v_m v_{l-m}e^{-i\Delta_{m,l}t} \qquad (3.179)\end{aligned}$$

Now we evaluate the last term in equation (3.169). Symmetrizing with respect to l and m we get:

$$\begin{aligned}&\frac{1}{2}\sum_{l=-\infty}^{\infty}\sum_{m=-\infty}^{\infty}K_l v_l^* v_{l-m}v_m e^{-i\Delta_{m,l}t}\\ &=\frac{1}{6}\sum_{l=-\infty}^{\infty}\sum_{m=-\infty}^{\infty}(K_l+K_m+K_{l-m})v_l^* v_{l-m}v_m e^{-i\Delta_{m,l}t} \qquad (3.180)\end{aligned}$$

Now the time derivative of the right hand side Eq. (3.180) is given by:

$$
\begin{aligned}
&-i\sum_{l=-\infty}^{\infty}\sum_{m=-\infty}^{\infty}\frac{\Delta_{m,l}}{6}(K_l+K_m+K_{l-m})v_l^*v_{l-m}v_m e^{-i\Delta_{m,l}t}\\
&+\frac{1}{6}\sum_{l=-\infty}^{\infty}\sum_{m=-\infty}^{\infty}(K_l+K_m+K_{l-m})\frac{d}{dt}(v_l^*v_{l-m}v_m)e^{-i\Delta_{m,l}t}
\end{aligned}
\tag{3.181}
$$

We simplify the last term on the right hand side of Eq. (3.181):

$$
\begin{aligned}
&-\frac{1}{6}\sum_{l=-\infty}^{\infty}\sum_{m=-\infty}^{\infty}(K_l+K_m+K_{l-m})\frac{d}{dt}(v_{-l}v_{l-m}v_m)e^{-i\Delta_{m,l}t} \qquad (3.182)\\
&=\frac{i}{12}\sum_{q=-\infty}^{\infty}\sum_{l=-\infty}^{\infty}\sum_{m=-\infty}^{\infty}(K_l+K_m+K_{l-m})\overline{X}_{-l,q}v_q v_{-q-l}v_{l-m}v_m e^{-i\Delta_{m,l}t}e^{-i\Delta_{q,-l}t}\\
&+\frac{i}{12}\sum_{q=-\infty}^{\infty}\sum_{l=-\infty}^{\infty}\sum_{m=-\infty}^{\infty}(K_l+K_m+K_{l-m})\overline{X}_{l-m,q}v_{-l}v_q v_{l-m-q}v_m e^{-i\Delta_{m,l}t}e^{-i\Delta_{q,l-m}t}\\
&+\frac{i}{12}\sum_{q=-\infty}^{\infty}\sum_{l=-\infty}^{\infty}\sum_{m=-\infty}^{\infty}(K_l+K_m+K_{l-m})\overline{X}_{m,q}v_{-l}v_{l-m}v_q v_{m-q}e^{-i\Delta_{m,l}t}e^{-i\Delta_{q,m}t}
\end{aligned}
$$

In the second term on the right hand side of Eq. (3.182) we change the dummy variables ($m=l'-m'$, $l=l'$), and in the first terms ($m=-l'$, $l=-m'$) and the simplified result for Eq. (3.182) is given by:

$$
\begin{aligned}
&\tfrac{1}{2}\partial_{\tau_1}\sum_{m=-\infty}^{\infty}K_l v_{-l}v_{l-m}v_m e^{-i\Delta_{m,l}t} \qquad (3.183)\\
&=-i\sum_{l=-\infty}^{\infty}\sum_{m=-\infty}^{\infty}\frac{\Delta_{m,l}}{6}(K_l+K_m+K_{l-m})v_l^*v_{l-m}v_m e^{-i\Delta_{m,l}t}\\
&+\frac{i}{4}\sum_{q=-\infty}^{\infty}\sum_{l=-\infty}^{\infty}\sum_{m=-\infty}^{\infty}(K_l+K_m+K_{l-m})\overline{X}_{m,q}v_{-l}v_{l-m}v_q v_{m-q}e^{-i\Delta_{m,l}t}e^{-i\Delta_{q,m}t}
\end{aligned}
$$

Substituting from Eq. (3.179) and Eq. (3.183) in Eq. (3.169) we get:

$$
\begin{aligned}
&\frac{d}{dt}E \qquad (3.184)\\
&=-\frac{i}{4}\sum_{q=-\infty}^{\infty}\sum_{l=-\infty}^{\infty}\sum_{m=-\infty}^{\infty}(K_l+K_m+K_{l-m})\overline{X}_{m,q}v_{-l}v_{l-m}v_q v_{m-q}e^{-i(\omega_q+\omega_{m-q}+\omega_{l-m}-\omega_l)t}
\end{aligned}
$$

If we were to work to the order ε^4 for energy E, by including the next terms of perturbation series i.e. $n^{(3)}$ and $v^{(3)}$, this will result in terms of the 4th order in ε, which will cancel out with the right hand side of Eq. (3.184) plus the terms of the order ε^5.

We analyze Eq. (3.184) and we estimate δE, the magnitude of the oscillation of energy E, for the two extreme limits:
i) In the limit of very small perturbations $|n_l| \sim \epsilon$, such that $|n_l| \ll (\omega_q+\omega_{m-q}+\omega_{l-m}-\omega_l)/\omega_l$, time scale for variation of energy in given by the detunings, $1/\delta t \sim \omega_q + \omega_{m-q} + \omega_{l-m} - \omega_l$, since the perturbation amplitudes are approximately constant. As a result for small perturbations Eq. (3.184) implies

$$\delta E \sim \delta t \frac{\omega_l^3}{k_l^2}\epsilon^4 \sim \epsilon^4 \tag{3.185}$$

This relation implies that energy of a system of small perturbations, in which the resonant wave-wave interactions are negligible, is conserved up to the 3rd order in ϵ ($\delta E \sim \mathcal{O}(\epsilon^4)$).
ii) In the limit where perturbations are large such that we have strong resonant wave-wave interactions in the system, $|n_l| \sim \epsilon \gg (\omega_q + \omega_{m-q} + \omega_{l-m} - \omega_l)/\omega_l$, the timescale for the evolution of the system is given by $\delta t \sim 1/\omega_l |n_l| \sim 1/\epsilon\omega_l$. This is the timescale for resonance growths of the perturbations (see Eq. 3.232). As a result, for large perturbations Eq. (3.184) implies

$$\delta E \sim \delta t \frac{\omega_l^3}{k_l^2}\epsilon^4 \sim \epsilon^3 \tag{3.186}$$

This relation implies that for a system of large perturbations at which wave-wave resonance is strong, the total energy of the system is conserved only up to the second order in ε ($\delta E \sim \mathcal{O}(\varepsilon^3)$).

3.5 Wave-wave Interaction between TG modes 1 and 2

Equation (3.138) describes the slow time evolution of mode amplitudes due to nonlinear coupling to the other modes. We focus on the interaction between modes 1 and 2, assuming all the other modes amplitudes are initially much smaller. We drop the multiple time scales perturbation notation and $\varepsilon = 1$. As a result $\tau_1 = t$ and we obtain the following equations describing the evolution of these two modes:

$$\dot{n}_1 = -iX_{1,2}\, n_2 n_1^* e^{i\Delta_{1,2}t}, \tag{3.187}$$

$$\dot{n}_2 = -iX_{2,1}\, (n_1)^2 e^{-i\Delta_{1,2}t}, \tag{3.188}$$

where nonlinear coupling coefficients are given by:

$$\begin{aligned} X_{1,2} &= \tfrac{\omega_1}{2}\left(1+\tfrac{\omega_2}{\omega_1}\right) \\ X_{2,1} &= \omega_1\left(1+\tfrac{\omega_1}{\omega_2}\right), \end{aligned} \tag{3.189}$$

and detuning is defined by:

$$\Delta_{1,2} = 2\omega_1 - \omega_2 \tag{3.190}$$

3.5.1 Phase-space analysis

We will study the evolution equations (3.187) and (3.188) using phase-space analysis. n_1 and n_2 are complex mode amplitudes which can be written in terms of a time dependent real amplitude and a time dependent phase.

$$\begin{aligned} n_1(t) &= a_1(t) e^{i\overline{\alpha}_1(t) + i\Delta_{1,2}t} \\ n_2(t) &= a_2(t) e^{i\overline{\alpha}_2(t) + i\Delta_{1,2}t}, \end{aligned} \tag{3.191}$$

where we define the real amplitude $a_l(t)$ as:

$$a_l(t) = |n_l(t)| \;=\; A_l^t/2, \quad \text{traveling waves} \tag{3.192}$$

$$\;=\; A_l^s/4. \quad \text{standing waves} \tag{3.193}$$

Also we define the phase $\overline{\alpha}(t)_l$ as:

$$\overline{\alpha}_l(t) = \alpha_l(t) - \Delta_{1,2}t, \quad l = 1,2 \tag{3.194}$$

where the phase $\alpha_l(t)$ for traveling and standing wave is respectively defined in Eq. (3.97) and Eq. (3.102). We eliminate the explicit time dependence on Eq. (3.187) and Eq. (3.188) by substituting from Eq. (3.191). Defining the total phase of the modes 1 and 2 as:

$$\phi_l = \overline{\alpha}_l(t) + \Delta_{1,2}t - \omega_l t, \quad l = 1,2 \tag{3.195}$$

we define the dynamic phase as:

$$\begin{aligned} \phi(t) &= 2\phi_1(t) - \phi_2(t) \\ &= 2\overline{\alpha}_1(t) - \overline{\alpha}_2(t), \end{aligned} \tag{3.196}$$

where we used (3.195) and (3.190) to get (3.196). Substituting from (3.191) in (3.187) we obtain:

$$\dot{a}_1 + i(\Delta_{1,2} + \dot{\overline{\alpha}}_1)a_1 = -iX_{1,2}a_2a_1e^{i(\overline{\alpha}_2 - 2\overline{\alpha}_1)} \tag{3.197}$$

$$\dot{a}_2 + i(\Delta_{1,2} + \dot{\overline{\alpha}}_2)a_2 = -iX_{2,1}a_1^2e^{-i(\overline{\alpha}_2 - 2\overline{\alpha}_1)} \tag{3.198}$$

Taking the real part of (3.197) and (3.198) we obtain:

$$\dot{a}_1 = -X_{1,2}a_2a_1\sin\phi \tag{3.199}$$

$$\dot{a}_2 = X_{2,1}a_1^2\sin\phi \tag{3.200}$$

Subtracting equation (3.198) from 2 times equation (3.197) we obtain:

$$\dot{\phi} = -\left(2X_{1,2}a_2 - X_{2,1}\frac{a_1^2}{a_2}\right)\cos\phi - \Delta_{1,2} \tag{3.201}$$

Furthermore, from eliminating $\sin\phi$ from equations (3.199) and (3.200) integrating in time we obtain an integral of motion A and the following conservation relation:

$$\frac{a_1^2}{X_{1,2}} + \frac{a_2^2}{X_{2,1}} = \frac{A^2}{X_{2,1}} \tag{3.202}$$

The left hand side of Eq. (3.202) is an exact constant of motion for equations (3.187) and (3.188). The conservation relation given by the Eq. (3.202) expresses the conservation of wave energy for the system of equations (3.187) and (3.188). In order to see that we substitute from Eq. (3.189) in Eq. (3.202) to get

$$\frac{a_1^2}{\frac{\omega_1}{2}\left(1+\frac{\omega_2}{\omega_1}\right)} + \frac{a_2^2}{\omega_1\left(1+\frac{\omega_1}{\omega_2}\right)} = \frac{A^2}{\omega_1\left(1+\frac{\omega_1}{\omega_2}\right)}$$

Now, multiplying both sides of the above by $\omega_1^2(\omega_1+\omega_2)/2k_1^2$ we get:

$$\begin{aligned} \frac{2\omega_1\omega_2}{k_2^2}A^2 &= \frac{\omega_1^2}{k_1^2}a_1^2 + \frac{2\omega_1\omega_2}{k_2^2}a_2^2 \\ &= \frac{\omega_1^2}{k_1^2}a_1^2 + \frac{\omega_2^2}{k_2^2}a_2^2 + \frac{\Delta_{1,2}}{\omega_2}\frac{\omega_2^2}{k_2^2}a_2^2 \end{aligned} \tag{3.203}$$

In the last line of the above equation, the first and second term are respectively the energies of the linear modes 1 and 2 and the last term is a small correction for small detuning $\Delta_{1,2}/\omega_2 \ll 1$, due to the nonlinear coupling between the waves.

Substituting (3.202) in (3.201) to eliminate a_1 and after scaling the time by introducing:

$$\overline{t} = t/X_{1,2}A \tag{3.204}$$

we obtain:

$$\frac{d}{d\overline{t}}\phi = [\frac{1}{x} - 3x]\cos\phi - 2\eta, \tag{3.205}$$

where the variable x and the parameter η are defined by

$$x = a_2/A \tag{3.206}$$

$$\eta = \frac{\Delta_{1,2}}{2X_{1,2}A} = \frac{\Delta_{1,2}}{(\omega_1+\omega_2)A} \tag{3.207}$$

η is the ratio of a measure of the dispersion, given by $\Delta_{1,2}/(\omega_1+\omega_2)$ to a measure of nonlinearity, given by A. Furthermore, from the conservation equation (3.202) we have the following relation for x:

$$x^2 + \frac{X_{1,2}}{X_{2,1}}a_1^2 = 1 \tag{3.208}$$

which dictates the condition that $x < 1$

$$x < 1 \tag{3.209}$$

We can elliminate a_1 from (3.200) by substituting from (3.202) and we obtain:

$$\frac{d}{d\bar{t}}x = [1-x^2]\sin\phi \tag{3.210}$$

Equations (3.205) and (3.210) describe the evolution of phase-space (ϕ, x). Topology of this phase-space is determined by the parameter η. These equations give the time evolution of an integrable system. This system is described by the canonical variables (ϕ, x^2) and the Hamiltonian:

$$H = 2[x-x^3]\cos\phi - 2\eta x^2 \tag{3.211}$$

$$\frac{d\phi}{d\bar{t}} = \frac{\partial H}{\partial x^2}, \tag{3.212}$$

$$\frac{dx^2}{d\bar{t}} = -\frac{\partial H}{\partial \phi} \tag{3.213}$$

Different curves in phase-space are given by different values of the Hamiltonian. For a curve with $H = E$, we can solve for $\cos\phi$ from Eq. (3.211) and substitute in (3.210)

to obtain

$$\dot{x} = \pm[1-x^2]\sqrt{1-\left[\frac{E+2\eta x^2}{2[x-x^3]}\right]^2}, \tag{3.214}$$

which can be integrated to give the time period of the curve as well as the amplitude x as a function of time.

We can map out the phase-space of (ϕ, x) by locating its fixed points. By lineaizing the equations (3.205) and (3.210) around fixed points in phase-space, we can determine their identity. Linearized equations in this 2D space is given by the following matrix

$$\mathbf{D}_0(\phi_p, x_p) = \begin{pmatrix} \partial_x f & \partial_\phi f \\ \partial_x g & \partial_\phi g \end{pmatrix}_{(\phi_p, x_p)} = \begin{pmatrix} -2x_p \sin\phi_p & [1-x_p^2]\cos\phi_p \\ -[\frac{1}{x_p^2}+3]\cos\phi_p & -[\frac{1}{x_p}-3x_p]\sin\phi_p \end{pmatrix} \tag{3.215}$$

where $f(\phi, x)$ is the right hand side of Eq. (3.210) and $g(\phi, x)$ is the right hand side of Eq. (3.205).

The eigenvalues λ of the linear matrix $\mathbf{D}_0$ at the fixed points are obtained from the characteristic equation $|\mathbf{D}_0 - \lambda\mathbf{I}| = 0$ which implies that:

$$\lambda^2 - \mathrm{tr}\,\mathbf{D}_0\lambda - \det\mathbf{D}_0 = 0 \tag{3.216}$$

We set the left hand side of Eq.'s (3.205) and (3.210) to zero and we solve for fixed points. For $\sin\phi = 0$ there are two *center* fixed points. For $\phi = 0$ we have:

$$\begin{aligned} \phi = 0 \quad &\Rightarrow \quad 3x^2 - 1 + 2\eta x = 0 \\ &\Rightarrow \quad x_0 = -\frac{\eta}{3} + \sqrt{\left(\frac{\eta}{3}\right)^2 + \frac{1}{3}} \end{aligned} \tag{3.217}$$

which gives the coordinates of the fixed point c_0 located at $(\phi, x) = (0, x_0)$ in the

phase-space. For $\phi = \pm\pi$ we have:

$$\begin{aligned} \phi = \pm\pi \quad &\Rightarrow \quad 3x^2 - 1 - 2\eta x = 0 \\ &\Rightarrow \quad x_\pi = \frac{\eta}{3} + \sqrt{\left(\frac{\eta}{3}\right)^2 + \frac{1}{3}} \end{aligned} \tag{3.218}$$

which gives the coordinates of the fixed point c_π located at $(\phi, x) = (\pi, x_\pi)$ in the phase-space. In obtaining c_0 and c_π, since by definition in Eq. (3.206) we have $x > 0$, solutions with $x < 0$ were discarded. Linearizing the equations (3.210) and (3.205) around the fixed points c_0 and c_π gives

$$\begin{aligned} \mathbf{D}_0 &= \begin{pmatrix} 0 & [1 - x_p^2]\cos\phi_p \\ -[\frac{1}{x_p^2} + 3]\cos\phi_p & 0 \end{pmatrix} \Rightarrow \\ \det \mathbf{D}_0 &= (1 - x_p^2)(\frac{1}{x_p^2} + 3)\cos^2\phi > 0 \\ \mathrm{tr}\, \mathbf{D}_0 &= 0 \end{aligned} \tag{3.219}$$

Eigenvalues of c_0 and c_π are obtained using Eq. (3.216). Since these pairs of eigenvalues are imaginary, fixed points c_0 and c_π are *center* points [38]. Using the condition that $x < 1$ obtained in Eq. (3.208) in the equation (3.218), we can see that the center point c_π exists in the finite phase-space of $\phi \in [-\pi, \pi]$ and $x \in [0, 1]$, only if $\eta < 1$ and disappears for $\eta > 1$.

For $x = 1$ and $\cos\phi_s = -\eta$ another two fixed points $s_\pm$ exist in phase-space. These fixed points are *saddle* points and are located at

$$s_\pm : (\pm\phi_s, 1), \quad \phi_s = \pi - \arccos\eta \geq 0 \tag{3.220}$$

These two fixed points only exist if $\eta < 1$. Linearizing around these fixed points we

get:

$$\begin{aligned} \mathbf{D}_0 &= \begin{pmatrix} \mp 2\sin\phi_s & 0 \\ 4\eta & \pm 2\sin\phi_s \end{pmatrix} \Rightarrow \\ \det \mathbf{D}_0 &= -4(1-\eta^2) < 0 \\ \mathrm{tr}\, \mathbf{D}_0 &= 0 \end{aligned} \tag{3.221}$$

We obtain the eigenvalues of the linearized system at these fixed points from the characteristic equation Eq. (3.216) which are given by:

$$\pm\lambda = \pm 2\sqrt{1-\eta^2} \tag{3.222}$$

Since these pair of eigenvalues are real and opposite in sign, $s_\pm$ are *saddle* points [38]. For $s_+ : (\phi_s, 1)$ we find the eigenvectors related to $\pm\lambda$. For $+\lambda$ the eigenvector $\mathbf{v}_+$ is given by:

$$\begin{aligned} [\mathbf{D}_0 - \lambda \mathbf{I}].\mathbf{v}_+ &= \begin{pmatrix} -4\sqrt{1-\eta^2} & 0 \\ 4\eta & 0 \end{pmatrix}.\mathbf{v}_+ = 0 \\ \Rightarrow \mathbf{v}_+ &= \begin{pmatrix} 0 \\ 1 \end{pmatrix} \end{aligned} \tag{3.223}$$

For $-\lambda$ the eigenvector $\mathbf{v}_-$ is given by:

$$\begin{aligned} [\mathbf{D}_0 + \lambda \mathbf{I}].\mathbf{v}_- &= \begin{pmatrix} 0 & 0 \\ 4\eta & 4\sqrt{1-\eta^2} \end{pmatrix}.\mathbf{v}_- = 0 \\ \Rightarrow \mathbf{v}_- &= \begin{pmatrix} \sqrt{1-\eta^2} \\ -\eta \end{pmatrix} \end{aligned} \tag{3.224}$$

Functional form for (ϕ, x) as a function of time near the saddle point $s_+ : (\phi_s, 1)$ can be constructed from the above solutions as:

$$\begin{pmatrix} x(\overline{t}) - 1 \\ \phi(\overline{t}) - \phi_s \end{pmatrix} = a_+ \begin{pmatrix} 0 \\ 1 \end{pmatrix} e^{\lambda \overline{t}} + a_- \begin{pmatrix} \sqrt{1-\eta^2} \\ -\eta \end{pmatrix} e^{-\lambda \overline{t}}, \tag{3.225}$$

where the constants a_+ and a_- are determined from the initial conditions. For the initial point in phase-space given by $(\phi(0), x(0))$ in the vicinity of $s_+ : (\phi_s, 1)$, the solution $(\phi(\overline{t}), x(\overline{t}))$ as a function of time is given by:

$$x(t) = (x(0)-1)e^{-\lambda \overline{t}} + 1 \tag{3.226}$$

$$\phi(t) = [\phi(0) - \phi_s + \tfrac{\eta}{\sqrt{1-\eta^2}}(x(0)-1)]e^{\lambda \overline{t}} - \tfrac{\eta}{\sqrt{1-\eta^2}}(x(0)-1)e^{-\lambda \overline{t}} + \phi_s \tag{3.227}$$

Above solution shows that $x(\overline{t})$ grows towards 1, and thus brings the point closer to s_+.From performing the same analysis for the saddle point $s_- : (-\phi_s, 1)$, we obtain the following solution $(\phi(t), x(t))$ as a function of time, starting from an initial point $(\phi(0), x(0))$ in the vicinity of $s_- : (-\phi_s, 1)$

$$x(\overline{t}) = (x(0)-1)e^{\lambda \overline{t}} + 1 \tag{3.228}$$

$$\phi(\overline{t}) = [\phi(0) + \phi_s - \tfrac{\eta}{\sqrt{1-\eta^2}}(x(0)-1)]e^{-\lambda \overline{t}} + \tfrac{\eta}{\sqrt{1-\eta^2}}(x(0)-1)e^{\lambda \overline{t}} - \phi_s \tag{3.229}$$

Due to the conservation relation (3.202), decay of $x = a_2/A$ at the fixed point $(-\phi_s, 1)$ will result in the growth of a_1. To find the functional form for the growth of a_1 near the saddle point at $(-\phi_s, 1)$, from (3.200) replacing a_2 with $(a_2(0)-A)e^{X_{1,2}A\lambda t} + A$ (after switching back to time t from $\overline{t}$) we get:

$$a_1(t) = \sqrt{\frac{\dot{a}_2}{X_{2,1}\sin\phi}} \approx \sqrt{\frac{X_{1,2}A\lambda(A-a_2(0))}{X_{2,1}\sin\phi_s}}\, e^{(X_{1,2}A\lambda/2)t}, \tag{3.230}$$

which states that $a_1(t)$ grows exponentially at a constant rate $X_{1,2}A\lambda/2$. Assuming that at $t = 0$ mode 2 was much more populated that mode 1:

$$a_2(0) \approx A, \tag{3.231}$$

we find the constant growth rate of mode 1 in Eq. (3.230) to be:

$$\Gamma = (\omega_1 + \omega_2)\frac{a_2(0)}{2}\sqrt{1 - \left[\tfrac{\Delta_{1,2}}{(\omega_1+\omega_2)a_2(0)}\right]^2} \tag{3.232}$$

There are another set of important points in phase-space: jump point J_1 located at

$(\phi, x) = (-\pi/2, 0)$, and jump point J_2 located at $(\phi, x) = (-\pi/2, 0)$, at which the solution is discontinuous. Solution curve $\widehat{J_2 J_1}$ connects these two points (see Fig. (3.5)) on a finite time ($\widehat{J_2 J_1}$ is not an invariant manifold), and with its direction from J_2 to J_1. $dx/d\phi$ for $\widehat{J_2 J_1}$ is finite at J_1 and J_2. Two solutions *jump* from J_1 to J_2 at $x = 0$, from $\phi = -\pi/2$ to $\phi = \pi/2$ and from $\phi = -\pi/2$ to $\phi = -3\pi/2$. When the solution has zero amplitude ($x = 0$) its phase is undefined; the phase can therefore change discontinuously.

The closed curve $\widehat{J_2 J_1 J_2}$ consisting of $\widehat{J_2 J_1}$ and the jump curve $\widehat{J_1 J_2}$, which jumps from J_1 to J_2 at $x = 0$, is a separatrix which contains a class of orbits encircling the center fixed point c_0. These orbits are the solutions in which phases of mode 1 and 2 are semi-locked, i.e. $\phi = 2\phi_1 - \phi_2$ oscillates around zero. The separatrix $\widehat{J_2 J_1 J_2}$ separates these solutions from the solutions which streams in phase-space, for which the time average of ϕ is non zero.

As η becomes larger the separatrix $\widehat{J_2 J_1 J_2}$ takes a smaller area in phase-space and in the limit $\eta \to \infty$ it disappears. We can see that from calculating the finite $dx/d\phi$ for $\widehat{J_2 J_1}$ at J_1 and J_2 and seeing that $dx/d\phi$ goes to zero as $1/\eta$ (see Fig. (3.5)): At these points $\dot{x}(\pi/2) = 1$ and $\dot{x}(-\pi/2) = -1$. In order for $dx/d\phi$, and thus $\dot{\phi}$ to be finite at these points, $\cos\phi$ to the lowest oder in small x must be given by:

$$\cos\phi \approx b\,x \quad \text{for} \quad (\phi, x) \approx (\pm\pi/2, 0) \text{ and } -\pi/2 < \phi < \pi/2, \tag{3.233}$$

Substituting Eq. (3.233) in the RHS of Eq. (3.210) we get:

$$\dot{\phi} = (\frac{1}{x} - 3x)(b\,x) - 2\eta \approx b - 2\eta, x \to 0 \tag{3.234}$$

Taking the derivative of $\cos\phi$ with respect to time we obtain:

$$\frac{d}{dt}\cos\phi = -\dot{\phi}\sin\phi \tag{3.235}$$

Since at $(\phi, x) \approx (\pm\phi/2, 0)$ we have $\sin\phi = \pm 1$, using Eq. (3.234) in Eq. (3.235) we

obtain:

$$\frac{d}{dt}\cos\phi = \mp(b-2\eta) \tag{3.236}$$

Also from Eq. (3.233) we have:

$$\frac{d}{dt}\cos\phi = b\dot{x} = \pm b \quad \text{for} \quad (\phi, x) = (\pm\pi/2, 0) \tag{3.237}$$

Equating (3.236) and (3.237) we get:

$$b = \eta \quad \text{for} \quad (\phi, x) = (\pm\pi/2, 0) \tag{3.238}$$

Since, from Eq. (3.233) we have $\dot{x}(\phi = \pm\pi/2) = \pm 1$, therefore

$$\frac{dx}{d\phi} = \mp\frac{1}{\eta} \quad (\phi, x) = (\pm\pi/2, 0) \tag{3.239}$$

There are also a class of solutions which are also semi-phase-locked and encircle center point c_π. These solutions are separated from the streaming solutions by the separatrix $\widehat{s_- s_+ s_-}$, which is the closed *invariant* curve that passes through the saddle points s_- and s_+. However, unlike the solutions trapped in the separatrix $\widehat{J_2 J_1 J_2}$, this region vanishes for $\eta > 1$. We can see the different forms of phase-space for the different values of η depicted schematically in figure (3.5).

In the two-wave approximation used throughout this section, the interaction between the isolated modes 1 and 2 is a reversible process. Even in the regime where mode 1 grows exponentially from a small amplitude, its amplitude will reach a maximum while mode 2 amplitude will decay and reach the minimum of its amplitude, and after this the reverse of the whole process happens i.e. mode 2 will grow as mode 1 decays and so on. Therefore amplitudes of both mode 2 and mode 1 are periodic functions of time in the whole parameter range of η. For each η we have a unique structure of (ϕ, x) phase-space. Since the energy between mode 1 and 2 is conserved (see Eq. (3.202)), whenever a_1 is at its minimum a_2 is at its maximum and vice versa. A given curve in the phase-space depends on the initial conditions, which can be distinguished by the ratio of the minimum of a_1 to the maximum of a_2

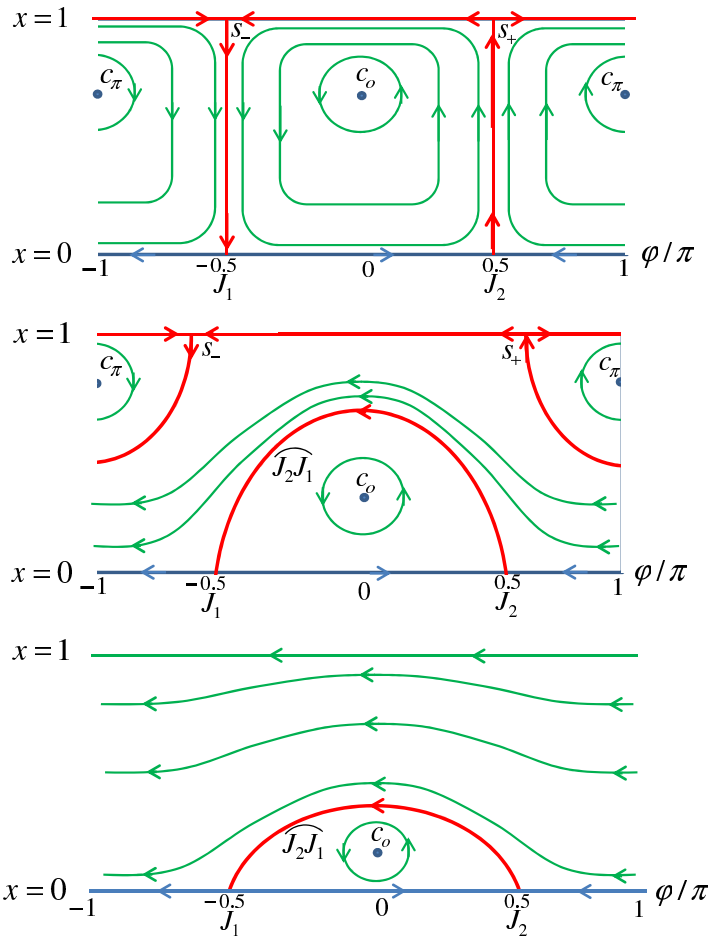

Figure 3.5: Schematic depiction of phase-space (ϕ, x) for different valus of η.

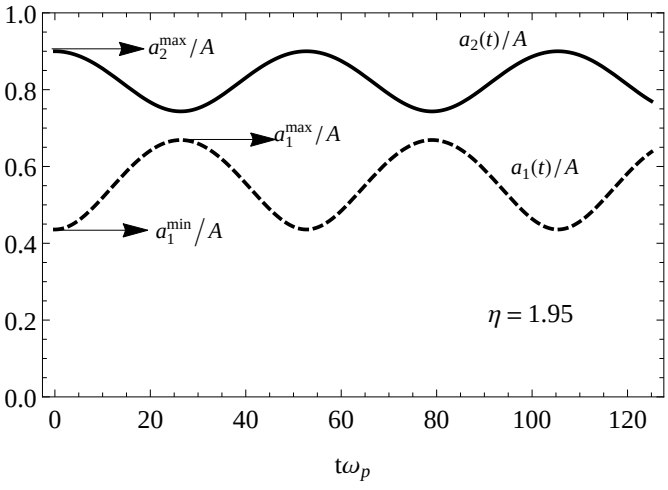

Figure 3.6: Plot of a_2 and a_1 vs. time for $\eta = 1.95$, for the ratio $a_1^{\min}/a_2^{\max} = 0.48$.

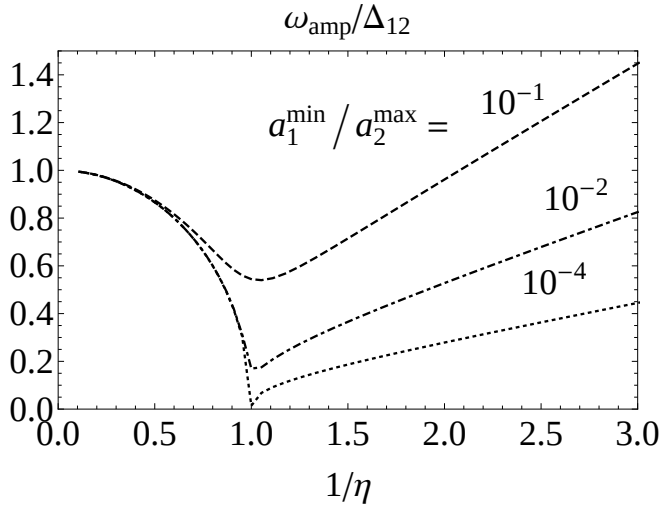

Figure 3.7: Frequency of the oscillation of mode amplitudes as a function of $1/\eta$, for $a_1^{min}/a_2^{max} = 10^{-1}, 10^{-2}$ and 10^{-4}.

(see Fig. (3.6)). Each curve can equivalently be identified by the Hamiltonian given by Eq. (3.211), however a_1^{min}/a_2^{max} is more practical since it does not involve ϕ.

Figure (3.7) shows the frequency of the amplitude oscillation as the function of parameter η for different values of a_1^{min}/a_2^{max} (horizontal axis is $1/\eta$ to be linear in terms of the nonlinearity A). In the limit of $\eta \gg 1$, which corresponds to large dispersion compared to nonlinearity, oscillation frequency tends to the detuning $\Delta_{1,2}$. As η approaches 1, the amplitude oscillation frequency reaches its minimum and for the case where $a_1^{min}/a_2^{max} \to 0$ this frequency tends to zero. In the large nonlinearity regime $\eta < 1$, ω_{amp} becomes larger with nonlinearity $A \approx a_2(0)$.

As the frequency of the the amplitudes oscillation changes with η the amplitude of this oscillation also changes. Figure (3.8) describes maximum value that a_1 can reach, starting from the same value of a_1^{min}, as a function of η. We can see that as $\eta \to 0$ and wave-wave interaction approaches exact resonance, the larger amplitude mode 2 shares more of its energy with mode 1, and therefore a_1^{max} becomes larger.

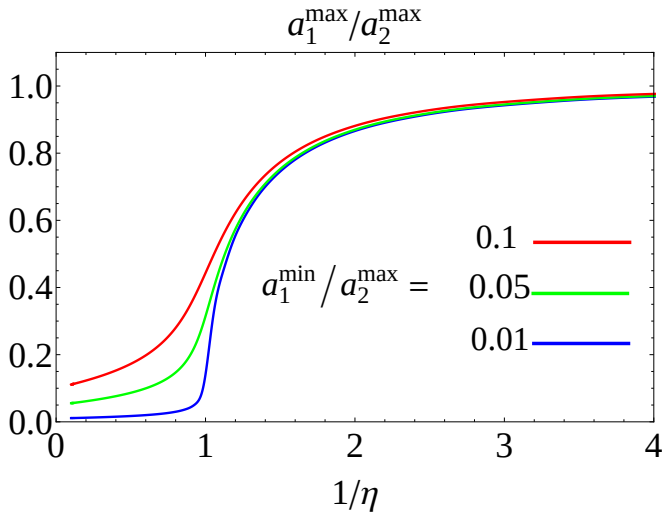

Figure 3.8: Plot of the maximum value the amplitude of mode 1 reaches (a_1^{max}) from a minimum (a_1^{min}), as a function of the parameter η, for initial conditions such that mode 2 is dominant, i.e. a_1^{min}/a_2^{max} is small.

3.5.2 Special case: Eigenmode 1 solution for the system of isolated modes 1 and 2: $|n_1(0)| \gg |n_2(0)|$

In this section, using only the equations (3.187) and (3.188), we obtain the nonlinear *eigenmode* 1 solution for which the full time variation of the spatial Fourier component 2 is a harmonic of mode 1:

$$n_1^{(1)}(t) = \overline{n}_1 e^{-i\overline{\omega}_1 t},\ n_2^{(1)}(t) = \overline{n}_2 e^{-i2\overline{\omega}_1 t} \tag{3.240}$$

where $\overline{n}_1$ and $\overline{n}_2$ are constants. $\overline{\omega}_1$ is the nonlinear mode 1 frequeny, which in the limit $\overline{n}_1 \to 0$, where the solutions are linear, must tend to the linear mode 1 frequency ω_1. We compare the eigenmode solution and mode frequency correction obtained here to Eq. (3.35) in section 3.2.1 for traveling waves, and Eq. (3.74) in section 3.2.2 for standing waves. Keeping the nonlinear equations relating Fourier terms 1 and 2 in Eq. (3.148), we obtain:

$$\dot{n}_1 = -iX_{1,2} n_2 n_1^* e^{i\Delta_{1,2} t} \tag{3.241}$$

$$\dot{n}_2 = -iX_{2,1} n_1^2 e^{-i\Delta_{1,2} t} \tag{3.242}$$

where $\Delta_{1,2} = 2\omega_1 - \omega_{21}$ and

$$X_{1,2} = \frac{\omega_1}{2}\left(1 + \frac{\omega_2}{\omega_1}\right), \quad X_{2,1} = \omega_1\left(1 + \frac{\omega_1}{\omega_2}\right),$$

Taking the time derivative of Eq. (3.241) we obtain:

$$\ddot{n}_1 = -iX_{1,2}\dot{n}_2 n_1^* e^{i\Delta_{1,2}t} - iX_{1,2}n_2\dot{n}_1^* e^{i\Delta_{1,2}t} + i\Delta_{1,2}\dot{n}_1 \tag{3.243}$$

We substitute for $\dot{n}_2$ from Eq. (3.242) and for $\dot{n}_1^*$ from the complex conjugate of (3.241) and obtain:

$$\ddot{n}_1 = -X_{2,1}X_{1,2}|n_1|^2 n_1 + (X_{1,2})^2|n_2|^2 n_1 + i\Delta_{1,2}\dot{n}_1 \tag{3.244}$$

Assuming oscillatory solutions for mode 1 and 2 of the forms $n_1 = |n_1|e^{qt}$, $n_2 = |n_2|e^{(2q-i\Delta_{1,2})t}$, with q being imaginary and $|n_1|$ and $|n_2|$ constants, we obtain:

$$q^2 + X_{2,1}X_{1,2}|n_1|^2 - (X_{1,2})^2|n_2|^2 - i\Delta_{1,2}q = 0 \tag{3.245}$$

Solving the above equation we get:

$$q_\pm = i\tfrac{\Delta_{1,2}}{2} \pm i\delta_\omega \tag{3.246}$$

$$\delta_\omega = \sqrt{(\tfrac{\Delta_{1,2}}{2})^2 + X_{2,1}X_{1,2}|n_1|^2 - (X_{1,2})^2|n_2|^2} \tag{3.247}$$

Based on the assumed ordering:

$$\Delta_{1,2}/\omega_1 \gg |n_1(0)| \gg |n_2(0)| \tag{3.248}$$

we neglect the smallest terms $-(X_{1,2})^2|n_2|^2$ in the square root in Eq. (3.247) and write δ_ω as:

$$\delta_\omega = \sqrt{(\tfrac{\Delta_{1,2}}{2})^2 + X_{2,1}X_{1,2}|n_1|^2} \tag{3.249}$$

Since both roots given by Eq. (3.246) are imaginary, mode 1 is stable. This means that the amplitudes of n_1 and n_2 may oscillate about their initial values, but they

are not going to grow or decay exponentially. The total solution comprising the two solutions related to $q_{\pm}$ is given by:

$$n_1(t) = Ae^{i(\frac{\Delta_{1,2}}{2}+\delta_\omega)t} + Be^{i(\frac{\Delta_{1,2}}{2}-\delta_\omega)t} \tag{3.250}$$

However the constants A and B are not independent complex numbers. Substituting for $n_1(t)$ from (3.250) in (3.241) we get:

$$\begin{aligned} &i(\tfrac{\Delta_{1,2}}{2}+\delta_\omega)Ae^{i(\frac{\Delta_{1,2}}{2}+\delta_\omega)t} + i(\tfrac{\Delta_{1,2}}{2}-\delta_\omega)Be^{i(\frac{\Delta_{1,2}}{2}-\delta_\omega)t} \\ &= -iX_{1,2}\, n_2\left(A^*e^{-i(\frac{\Delta_{1,2}}{2}+\delta_\omega)t} + B^*e^{-i(\frac{\Delta_{1,2}}{2}-\delta_\omega)t}\right)e^{i\Delta_{1,2}t} \\ &= -iX_{1,2}\left(n_2A^*e^{i(\frac{\Delta_{1,2}}{2}-\delta_\omega)t} + n_2B^*e^{i(\frac{\Delta_{1,2}}{2}+\delta_\omega)t}\right) \end{aligned} \tag{3.251}$$

From Equation (3.251) we obtain the following relation between A and B:

$$(\tfrac{\Delta_{1,2}}{2}+\delta_\omega)A = -X_{1,2}\, n_2B^* \tag{3.252}$$

$$(\tfrac{\Delta_{1,2}}{2}-\delta_\omega)B = -X_{1,2}\, n_2A^* \tag{3.253}$$

We can rewrite (3.250) using (3.253) as

$$n_1(t) = Be^{i(\frac{\Delta_{1,2}}{2}-\delta_\omega)t} - \frac{X_{1,2}}{(\frac{\Delta_{1,2}}{2}+\delta_\omega)}\, n_2B^*e^{i(\frac{\Delta_{1,2}}{2}+\delta_\omega)t} \tag{3.254}$$

Based on the ordering assumption in Eq. (3.248), the second term in Eq. (3.254) is small compared to the first term we can approximate $n_1(t)$ as:

$$n_1(t) \approx Be^{i(\frac{\Delta_{1,2}}{2}-\delta_\omega)t} \tag{3.255}$$

The full time variation of mode 1 is given by:

$$n_1^{(1)}(t) = Be^{-i\overline{\omega}_1 t}, \tag{3.256}$$

where the frequency of the nonlinear mode is given by

$$\overline{\omega}_1 = \omega_1 + \overline{\omega}_1^{(2)}, \quad \overline{\omega}_1^{(2)} = \sqrt{(\tfrac{\Delta_{1,2}}{2})^2 + X_{2,1}X_{1,2}|n_1|^2} - \tfrac{\Delta_{1,2}}{2} \tag{3.257}$$

$\overline{\omega}_1^{(2)}$ is the nonlinear frequency correction term. Substituting from Eq. (3.255) in Eq. (3.242) we solve for n_2 to obtain:

$$\dot{n}_2 = -iX_{2,1}B^2 e^{-2i\delta_\omega t} \tag{3.258}$$

which implies that

$$n_2(t) = C + \frac{X_{2,1}}{2\delta_\omega} B^2 e^{-2i\delta_\omega t} \tag{3.259}$$

C is a constant of integration. The full time variation of spatial Fourier mode 2 is given by:

$$n_2^{(1)}(t) = n_2 e^{-i\omega_2 t} = C e^{-i\omega_2 t} + \frac{X_{2,1}}{2\delta_\omega} B^2 e^{-i2\overline{\omega}_1 t} \tag{3.260}$$

Assuming that only the nonlinear mode 1 is present in the plasma, the only frequencies present in the plasma must be $\overline{\omega}_1$ and all its harmonics. Therefore, we set $C = 0$ and obtain:

$$n_2(t) = \frac{X_{2,1}}{2\delta_\omega} B^2 e^{-2i\delta_\omega t} \tag{3.261}$$

$$n_2^{(1)}(t) = \frac{X_{2,1}}{2\delta_\omega} B^2 e^{-i2\overline{\omega}_1 t} \tag{3.262}$$

Substituting $n_2(t)$ from Eq. (3.266) in the second term on the right hand side of Eq. (3.254), which we neglected due to smallness we get:

$$n_1(t) = \overline{n}_1 e^{i(\frac{\Delta_{1,2}}{2} - \delta_\omega)t} \tag{3.263}$$

$$n_1^{(1)}(t) = \overline{n}_1 e^{-i\overline{\omega}_1 t} \tag{3.264}$$

$$\overline{n}_1 = \left[1 - \frac{X_{1,2}X_{2,1}}{2\delta_\omega(\frac{\Delta_{1,2}}{2} + \delta_\omega)} |B|^2\right] B \tag{3.265}$$

Comparing Eq. (3.264) to Eq. (3.262) we can see that we have obtained the eigenmode 1 solution for which $n_2^{(1)}(t)$ is a harmonic of $n_1^{(1)}(t)$, oscillating at twice its base frequency $\overline{\omega}_1$. Now, in the limit $\frac{X_{1,2}X_{2,1}}{2\delta_\omega(\frac{\Delta_{1,2}}{2}+\delta_\omega)}|\overline{n}_1|^2 \ll 1$, we have $\overline{n}_1 \approx B$ and therefore we can write:

$$n_2(t) = \frac{X_{2,1}}{2\delta_\omega}\overline{n}_1^2 e^{-2i\delta_\omega t} \tag{3.266}$$

$$n_2^{(1)}(t) = \frac{X_{2,1}}{2\delta_\omega}\overline{n}_1^2 e^{-i2\overline{\omega}_1 t} \tag{3.267}$$

Although the results from this section i.e. Eq. (3.255), Eq. (3.266) and Eq. (3.257), are obtained for mode 1 and 2, they are valid for any pair of isolated modes $m, 2m$ with substituting $1 \to m$ and $2 \to 2m$.

The assumption of small detuning compared to mode frequency $\Delta_{1,2}/\omega_1 \ll 1$, which we made in section 3.4, and later we used its results in section 3.5, is valid for a long, thin plasma ($k_1 \ll k_\perp$). We can expand $\Delta_{1,2}/\omega_1$ in terms of small $k_1/k_\perp$ and to the lowest order we get:

$$\Delta_{1,2}/\omega_1 \approx 3\frac{k_1^2}{k_\perp^2}, \tag{3.268}$$

which shows that $\Delta_{1,2}/\omega_1 \ll 1$ for $k_1 \ll k_\perp$.

Here we find the connection between the mode frequency correction which we obtained in Eq. (3.257), and the frequency corrections which we obtained previously in Eq.(3.99) and Eq.(3.103). For a small amplitude $|n_1|$, which satisfies the inequality:

$$|n_1|^2 \ll \frac{(\Delta_{1,2})^2}{4X_{2,1}X_{1,2}}, \tag{3.269}$$

we expand Eq. (3.257) and to the lowest order in $|n_1|$ we obtain:

$$\overline{\omega}_1^{(2)} \approx \frac{X_{2,1}X_{1,2}}{\Delta_{1,2}}|n_1|^2 \tag{3.270}$$

Now for small detuning, from expanding the right hand side of Eq. (3.270) in terms

of small $k_1/k_\perp$, to the lowest order in $k_1/k_\perp$, is given by:

$$\omega_1^{(2)} \approx \omega_1 \frac{3}{4} \frac{k_\perp^2}{k_1^2} |\overline{n}_1|^2 \tag{3.271}$$

Also, the inequality given by Eq. (3.269) for small detuning, to the lowest order in $k_1/k_\perp$ is given by:

$$|n_1| \ll k_1^2/k_\perp^2 \tag{3.272}$$

Comparing the above condition to Eq. (3.36) and Eq. (3.75) we can see that this is the condition for which the perturbation formalisms in section 3.2.1 and 3.2.2 were valid for a long and thin plasma, i.e. the condition of large detuning compared to nonlinearity. Using Eq. (3.271) we obtain a frequency correction for traveling waves (from Eq.(3.99) we have $|\overline{n}_1| = |n_1| = A_1^t/2$) and standing waves (from Eq.(3.103) we have $|\overline{n}_1| = |n_1| = A_1^t/4$):

$$\omega_1^{(2)} \approx \omega_1 \frac{3}{16} \frac{k_\perp^2}{k_1^2} (A_1^t)^2 \tag{3.273}$$

$$\omega_1^{(2)} \approx \omega_1 \frac{3}{64} \frac{k_\perp^2}{k_1^2} (A_1^s)^2 \tag{3.274}$$

We can now compare the above results in Eq. (3.273) and Eq. (3.274) to the frequency corrections obtained in sections 3.2.1 and 3.2.2, for the case of large detuning compared to mode amplitude. We can see that for a long and thin plasma, the results are identical to Eq. (3.37) for traveling waves and Eq. (3.76) for standing waves. Figure (3.9) compares $\overline{\omega}_2$, the nonlinear frequency of mode 2, obtained from Eq. (3.257) with $1 \rightarrow 2$ and depicted in a dashed curve, to $\overline{\omega}_2$ obtained from Eq. (3.35) for traveling waves, depicted in a solid curve, and computer simulation results with the number of spatial Fourier terms $M = 4, 8, 16$. For the computer simulations we used the following external potential to excite a nonlinear mode 2 adiabatically:

$$V^{\text{ext}}(z,t) = 2\overline{V}_2 g^{\text{slow}}(t) \cos[k_2 z - \omega_2 t] \tag{3.275}$$

with $g^{\text{slow}}(t)$ given by Eq. (F.6), and integrate Eqs (F.2) and (F.3) in time with the num-

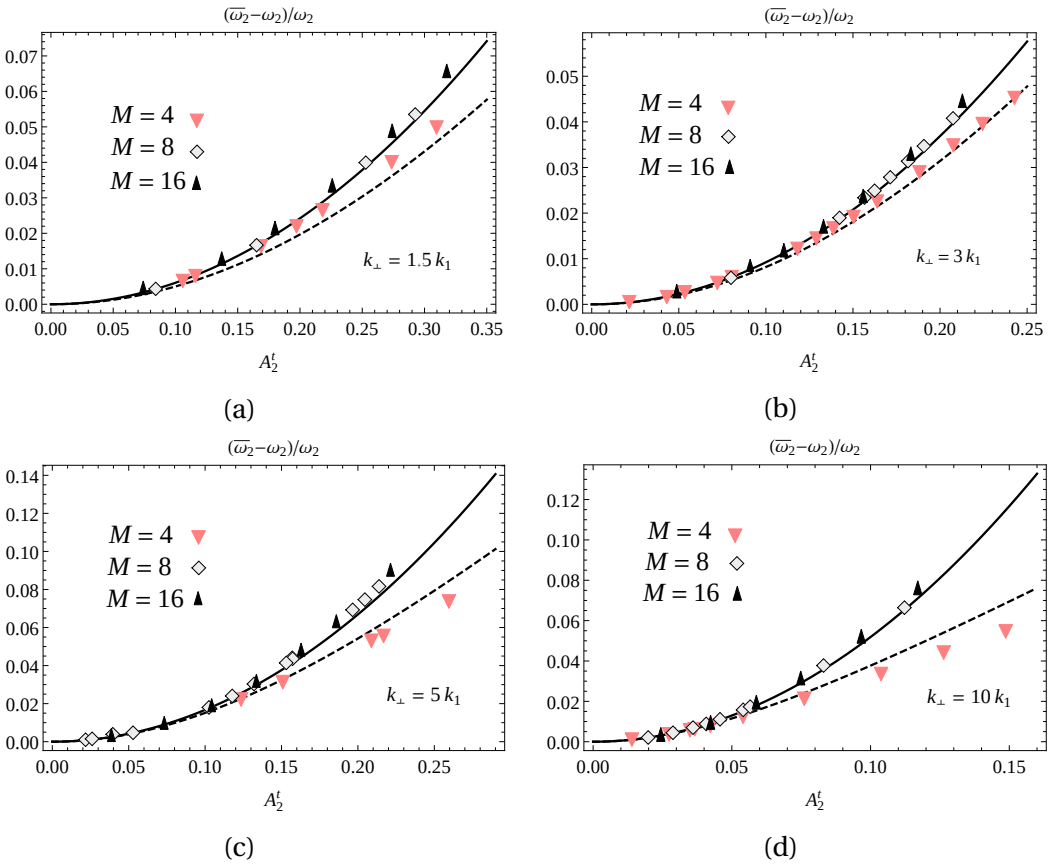

Figure 3.9: Plot of the change in mode 2 eigenfrequency of a traveling wave due to the its large amplitude(nonlinearity) for 4 values of $k_\perp/k_1$. The analytically evaluated frequency obtained from Eq. (3.257) and Eq. (3.35) are depicted respectively in dashed and solid curves. Numerically evaluated results for $M = 4, 8, 16$ are also depicted.

ber of terms kept being $M = 4, 8, 16$. Due to the even symmetry of this drive, all the odd Fourier components remain zero. For $M = 4$ only two harmonics $m = 2$ with frequency $\overline{\omega}_2$ and $m = 4$ with frequency $2\overline{\omega}_2$ constitute the nonlinear mode 2. For $M = 8$, four harmonics, and for $M = 16$, eight harmonics constitute the nonlinear mode 2. The dashed curve depicts the analytical relation Eq. (3.257) and the solid curve depicts the analytical relation Eq. (3.35). The analytical mode frequency given by Eq. (3.257) is obtained from Eqs. (3.241) and (3.242), which are the reduced version of Eqs (F.2) and (F.3) truncated at $M = 4$, with the same interacting modes 2 and 4. Therefore, the numerically calculated results with $M = 4$ have a good agreement with Eq. (3.257). However, the analytical relation Eq. (3.35) was obtained as a frequency correction for a nonlinear cnoidal eigenmode and is closer to the numerical data containing more number of harmonics $M = 8, 16$, which are better approximations for a cnoidal wave.

3.5.3 Special case: $|n_2(0)| \gg |n_1(0)|$

We are interested in the time evolution of n_1 due to nonlinear coupling to n_2, from initial conditions such that

$$|n_2(0)| \gg |n_1(0)|, \tag{3.276}$$

and we exclude all the other spatial Fourier terms of perturbation n_m with $m \neq 1$ or 2. Looking back at equations (3.187) and (3.188), we can see that assuming $|n_1(0)| \approx \varepsilon |n_2(0)|$ where $\varepsilon \ll 1$, the RHS of (3.187) is of the first order w.r.t. ε, whereas the RHS of (3.188) is of the second order w.r.t. ε. Hence we assume to the first order in ε, n_2 is constant in time. Following the same derivations as Eq. (3.241) through Eq. (3.244), with the assumption Eq. (3.276) we neglect the term $-X_{2,1}X_{1,2}|n_1|^2 n_1$ in Eq. (3.244) and obtain:

$$\ddot{n}_1 = (X_{1,2})^2 |n_2|^2 n_1 + i\Delta_{1,2}\dot{n}_1 \tag{3.277}$$

Assuming a solution for n_1 of the form $n_1 = Ae^{qt}$, with q being complex and n_2 constant, we solve for q and obtain:

$$q_\pm = i\tfrac{\Delta_{1,2}}{2} \pm i\tilde{\delta}_\omega \tag{3.278}$$

$$\tilde{\delta}_\omega = \sqrt{\tfrac{(\Delta_{1,2})^2}{4} - (X_{1,2})^2 |n_2|^2} \tag{3.279}$$

From Eq. (3.278) we can see that for $\Delta_{1,2}/2X_{1,2}|n_2| < 1$ we get exponentially growing and decaying solutions and for $\Delta_{1,2}/2X_{1,2}|n_2| > 1$ we get two oscillatory solutions. These regimes are identically seen from the phase-space: For $\eta \approx \Delta_{1,2}/2X_{1,2}|n_2(0)| < 1$(see Eq. (3.207)) saddle points exist in phase-space and solutions in the neighborhood of these saddle points are in the form of exponential phase locked growth and decay for n_1, as we obtained in (3.230). However, for $\eta > 1$ saddle points vanish from the phase-space and solutions for n_1 are of oscillatory form. In the oscillatory regime i.e. $\Delta_{1,2}/2X_{1,2}|n_2| > 1$, n_1 will oscillate at a slow frequency in the vicinity of its initial value, but it will not grow and as a result, $|n_2|$ will stay constant. As a result, our assumption that $|n_2| \gg |n_1|$ is satisfied for all time. Hence our solution is a steady

solution in time.

For the unstable regime i.e. $\Delta_{1,2}/2X_{1,2}|n_2| < 1$, n_1 will grow and $|n_2|$ will decay due to conservation of energy. As a result, the solutions that we obtain for n_1 from (Eq. 3.277) are only valid for initial times at which our assumption that $|n_2| \gg |n_1|$ is still satisfied. This means that the exponential growth rate of mode 1 is a function of time.

Oscillatory regime for n_1: $\Delta_{1,2}/2X_{1,2}|n_2| > 1$

Solution to Eq. (3.277) is of the following form:

$$n_1(t) = Ae^{i(\frac{\Delta_{1,2}}{2}+\tilde{\delta}_\omega)t} + Be^{i(\frac{\Delta_{1,2}}{2}-\tilde{\delta}_\omega)t} \tag{3.280}$$

Using Eq. (3.280) in Eq. (3.241), we perform the same derivation as Eq. (3.250) through Eq. (3.254) and obtain:

$$n_1(t) = Be^{i(\frac{\Delta_{1,2}}{2}-\tilde{\delta}_\omega)t} - \frac{X_{1,2}}{(\frac{\Delta_{1,2}}{2}+\tilde{\delta}_\omega)} n_2 B^* e^{i(\frac{\Delta_{1,2}}{2}+\tilde{\delta}_\omega)t} \tag{3.281}$$

Writing $B = |\overline{n}_1|e^{i\phi_1}$, the full time variation for a traveling mode is given by

$$\begin{aligned} &n_1^{(1)}(t) \\ &= n_1(t)e^{-i\omega_1 t} = |\overline{n}_1|\left[e^{-i\overline{\omega}_1 t + i\phi_1} - \frac{X_{1,2}}{(\frac{\Delta_{1,2}}{2}+\tilde{\delta}_\omega)}|n_2|e^{-i(\omega_2-\overline{\omega}_1)t+i(\phi_2-\phi_1)}\right] \end{aligned} \tag{3.282}$$

where in the second term of the above equation we used:

$$\tfrac{\Delta_{1,2}}{2} + \tilde{\delta}_\omega - \omega_1 = 2\tilde{\delta}_\omega - \overline{\omega}_1 = \overline{\omega}_1 - \omega_2 \tag{3.283}$$

The total spatio-temporal solution of the traveling mode 1 is therefore given by:

$$\begin{aligned} &n_1(z,t) = n_1^{(1)}(t)e^{ik_1 z} + n_{-1}^{(1)}(t)e^{-ik_1 z} \\ &= 2|\overline{n}_1|\left[\cos[k_1 z - \overline{\omega}_1 t + \phi_1] - \frac{X_{1,2}}{(\frac{\Delta_{1,2}}{2}+\tilde{\delta}_\omega)}|n_2|\cos[k_1 z - (\omega_2-\overline{\omega}_1)t + \phi_2 - \phi_1]\right] \end{aligned} \tag{3.284}$$

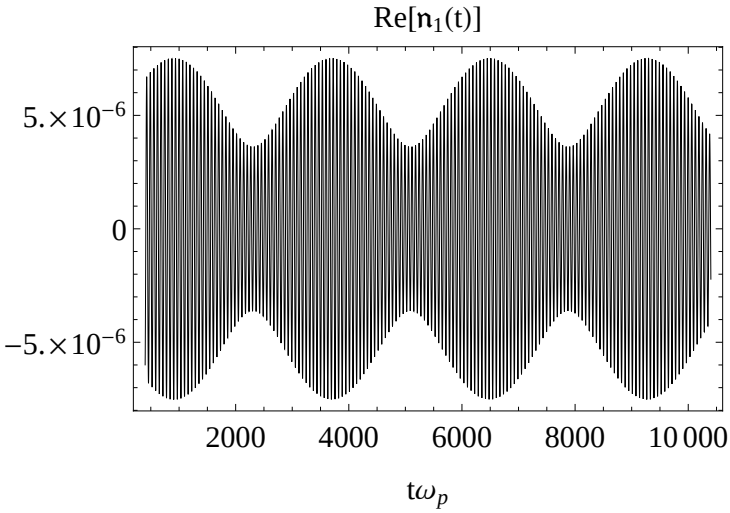

Figure 3.10: Plot of $\mathrm{Re}[\mathrm{n}_1(t)]$ for $k_\perp = 10k_1$ and $|\mathrm{n}_1| = 10^{-3}|\mathrm{n}_2|$, where $|\mathrm{n}_2| = 6.2\times10^{-3}$. Forcing time was $T_F\omega_p = 400$ and drive potential $\overline{V}_2 = 2\times10^{-6} m_q(\omega_p L/2\pi)^2$.

$\overline{\omega}_1$ is the nonlinear mode frequency of mode 1, modified due to nonlinear coupling to mode 2:

$$\begin{aligned}\overline{\omega}_1 &= \omega_1 + \tilde{\tilde{\delta}}_\omega - \tfrac{\Delta_{1,2}}{2} \\ &= \frac{\omega_2}{2} + \sqrt{\tfrac{(\Delta_{1,2})^2}{4} - (X_{1,2})^2|n_2|^2}\end{aligned} \tag{3.285}$$

From the above result we see that as $A_2^t = 2|n_2|$ grows from zero to the threshold amplitude of instability at $A_2^{\mathrm{t,\,th}} = \Delta_{1,2}/X_{1,2}$, mode 1 frequency $\overline{\omega}_1$ goes down from ω_1 to $\omega_2/2$. As we will see later on from Eq. (3.290), beyond the threshold amplitude, mode 1 fast-time frequency will stay at $\overline{\omega}_1 = \omega_2/2$ and will not change with $|n_2|$ at the time of phase-locked growth.

Figure (3.10) shows $\mathrm{Re}[\mathrm{n}_1(t)]$, which is the solution of the equations Eq. (F.2) with $M = 2$, $k_\perp = 10k_1$, and $|\mathrm{n}_1| = 10^{-3}|\mathrm{n}_2|$. There are two observable frequencies: the frequency of the fast mode oscillation $\overline{\omega}_1 = 0.0992\omega_p$, which comes from the first term on the right hand side of Eq. (3.282), and the frequency of the slow oscillation of the amplitude $\omega_{\mathrm{amp}} \approx 0.77\Delta_{1,2} = 2.2\times10^{-3}\omega_p$ which comes from the beating between the second term on the right hand side of Eq. (3.282) and the first term, with

their frequency difference given by:

$$\omega_{\text{amp}} = \overline{\omega}_1 - \omega_2 = 2\tilde{\delta}_\omega \tag{3.286}$$

$\overline{\omega}_1$ decreases with the increase in the amplitude of mode 2 and reaches a minimum $\omega_1 - \frac{\Delta_{1,2}}{2}$, when $\tilde{\delta}_\omega = 0$ (see Eq. (3.278)), which is the border between the stability and instability regimes.

In the limit $A_2^t \to 0$, ω_{amp} tends to $\Delta_{1,2}$, as we can see from Eq. (3.278). Figure (3.19) compares $\omega_{\text{amp}}/\Delta_{1,2}$ obtained from Eq. (3.286) depicted in a dashed curve, to numerical results with $M = 2, 4, 8$ number of spatial modes, vs. the amplitude of mode 2, A_2^t. As A_2^t grows from zero ω_{amp} decreases and eventually goes to zero at the threshold of instability for which $\omega_{\text{amp}}/\Delta_{1,2} = 0$. Presence of more spatial Fourier terms pushes the threshold of instability further to higher values of A_2^t and makes the nonlinear mode 2 more stable to a small sub-harmonic mode 1 perturbation.

Turning now to the standing modes, the time variation of a standing mode 1 is given by:

$$\begin{aligned}
&n_1^{(1)}(t) = n_1(t)e^{-i\omega_1 t} + c.c. \\
&= |\overline{n}_1| \left[e^{-i\overline{\omega}_1 t + i\phi_1} - \frac{X_{1,2}}{(\frac{\Delta_{1,2}}{2} + \tilde{\delta}_\omega)} |n_2| e^{-i(\omega_2 - \overline{\omega}_1)t + i(\phi_2 - \phi_1)} \right] + c.c. \\
&= 2|\overline{n}_1| \left[\cos[\overline{\omega}_1 t - \phi_1] - \frac{X_{1,2}}{(\frac{\Delta}{2} + \tilde{\delta}_\omega)} |n_2| \cos[(\omega_2 - \overline{\omega}_1)t - \phi_2 + \phi_1] \right]
\end{aligned} \tag{3.287}$$

Equation (3.287) shows the oscillation of the amplitude of mode 1, due to the beating of the two terms on right hand side with the beat frequency $\omega_{\text{amp}} = 2\tilde{\delta}_\omega$.

Unstable regime for n_1: $\Delta_{1,2}/2X_{1,2}|n_2| < 1$

For the case of exponential growing-decaying solutions, i.e. $\tilde{\delta}_\omega$ imaginary, defining the exponential growth rate as

$$\overline{\delta}_\omega = i\tilde{\delta}_\omega = \sqrt{(X_{1,2})^2 |n_2|^2 - \frac{(\Delta_{1,2})^2}{4}}, \tag{3.288}$$

Solution to Eq. (3.277) is of the following form:

$$n_1(t) = Ae^{(i\frac{\Delta_{1,2}}{2}+\overline{\delta}_\omega)t} + Be^{(i\frac{\Delta_{1,2}}{2}-\overline{\delta}_\omega)t} \tag{3.289}$$

From Eqs. (3.94) and (3.289), the full time dependence for a traveling mode 1 is given by:

$$\begin{aligned} n_1^{(1)}(t) &= n_1(t)e^{-i\omega_1 t} \\ &= e^{-i\frac{\omega_2}{2}t}\left(Ae^{\overline{\delta}_\omega t} + Be^{-\overline{\delta}_\omega t}\right) \end{aligned} \tag{3.290}$$

From the above equation we can see that in the unstable regime, the fast time oscillation frequency has shifted from ω_1 to $\omega_2/2$ due to nonlinearity, at the time of phase-locked exponential growth of mode 1 and does not change with the amplitude $A_2^t = 2|n_2|$. This means that while mode 1 and 2 are phase-locked the mode 1 is the exact *sub-harmonic* of mode 2.

Substituting from (3.289) in (3.241) we get:

$$\begin{aligned} &(i\tfrac{\Delta_{1,2}}{2}+\overline{\delta}_\omega)Ae^{(i\frac{\Delta_{1,2}}{2}+\overline{\delta}_\omega)t} + (i\tfrac{\Delta_{1,2}}{2}-\overline{\delta}_\omega)Be^{(i\frac{\Delta_{1,2}}{2}-\overline{\delta}_\omega)t} \\ &= -iX_{1,2}\,n_2\left(A^*e^{(-i\frac{\Delta_{1,2}}{2}+\overline{\delta}_\omega)t} + B^*e^{(-i\frac{\Delta_{1,2}}{2}-\overline{\delta}_\omega)t}\right)e^{i\Delta_{1,2}t} \\ &= -iX_{1,2}\left(n_2A^*e^{(i\frac{\Delta_{1,2}}{2}+\overline{\delta}_\omega)t} + n_2B^*e^{(i\frac{\Delta_{1,2}}{2}-\overline{\delta}_\omega)t}\right) \end{aligned} \tag{3.291}$$

From Eq. (3.251) we obtain the following relation between A and B:

$$(i\tfrac{\Delta_{1,2}}{2}+\overline{\delta}_\omega)A = -iX_{1,2}\,n_2A^* \tag{3.292}$$

$$(i\tfrac{\Delta_{1,2}}{2}-\overline{\delta}_\omega)B = -iX_{1,2}\,n_2B^* \tag{3.293}$$

Dividing both sides of Eq. (3.292) by $(i\frac{\Delta_{1,2}}{2}+\overline{\delta}_\omega)A^*$ we obtain:

$$\frac{A}{A^*} = -i\frac{X_{1,2}n_2}{i\frac{\Delta_{1,2}}{2}+\overline{\delta}_\omega} \tag{3.294}$$

Taking the absolute value of the above equation we get:

$$\left| \frac{X_{1,2} n_2}{i\frac{\Delta_{1,2}}{2} + \overline{\delta}_{\omega}} \right| = 1 \tag{3.295}$$

Similarly from Eq. (3.293) we get:

$$\left| \frac{X_{1,2} n_2}{i\frac{\Delta_{1,2}}{2} - \overline{\delta}_{\omega}} \right| = 1 \tag{3.296}$$

Based on Eq. (3.295) and Eq. (3.296) we define ψ_- and ψ_+ as:

$$e^{i2\psi_{\pm}} = -i \frac{X_{1,2} n_2}{i\frac{\Delta_{1,2}}{2} \pm \overline{\delta}_{\omega}} \tag{3.297}$$

Substituting from Eq. (3.297) in Eq. (3.292) and Eq. (3.293) we obtian:

$$A = e^{i2\psi_+} A^*, \quad B = e^{i2\psi_-} B^* \tag{3.298}$$

Defining $A = |A| e^{i\alpha}$ and $B = |B| e^{i\beta}$ and using equation (3.298) we get:

$$\alpha = \psi_+, \quad \beta = \psi_- \tag{3.299}$$

Thus, the total solution for n_1, given by equation (3.250) can be rewritten as:

$$n_1(t) = e^{i\frac{\Delta_{1,2}}{2}t + i\psi_+} \left[|A| e^{\overline{\delta}_{\omega} t} + e^{i(\psi_- - \psi_+)} |B| e^{-\overline{\delta}_{\omega} t} \right] \tag{3.300}$$

As mentioned before, the above solution is valid only for times where the assumption $|n_2| \gg |n_1|$ is still satisfied. The absolute value of the amplitudes of the growing and damping solution in Eq. (3.300) which are $|A|$ and $|B|$, are independent values. However their relative phase $\psi_- - \psi_+$ is not an independent parameter. In order to

evaluate this phase difference, from Eq. (3.297) for $e^{i2(\psi_- - \psi_+)}$ we write:

$$\begin{aligned} e^{i2(\psi_- - \psi_+)} &= \frac{i\Delta_{1,2} + 2\overline{\delta}_\omega}{i\Delta_{1,2} - 2\overline{\delta}_\omega} = \frac{\Delta_{1,2}^2 - 4\overline{\delta}_\omega^2 - 4i\overline{\delta}_\omega\Delta_{1,2}}{\Delta_{1,2}^2 + 4\overline{\delta}_\omega^2} \\ &= \frac{4X_{1,2}^2|n_2|^2 - i4\overline{\delta}_\omega\Delta_{1,2}}{2\Delta_{1,2}^2 - X_{1,2}^2|n_2|^2} \end{aligned} \tag{3.301}$$

Substituting for $X_{1,2}$ from Eq. (3.189) we obtain

$$\tan[2(\psi_- - \psi_+)] = -\frac{4\overline{\delta}_\omega\Delta_{1,2}}{(\omega_1+\omega_2)^2|n_2|^2} \tag{3.302}$$

3.5.4 Special case: Isolated modes 1, 2 and 3 with $|n_2(0)| \gg |n_1(0)|, |n_3(0)|$

In the previous section 3.5.3, all of the spatial Fourier terms, except mode 1 and 2, were excluded from the plasma. In this section we keep three spatial Fourier terms 1,2 and 3 and exclude the rest, with the initial condition such that $|n_2(0)| \gg |n_1(0)|, |n_2(0)|$. We are interested in seeing the effect that mode 3 has on the nonlinear interaction of modes 1 and 2. The evolution equations describing this system are given by the Eq. (3.148) with $l = 1, 2, 3$, and $n_l = 0$ for $l > 3$:

$$\dot{n}_2 = -i\chi_{2,1}(n_1)^2 e^{-i\Delta_{1,2}t} - i\chi_{2,3} n_1^* n_3 e^{-i\Delta_{1,3}t}, \tag{3.303}$$

$$\dot{n}_1 = -i\chi_{1,2} n_2 n_1^* e^{i\Delta_{1,2}t} - i\chi_{1,3} n_3 n_2^* e^{i\Delta_{1,3}t}, \tag{3.304}$$

$$\dot{n}_3 = -i\chi_{3,1} n_2 n_1 e^{-i\Delta_{1,3}t}, \tag{3.305}$$

where $\Delta_{1,2} = 2\omega_1 - \omega_2$ and $\Delta_{1,3} = \omega_1 + \omega_2 - \omega_3$ and

$$\chi_{l,m} = X_{l,m} + X_{l,l-m}, \quad l \neq 2m \tag{3.306}$$
$$\chi_{2m,m} = X_{2m,m}.$$

With the assumption that $n_1, n_3 \sim \varepsilon n_2$, since $\dot{n}_2$ is of order ε^2 and is smaller compared to $\dot{n}_1, \dot{n}_3 \sim \varepsilon$, to the lowest order n_2 satisfies:

$$\dot{n}_2 \approx 0, \tag{3.307}$$

Therefore to the lowest order, n_2 is a constant and the solutions to equations (3.304) and (3.305) are of the following forms:

$$n_1 = Ae^{qt} + Be^{(q^* + i\Delta_{1,2})t}, n_3 = Ce^{(q - i\Delta_{1,3})t} + De^{(q^* + i\Delta_{1,2} - i\Delta_{1,3})t} \tag{3.308}$$

Substituting from Eq. (3.308) in Eq. (3.304) and Eq. (3.305) we obtain the following equations:

$$qA + i\chi_{1,2} n_2 B^* + i\chi_{1,3} n_2^* C = 0, \tag{3.309}$$

$$(q - i\Delta_{1,2})B^* - i\chi_{1,2} n_2^* A - i\chi_{1,3} n_2 D^* = 0, \tag{3.310}$$

$$(q - i\Delta_{1,3})C + i\chi_{1,3} n_2 A = 0, \tag{3.311}$$

$$(q - i\Delta_{1,2} + i\Delta_{1,3})D^* - i\chi_{1,3} n_2^* B^* = 0. \tag{3.312}$$

where A, B, C, D are undetermined complex constants. Above equations can be written in terms of a matrix equation:

$$\mathbf{M}(q).\mathbf{e} = 0, \tag{3.313}$$

where $\mathbf{e}$ is the eigenvector related to q given by:

$$\mathbf{e} = \begin{pmatrix} A \\ B^* \\ C \\ D^* \end{pmatrix} \tag{3.314}$$

and matrix $\mathbf{M}(q)$ is given by

$$\begin{pmatrix} q & i\chi_{1,2} n_2 & i\chi_{1,3} n_2^* & 0 \\ -i\chi_{1,2} n_2^* & q - i\Delta_{1,2} & 0 & -i\chi_{1,3} n_2 \\ i\chi_{3,1} n_2 & 0 & q - i\Delta_{1,3} & 0 \\ 0 & -i\chi_{3,1} n_2^* & 0 & q - i\Delta_{1,2} + i\Delta_{1,3} \end{pmatrix} \tag{3.315}$$

The four roots of the determinant of $\mathbf{M}$ give the complex frequencies of the n_1 and n_3 system. Figure (3.12) shows the real and figure (3.11) shows the imaginary part of the four roots for q scaled to $\Delta_{1,2}$. These roots are q_1, q_2, q_3 and q_4, with their related eigenvectors $\mathbf{e}_1, \mathbf{e}_2, \mathbf{e}_3$, and $\mathbf{e}_4$ which satisfy:

$$\mathbf{M}(q_i).\mathbf{e}_i = 0,\ i = 1, 2, 3, 4 \tag{3.316}$$

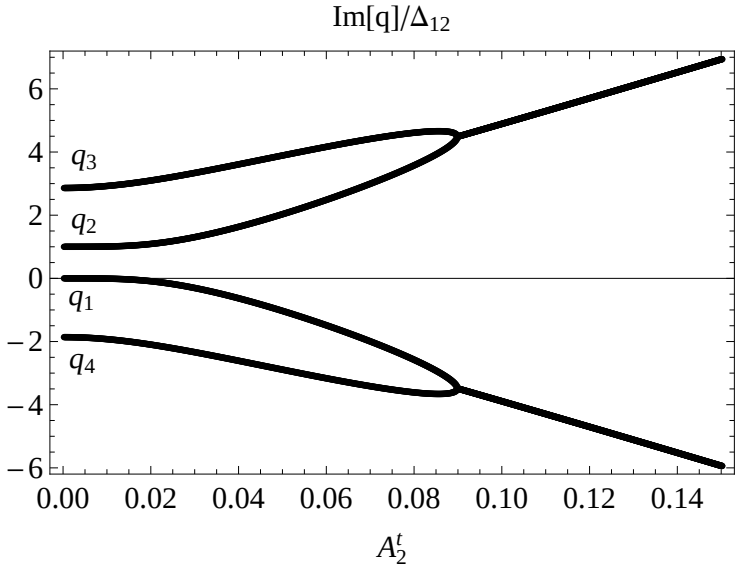

Figure 3.11: Imaginary parts of the four roots, q_1, q_2, q_3, q_4 vs. the amplitude of mode 2, for $k_\perp = 10k_1$.

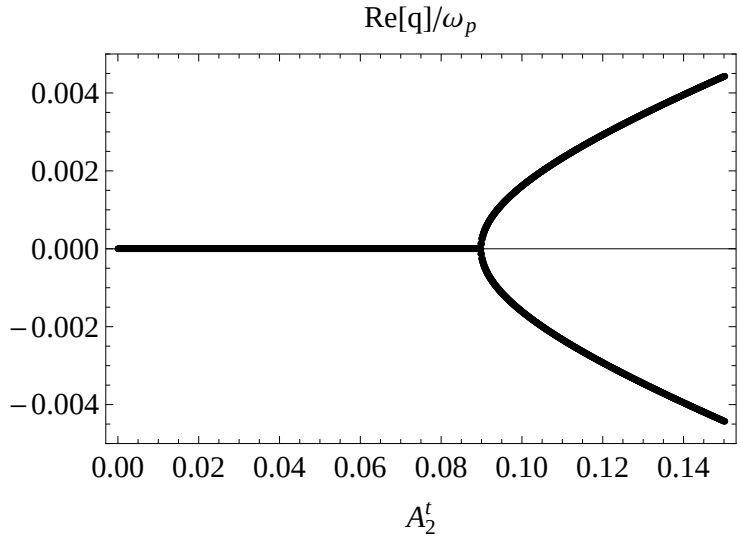

Figure 3.12: Real parts of the four roots, q_1, q_2, q_3, q_4 vs. the amplitude of mode 2, for $k_\perp = 10k_1$.

The un-normalized eigenvector related to eigenvalue q is given by:

$$\mathbf{e}_j^T = \left(1\,, \frac{q_j + \frac{\chi_{1,3}\chi_{3,1}|n_2|^2}{q_j - i\Delta_{1,3}}}{-i\chi_{1,2}}, -\frac{i\chi_{3,1}n_2}{q_j - i\Delta_{1,3}}, \frac{i\chi_{3,1}n_2^*}{q_j - i\Delta_{1,2} + i\Delta_{1,3}} \frac{q_j + \frac{\chi_{1,3}\chi_{3,1}|n_2|^2}{q_j - i\Delta_{1,3}}}{-i\chi_{1,2}} \right) \tag{3.317}$$

which can be rewritten as:

$$\mathbf{e}_j = \begin{pmatrix} (q_j - i\Delta_{1,2} + i\Delta_{1,3})(q_j - i\Delta_{1,3}) \\ i(q_j - i\Delta_{1,2} + i\Delta_{1,3})[q_j(q_j - i\Delta_{1,3}) + \chi_{1,3}\chi_{3,1}|n_2|^2]/\chi_{1,2} \\ -i\chi_{3,1}n_2(q_j - i\Delta_{1,2} + i\Delta_{1,3}) \\ -\frac{\chi_{3,1}}{\chi_{1,2}}n_2^*[q_j(q_j - i\Delta_{1,3}) + \chi_{1,3}\chi_{3,1}|n_2|^2] \end{pmatrix} \tag{3.318}$$

There is a value of amplitude of mode 2, $A_2^t = 2|n_2|$ (see Eq. (3.99)) below which all the roots are imaginary and above which there are 2 pairs of growing and decaying roots. In figure (3.12) this value, which we call the instability threshold is given by $A_2^{\mathrm{t,\,thr}} = 0.09$. In the values $A_2^{\mathrm{t}} < A_2^{\mathrm{t,\,thr}}$ where all the roots are imaginary, there is the following relation between the roots:

$$q_1 = iq_{1i},\; q_2 = i\Delta_{1,2} - iq_{1i},\; q_3 = iq_{3i},\; q_4 = i\Delta_{1,2} - iq_{3i} \tag{3.319}$$

In the limit $n_2 \to 0$ these frequencies are given by:

$$q_1 = 0,\; q_2 = i\Delta_{1,2},\; q_3 = i\Delta_{1,3},\; q_4 = i\Delta_{1,2} - i\Delta_{1,3} \tag{3.320}$$

n_1 and n_3 as a function of time are linear combinations of the four eigenvectors with real arbitrary coefficients a_1, a_2, a_3, a_4, which are determined from the initial conditions. As a result, $n_1(t)$ has the form:

$$\begin{aligned} n_1(t) &= a_1\mathrm{e}_{11}e^{iq_{1i}t} + a_2\mathrm{e}_{21}e^{i(\Delta_{1,2}-q_{1i})t} + a_3\mathrm{e}_{31}e^{iq_{3i}t} + a_4\mathrm{e}_{41}e^{i(\Delta_{1,2}-q_{3i})t} \\ &+ a_1\mathrm{e}_{12}^*e^{i(\Delta_{1,2}-q_{1i})t} + a_2\mathrm{e}_{22}^*e^{iq_{1i}t} + a_3\mathrm{e}_{32}^*e^{i(\Delta_{1,2}-q_{3i})t} + a_4\mathrm{e}_{42}^*e^{iq_{3i}t}, \end{aligned} \tag{3.321}$$

The full time dependence of mode 1 is given by:

$$n_1^{(1)}(t) = (a_1 \mathrm{e}_{11} + a_2 \mathrm{e}_{22}^*) e^{i q_{1i} t - i\omega_1 t} + (a_1 \mathrm{e}_{12}^* + a_2 \mathrm{e}_{21}) e^{i(\Delta_{1,2} - q_{1i})t - i\omega_1 t}$$
$$+ (a_3 \mathrm{e}_{31} + a_4 \mathrm{e}_{42}^*) e^{i q_{3i} t - i\omega_1 t} + (a_4 \mathrm{e}_{41} + a_3 \mathrm{e}_{32}^*) e^{i(\Delta_{1,2} - q_{3i})t - i\omega_1 t} \tag{3.322}$$

Similarly for mode 3 we obtain:

$$n_3^{(1)}(t) = (a_1 \mathrm{e}_{13} + a_2 \mathrm{e}_{24}^*) e^{i(q_{1i} - \Delta_{1,3})t - i\omega_3 t} + (a_1 \mathrm{e}_{14}^* + a_2 \mathrm{e}_{23}) e^{i(\Delta_{1,2} - \Delta_{1,3} - q_{1i})t - i\omega_3 t}$$
$$+ (a_3 \mathrm{e}_{33} + a_4 \mathrm{e}_{44}^*) e^{i(q_{3i} t - \Delta_{1,3})t - i\omega_3 t} + (a_4 \mathrm{e}_{43} + a_3 \mathrm{e}_{34}^*) e^{i(\Delta_{1,2} - \Delta_{1,3} - q_{3i})t - i\omega_3 t} \tag{3.323}$$

We used the following definition for the nonlinear mode 1 frequency:

$$\overline{\omega}_1 = \omega_1 - q_{1i}, \tag{3.324}$$

which is the sum of the linear mode frequency ω_1, and $-q_{1i}$ which is the frequency correction due to nonlinear coupling to mode 2. There is also a correction to the frequency of mode 3 due to coupling to mode 2. We define the nonlinear mode 3 frequency as $\overline{\omega}_3$:

$$\overline{\omega}_3 = \omega_3 - q_{3i} + \Delta_{1,3} \tag{3.325}$$

Using the definitions in Eq. (3.330) and Eq. (3.325) we can rewrite Eq. (3.322) as:

$$n_1^{(1)}(t) = (a_1 \mathrm{e}_{11} + a_2 \mathrm{e}_{22}^*) e^{-i\overline{\omega}_1 t} + (a_1 \mathrm{e}_{12}^* + a_2 \mathrm{e}_{21}) e^{-i(\omega_2 - \overline{\omega}_1)t}$$
$$+ (a_3 \mathrm{e}_{31} + a_4 \mathrm{e}_{42}^*) e^{-i(\overline{\omega}_3 - \omega_2)t} + (a_4 \mathrm{e}_{41} + a_3 \mathrm{e}_{32}^*) e^{i(\overline{\omega}_3 - 2\omega_2)t} \tag{3.326}$$

For mode 3 we can rewrite Eq. (3.323) as:

$$n_3^{(1)}(t) = (a_1 \mathrm{e}_{13} + a_2 \mathrm{e}_{24}^*) e^{-i(\overline{\omega}_1 + \omega_2)t} + (a_1 \mathrm{e}_{14}^* + a_2 \mathrm{e}_{23}) e^{i(\overline{\omega}_1 - 2\omega_2)t}$$
$$+ (a_3 \mathrm{e}_{33} + a_4 \mathrm{e}_{44}^*) e^{-i\overline{\omega}_3 t} + (a_4 \mathrm{e}_{43} + a_3 \mathrm{e}_{34}^*) e^{i(\overline{\omega}_3 - 3\omega_2)t} \tag{3.327}$$

We are interested in the effect of a dominant nonlinear mode 2 on small amplitude mode 1, in the presence of a small mode 3 in the plasma. Thus, for three

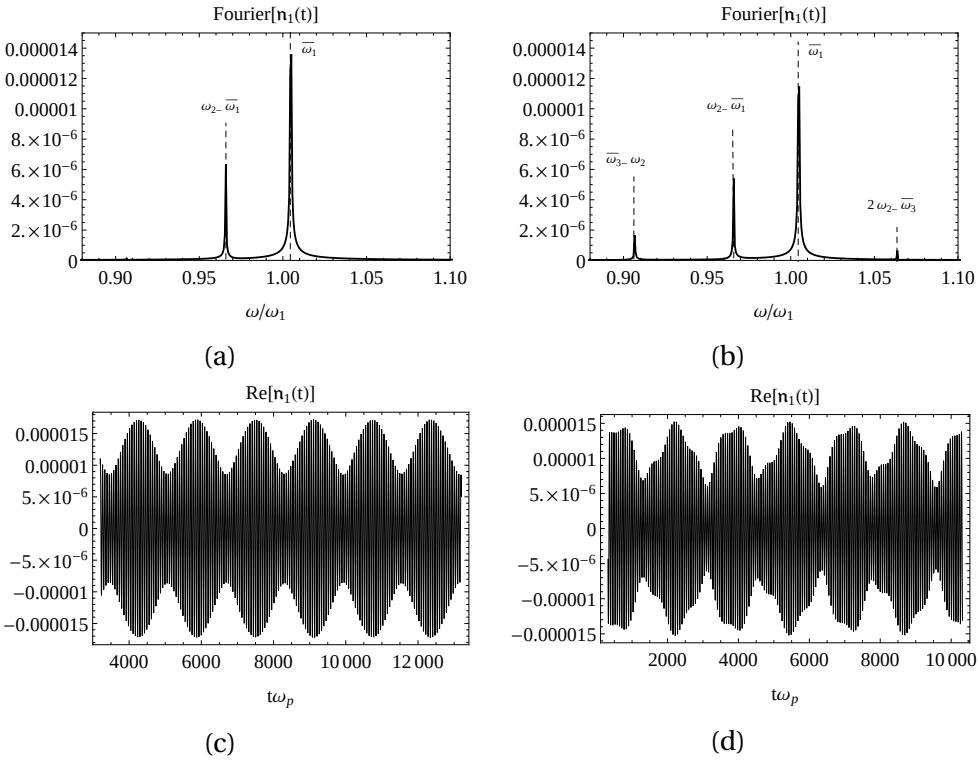

Figure 3.13: Figures (3.13c) and (3.13d) are Re[$n_1(t)$] vs. time, obtained from the time integration of Eqs. (F.2) and (F.3) with $M = 3$. Figures (3.13a) and (3.13b) are their respective Fourier transforms for $k_\perp = 10k_1$, $|n_1| = 10^{-3}|n_2|$, and $|n_2| = 1.24\times10^{-2}$. The vertical dashed lines are the analytically obtained frequencies from Eq. (3.324) and Eq. (3.325). Figures (3.13c) and (3.13a) are the result of driving the plasma at the potential $\overline{V}_2 = 5\times10^{-7} m_q(\omega_p L/2\pi)^2$ for a forcing time $T_F\omega_p = 3200$. Figures (3.13d) and (3.13b) are the results of driving the plasma at the potential $\overline{V}_2 = 5\times10^{-6} m_q(\omega_p L/2\pi)^2$ for a forcing time $T_F\omega_p = 320$.

isolated spatial Fourier terms in the plasma, we use the following external potential to excite a mode 2 and a small mode 1 as a seed:

$$V^{\text{ext}}(z,t) = 2g^{\text{slow}}(t)\left[\overline{V}_2\cos[k_2 z-\omega_2 t]+\epsilon\overline{V}_2\cos[k_1 z-\omega_1 t]\right] \tag{3.328}$$

were $g^{\text{slow}}(t)$ is a slowly varying function of time with the form given by Eq. (F.6). Although our drive potential includes frequencies ω_1 and ω_2, mode 3 and its related frequencies are also nonlinearly excited (see Eqs. (3.326) and (3.327)). Since our focus is on the interacting modes 1 and 2, we want to minimize the effects related to mode 3. We find that the response of plasma to the drive potential depends on how

it was driven, i.e. depends on the values of the parameters of the drive, which are the drive time and drive amplitude. Comparing Figs. (3.13c) and (3.13d) to Fig. (3.10), we find the prescription for receiving a response from plasma that contains the least effects related to mode 3: Adiabaticaly driving the plasma by choosing smaller potential amplitudes and longer drive times results a plasma response in which $\mathrm{n}_1(t)$ (or $n_1^{(1)}(t)$ of the reduced system given by Eq. (3.326)) contains large signals related to $\overline{\omega}_1$ and $\overline{\omega}_1-\omega_2$ and much smaller signals related to the frequencies $\overline{\omega}_3-\omega_2$ and $2\omega_2-\overline{\omega}_3$. Figure (3.13c) shows the time variation of $\mathrm{Re}[\mathrm{n}_1(t)]$, which is the solution of Eq. (F.2) with $M=3$ and $|\mathrm{n}_1|=10^{-3}|\mathrm{n}_2|$. Our analytical perturbation solution for n_1 is the function $n_1^{(1)}(t)$ which has the form given by Eq. (3.326). Figure (3.13a) depicts the Fourier transform of $\mathrm{n}_1(t)$ from the computer simulations, for a case of slower and smaller drive vs figure (3.13a) for a faster larger drive, for the same value of $|\mathrm{n}_2|=1.24\times10^{-2}$. For the faster larger drive we can see that all the four frequencies in Eq. (3.326) are present. On the other hand, as the result of adiabatically driving the plasma (slow drive) terms 3 and 4 on the right hand side of Eq. (3.326) are absent from the plasma, since they are not resonant with the drive potential, i.e. their frequencies are not close to ω_1. This results in a solution with $a_3\approx0, a_4\approx0$. The only term that is close enough to be driven resonantly is the first term in Eq. (3.326). However, due to nonlinear coupling of mode 1 to mode 2, we can not excite the first term in Eq. (3.326) without exciting the second term. From Eq. (3.326) we can see that there is no solution such that the first term is nonzero and the second term becomes zero, and vice versa, since a_1 and a_2 are real and e_{11}, e_{22}^*, e_{12}^*, e_{21} are complex. Therefore the response of adiabaticaly driving Eq. (3.328) is of the form:

$$n_1^{(1)}(t)\approx(a_1\mathrm{e}_{11}+a_2\mathrm{e}_{22}^*)e^{-i\overline{\omega}_1t}+(a_1\mathrm{e}_{12}^*+a_2\mathrm{e}_{21})e^{i(\overline{\omega}_1-\omega_2)t}, \tag{3.329}$$

The frequencies of the two terms in Eq. (3.329) i.e. $\overline{\omega}_1$ and $\omega_2-\overline{\omega}_1$ are close to each other and the beating between these two terms gives the slow time varying envelope of amplitude oscillation with the beat frequency (see Fig. (3.13c)):

$$\omega_{\mathrm{amp}}=2\overline{\omega}_1-\omega_2 \tag{3.330}$$

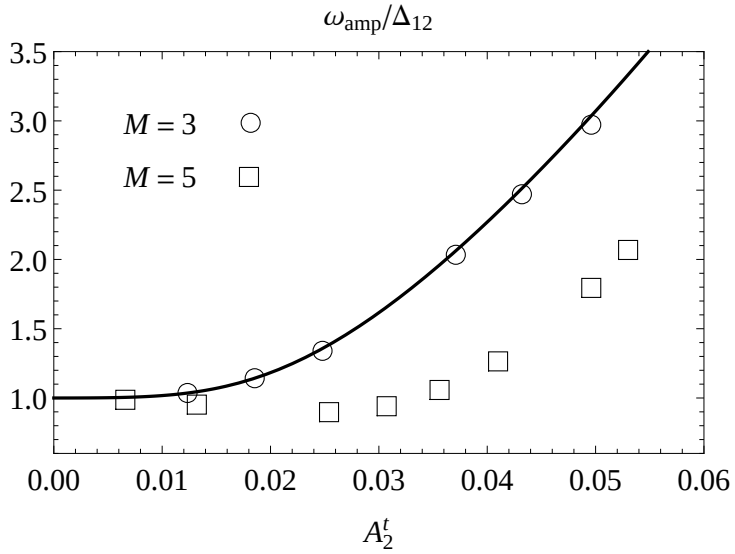

Figure 3.14: Plot of the beat frequency of the mode 1 amplitude, as a function of the amplitude of mode 2, for $k_\perp = 10k_1$. The analytical result is obtained from Eq. (3.330) and depicted in a solid curve. The numerical result for $M = 3$ and $M = 5$ are depicted in circles and squares.

Figure (3.14) depicts ω_{amp}, obtained from Eq. (3.330), scaled by $\Delta_{1,2}$ in a solid curve, and the beat frequency measured from the numerical simulation results($k_\perp/k_1 = 10$), with 3 isolated waves depicted in circles and the results for 5 isolated waves depicted in squares. From Fig (3.11) and Eq. (3.324) we observe that as the mode 2 amplitude $A_2^t = 2|n_2|$ grows, the frequency of mode 1 $\overline{\omega}_1$ also grows. This behaviour is opposite to the case of isolated modes 1 and 2 for which the frequency of mode 1 was given by the relation Eq. (3.285), and is also opposite to the case of isolated modes 1, 2, 3 and 4, which we study in the next section. Thus, from Eq. (3.330), ω_{amp} also grows with A_2^t as is depicted in Fig (3.14). Furthermore, from Fig (3.11) and Eq. (3.325) we observe that mode 3 frequency $\overline{\omega}_3$ goes down as the mode 2 amplitude A_2^t grows. For $A_2^{\text{t}} \geq A_2^{\text{t, th}}$ which is the unstable regime, the following condition holds between the frequencies:

$$\omega_2 = (\overline{\omega}_3 + \overline{\omega}_1)/2 \tag{3.331}$$

The above condition is different from the sub-harmonicity condition $\omega_2 = 2\overline{\omega}_1$ which was satisfied in the unstable regime, for isolated waves 1 and 2.

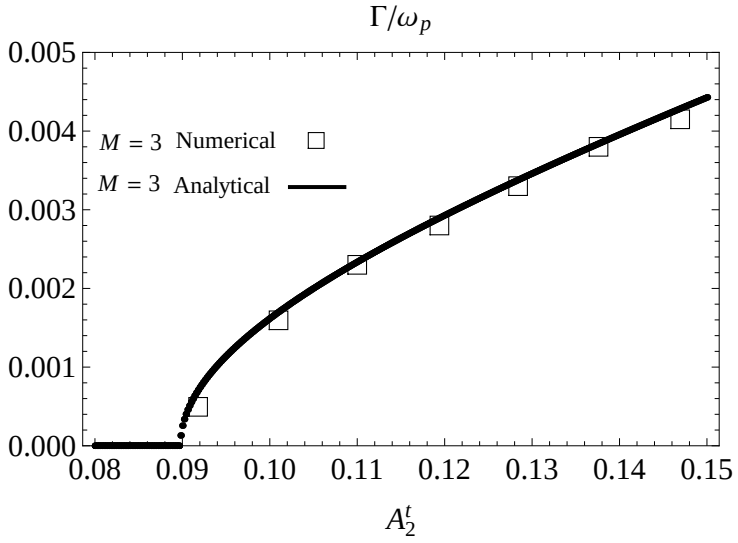

Figure 3.15: Plot of the growth rate of mode 1 vs. the amplitude of mode 2, for $M = 3$ interacting modes, for $k_\perp = 10k_1$. The analytical growth rate Γ is defined in Eq. (3.332). The numerical results are depicted in squares.

From Fig. (3.12) we can see that for $k_\perp = 10k_1$ the instability threshold is at $A_2^{\mathrm{t,\,thr}} \approx 0.09$. for values of amplitude below $A_2^{\mathrm{t,\,thr}}$, all four q's are imaginary. For values of amplitude above this threshold, frequencies will have a real part:

$$\begin{aligned} q_1 &= \Gamma + i q_{1i} \\ q_2 &= -\Gamma + i\Delta_{1,2} - i q_{1i} \\ q_3 &= \Gamma + i\Delta_{1,2} - i q_{1i} \\ q_4 &= -\Gamma + i q_{1i} \end{aligned} \tag{3.332}$$

Γ is the growth rate of modes 1 and 3. Due to energy conservation, growth of these modes will cause the decay of the dominant mode 2. As we can see in figure (3.15), the growth rate Γ increases with the amplitude of mode 2. For larger Γ, mode 2 shares more of its energy and decays to smaller values, and the amplitudes of mode 1 and 3 grow to larger values.

3.5.5 Special case: Four isolated modes 1, 2, 3 and 4 with $|n_2(0)| \gg |n_4(0)| \gg |n_1(0)|, |n_3(0)|$

In this section the isolated spatial Fourier terms 1,2,3,4 are present and all the other terms are excluded. We assume a dominant nonlinear mode 2 in the plasma and the spatial Fourier term 4 is just a harmonic of term 2 due to mode 2 being nonlinear: $n_2(t)$ oscillates at the frequency $\overline{\omega}_2$ and, $n_4(t)$ oscillates at frequency $2\overline{\omega}_2$. Initial condition are such that

$$|n_2(0)| \gg |n_4(0)| \gg |n_1(0)|, |n_3(0)| \tag{3.333}$$

The evolution equations describing this system are given by the Eq. (3.148) with $l = 1,2,3,4$, and $n_l = 0$ for $l > 4$:

$$\dot{n}_1 = -i\chi_{1,2} n_2 n_1^* e^{i\Delta_{1,2}t} - i\chi_{1,3} n_3 n_2^* e^{i\Delta_{1,3}t} - i\chi_{1,4} n_4 n_3^* e^{i\Delta_{1,4}t}, \tag{3.334}$$

$$\dot{n}_3 = -i\chi_{3,1} n_2 n_1 e^{-i\Delta_{1,3}t} - i\chi_{3,4} n_4 n_1^* e^{i\Delta_{1,4}t}, \tag{3.335}$$

$$\dot{n}_2 = -i\chi_{2,4} n_4 n_2^* e^{i\Delta_{2,4}t} - i\chi_{2,3} n_3 n_1 e^{i\Delta_{1,3}t}, \tag{3.336}$$

$$\dot{n}_4 = -i\chi_{4,2} (n_2)^2 e^{-i\Delta_{2,4}t} - i\chi_{4,3} n_3 n_1 e^{-i\Delta_{1,4}t}, \tag{3.337}$$

where $\Delta_{1,2} = 2\omega_1 - \omega_2$, $\Delta_{1,3} = \omega_1 + \omega_2 - \omega_3$ and $\Delta_{2,4} = 2\omega_2 - \omega_4$. With the assumption that $n_1, n_3 \sim \varepsilon n_4 \ll n_4$, the second term on the right hand side of Eq. (3.336) and Eq. (3.337) are of order ε^2 with the respect to the first terms and we can drop them to the lowest order:

$$\dot{n}_2 = -i\chi_{2,4} n_4 n_2^* e^{i\Delta_{2,4}t} \tag{3.338}$$

$$\dot{n}_4 = -i\chi_{4,2} (n_2)^2 e^{-i\Delta_{2,4}t} \tag{3.339}$$

As the result, the evolution of n_2 and n_4 decouples from small amplitude n_1 and n_3. The solution to equations Eq. (3.338) and Eq. (3.339) for a nonlinear mode 2 are

given by Eq. (3.255), Eq. (3.266) and Eq. (3.257), with $1 \rightarrow 2$ and $2 \rightarrow 4$:

$$n_2(t) = \overline{n}_2 e^{i(\frac{\Delta_{2,4}}{2} - \delta_\omega)t} \tag{3.340}$$

$$n_4(t) = \frac{\chi_{4,2}}{2\delta_\omega} \overline{n}_2^2 e^{-2i\delta_\omega t} \tag{3.341}$$

$$\delta_\omega = \sqrt{(\tfrac{\Delta_{2,4}}{2})^2 + \chi_{2,4}\chi_{4,2}|\overline{n}_2|^2}, \tag{3.342}$$

where $\overline{n}_2$ is constant. Using the definition of $\overline{\omega}_2$ which is the frequency of the nonlinear mode 2 (see Eq. (3.257) with $1 \rightarrow 2$):

$$\overline{\omega}_2 = \omega_2 + \delta_\omega - \tfrac{\Delta_{2,4}}{2}, \tag{3.343}$$

We have the following definitions:

$$\overline{\Delta}_{1,2} = 2\omega_1 - \overline{\omega}_2 = \Delta_{1,2} - \delta_\omega + \tfrac{\Delta_{2,4}}{2} \tag{3.344}$$

$$\overline{\Delta}_{1,3} = \overline{\omega}_2 + \omega_1 - \omega_3 = \Delta_{1,3} + \delta_\omega - \tfrac{\Delta_{2,4}}{2} \tag{3.345}$$

$$\overline{\Delta}_{2,4} = 2\overline{\omega}_2 - \omega_4 = 2\delta_\omega \tag{3.346}$$

We substitute from Eq. (3.340) and Eq. (3.341) in Eq. (3.334) and Eq. (3.335) and use Eq. (3.344) through Eq. (3.346) and we obtain:

$$\begin{aligned} &\dot{n}_1 = \\ &-i\chi_{1,2}\overline{n}_2 n_1^* e^{i\overline{\Delta}_{1,2}t} - i\chi_{1,3} n_3 \overline{n}_2^* e^{i\overline{\Delta}_{1,3}t} - i\chi_{1,4}\frac{\chi_{4,2}}{2\delta_\omega}(\overline{n}_2)^2 n_3^* e^{i(\Delta_{1,4} - \overline{\Delta}_{2,4})t} \end{aligned} \tag{3.347}$$

$$\dot{n}_3 = -i\chi_{3,1}\overline{n}_2 n_1 e^{-i\overline{\Delta}_{1,3}t} - i\chi_{3,4}\frac{\chi_{4,2}}{2\delta_\omega}(\overline{n}_2)^2 n_1^* e^{i(\Delta_{1,4} - \overline{\Delta}_{2,4})t}, \tag{3.348}$$

The solution to above equations is of the following form:

$$n_1 = Ae^{qt} + Be^{(q^* + i\overline{\Delta}_{1,2})t}, n_3 = Ce^{(q - i\overline{\Delta}_{1,3})t} + De^{(q^* + i\overline{\Delta}_{1,2} - i\overline{\Delta}_{1,3})t} \tag{3.349}$$

Substituting from Eq. (3.349) in Eq. (3.347) and Eq. (3.348) we obtain the following equations:

$$qA + i\chi_{1,2}\overline{n}_2 B^* + i\chi_{1,3}\overline{n}_2^* C + i\chi_{1,4}\frac{\chi_{4,2}}{2\delta_\omega}\overline{n}_2^2 D^* = 0 \tag{3.350}$$

$$(q - i\overline{\Delta}_{1,2})B^* - i\chi_{1,2}\overline{n}_2^* A - i\chi_{1,4}\frac{\chi_{4,2}}{2\delta_\omega}(\overline{n}_2^2)^* C - i\chi_{1,3}\overline{n}_2 D^* = 0 \tag{3.351}$$

$$(q - i\overline{\Delta}_{1,3})C + i\chi_{1,3}\overline{n}_2 A + i\chi_{3,4}\frac{\chi_{4,2}}{2\delta_\omega}\overline{n}_2^2 B^* = 0 \tag{3.352}$$

$$(q - i\overline{\Delta}_{1,2} + i\overline{\Delta}_{1,3})D^* - i\chi_{1,3}\overline{n}_2^* B^* - i\chi_{3,4}\frac{\chi_{4,2}}{2\delta_\omega}(\overline{n}_2^2)^* B^* = 0 \tag{3.353}$$

Above equations can be written in terms of a matrix equation:

$$\mathbf{M}(q).\mathbf{n} = 0, \tag{3.354}$$

where $\mathbf{n}$ is a vector givn by:

$$\mathbf{n} = \begin{pmatrix} A \\ B^* \\ C \\ D^* \end{pmatrix} \tag{3.355}$$

and matrix $\mathbf{M}(q)$ is given by

$$\mathbf{M}(q) = \begin{pmatrix} q & i\chi_{1,2}\overline{n}_2 & i\chi_{1,3}\overline{n}_2^* & i\chi_{1,4}\frac{\chi_{4,2}}{2\delta_\omega}\overline{n}_2^2 \\ -i\chi_{1,2}\overline{n}_2^* & q - i\overline{\Delta}_{1,2} & -i\chi_{1,4}\frac{\chi_{4,2}}{2\delta_\omega}(n_2^2)^* & -i\chi_{1,3}\overline{n}_2 \\ i\chi_{3,1}\overline{n}_2 & i\chi_{3,4}\frac{\chi_{4,2}}{2\delta_\omega}(\overline{n}_2)^2 & q - i\overline{\Delta}_{1,3} & 0 \\ -i\chi_{3,4}\frac{\chi_{4,2}}{2\delta_\omega}(\overline{n}_2^2)^* & -i\chi_{3,1}\overline{n}_2^* & 0 & q - i\overline{\Delta}_{1,2} + i\overline{\Delta}_{1,3} \end{pmatrix} \tag{3.356}$$

The four roots of the determinant of $\mathbf{M}$ give the complex frequencies of the n_1 and n_3 system. Figure (3.17) shows the real and figure (3.16) shows the imaginary part of the four roots for q scaled to $\Delta_{1,2}$. These roots are q_1, q_2, q_3 and q_4, with their related eigenvectors $\mathbf{e}_1, \mathbf{e}_2, \mathbf{e}_3$, and $\mathbf{e}_4$ which satisfy:

$$\mathbf{M}(q_i).\mathbf{e}_i = 0,\ i = 1,2,3,4 \tag{3.357}$$

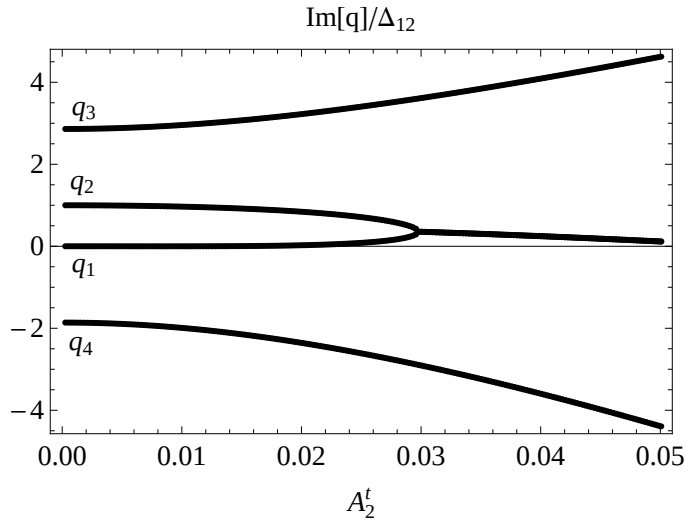

Figure 3.16: Imaginary parts of the roots q_1, q_2, q_3, q_4 vs. the amplitude of mode 2, for $k_\perp = 10k_1$.

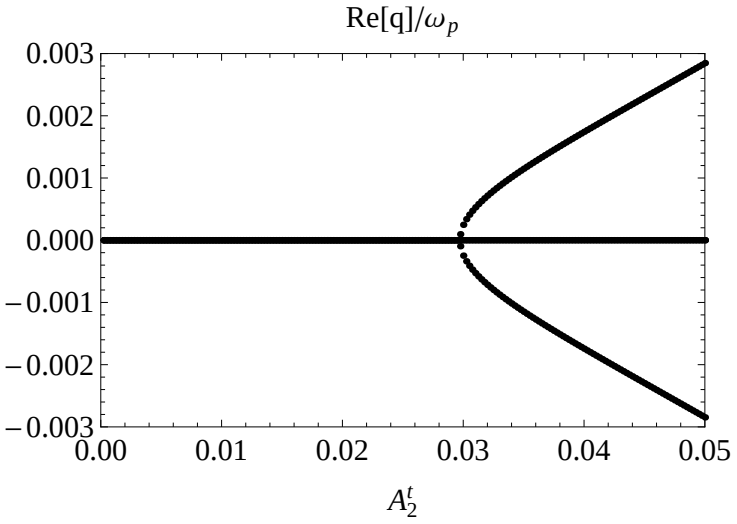

Figure 3.17: Real parts of the roots q_1, q_2, q_3, q_4 vs. the amplitude of mode 2, for $k_\perp = 10k_1$.

Here we follow the discussion we had in the last section, for the response of the plasma to a drive potential given by Eq. (3.328), which will excite a nonlinear mode 2 and a small amplitude mode 1 coupled to mode 2 due to nonlinearity. There is a threshold value for the amplitude of mode 2, $A_2^t = 2|n_2|$ (see Eq. (3.99)) below which all the roots are imaginary and above which there is pair of growing-decaying roots. In figure (3.12) this instability threshold is given by $A_2^{\mathrm{t,\,thr}} = 0.03$. In the values $A_2^{\mathrm{t}} < A_2^{\mathrm{t,\,thr}}$ where all the roots are imaginary, there is the following relation between the roots:

$$q_1 = iq_{1i},\ q_2 = i\overline{\Delta}_{1,2} - iq_{1i},\ q_3 = iq_{3i},\ q_4 = i\overline{\Delta}_{1,2} - iq_{3i} \tag{3.358}$$

In the limit $n_2 \to 0$ these frequencies are given by:

$$q_1 = 0,\ q_2 = i\Delta_{1,2},\ q_3 = i\Delta_{1,3},\ q_4 = i\Delta_{1,2} - i\Delta_{1,3} \tag{3.359}$$

n_1 and n_3 as a function of time are linear combinations of the four eigenvectors with real arbitrary coefficients a_1, a_2, a_3, a_4, which are determined from the initial conditions. As a result the full time dependence of mode 1 is given by:

$$\begin{aligned} n_1^{(1)}(t) &= (a_1 \mathrm{e}_{11} + a_2 \mathrm{e}_{22}^*) e^{iq_{1i}t - i\omega_1 t} + (a_1 \mathrm{e}_{12}^* + a_2 \mathrm{e}_{21}) e^{i(\overline{\Delta}_{1,2} - q_{1i})t - i\omega_1 t} \\ &+ (a_3 \mathrm{e}_{31} + a_4 \mathrm{e}_{42}^*) e^{iq_{3i}t - i\omega_1 t} + (a_4 \mathrm{e}_{41} + a_3 \mathrm{e}_{32}^*) e^{i(\overline{\Delta}_{1,2} - q_{3i})t - i\omega_1 t} \end{aligned} \tag{3.360}$$

Similarly for mode 3 we obtain:

$$\begin{aligned} n_3^{(1)}(t) &= (a_1 \mathrm{e}_{13} + a_2 \mathrm{e}_{24}^*) e^{i(q_{1i} - \overline{\Delta}_{1,3})t - i\omega_3 t} + (a_1 \mathrm{e}_{14}^* + a_2 \mathrm{e}_{23}) e^{i(\overline{\Delta}_{1,2} - \overline{\Delta}_{1,3} - q_{1i})t - i\omega_3 t} \\ &+ (a_3 \mathrm{e}_{33} + a_4 \mathrm{e}_{44}^*) e^{i(q_{3i}t - \overline{\Delta}_{1,3})t - i\omega_3 t} + (a_4 \mathrm{e}_{43} + a_3 \mathrm{e}_{34}^*) e^{i(\overline{\Delta}_{1,2} - \overline{\Delta}_{1,3} - q_{3i})t - i\omega_3 t} \end{aligned} \tag{3.361}$$

We define the nonlinear mode 1 frequency which as:

$$\overline{\omega}_1 = \omega_1 - q_{1i}, \tag{3.362}$$

which is the sum of the linear frequency and $-q_{1i}$, which is the frequency correction due to nonlinear coupling to mode 2. Furthermore we define the nonlinear mode 3

frequency as:

$$\overline{\omega}_3 = \omega_3 - q_{3i} + \overline{\Delta}_{1,3} \tag{3.363}$$

Using Eq. (3.362) and Eq. (3.363) we can rewrite Eq. (3.360) and Eq. (3.361) as:

$$\begin{aligned} n_1^{(1)}(t) &= (a_1 \mathrm{e}_{11} + a_2 \mathrm{e}_{22}^*) e^{-i\overline{\omega}_1 t} + (a_1 \mathrm{e}_{12}^* + a_2 \mathrm{e}_{21}) e^{-i(\overline{\omega}_2 - \overline{\omega}_1)t} \\ &+ (a_3 \mathrm{e}_{31} + a_4 \mathrm{e}_{42}^*) e^{-i(\overline{\omega}_3 - \overline{\omega}_2)t} + (a_4 \mathrm{e}_{41} + a_3 \mathrm{e}_{32}^*) e^{i(\overline{\omega}_3 - 2\overline{\omega}_2)t} \end{aligned} \tag{3.364}$$

$$\begin{aligned} n_3^{(1)}(t) &= (a_1 \mathrm{e}_{13} + a_2 \mathrm{e}_{24}^*) e^{-i(\overline{\omega}_1 + \overline{\omega}_2)t} + (a_1 \mathrm{e}_{14}^* + a_2 \mathrm{e}_{23}) e^{i(\overline{\omega}_1 - 2\overline{\omega}_2)t} \\ &+ (a_3 \mathrm{e}_{33} + a_4 \mathrm{e}_{44}^*) e^{-i\overline{\omega}_3 t} + (a_4 \mathrm{e}_{43} + a_3 \mathrm{e}_{34}^*) e^{i(\overline{\omega}_3 - 3\overline{\omega}_2)t} \end{aligned} \tag{3.365}$$

We are interested in the effect of a dominant nonlinear mode 2 on small amplitude mode 1. Thus we use the external potential given by Eq. (3.328) to excite a nonlinear mode 2 and a small mode 1 as a seed. Following the same discussion as in section 3.5.4 in order ot minimize the effects related to mode 3, we drive the plasma using the potential Eq. (3.328) adiabatically, which results in a solution with $a_3 \approx 0$, $a_4 \approx 0$ in Eq. (3.364).

Figure (3.18a) shows the full time variation of $\mathrm{Re}[\mathrm{n}_1(t)]$, which is the solution of the equations Eq. (F.2) with $M = 4$ and $|\mathrm{n}_1| = 10^{-4}|\mathrm{n}_2|$. Our analytical perturbation solution for n_1 is the function $n_1^{(1)}(t)$ which has the form given by Eq. (3.360). Figure (3.18c) depicts the Fourier transform of $\mathrm{n}_1(t)$ from the computer simulations, for a case of slower and smaller drive vs. Figure (3.18d) for faster and larger drive, for the same value of $|\mathrm{n}_2| = 1.2 \times 10^{-2}$.

For the faster larger drive we can see that three of the four frequencies in Eq. (3.360) are visible on the depicted scale. On the other hand, as the result of adiabatically driving the plasma (slow drive) terms 3 and 4 on the right hand side of Eq. (3.360) are absent from the plasma. Therefore the response of slowly driving the potential in Eq. (3.328) is given by Eq. (3.360) with only the first two terms. The frequencies of the two terms, i.e. $\overline{\omega}_1$ and $\overline{\omega}_2 - \overline{\omega}_1$ are close to each other and the beating between these two terms gives the slow time varying envelope of amplitude

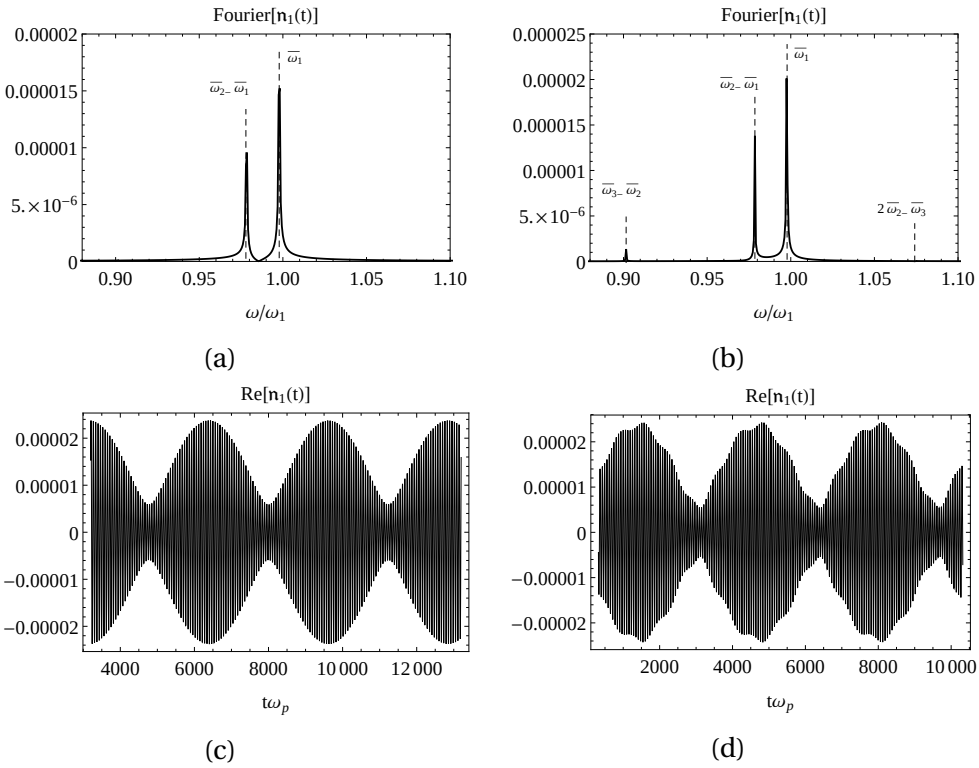

Figure 3.18: Figures (3.18a) and (3.18b) are $\mathrm{Re}[\mathrm{n}_1(t)]$ vs. time, obtained from the time integration of Eqs. (F.2) and (F.3) with $M = 4$. Figures (3.18c) and (3.18d) are their respective Fourier transforms for $k_\perp = 10k_1$, $|\mathrm{n}_1| = 10^{-3}|\mathrm{n}_2|$, and $|\mathrm{n}_2| = 1.2 \times 10^{-2}$ and the vertical dashed lines are the analytically obtained frequencies from Eq. (3.343), Eq. (3.362) and Eq. (3.363). Figures (3.18a) and (3.18c) are the reslut of driving the plasma at the potential $\overline{V}_2 = 5 \times 10^{-7} m_q(\omega_p L/2\pi)^2$ for a forcing time $T_F\omega_p = 3200$. Figures (3.18b) and (3.18d) are the reslut of driving the plasma at the potential $\overline{V}_2 = 5 \times 10^{-6} m_q(\omega_p L/2\pi)^2$ for a forcing time $T_F\omega_p = 320$.

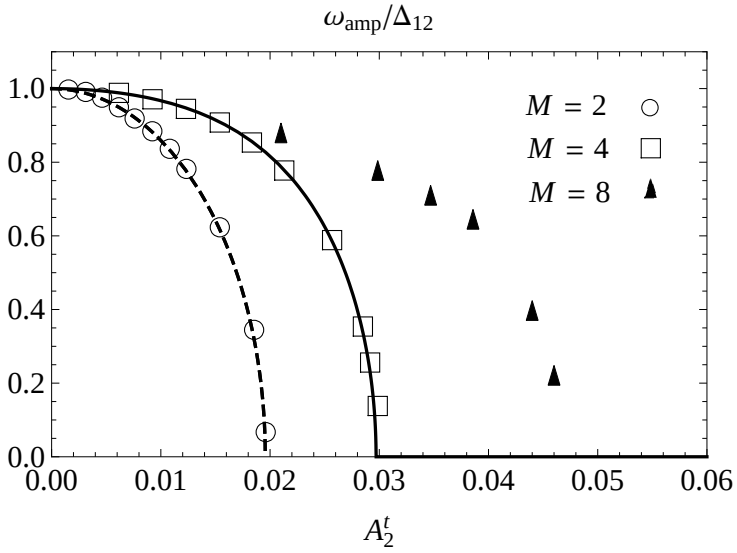

Figure 3.19: Beat frequency of the amplitude of mode 1 vs. the amplitude of mode 2, for $k_\perp = 10k_1$. The analytical result for $M = 2$, obtained in Eq. (3.286), is depicted in a dashed curve. Analytical result for $M = 4$ and given by Eq. (3.366), is depicted in a solid curve. Numerical results obtained for $M = 2, 4$ and 8 number of the present spatial Fourier terms are depicted respectively with circles, squares and triangles.

oscillation with the beat frequency (see figure (3.18a)):

$$\omega_{\rm amp} = 2\overline{\omega}_1 - \overline{\omega}_2 \tag{3.366}$$

Contrary to the section 3.5.4 for three waves 1, 2 and 3, and similar to the section 3.5.3 for two waves 1 and 2, $\omega_{\rm amp}$ decreases with growing A_2^t's. At the threshold of instability we have $q_{1i} = \overline{\Delta}_{1,2}/2$, and as a result $\omega_{\rm amp} = 0$. Figure (3.19) shows the beat frequency measured from the numerical simulations ($k_\perp/k_1 = 10$) scaled to $\Delta_{1,2}$. Frequencies obtained from $M = 2, 4$ and 8 number of the present spatial Fourier terms are depicted respectively with circles, squares and triangles. Analytical result for 2 waves, given by Eq. (3.286), is depicted in a dashed curve, and the analytical result for 4 waves, given by Eq. (3.366), is depicted in a solid curve. The threshold of instability moves to higher values of A_2^t with more number waves kept: for 2 waves at $A_2^{\rm t,\,thr} \approx 0.02$ for 4 waves at $A_2^{\rm t,\,thr} \approx 0.03$ and for 8 waves at $A_2^{\rm t,\,thr} \approx 0.048$. This implies that larger number of interacting waves will result in a more stable nonlinear mode 2, in the presence of a small amplitude mode 1. Fig. (3.20) compares the beat

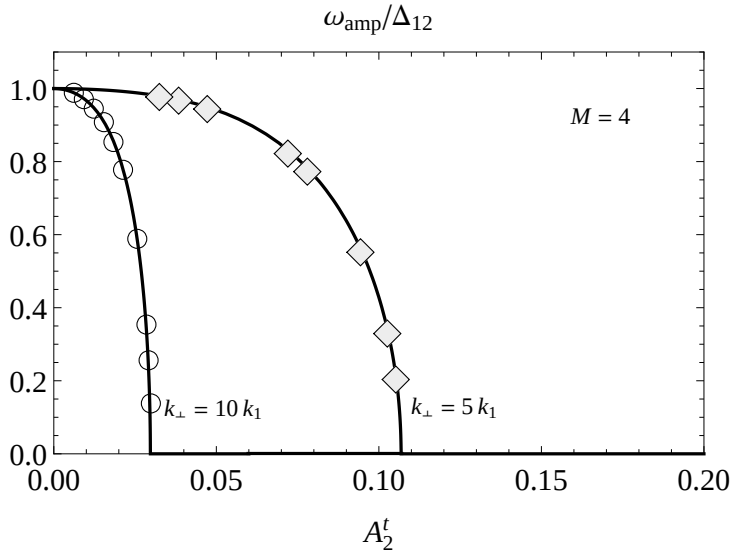

Figure 3.20: Beat frequency of the amplitude of mode 1 vs. the amplitude of mode 2, for $k_\perp = 10k_1$ and $k_\perp = 5k_1$. Analytical result for $M = 4$ is given by Eq. (3.366) and is depicted in a solid curve. Numerical results obtained for $M = 4$ number of the present spatial Fourier terms are depicted respectively squares for $k_\perp = 10k_1$ and diamonds for $k_\perp = 5k_1$.

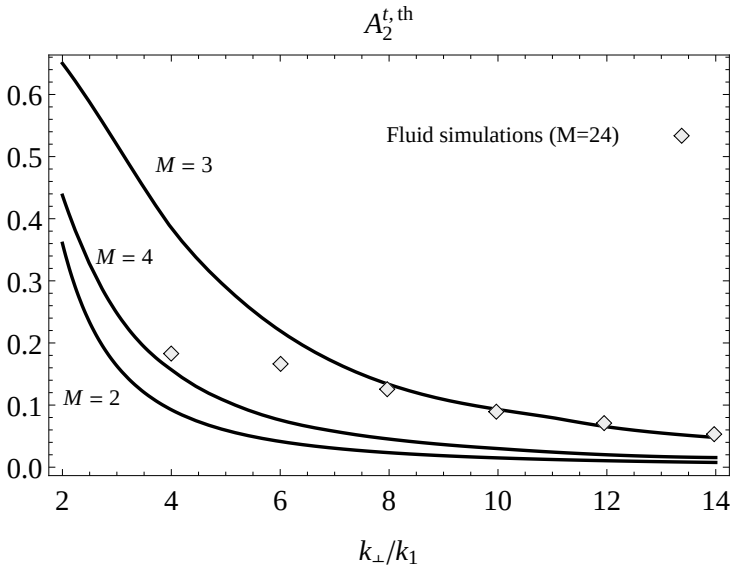

Figure 3.21: Plot of the amplitude of threshold for instability $A_2^{t,th}$ versus $k_\perp/k_1$. Fluid simulations of Eqs. (F.2) and (F.3) with $M = 24$ Fourier terms are depicted in diamonds.

frequency of mode 1 vs. the amplitude of mode 2 for $k_\perp/k_1 = 10$ and $k_\perp/k_1 = 5$. The latter case is more dispersive (has a larger detuning compared to mode frequency) and thus, mode 2 is more stable with respect to nonlinearity, in comparison to the former case.

In Fig. (3.21) the threshold amplitude for instability $A_2^{\mathrm{t,th}}$ due to resonant growth of mode 1, is depicted vs. $k_\perp/k_1$, for $M = 2,3,4$ in solid lines, and $M = 24$ in diamonds, the latter is closest to the realistic model of 1D plasma due to the large number of present terms. For larger $k_\perp/k_1$ the detuning between mode 2 and 1 ($\Delta_{1,2}$) is smaller compared to mode frequency, and as a result the onset of resonant instability of mode 2 is at smaller amplitudes $A_2^{\mathrm{t,th}}$. We can also observe that for any $k_\perp/k_1$, $A_2^{\mathrm{t,th}}$ for 2 waves is smaller than for 4 waves. However, anomalously for 3 waves $A_2^{\mathrm{t,th}}$ is larger than the $A_2^{\mathrm{t,th}}$ for 4 waves. For $M = 24$ and $k_\perp/k_1 \leq 2$ the threshold of instability of mode 1 ($A_2^{\mathrm{t,th}}$) could not be reached. In order to obtain larger A_2^t's with the driving technique described in appendix F we had to raise the drive potential and shorten the drive time. Otherwise, had we not shortened the drive time, the amplitude of mode 2 would be driven up and then down again. Thus for larger amplitudes the short driving time is not sufficient to excite nonlinear cnoidal mode 2, with phase-locked harmonics, instead the resonse of the plasma is more chaotic than wave-like. For $M = 24$ and $k_\perp/k_1 = 2$, A_2^t was driven up to 0.3 and still mode 1 was stable and oscillatory. This is due to the fact that satisfying the frequency condition for 3-wave interactions (see Eq. (3.1)) becomes harder for smaller values of $k_\perp/k_1$. On the other hand, satisfying the condition for the 4-waves interactions which is given by:

$$\omega_m + \omega_{m'} = \omega_n + \omega_{n'}, \quad k_m + k_{m'} = k_n + k_{n'} \tag{3.367}$$

is possible for large wave number modes, due to the fact that from Eq. (3.105), for $m \gg 1$ we have $\omega_m \approx 1$ ($\omega_m \approx \omega_p$ in proper unit of time). As a result, In our simulations with large number of terms, for example $M = 24$, the highest number modes become unstable and grow exponentialy, which leads to the decay or possible collapse (irreversible decay) of the large amplitude mode 2, before mode 1 gets the chance to become unstable. Figure (3.22) shows this decay for a traveling, nonlinear TG mode $m = 2$ with amplitude $A_2^t = 0.17$, obtained from the fluid simulation of

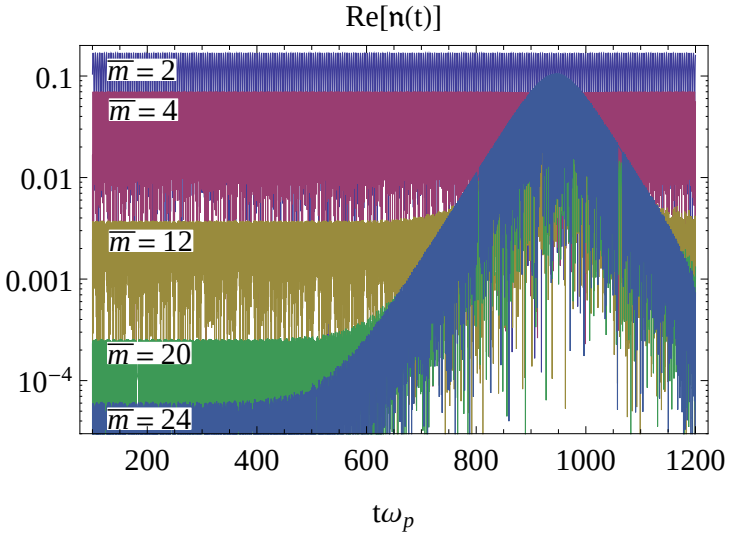

Figure 3.22: Plot of the Fourier components $\overline{m} = 2, 4, 12, 20, 24$ of density, for a nonlinear traveling mode $m = 2$, with amplitude $A_2^t = 0.17$, obtained from the fluid simulation of a plasma with $k_\perp/k_1 = 2$ and $M = 24$.

a plasma with $k_\perp/k_1 = 2$ and $M = 24$. Drive time was $T_F\omega_p = 100$ and drive potential was $\overline{V}_2 = 10^{-3} m_q(\omega_p L/2\pi)^2$. We can see that instability starts from the smallest length scale with $\overline{m} = 24$. As the term $\overline{m} = 24$ grows exponentially, it leads to the exponential growth of the terms $\overline{m} = 20$ and then $m = 12$, with the same rate. Terms $\overline{m} = 2$ and $\overline{m} = 4$ provide the enegy for this exponential growth and as a result, they decay as the higher $\overline{m}$ terms grow. Furthermore, we can see that the instability does not appear until $t\,\omega_p \approx 380$. Keeping smaller number of terms makes this wait period before the onset of instability longer and we obtained the frequency shift for larger amplitudes during this time, in Figs. (3.9a) and (3.9b), which repectively have $k_\perp = 1.5k_1$ and $k_\perp = 3k_1$. Note that this decay of the large amplitude, nonlinear mode 2 is independent of the presence of the small amplitude mode 1 seed.

For values of A_2^t larger than $A_2^{\mathrm{t,\,thr}}$: the four roots of the determinant of **M** are

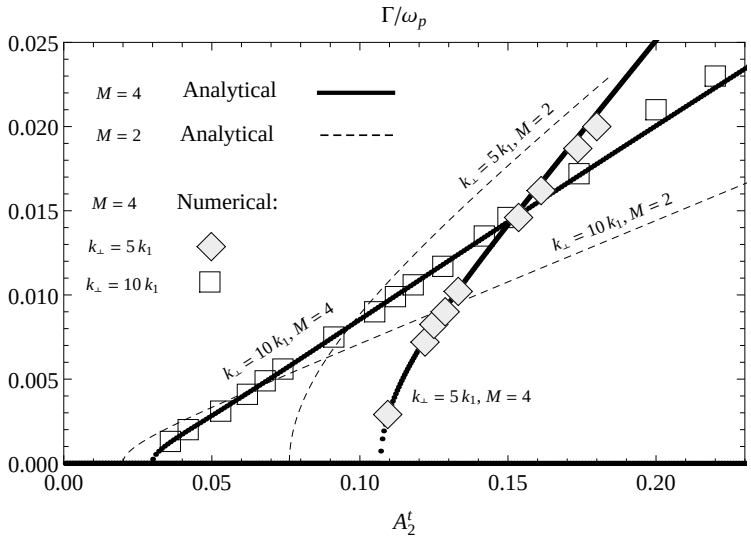

Figure 3.23: Growth rate of mode 1 vs. the amplitude of mode 2. The analytical growth rate for $M = 4$, which is Γ defined in Eq. (3.368), is depicted in a solid curve, numerical result for $M = 4$ is depicted in squares for $k_\perp = 10k_1$ and diamonds for $k_\perp = 5k_1$; and for comparison the analytical result for $M = 2$, given by Eq. (3.288), is depicted in dashed curves.

given by:

$$
\begin{aligned}
q_1 &= \Gamma + i\overline{\Delta}_{1,2}/2 \\
q_2 &= -\Gamma + i\overline{\Delta}_{1,2}/2 \\
q_3 &= i\,q_{3i} \\
q_4 &= i\overline{\Delta}_{1,2} - i\,q_{3i}
\end{aligned}
\tag{3.368}
$$

Substituting from Eq. (3.368) in Eqs. (3.360) and (3.361) we find the unstable solutions of modes 1 and 3:

$$
\begin{aligned}
n_1^{(1)}(t) &= \left[(a_1 \mathrm{e}_{11} + a_2 \mathrm{e}_{22}^*)e^{\Gamma t} + (a_1 \mathrm{e}_{12}^* + a_2 \mathrm{e}_{21})e^{-\Gamma t}\right] e^{-i\frac{1}{2}\overline{\omega}_2 t} \\
&+ (a_3 \mathrm{e}_{31} + a_4 \mathrm{e}_{42}^*)e^{-i(\overline{\omega}_3 - \overline{\omega}_2)t} + (a_4 \mathrm{e}_{41} + a_3 \mathrm{e}_{32}^*)e^{i(\overline{\omega}_3 - 2\overline{\omega}_2)t}
\end{aligned}
\tag{3.369}
$$

$$
\begin{aligned}
n_3^{(1)}(t) &= \left[(a_1 \mathrm{e}_{13} + a_2 \mathrm{e}_{24}^*)e^{\Gamma t} + (a_1 \mathrm{e}_{14}^* + a_2 \mathrm{e}_{23})e^{-\Gamma t}\right] e^{-i\frac{3}{2}\overline{\omega}_2 t} \\
&+ (a_3 \mathrm{e}_{33} + a_4 \mathrm{e}_{44}^*)e^{-i\overline{\omega}_3 t} + (a_4 \mathrm{e}_{43} + a_3 \mathrm{e}_{34}^*)e^{i(\overline{\omega}_3 - 3\overline{\omega}_2)t}
\end{aligned}
\tag{3.370}
$$

From Eq. (3.369) we can see that for mode 1, the fast time variation of the expo-

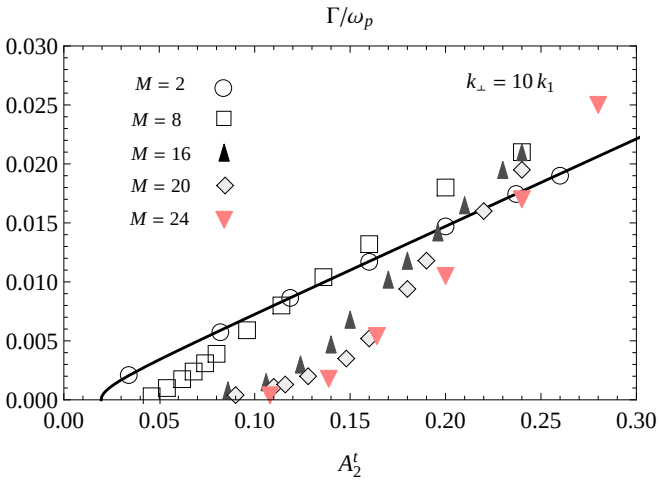

(a)

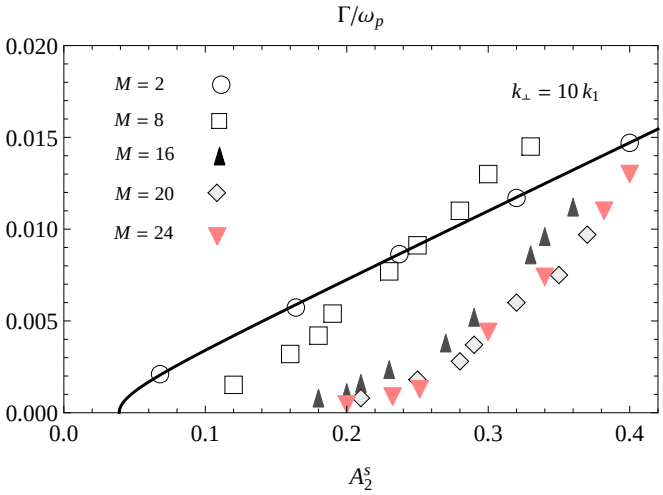

(b)

Figure 3.24: Growth rate of mode 1 vs. the amplitude of mode 2, for traveling waves (3.24a) and standing waves (3.24b). The numerical results for $M = 2, 8, 16, 20, 24$ are depicted in circles, squares, trangles and diamonds and inverse triangles. For comparison, the analytical result for $M = 2$, given by Eq. (3.288), is depicted in solid curves.

nentially growing and decaying solutions has a frequency $\overline{\omega}_1 = \overline{\omega}_2/2$, which means that these terms are exact *sub-harmonics* of mode 2. We have previously seen this happening in the unstable regime for isolated modes 1 and 2, as can be seen in Eq. (3.290). However, in the unstable regime of the isolated modes 1,2 and 3 a different kind of resonance condition was satisfied, which was given by Eq. (3.331).

Moreover, from Eq. (3.370) we can see that the exponentially growing and decaying terms of mode 3 have a fast time variation frequency of $3\overline{\omega}_2/2$, which means that these terms are *fractional* harmonics of mode 2.

By driving mode 2 to an amplitude larger than the threshold amplitude $A_2^{\text{t,th}}$, the solution for the small amplitude mode 1 grows exponentially. Figure (3.23) depicts Γ/ω_p. The analytical growth rate for $M = 4$, which is Γ defined in Eq. (3.368), is depicted in solid curve, numerical result for $M = 4$ is depicted in squares, and for comparison, analytical result, given by Eq. (3.288), for $M = 2$ are depicted in dashed curve.

We compare the growth rates of mode 1 due to the dominant mode 2, for larger number of Fourier terms M kept. In order to launch a large amplitude nonlinear mode 2, where the even Fourier terms are harmonics of the basis mode 2, we choose longer drive times and smaller drive potentials to avoid exciting unwanted waves. However, using the driving technique described in appendix F, in order to reach larger mode amplitudes we have to raise the drive potential and lower the drive time, otherwise, if we don't shorten the drive time, the mode amplitude will be driven up and the down again. Based on this limitation of the driving technique, we drive the plasma as slowly as possible to reach the desired amplitude.

Driving the mode 2 amplitude beyond the threshold amplitude $A_2^{\text{t,th}}$, which is a function of M, will result in the exponential growth of mode 1 from its small initial value. Figure (3.26) shows an example of the exponential growth mode 1 vs. time, for $M = 24$. Figure (3.24a) depicts the growth rates of mode 1 due to dominant mode 2 with $M = 2, 8, 16, 20$ and 24 present. Figure (3.24a) is the growth rates for traveling waves. We can see clearly that presence of more number of spatial Fourier terms pushes the instability thershold to higher values of A_2^t. However as M grows larger, $A_2^{\text{t, th}}$ tends toward the value $A_2^{\text{t, th}} \approx 0.086$ ($A_2^{\text{s, th}} \approx 0.173$ for standing waves),

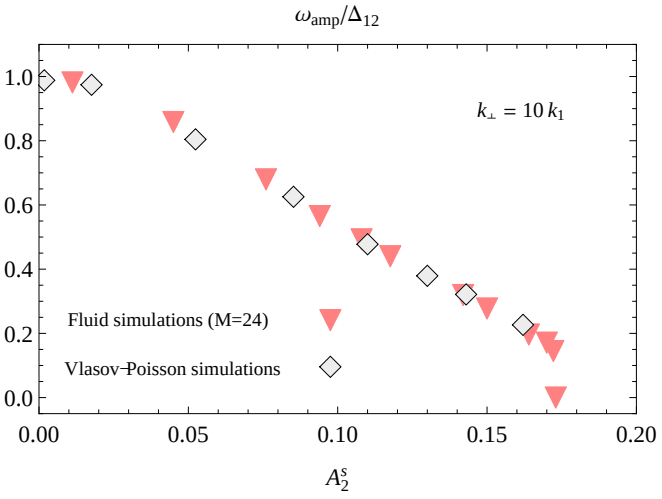

(a)

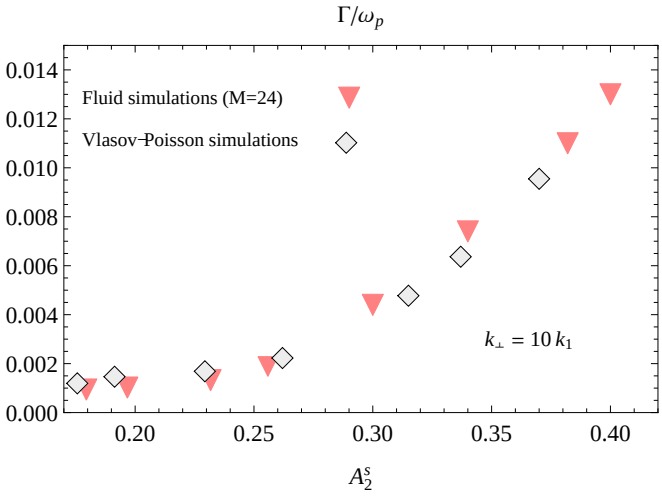

(b)

Figure 3.25: Comparison between the results from exciting a dominant mode 2 standing wave and a small amplitude mode 1 standing wave, in cold fluid simulations by integrating Eqs. (F.2) and (F.3), and Vlasov-Poisson simulation of a cold system ($\omega_2/k_2 v_T = 12.2$) by using method of lines [5]. In both simulations $k_\perp = 10k_1$. Fig. (3.25a) is the plot of the beat frequency of mode 1 ω_{amp} versus A_2^s. Fig. (3.25b) is the plot of the growth rate of the amplitude of mode 1 versus A_2^s.

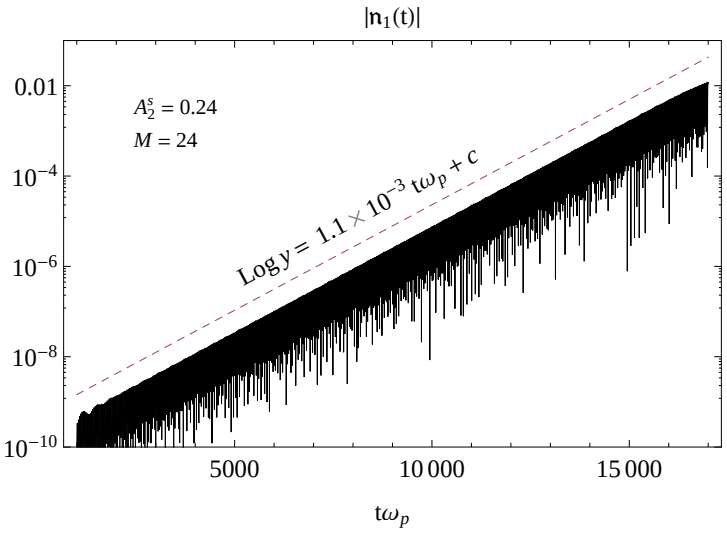

Figure 3.26: Plot of $|\mathrm{n}_1(t)|$ vs. time, for $k_\perp = 10k_1$ and $|A_2^s| = 0.24$. The plasma was driven by the potential $\overline{V}_2 = 1\times10^{-4} m_q(\omega_p L/2\pi)^2$ for a forcing time $T_F\omega_p = 180$.

which is independent of the number of terms kept in the Fourier series. The result for standing waves, depicted in Fig. (3.24b), are homologous to the traveling waves, with the scaling $A^t \rightarrow A^s/2$. This is due to the fact that resonant wave-wave interaction comes from the waves which are traveling in the same directions (see Eq. (3.138)), and for a standing wave with amplitude A^s, the amplitude of the waves in each direction is $A^s/2$.

Furthermore, we compare our fluid simulation results to the Vlasov-Poisson simulation of a dominant standing mode 2 and a small amplitude mode 1 of a cold system ($\omega_2/k_2 v_T = 12.2$) and for $k_\perp = 10k_1$, by using method of lines which is described in Ref. 5. In these simulations the distributuion function is evaluated self-consistently at grid-points in (z,v) phasespace. Fig. (3.25a) compares the beat frequency of mode 1 ω_{amp} versus A_2^s, from fluid simulations with $M = 24$ and Vlasov-Poisson simulations. For the unstable regime, Fig. (3.25b) is the plot of the growth rate of the amplitude of mode 1 versus A_2^s, from fluid simulations with $M = 24$ and Vlasov-Poisson simulations.

3.6 Summary

In a cold fluid regime, resonant wave-particle interactions are absent and the time development of the plasma is controlled by 3-wave interactions. For a long thin plasma, the dispersion relation is near acoustic and large amplitude perturbations can lead to resonant instabilities. Specifically for the case of a large amplitude mode 2, a small amplitude mode 1 can grow exponentially due to nonlinear coupling to mode 2. We studied the interaction of the isolated modes 2 and 1, as a simple approximate model to the real system. For our analytical study we obtain a reduced system of evolution equations using a weakly nonlinear perturbation equations. We observe that for a system initially set with a dominant mode 2 and small amplitude mode 1, the dynamics of the system depends on the amplitude of mode 2 and the detuning between modes 2 and 1, which represents the strength of the dispersion. For a small amplitude mode 2, the amplitude of mode 1 remains near its initial value. A large amplitude mode 2 shares its energy with mode 1 and causes mode 1 to grow exponentially. In a realistic plasma exciting modes 2 and 1 will lead to exciting other higher modes. We extend our analytical study of mode 2 and 1 interaction by including modes 3, and then modes 3 and 4. In each case presence of more number of terms leads to a more stable large amplitude mode 2 since the threshold of instability for mode 2 amplitude is pushed to higher values. Furthermore, we extend our analysis using numerical evaluation of the larger number of interacting modes in the system. As the number of present modes increases the threshold of instability, beat frequency of mode 1 (ω_{amp}), and the growth rate of mode 1 (Γ) tend toward values independent of the number of present terms in the fluid simulation. For a short plasma such that $k_\perp \lesssim k_1$, 3-wave interactions cannot occur, however condition allow for satisfying 4-wave interactions. In our fluid simulations of short plasmas we observe an instability of the nonlinear eigenmodes which has signatures of the 4-wave interactions.

Some of the material in this Chapter is in preparation for publication. The dissertation author was the primary investigator and author of this material.

Chapter 4

Nonlinear interaction between EAWs

EAWs are undamped plasma waves which are absent from the fluid description of plasma. EAWs are nonlinear BGK waves and can exist in a non-Maxwellian particle distribution. Trapped particles in the wave troughs flatten the velocity distribution at the phase velocity and allow it to propagate, without being Landau damped. Since the existance of EAWs depends on the velocity distribution, wave-wave interaction between EAWs requires the Vlasov-Poisson description of plasma.

In the first part of this section we will obtain the evolution equation for wave amplitudes due to nonlinear wave-wave interaction between standing waves in a 1D plasma from the Vlasov-Poisson desciption of plasma with length L and perpendicular mode number $k_\perp$, as a parameter to maintain the effect of radial confinement.

Although the EAWs are undamped nonlinear modes, a linear dispersion relation and linear frequency can be obtained for small amplitude undamped EAWs, by assuming a Maxwellian velocity distribution which is locally flattened over an infinitesimally narrow region around the phase velocity. This is implemented by taking the principal value of the integrals over the velocity. Since the velocity distribution is flattened at the phase velocity, linear EAWs will be undamped.

Similar to the TG modes, in the cylindrical geometry of Malmberg-Penning traps, EAWs also have near-acoustic dispersion relations, i.e. dispersion is weak. Thus three wave interactions are important nonlinear effects for the evolution of mode amplitudes. For the special case of interaction between modes 1 and 2, with initial amplitude of mode 2 being much larger than mode 1, we will evaluate the res-

onant exponential growth rate of mode 1, which we will compare to the numerically evaluated growth rates from our 1D Vlasov-Poisson computer simulations.

4.0.1 1D wave-wave interaction in a Vlasov-Poisson system

We begin with 1D Vlasov-Poisson equations for a cylindrically symmetric electrostatic wave along the axis of plasma

$$\partial_t \mathrm{f} + v\partial_z \mathrm{f} - \tfrac{1}{m_q}\partial_z \varphi \partial_v \mathrm{f} = 0 \tag{4.1}$$

$$\left[k_\perp^2 - \partial_z^2\right]\varphi = 4\pi q^2 \int \mathrm{f}\, dv \tag{4.2}$$

We assume we have standing waves with Neumann boundary conditions for φ at the plasma ends $\partial_z \varphi(\pm L/2) = 0$. Thus mode potential is of the following form:

$$\begin{aligned}\varphi_m(z;t) &= \varphi_m^{lab}(t)\cos[k_m z] \\ &= [\varphi_m(t) + \varphi_m^*(t)]\left[e^{ik_m z} + e^{-ik_m z}\right],\end{aligned} \tag{4.3}$$

and we will have electrostatic potential and distribution function of the form:

$$\mathrm{f}(z,v,t) = n_0(F_0(v,t) + \sum_{m=-\infty}^{\infty} \mathrm{f}_m(v,t)e^{ik_m z}) \tag{4.4}$$

where n_0 is the equilibrium plasma density, $\mathrm{f}_{-m}(v,t) = \mathrm{f}_m^*(v,t)$ and the sum excludes $m = 0$ term. We can write the Vlasov-Poisson in terms of Fourier variables

$$\begin{aligned}&\partial_t \mathrm{f}_m(v,t) + ik_m v\mathrm{f}_m(v,t) - \tfrac{i}{m_q}k_m \varphi_m(t)\partial_v F_0(v,t) \\ &= \frac{i}{m_q}\sum_{m'=-\infty}^{\infty}(k_m - k_{m'})\phi_{m-m'}(t)\partial_v \mathrm{f}_{m'}(v,t)\end{aligned} \tag{4.5}$$

$$\partial_t F_0(v,t) = -\frac{i}{m_q}\sum_{m'=-\infty}^{\infty} k'_m \phi_{m-m'}(t)\partial_v \mathrm{f}_{m'}(v,t) \tag{4.6}$$

$$\varphi_m(t) = K_m^{-2} 4\pi q^2 n_0 \int dv\, \mathrm{f}_m(v,t) \tag{4.7}$$

where $K_m^2 = k_\perp^2 + k_m^2$. Equation (4.6) describes the evolution of the background distribution. In the following analysis we assume that the perturbation is small $|\mathrm{f}_m| \ll F_0$. We carry out a weakly nonlinear analysis correct up to second order in the amplitude of perturbed potential. We will expand using multiple time-scale expansion:

$$\mathrm{f}_m(v,t) \simeq \varepsilon \mathrm{f}_m^{(1)}(v,\tau_0,\tau_1,\ldots) + \varepsilon^2 \mathrm{f}_m^{(2)}(v,\tau_0,\tau_1,\ldots) + \ldots \tag{4.8}$$

$$\varphi_m(t) \simeq \varepsilon \varphi_m^{(1)}(\tau_0,\tau_1,\ldots) + \varepsilon^2 \varphi_m^{(2)}(\tau_0,\tau_1,\ldots) + \ldots \tag{4.9}$$

$$F_0(v,t) \simeq F_0^{(0)}(v,\tau_0,\tau_1,\ldots) + \varepsilon F_0^{(1)}(v,\tau_0,\tau_1,\ldots) + \ldots \tag{4.10}$$

where $\varepsilon \ll 1$ measures the strength of perturbation. in Eqs. (4.8) through (4.10) time scales satisfy:

$$\partial_t \tau_0 = 1, \quad \partial_t \tau_1 = \varepsilon, \quad \partial_t \tau_2 = \varepsilon^2, \tag{4.11}$$

So that time derivative is expanded as:

$$\partial_t = \partial_{\tau_0} + \varepsilon \partial_{\tau_1} + \varepsilon^2 \partial_{\tau_2} + \ldots \tag{4.12}$$

Time-scales are treated as independent. We substitute the expansions Eqs. (4.8) and (4.10) in the Vlasov and Poisson equations, we can separate each order of ε in

these equations:

$$\partial_{\tau_0} \mathrm{f}_m^{(1)}(v,\tau_0,\tau_1) + i v k_m \mathrm{f}_m^{(1)}(v,\tau_0,\tau_1) - \tfrac{ik_m}{m_q}\varphi_m(\tau_0,\tau_1)\partial_v F_0^{(0)}(v,\tau_0,\tau_1) = 0 \tag{4.13}$$

$$\begin{aligned}&\partial_{\tau_0} \mathrm{f}_m^{(2)}(v,\tau_0,\tau_1) + \partial_{\tau_1} \mathrm{f}_m^{(1)}(v,\tau_0,\tau_1) + i k_m v \mathrm{f}_m^{(2)}(v,\tau_0,\tau_1) - \tfrac{ik_m}{m_q}\varphi_m^{(2)}(\tau_0,\tau_1)\partial_v F_0^{(0)}(v,\tau_0,\tau_1)\\ &= \frac{i}{m_q}\sum_{m'=-\infty}^{\infty}(k_m - k_{m'})\varphi_{m-m'}^{(1)}(\tau_0,\tau_1)\partial_v \mathrm{f}_{m'}^{(1)}(v,\tau_0,\tau_1)\\ &+ \tfrac{ik_m}{m_q}\varphi_m^{(1)}(\tau_0,\tau_1)\partial_v F_0^{(1)}(v,\tau_0,\tau_1)\end{aligned} \tag{4.14}$$

$$\phi_m^{(1)}(\tau_0,\tau_1) = K_m^{-2} 4\pi q^2 n_0 \int dv\, \mathrm{f}_m^{(1)}(v,\tau_0,\tau_1) \tag{4.15}$$

$$\phi_m^{(2)}(\tau_0,\tau_1) = K_m^{-2} 4\pi q^2 n_0 \int dv\, \mathrm{f}_m^{(2)}(v,\tau_0,\tau_1) \tag{4.16}$$

$$\partial_{\tau_0} F_0^{(0)}(v,\tau_0,\tau_1) = 0 \tag{4.17}$$

$$\partial_{\tau_1} F_0^{(0)}(v,\tau_0,\tau_1) + \partial_{\tau_0} F_0^{(1)}(v,\tau_0,\tau_1) = 0 \tag{4.18}$$

From Eq. (4.17) we see that $F_0^{(0)}$ does not depend on the fast timescale τ_0 thus $F_0^{(0)} = F_0^{(0)}(v,\tau_1)$. Thus Eq. (4.18) can be integrated over τ_0:

$$F_0^{(1)}(v,\tau_0,\tau_1) = F_0^{(1)}(v,\tau_0=0,\tau_1) - \tau_0 \quad \partial_{\tau_1} F_0^{(0)}(v,\tau_1) \tag{4.19}$$

Removing secular term on the RHS, we see that $F_0^{(0)}$ does not vary on the slow time scale τ_1. Thus for the current purpose $F_0^{(0)}(v)$ is constant in time. Later on we will take it to be of the Maxwellian form:

$$F_0^{(0)}(v) = \frac{1}{v_T\sqrt{2\pi}}\exp(-v^2/2v_T^2) \tag{4.20}$$

where $v_T = \sqrt{T/m_q}$ is the thermal velocity. Now we assume that the first order potential and distribution are oscillatory in the fast time scale with an amplitude which varies slowly with τ_1:

$$\varphi_m^{(1)}(\tau_0,\tau_1) = \varphi_m(\tau_1)e^{-i\omega_m\tau_0} + \varphi_m^*(\tau_1)e^{i\omega_m^*\tau_0} \tag{4.21}$$

$$\mathrm{f}_m^{(1)}(v,\tau_0,\tau_1) = f_m(v,\tau_1)e^{-i\omega_m\tau_0} + f_{-m}(v,\tau_1)e^{i\omega_m^*\tau_0}, \tag{4.22}$$

where $\varphi_m^*(\tau_1)=\varphi_{-m}(\tau_1)$ and $\omega_m=\omega_m^r+i\gamma_m$ is the linear complex mode frequency. Using above relation in the first order Vlasov equation (4.13) gives:

$$f_m(v,\tau_1)=\frac{m_q^{-1}\varphi_m(\tau_1)\partial_v F_0^{(0)}(v)}{v-\omega_m/k_m} \tag{4.23}$$

$$f_{-m}(v,\tau_1)=\frac{m_q^{-1}\varphi_{-m}(\tau_1)\partial_v F_0^{(0)}(v)}{v+\omega_m^*/k_m} \tag{4.24}$$

Using Eqs. (4.21), (4.22), (4.23) and (4.24), and also the Poisson equation (4.15) we get the first order dispersion relation:

$$\left[1-\frac{\omega_p^2}{K_m^2}\int dv\,\frac{\partial_v F_0^{(0)}(v)}{v-\omega_m/k_m}\right]\varphi_m=0 \tag{4.25}$$

$$\left[1-\frac{\omega_p^2}{K_m^2}\int dv\,\frac{\partial_v F_0^{(0)}(v)}{v+\omega_m^*/k_m}\right]\varphi_m^*=0 \tag{4.26}$$

where $\omega_p=\sqrt{4\pi n_0 q^2/m_q}$. Defining the linear dispersion function $D(s,k)$ as:

$$D(s,k_m)=1-\frac{\omega_p^2}{K_m^2}\int dv\,\frac{ik_m\partial_v F_0^{(0)}(v)}{ik_m v+s} \tag{4.27}$$

Equations (4.25) and (4.26) can simply be written as:

$$D(-i\omega_m,k_m)\varphi_m=0$$

$$D(i\omega_m^*,k_m)\varphi_m^*=0$$

For long, thin plasmas i.e. $L\gg r_p$, which is our interest, the frequency mismatch, also known as the detuning, between linear modes m, $l-m$, and l is also small and can be comparable to the mode amplitude:

$$(\omega_m+\omega_{l-m}-\omega_l)/\omega_m\ll 1 \tag{4.28}$$

Thus we define the detuning $\Delta_{m,l}$ as:

$$\omega_m + \omega_{l-m} - \omega_l = \varepsilon \Delta_{m,l} \tag{4.29}$$

$$\tau_0(\omega_m + \omega_{l-m} - \omega_l) = \varepsilon \tau_0 \Delta_{m,l} = \tau_1 \Delta_{m,l} \tag{4.30}$$

From the second order Vlasov equation we get:

$$\begin{aligned}
&\partial_{\tau_0} \mathrm{f}_m^{(2)} + i k_m v \mathrm{f}^{(2)} - \tfrac{i k_m}{m_q} \varphi_m^{(2)} \partial_v F_0^{(0)} \\
&= -\frac{m_q^{-1} \partial_{\tau_1} \varphi_m(\tau_1) \partial_v F_0^{(0)}}{v - \omega_m / k_m} e^{-i\omega_m \tau_0} - \frac{m_q^{-1} \partial_{\tau_1} \varphi_m^*(\tau_1) \partial_v F_0^{(0)}}{v + \omega_m^* / k_m} e^{i\omega_m \tau_0} \\
&+ \frac{i}{2 m_q} \sum_{m',m''} \varphi_{m'} \varphi_{m''} \partial_v \left[\frac{k_{m''} \partial_v F_0^{(0)}}{v - \omega_{m'} / k_{m'}} + \frac{k_{m'} \partial_v F_0^{(0)}}{v - \omega_{m''} / k_{m''}} \right] e^{-i\Delta_{m,m'} \tau_1} e^{-i\omega_m \tau_0} \\
&+ \frac{i}{2 m_q} \sum_{m',m''} \varphi_{m'}^* \varphi_{m''}^* \partial_v \left[\frac{k_{m''} \partial_v F_0^{(0)}}{v + \omega_{m'}^* / k_{m'}} + \frac{k_{m'} \partial_v F_0^{(0)}}{v + \omega_{m''}^* / k_{m''}} \right] e^{i\Delta_{m,m'}^* \tau_1} e^{i\omega_m^* \tau_0} \\
&+ \frac{i}{2 m_q} \sum_{m',m''} \varphi_{m'} \varphi_{m''}^* \partial_v \left[\frac{k_{m''} \partial_v F_0^{(0)}}{v - \omega_{m'} / k_{m'}} + \frac{k_{m'} \partial_v F_0^{(0)}}{v + \omega_{m''}^* / k_{m''}} \right] e^{-i(\omega_{m'} - \omega_{m''}^*) \tau_0} \\
&+ \frac{i}{2 m_q} \sum_{m',m''} \varphi_{m'}^* \varphi_{m''} \partial_v \left[\frac{k_{m''} \partial_v F_0^{(0)}}{v + \omega_{m'}^* / k_{m'}} + \frac{k_{m'} \partial_v F_0^{(0)}}{v - \omega_{m''}^* / k_{m''}} \right] e^{i(\omega_{m'}^* - \omega_{m''}) \tau_0}
\end{aligned} \tag{4.31}$$

In the above sums $m'' = m - m'$. Laplace transform is performed on Eqs. (4.31) and (4.16) w.r.t. fast time variable τ_0, using:

$$\begin{aligned}
\hat{\varphi}_k^{(2)}(s, \tau_1) &= \int_0^\infty d\tau_0 \varphi_k^{(2)}(\tau_0, \tau_1) e^{-s\tau_0} \\
\varphi_k^{(2)}(\tau_0, \tau_1) &= \frac{1}{2\pi i} \int_C d\tau_0 \hat{\varphi}_k^{(2)}(s, \tau_1) e^{s\tau_0}
\end{aligned} \tag{4.32}$$

With $\mathrm{f}_m^{(2)}(v,\tau_0=0,\tau_1)=0$ we get:

$$
\begin{aligned}
&(s+ik_m v)\hat{\mathrm{f}}_m^{(2)}(s)-\tfrac{ik_m}{m_q}\hat{\varphi}_m^{(2)}(s)\partial_v F_0^{(0)}= \\
&=-\frac{1}{s+i\omega_m}\frac{m_q^{-1}\partial_{\tau_1}\varphi_m(\tau_1)\partial_v F_0^{(0)}}{v-\omega_m/k_m}-\frac{1}{s-i\omega_m^*}\frac{m_q^{-1}\partial_{\tau_1}\varphi_m^*(\tau_1)\partial_v F_0^{(0)}}{v+\omega_m^*/k_m} \\
&+\frac{i}{2m_q}\sum_{m',m''}\varphi_{m'}\varphi_{m''}\partial_v\left[\frac{k_{m''}\partial_v F_0^{(0)}}{v-\omega_{m'}/k_{m'}}+\frac{k_{m'}\partial_v F_0^{(0)}}{v-\omega_{m''}/k_{m''}}\right]\frac{e^{-i\Delta_{m,m'}\tau_1}}{s+i\omega_m} \\
&+\frac{i}{2m_q}\sum_{m',m''}\varphi_{m'}^*\varphi_{m''}^*\partial_v\left[\frac{k_{m''}\partial_v F_0^{(0)}}{v+\omega_{m'}^*/k_{m'}}+\frac{k_{m'}\partial_v F_0^{(0)}}{v+\omega_{m''}^*/k_{m''}}\right]\frac{e^{i\Delta_{m,m'}^*\tau_1}}{s-i\omega_m^*} \\
&+\frac{i}{2m_q}\sum_{m',m''}\varphi_{m'}\varphi_{m''}^*\partial_v\left[\frac{k_{m''}\partial_v F_0^{(0)}}{v-\omega_{m'}/k_{m'}}+\frac{k_{m'}\partial_v F_0^{(0)}}{v+\omega_{m''}^*/k_{m''}}\right]\frac{1}{s+i\omega_m'-i\omega_{m''}^*} \\
&+\frac{i}{2m_q}\sum_{m',m''}\varphi_{m'}^*\varphi_{m''}\partial_v\left[\frac{k_{m''}\partial_v F_0^{(0)}}{v+\omega_{m'}^*/k_{m'}}+\frac{k_{m'}\partial_v F_0^{(0)}}{v-\omega_{m''}/k_{m''}}\right]\frac{1}{s-i\omega_{m'}^*+i\omega_{m''}}
\end{aligned}
\tag{4.33}
$$

Performing the Laplace transform on the second order Poisson equation we get:

$$
\hat{\varphi}_m^{(2)}(s,\tau_0,\tau_1)=K_m^{-2}4\pi q^2 n_0\int d\,v\hat{\mathrm{f}}_m^{(2)}(v,\tau_0,\tau_1) \tag{4.34}
$$

From Eq. (4.33) we solve for $\hat{\mathrm{f}}_m^{(2)}(s)$ and substitute in Eq. (4.34) we get:

$$
\begin{aligned}
&\hat{\varphi}_m^{(2)}(s,\tau_0,\tau_1)=\frac{K_m^{-2}\omega_p^2}{D(s,k_m)}\int\frac{d\,v}{s+ik_m v}\Bigg\{ \\
&-\frac{1}{s+i\omega_m}\frac{\partial_{\tau_1}\varphi_m(\tau_1)\partial_v F_0^{(0)}}{v-\omega_m/k_m}-\frac{1}{s-i\omega_m^*}\frac{\partial_{\tau_1}\varphi_m^*(\tau_1)\partial_v F_0^{(0)}}{v+\omega_m^*/k_m} \\
&+\frac{i}{2}\sum_{m',m''}\varphi_{m'}\varphi_{m''}\partial_v\left[\frac{k_{m''}\partial_v F_0^{(0)}}{v-\omega_{m'}/k_{m'}}+\frac{k_{m'}\partial_v F_0^{(0)}}{v-\omega_{m''}/k_{m''}}\right]\frac{e^{-i\Delta_{m,m'}\tau_1}}{s+i\omega_m} \\
&+\frac{i}{2}\sum_{m',m''}\varphi_{m'}^*\varphi_{m''}^*\partial_v\left[\frac{k_{m''}\partial_v F_0^{(0)}}{v+\omega_{m'}^*/k_{m'}}+\frac{k_{m'}\partial_v F_0^{(0)}}{v+\omega_{m''}^*/k_{m''}}\right]\frac{e^{i\Delta_{m,m'}^*\tau_1}}{s-i\omega_m^*} \\
&+\frac{i}{2}\sum_{m',m''}\varphi_{m'}\varphi_{m''}^*\partial_v\left[\frac{k_{m''}\partial_v F_0^{(0)}}{v-\omega_{m'}/k_{m'}}+\frac{k_{m'}\partial_v F_0^{(0)}}{v+\omega_{m''}^*/k_{m''}}\right]\frac{1}{s+i\omega_m'-i\omega_{m''}^*} \\
&+\frac{i}{2}\sum_{m',m''}\varphi_{m'}^*\varphi_{m''}\partial_v\left[\frac{k_{m''}\partial_v F_0^{(0)}}{v+\omega_{m'}^*/k_{m'}}+\frac{k_{m'}\partial_v F_0^{(0)}}{v-\omega_{m''}/k_{m''}}\right]\frac{1}{s-i\omega_{m'}^*+i\omega_{m''}}\Bigg\}
\end{aligned}
\tag{4.35}
$$

Performing the inverse Laplace transform will result in secular as well as nonsecular terms. $D(s,k_m)$ has roots at $s=i\omega_m$ and $s=i\omega_m$. Secular term resulting from the first term of the integral on the right hand side of Eq. (4.35) is given by:

$$\begin{aligned}
&-K_m^{-2}\omega_p^2\int dv\,\frac{\partial_{\tau_1}\varphi_m(\tau_1)\partial_v F_0^{(0)}}{v-\omega_m/k_m}\int\frac{ds/(2\pi i)}{s+ik_m v}\frac{e^{s\tau_0}}{D(s,k_m)(s+i\omega_m)}\\
&\simeq -K_m^{-2}\omega_p^2\int dv\,\frac{\partial_{\tau_1}\varphi_m(\tau_1)\partial_v F_0^{(0)}}{v-\omega_m/k_m}\int\frac{ds/(2\pi i)}{s+ik_m v}\frac{e^{s\tau_0}}{\partial_s D(s,k_m)|_{s=-i\omega_m}(s+i\omega_m)^2}\\
&=\tau_0 e^{-i\omega_m\tau_0}\left[i\frac{K_m^{-2}\omega_p^2}{\partial_s D(s,k_m)|_{s=-i\omega_m}}\int dv\,\frac{\partial_{\tau_1}\varphi_m(\tau_1)\partial_v F_0^{(0)}}{k_m(v-\omega_m/k_m)^2}\right]\quad\text{(secular part only)}\\
=\;&-\tau_0 e^{-i\omega_m\tau_0}\partial_{\tau_1}\varphi_m
\end{aligned}\tag{4.36}$$

where we used

$$\partial_s D(s,k_m)|_{s=-i\omega_m}=\frac{K_m^{-2}\omega_p^2}{ik_m}\int dv\,\frac{\partial_v F_0^{(0)}}{(v-\omega_m/k_m)^2}$$

Above equation can identically be written for $s=-i\omega_m^*$ for the second term of the integral on the right hand side of Eq. (4.35). Secular terms resulting from terms 3 and 4 from the integral on the right hand side of Eq. (4.35) is given by:

$$+\tau_0\frac{e^{-i\omega_l\tau_0}}{2}\sum_{m',m''}\varphi_{m'}\varphi_{m''}e^{-i\Delta_{m,m'}\tau_1}\frac{\int\partial_v\left[\frac{k_{m''}\partial_v F_0^{(0)}}{v-\omega_{m'}/k_{m'}}+\frac{k_{m'}\partial_v F_0^{(0)}}{v-\omega_{m''}/k_{m''}}\right]\frac{dv}{k_m v-\omega_m}}{K_m^2\omega_p^{-2}\partial_s D(s,k_m)|_{s=i\omega_m}}$$

$$+\tau_0\frac{e^{i\omega_l^*\tau_0}}{2}\sum_{m',m''}\varphi^*_{m'}\varphi^*_{m''}e^{i\Delta^*_{m,m'}\tau_1}\frac{\int\partial_v\left[\frac{k_{m''}\partial_v F_0^{(0)}}{v+\omega^*_{m'}/k_{m'}}+\frac{k_{m'}\partial_v F_0^{(0)}}{v+\omega^*_{m''}/k_{m''}}\right]\frac{dv}{k_m v+\omega^*_m}}{K_m^2\omega_p^{-2}\partial_s D(s,k_m)|_{s=-i\omega^*_m}}$$

In order to remove the secular terms from RHS of Eq. (4.35) the following equations must be satisfied:

$$\frac{d}{dt}\varphi_m = \sum_{m',m''} \mathrm{M}(m;m',m'')\varphi_{m'}\varphi_{m''}e^{-i\Delta_{m,m'}t} \tag{4.37}$$

$$\mathrm{M}(m;m',m'') = \frac{M(m;m',m'')}{2K_m^2\omega_p^{-2}\partial_s D(s,k_m)|_{s=-i\omega_m}} \tag{4.38}$$

$$M(m;m',m'') = \int \partial_v \left[\frac{k_{m''}\partial_v F_0^{(0)}}{v-\omega_{m'}/k_{m'}} + \frac{k_{m'}\partial_v F_0^{(0)}}{v-\omega_{m''}/k_{m''}}\right]\frac{dv}{k_m v-\omega_m} \tag{4.39}$$

$$k_m = k_{m'} + k_{m''} \tag{4.40}$$

$$\Delta_{m,m'} = \omega_m - \omega_{m'} - \omega_{m''} \tag{4.41}$$

where we dropped the multiple time scale notation. Coefficients $M(m;m',m'')$ given by Eq. (4.38) can be simplified. The numerator can be written as:

$$\begin{aligned}
M(m;m',m'') &= \int \partial_v \left[\frac{k_{m''}\partial_v F_0^{(0)}}{v-\omega_{m'}/k_{m'}} + \frac{k_{m'}\partial_v F_0^{(0)}}{v-\omega_{m''}/k_{m''}}\right]\frac{dv}{k_m v-\omega_m} \\
&= \int \left[\frac{k_{m''}\partial_v F_0^{(0)}}{v-\omega_{m'}/k_{m'}} + \frac{k_{m'}\partial_v F_0^{(0)}}{v-\omega_{m''}/k_{m''}}\right]\frac{dv}{k_m(v-\omega_m/k_m)^2} \\
&= \int \frac{dv\,\partial_v F_0^{(0)}(v-(\omega_{m'}+\omega_{m''})/k_m)}{(v-\omega_{m'}/k_{m'})(v-\omega_{m''}/k_{m''})(v-\omega_m/k_m)^2} \\
&\approx \int \frac{\partial_v F_0^{(0)} dv}{(v-\omega_m/k_m)^3} \quad (\Delta_{m,m'}/\omega_m \ll 1)
\end{aligned} \tag{4.42}$$

Assuming a Maxwellian distribution, we can substitute for $F_0^{(0)}$ from Eq. (4.20) to obtain:

$$M(m;m',m'') = -\frac{1}{v_T^3}\int \frac{v\exp[-v^2/2v_T^2]dv}{(v-\omega_m/k_m)^3} \tag{4.43}$$

For the EAWs, we assume a Maxwellian equilibrium which is flattened at the phase velocities, so that the waves are undamped and we can take the principal value of integrals. Above result can be further simplified and written as:

$$M(m;m',m'') = -\frac{1}{v_T^4}\partial_b^2 \mathrm{W}(b)/2 \tag{4.44}$$

Since we have the following relation:

$$\partial_b^2 \mathrm{W}(b) = (b^2-3)\mathrm{W}(b)+1, \tag{4.45}$$

we can write:

$$M(m;m',m'') = -\frac{1}{2v_T^4}[(b^2-3)\mathrm{W}(b)+1]|_{b=\frac{\omega_m}{v_T k_m}} \quad (\Delta_{m,m'}/\omega_m \ll 1) \tag{4.46}$$

Substituting for $F_0^{(0)}$ from Eq. (4.20), the denominator of Eq. (4.38) is given by:

$$\begin{aligned} 2K_m^2\omega_p^{-2}\partial_s D(s,k_m)|_{s=-i\omega_m} &= -\frac{2}{ik_m v_T^3}\int dv \frac{v e^{-v^2/2v_T^2}}{(v-\omega_m/k_m)^2} \\ &= -\frac{2}{ik_m v_T^3}\partial_b \mathrm{W}(b)|_{b=\frac{\omega_m}{v_T k_m}} \\ &\frac{2}{ik_m v_T^3}([1-\mathrm{W}(b)]/b + b\mathrm{W}(b))|_{b=\frac{\omega_m}{v_T k_m}} \end{aligned} \tag{4.47}$$

Finally, the nonlinear coupling coefficient for the evolution of mode m due to the coupling of modes l and $l-m$, in the limit of $\Delta_{m,m'}/\omega_m \ll 1$ can be written as:

$$\begin{aligned} &\mathrm{N}(m,l) = i\mathrm{M}(m;m/2,m/2) \\ &= \frac{k_m}{4v_T}\left[\frac{(b^2-3)\mathrm{W}(b)+1}{[1-\mathrm{W}(b)]/b+b\mathrm{W}(b)}\right]\Bigg|_{b=\frac{\omega_m}{v_T k_m}}, \quad m=2l \\ &\mathrm{N}(m,l) = i\mathrm{M}(m;l,m-l)+i\mathrm{M}(m;m-l,m) \\ &= \frac{k_m}{2v_T}\left[\frac{(b^2-3)\mathrm{W}(b)+1}{[1-\mathrm{W}(b)]/b+b\mathrm{W}(b)}\right]\Bigg|_{b=\frac{\omega_m}{v_T k_m}}, \quad m\neq 2l \end{aligned} \tag{4.48}$$

In the limit of $\frac{\omega_m}{v_T k_m} \gg 1$ from Eq. (4.48) we obtain

$$-i\mathrm{N}(m,l)\mathrm{M}(m;l,l-m)+\mathrm{M}(m;m-l,l) \approx -i\frac{3k_m^2}{2\omega_m} \tag{4.49}$$

In the limit of small detuning $\Delta_{m,l}/\omega_m \ll 1$, the result given by Eq. (4.49) is identical to the nonlinear coupling coefficient obtained from the fluid picture of wave-wave

interaction given by Eq. (3.148):

$$
\begin{aligned}
-i\frac{\frac{\omega_m^2}{k_m^2}}{\frac{\omega_l^2}{k_l^2}\frac{\omega_{l-m}^2}{k_{l-m}^2}}\left(X_{m,l}+X_{m,m-l}\right) &= -i\frac{\frac{\omega_m^2}{k_m^2}}{\frac{\omega_l^2}{k_l^2}\frac{\omega_{l-m}^2}{k_{l-m}^2}}\left[k_m\frac{\omega_{m-l}}{2k_{m-l}}\left(1+\frac{\omega_l}{\omega_m}\right)+k_m\frac{\omega_l}{2k_l}\left(1+\frac{\omega_{m-l}}{\omega_m}\right)\right] \\
&\approx -i\frac{3k_m^2}{2\omega_m} \qquad (4.50)
\end{aligned}
$$

Interaction between EAW modes 2 and 1

We obtain the EAW mode frequencies from the linear dispersion relation

$$\mathrm{P}D(-i\omega_m, k_m) = 0 \tag{4.51}$$

with D given by Eq. (4.27). This equation has two roots. The root with the higher phase velocity corresponds to the TG mode. The root with lower phase velocity $\omega_m/k_m v_T \sim 1.4$ is heavily damped, unless we assume an equilibrium distribution which is flattened locally at this phase velocity. Taking the principal value of D in Eq. (4.51) is equivalent to flattening the distribution function at the phase velocity. This modified distribution function will allow the existence of undamped EAWs in the linear limit. Similar to TG modes, dispersion relation for the linear EAWs is near acoustic, with a dispersion much weaker than that of the TG modes, which allows strong resonance wave-wave interactions for relatively smaller amplitude waves.

Time evolution of EAW mode amplitudes due to nonlinear wave-wave interactions can be obtained by the Vlasov-Poisson description of plasma i.e. Eqs. (4.37) through (4.41) with coupling coefficients given by the principal value of Eq. (4.48), since the Maxwellian is flattened at ω_m/k_m. From Eq. (4.37) for EAW modes 2 and 1 we obtain

$$\tfrac{d}{dt}\varphi_1 = -i\mathrm{N}(1,2)\varphi_1^*\varphi_2 e^{i\Delta t} \tag{4.52}$$

$$\tfrac{d}{dt}\varphi_2 = -i\mathrm{N}(2,1)\varphi_1^2 e^{-i\Delta t} \tag{4.53}$$

$$\Delta = 2\omega_1 - \omega_2, \tag{4.54}$$

where $N(m,l)$ is defined in Eq. (4.48) and the coupling coefficients in Eqs (4.52) and (4.53) are given by

$$\mathrm{N}(2,1) = \mathrm{N}(1,2) = \frac{k_1}{2v_T}\left[\frac{(b^2-3)\mathrm{PW}(b)+1}{[1-\mathrm{PW}(b)]/b + b\,\mathrm{PW}(b)}\right]\Bigg|_{b=\frac{\omega_1}{v_T k_1}} \tag{4.55}$$

We are interested in the exponential growth of mode 1 amplitude in a regime where $|\varphi_1|/|\varphi_2| \ll 1$. We follow the same steps taken in section 3.5.3 for TG modes from we

obtain the following solution for mode 1:

$$\varphi_1 = |A| e^{(i\frac{\Delta}{2}+\delta)t+i\psi_+} + |B| e^{(i\frac{\Delta}{2}-\delta)t+i\psi_-} \tag{4.56}$$

$$\delta = \sqrt{(\mathrm{N}(1,2))^2 |\varphi_2|^2 - \frac{\Delta^2}{4}} \tag{4.57}$$

Real amplitudes of the growing and decaying solutions, i.e. respectively $|A|$ and $|B|$, are independent parameters set by initial conditions. However their phases i.e. ψ_+ and ψ_- are given by:

$$e^{i2\psi_\pm} = -i\frac{N(1,2)\varphi_2}{i\frac{\Delta}{2} \pm \delta} \tag{4.58}$$

δ is exponential growth rate which we will compare to the numerical result obtained from our nonlinear 1D Vlasov-Poisson computer simulations.

4.0.2 computer simulations

We use the method of lines to simulate the 1D nonlinear Vlasov and Poisson system with their equations respectively given by Eq. (4.1) and Eq. (4.2). Details of the method are described in REF.

In order to launch a standing EAW of mode number m, we use the following external drive potential:

$$\delta\varphi_D(z,t) = \varphi_D(t)\cos[m\pi z/L]\cos[\omega_m t] \tag{4.59}$$

where

$$\begin{aligned} \varphi_D(t) &= \overline{\varphi}_D \exp[-(t-t_0)^2/2\Delta_D^2], \quad t < t_0 \\ &= \overline{\varphi}_D, \quad t_0 < t < t_0 + t_D \\ &= \overline{\varphi}_D \exp[-(t-t_0-t_D)^2/2\Delta_D^2], \quad t_0 + t_D < t \end{aligned} \tag{4.60}$$

We take the drive frequency in Eq. (4.59) from the linear dispersion relation in (4.51). External drive potential is driven for approximately 30 to 60 cycles. As the drive is being turned off, plasma settles itself into the stationary(periodic in time with fre-

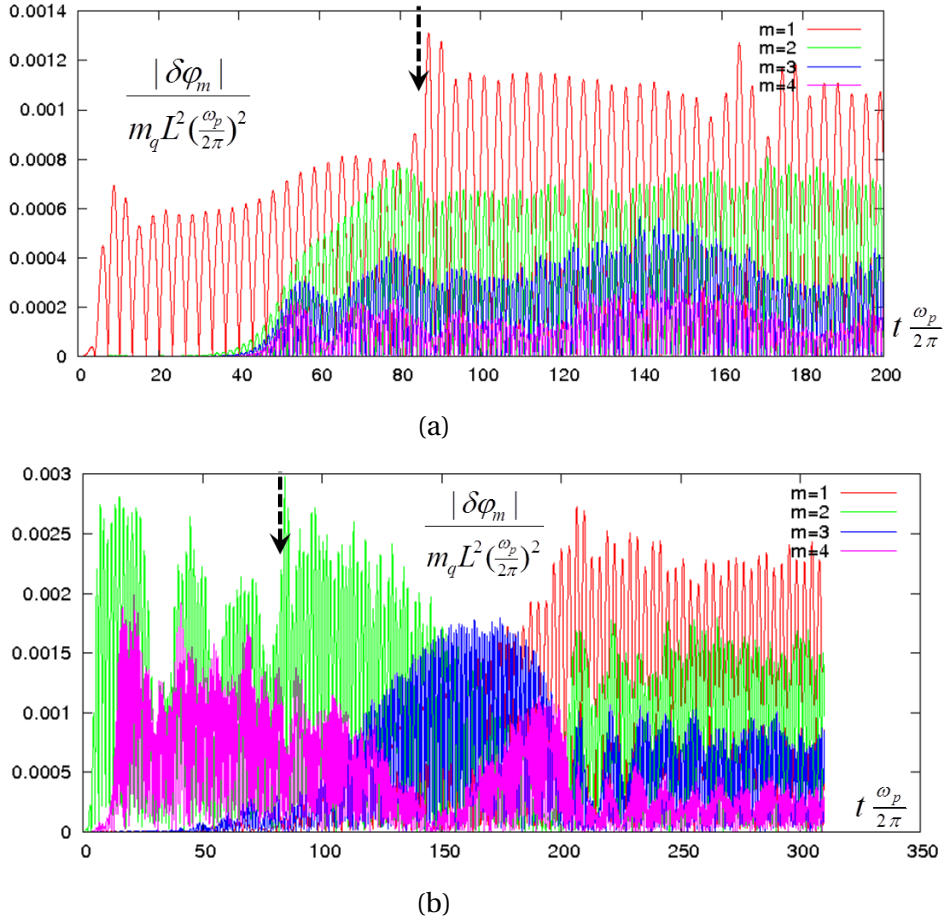

Figure 4.1: Amplitudes of the first four spatial Fourier components, $m = 1,2,3$ and $m = 4$, as a function of time. In figure (4.1a) external drive potential is $\cos[k_1 z]$ to excite EAW_1. In figure (4.1b) external drive potential is $\cos[k_2 z]$ to excite EAW_2. Dashed arrow shows the point in time where the drive is turned off. The physical parameters of the plasma are $k_\perp L = 18.44, L/\lambda = 37.3$

quency ω_m) mode EAW$_m$. EAW$_m$, are nonlinear plasma modes and the form of the mode in space is the superposition of many spatial harmonics, with $\cos[m\pi z/L]$ having the biggest amplitude. Therefore we can analyze the evolution of the mode from the evolution of the time dependent amplitudes of the individual spatial harmonics.

In Figures (4.1a) and (4.1b) we have respectively excited EAW$_1$ and EAW$_2$. Amplitudes of the first four spatial harmonics ($m = 1,2,3$ and 4) are depicted as functions of time. In figure (4.1a), after the drive is turned off plasma quickly settles into EAW$_1$ and as we can see it is stable. Time dependent variation of the spatial harmonics of EAW$_1$ are phase locked. This means that for mode EAW$_m$ the rmth spatial harmonics oscillates in time with frequency $r\omega_m$. In Fig. (4.2a) we can see that for EAW$_1$, m=1 harmonic oscillates at ω_1 and m=2 harmonic oscillates at ω_2 and they are phase locked.

In Fig. (4.1b), after the drive is turned off plasma quickly settles into EAW$_2$, however this mode is not stable and we can see the $m = 1$ and $m = 3$ harmonics growing as $m = 2$ and $m = 4$ decaying. Since the drive potential was $m = 2$ harmonic with even symmetry with respect to the center of plasma, $m = 1$ and $m = 3$ harmonics which have odd symmetry, grow out of the noise level. We can see that after t plasma reaches a steady state which, from comparing to the end state of Fig. (4.1a), we can see that it is in fact EAW$_1$. Therefore EAW$_2$ is unstable and collapses into EAW$_1$.

Figure (4.3) shows the distribution function $f(z,v,t)$ in the (z,v) phase-space and their related plasma density perturbations for EAW$_1$, in times $t = 0$, $t = T/4$ and $t = T/2$. We can see that the phase-space related to EAW$_1$ consists of a single hole orbiting the phase-space in a relatively flattened region at $v = \pm v_{ph}$. However this EAW$_1$ is in its earlier stages of its formation and is not fully developed in these figures, as can be seen from the evolving filaments and fine structures in phase-space. As seen from the mode density plot, since EAW$_1$ consists of both even and odd harmonics in space, EAW$_1$ does not have an either even or odd symmetry with respect to the center of plasma.

Furthermore, from comparing the distribution function plots to the plasma

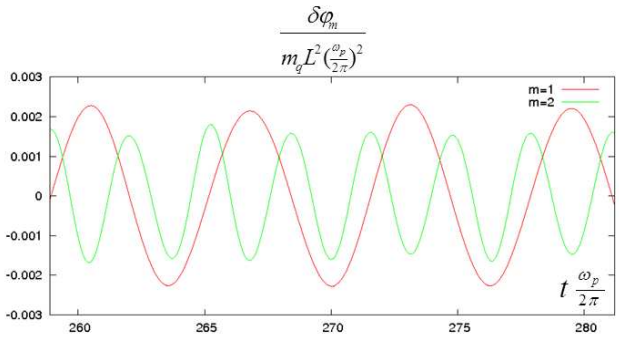

(a)

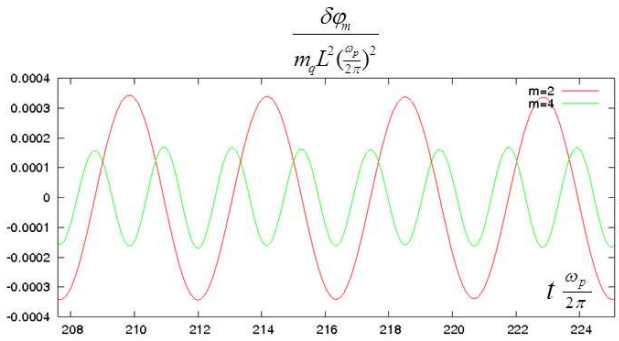

(b)

Figure 4.2: (4.2a): Amplitudes of the two largest spatial Fourier components of EAW_1, which are $m=1$ and $m=2$, oscillating phase-locked in time, with frequency of $m=2$ being 2 times the frequency of $m=1$. (4.2b): Amplitudes of the two largest spatial Fourier components of EAW_2, which are $m=2$ and $m=4$, oscillating phase-locked in time, with frequency of $m=4$ being 2 times the frequency of $m=2$. The physical parameters of the plasma are $k_\perp L = 18.44, L/\lambda = 37.3$

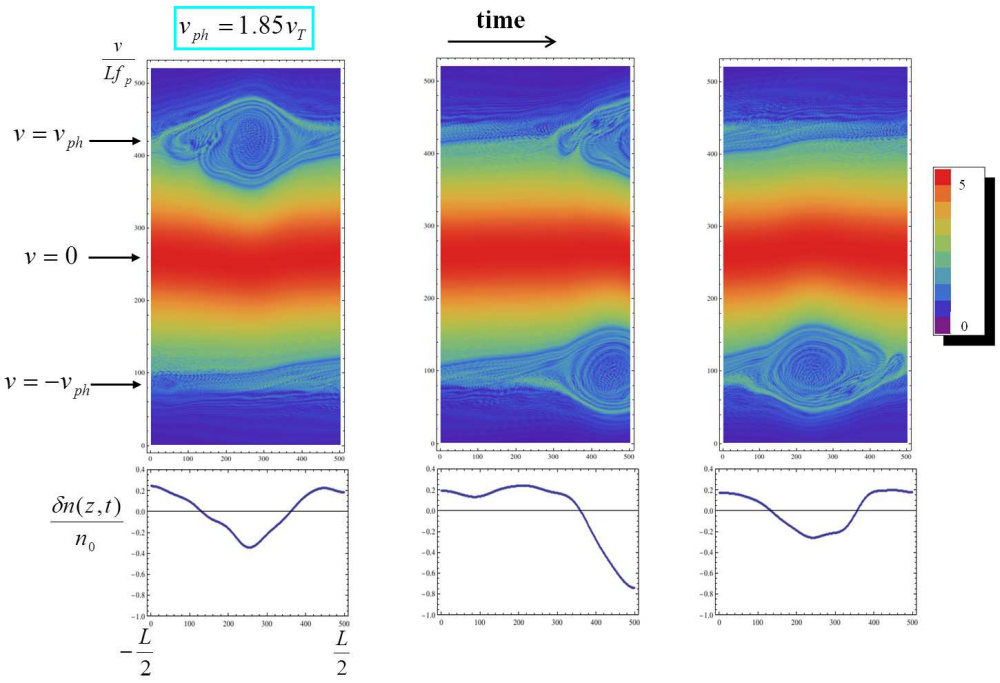

Figure 4.3: The three upper plots are density plots of the distribution function $f(z,v)$ of the EAW$_1$. Horizontal axis is the position along the plasma from $-L/2$ to $L/2$, and the horizontal axis is the particle velocity from $v = -2.8 v_T$ to $v = 2.8 v_T$. The three lower plots are density perturbations related to the distribution function plots. The physical parameters of the plasma are $k_\perp L = 18.44, L/\lambda = 37.3$

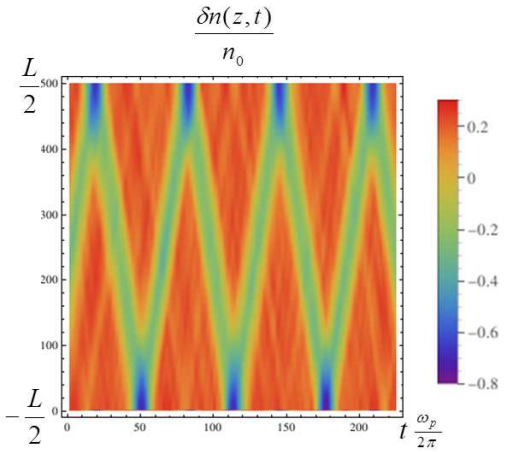

Figure 4.4: Plot of the density perturbation of EAW$_1$ along the plasma as a function of time, in a plasma with $k_\perp L = 18.44, L/\lambda = 37.3$.

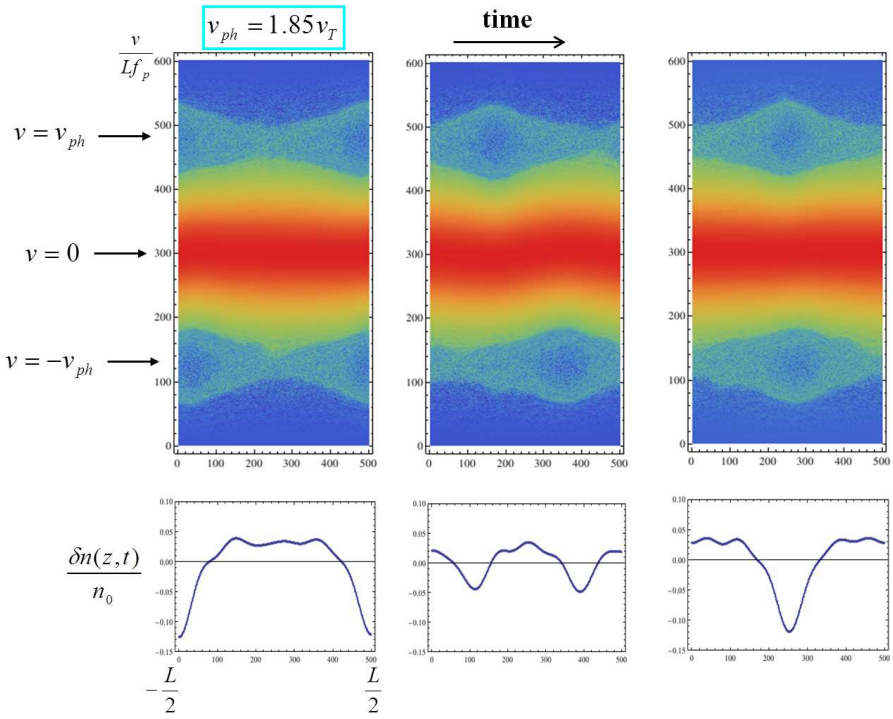

Figure 4.5: The three upper plots are density plots of the distribution function $f(z,v)$ of the EAW$_2$. Horizontal axis is the position along the plasma from $-L/2$ to $L/2$, and the horizontal axis is the particle velocity from $v = -2.8 v_T$ to $v = 2.8 v_T$. The three lower plots are density perturbations related to the distribution function plots. The physical parameters of the plasma are $k_\perp L = 18.44$, $L/\lambda = 37.3$.

density plots, the location of the hole in the distribution function corresponds to the location of the negative density perturbations along the plasma. In Fig. (4.4) we can see the negative density peak (dark blue color) as it is traveling to the left or right along the plasma and reflects from the plasma ends.

Figure (4.5) shows the distribution function $f(z,v,t)$ in the (z,v) phase-space and their related plasma density perturbations for EAW$_2$, in times $t = 0$, $t = T/4$ and $t = T/2$. The phase-space related to EAW$_2$ consists of two holes orbiting the phase-space in the flattened region $\partial f/\partial_v = 0$ at $\pm v = v_{ph}$. Comparing to the distribiution function depicted for EAW$_1$ in Fig. (4.3), we can see that this EAW$_2$ is well developed, with a more homogeneous and smooth distribution function and also the distribution function has a well formed flattened region at $v = \pm v_{ph}$.

Furthermore, comparing the density perturbation vs. position plots for EAW$_1$

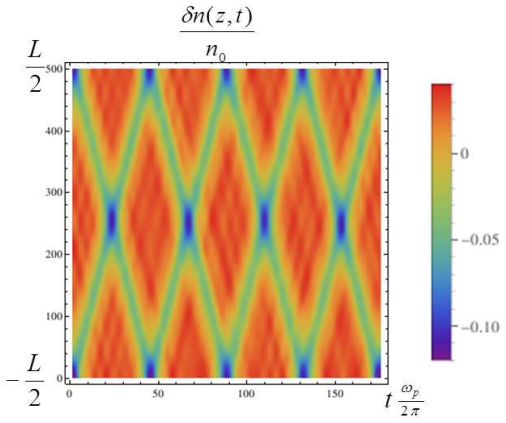

Figure 4.6: Plot of the density perturbation of EAW_2 along the plasma as a function of time in a plasma with $k_\perp L = 18.44$, $L/\lambda = 37.3$.

in Fig. (4.3) and for EAW_2 in Fig. (4.5), to TG nonlinear standing eigenmodes $m = 1$ and $m = 2$, respectively depicted in Figs. (3.2) and (3.3), we can see that the standing nonlinear TGs consists of (upward pointing) peeks or *density clumps*, traveling the length of plasma and reflecting off of plasma ends, whereas the EAWs density consists of traveling upside-down peeks or *density holes*.

Comparing the plots of the distribution function to the density perturbation plots, the two holes in the distribution function correspond to the negative density perturbations. EAW_2 is symmetric with respect to the center of plasma. The left and right half of the EAW_2 are two EAW_1s which are the mirror images of each other with respect to the center of plasma. In Fig. (4.6) we can see the two negative density peaks traveling in the opposite directions along plasma.

Figure (4.7) shows the process of decay of EAW_2 into EAW_1. Amplitude of $m = 1$ harmonic grows exponentially from the noise level with oscillation frequency $\omega_1 = \omega_2/2$. The growth of $m = 1$ is due to the nonlinear coupling to $m = 2$, which is the largest component of EAW_2. As the EAW_2 decays in time and EAW_1 grows, the two holes get close to each other along their bounce orbit in phase-space. Finally the holes catch up with each other and merge into a single hole orbiting the phase-space at the phase velocity. The process of hole merger is irreversible and the final state, which is EAW_1, is stable.

The growth of EAW_1 is exponential in its early stage and as its amplitude gets

larger and amplitude of EAW_2 gets smaller growth rate decreases, and finally after the hole merger, becomes zero. The onset of growth of EAW_1 is due to wave-wave resonant interaction.

We evaluated the maximum exponential growth rates from the relation which we obtained from our weakly nonlinear Vlasov-Poisson fromalism. The growth rate of the numerical method is obtained using fitting. In Fig. (4.8) we compared the exponential growth rates obtained from our analytical and numerical methods, which are in good agreement.

4.1 Summary

Decay of EAW_2 to EAW_1 was studied using both numerical and analytical methods. For our numerical method we used the method of lines for the simulation of 1D nonlinear Vlasov-Poisson system. We used a weakly nonlinear perturbation theory performed on the Vlasov-Poisson system to obtain the relations describing the nonlinear wave-wave interaction of EAWs.

The maximum growth rate of EAW_1 at the onset of its growth (and decay of EAW_2), obtained from our numerical method is in agreement with the growth rate we evaluated from the weakly nonlinear wave-wave interaction theory.

Some of the material in this Chapter is in preparation for publication. The dissertation author was the primary investigator and author of this material.

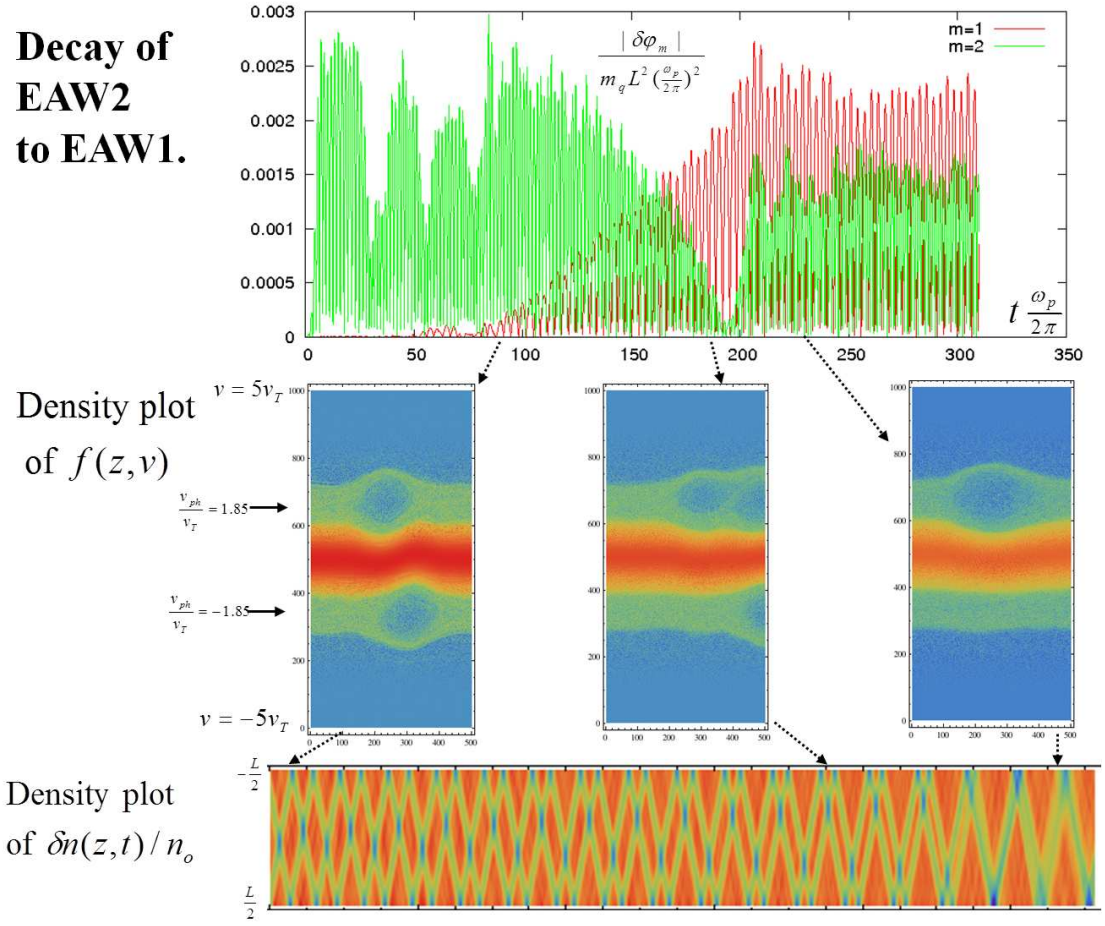

Figure 4.7: Decay of EAW_2 to EAW_1 in a plasma with $k_\perp L = 18.44, L/\lambda = 37.3$.

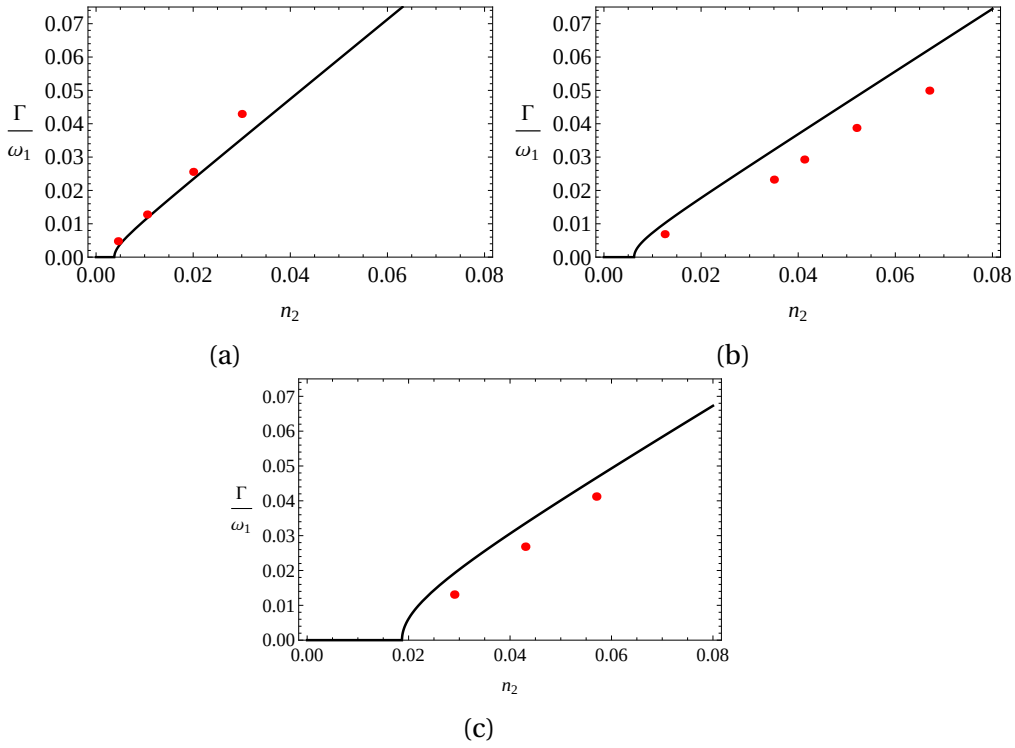

Figure 4.8: Exponential growth rate of small amplitude EAW_1 in the presence of large amplitude EAW_2. Solid curves are obtained from Eq. (4.57). Physical parameters related to the plot are (4.8a):$k_\perp L = 15, L/\lambda = 44.5$, (4.8b):$k_\perp L = 19.5, L/\lambda = 45.9$, (4.8c):$k_\perp L = 18.44, L/\lambda = 37.3$

Appendix A

Orbit calculations

For a small squeeze potential such that $\varphi_s/T \ll 1$, the energy of a majority of particles is much larger than φ_s. We would like to expand the functions of energy in the system in terms of the smallness ordering parameter ε introduced in Eq. (1.23), assuming that adding the squeeze potential will result in a first order perturbative correction to these functions. Thus for passing particles which have scaled energies $u > \varepsilon\overline{\varphi}_s$, we expand the functions of energy in terms of ε to first order in ε. From Eq. (1.27) we calculate the period of the orbit for a passing particle at energy u which orbits the whole length of the plasma:

$$\tau(u) = 2\int_{-\frac{L}{2}}^{\frac{L}{2}} \frac{dz}{v_T\sqrt{2(u-\varepsilon\overline{\varphi}_1(z))}} \tag{A.1}$$

$$\omega_b \approx \omega_0\left[1-\varepsilon\frac{\langle\overline{\varphi}_1(z)\rangle}{2u}\right], \tag{A.2}$$

where the symbol $\langle\ldots\rangle$ represents the spatial average along the length of plasma L. Here, $\tau_0 = 2L/v_T\sqrt{2u}$ and $\omega_0 = \frac{\pi}{L}v_T\sqrt{2u}$ are respectively the time period and the bounce frequency of the motion of particle with energy u in the absence of the

squeeze potential. The angle variable as a function of z, for $v>0$ is given by:

$$\begin{aligned}\psi &= \frac{2\pi}{\tau}\int_{-L/2}^{z}\frac{dz'}{v(z')} \\ &\approx \frac{\pi}{L}\left[z+\frac{L}{2}+\varepsilon\int_{-L/2}^{z}dz'\frac{\{\overline{\varphi}_1(z')\}}{2u}\right].\end{aligned} \tag{A.3}$$

In the above equation we substituted $\tau(E)$ from Eq. (A.1). Furthermore we defined $\{\overline{\varphi}_1(z)\}=\overline{\varphi}_1(z)-\left\langle\overline{\varphi}_1(z)\right\rangle$, which is the size of the deviation of $\overline{\varphi}_1(z)$ from its spatial average $\left\langle\overline{\varphi}_1(z)\right\rangle$. For $v<0$ we have:

$$\psi=\pi-\frac{\pi}{L}\left[z-L/2+\varepsilon\int_{L/2}^{z}dz'\frac{\{\overline{\varphi}_1(z')\}}{2u}\right]. \tag{A.4}$$

Thus, the angle variable can be written in terms of the angle variable in the absence of squeeze, plus a first order correction due to squeeze potential:

$$\psi = \psi_0+\psi_1 \tag{A.5}$$

$$\begin{aligned}\psi_0 &= \frac{\pi}{L}[z+L/2], \qquad v>0 \\ &= \pi-\frac{\pi}{L}[z-L/2], \quad v<0,\end{aligned} \tag{A.6}$$

$$\psi_1 = \varepsilon\,\mathrm{sign}(v)\frac{\pi}{L}\left[\int_{-L/2}^{z}dz'\frac{\{\overline{\varphi}_1(z')\}}{2u}\right]. \tag{A.7}$$

The action variable is:

$$\begin{aligned}I &= \frac{1}{2\pi}\oint p_z\,dz=\pi^{-1}\int_{-L/2}^{L/2}m_q v_T\sqrt{2u}\left(1-\varepsilon\overline{\varphi}_1(z)/u\right)^{1/2}dz \\ &\approx \frac{m_q v_T\sqrt{2u}L}{\pi}\left[1-\varepsilon\frac{\left\langle\overline{\varphi}_1\right\rangle}{2u}\right].\end{aligned} \tag{A.8}$$

Comparing Eq. (A.8) to Eq. (A.2) we get the following relation

$$I=m_q\omega_b\frac{L^2}{\pi^2}. \tag{A.9}$$

Since in Eq. (A.8), action variable I is given as a function of energy, we can reverse this relation to obtain energy as a function of I to the first order of perturbation:

$$u = \frac{\pi^2 I^2}{2m_q L^2 T} + \varepsilon \left\langle \overline{\varphi}_1 \right\rangle. \tag{A.10}$$

The position dependent part of the mode potential $\delta\varphi(z)$ can be written as a(periodic) function of action-angle variable $\delta\varphi(z) = \delta\varphi(\psi, I)$. Furthermore we can Fourier expand $\delta\varphi$ in terms of action-angle variables and calculate the nth Fourier component:

$$\begin{aligned}
\delta\varphi_n(I) &= \frac{1}{2\pi}\int_0^{2\pi} e^{-in\psi}\delta\varphi(z)d\psi \\
&\approx \delta\varphi_n^{(0)}(I) + \frac{1}{2\pi}\int_0^{2\pi} e^{-in(\psi_0+\psi_1)}\delta\varphi(z)(d\psi_0 + d\psi_1) \\
&\approx \delta\varphi_n^{(0)}(I) + \frac{1}{2\pi}\int_0^{2\pi} (d\psi_1 - in\psi_1 d\psi_0)e^{-in\psi_0}\delta\varphi(z) \\
&\approx \delta\varphi_n^{(0)}(I) + \frac{1}{2\pi}\int_0^{2\pi} d\left(\psi_1 e^{-in\psi_0}\right)\delta\varphi(z).
\end{aligned} \tag{A.11}$$

Integrating by parts on the last line of Eq. (A.11), since $\psi_1(z = \pm L/2) = 0$ we obtain:

$$\begin{aligned}
&\delta\varphi_n(I) \\
&\approx \delta\varphi_n^{(0)}(I) - \frac{1}{2\pi}\int_0^{2\pi} \psi_1 e^{-in\psi_0} d(\delta\varphi(z)),
\end{aligned} \tag{A.12}$$

where $\delta\varphi_n^{(0)}(I)$ is the Fourier component in terms of action-angle variables, in the absence of squeeze potential for which ψ_0 is given by Eq. (A.5):

$$\begin{aligned}
\delta\varphi_n^{(0)}(I) \quad &= \frac{1}{2\pi}\int_0^{2\pi} e^{-in\psi_0}\delta\varphi(z)d\psi_0 \\
&= \int_{-\frac{L}{2}}^{\frac{L}{2}} \frac{dz}{L}\cos[\tfrac{n\pi}{L}(z+\tfrac{L}{2})]\delta\varphi(z).
\end{aligned} \tag{A.13}$$

Using Eqs. (A.6) and (A.7) we can write Eq. (A.11) as:

$$\begin{aligned}&\delta\varphi_n(I)-\delta\varphi_n^{(0)}(I) \\ &=-\varepsilon\int_{-\frac{L}{2}}^{\frac{L}{2}}\frac{dz}{L}\cos[\tfrac{n\pi}{L}(z+\tfrac{L}{2})]\int_{-\frac{L}{2}}^{z}dz'\frac{\{\overline{\varphi}_1(z')\}}{2u}\frac{d}{dz}\delta\varphi(z).\end{aligned} \tag{A.14}$$

We will now use these results to determine the Fourier coefficients $C_m^n(I)$ given by Eq. (1.34), to the first order in ε. For the squeeze potential we use the symmetric form given by Eq. (1.17). From the wave potential $\delta\varphi(z,t)$ given by Eq. (1.31) we can see that the wave is a superposition of cosine waves. For the mth cosine, we substitute $\cos[\frac{m\pi}{L}(z+\frac{L}{2})]$ for $\delta\varphi(z)$. Substituting from Eq. (1.31) in Eq. (A.13) we obtain the unsqueezed Fourier components:

$$\begin{aligned}[C_m^n(I)]^{(0)} &= \int_{-L/2}^{L/2}\frac{dz}{L}\cos\Big[\frac{n\pi}{L}(z+L/2)\Big]\delta\bar{\phi}\cos\Big[\frac{m\pi}{L}(z+L/2)\Big] \\ &= \frac{1}{2}\big(\delta_{n,m}+\delta_{n,-m}\big)\end{aligned} \tag{A.15}$$

Using the relation:

$$\int_{-L/2}^{z}\frac{\{\overline{\varphi}_1(z')\}}{2u}dz' = \sum_{\overline{m}=1}^{\infty}\frac{\overline{\varphi}^1_{\overline{m}}}{2u}\frac{L}{2\pi\overline{m}}\sin\Big[2\pi\frac{\overline{m}}{L}(z+L/2)\Big]$$

first we calculate perturbation to mth Fourier mode in angle space:

$$\begin{aligned}C_m^m(I)-[C_m^m(I)]^{(0)} &= \varepsilon\int_{-L/2}^{L/2}\frac{dz}{L}\frac{m\pi}{L}\cos\Big[\frac{m\pi}{L}(z+L/2)\Big]\sin\Big[\frac{m\pi}{L}(z+L/2)\Big] \\ &\times \sum_{m'=1}^{\infty}\frac{\overline{\varphi}^1_{m'}}{2u}\frac{L}{2\pi m'}\sin\Big[2\pi\frac{m'}{L}(z+L/2)\Big] \\ &= \varepsilon\int_0^{L}\frac{dy}{L}\frac{m\pi}{2L}\sin\Big[\frac{2m\pi}{L}y\Big]\sum_{m=1}^{\infty}\frac{\overline{\varphi}^1_m}{2u}\frac{L}{2\pi m'}\sin\Big[2\pi m'\frac{y}{L}\Big] \\ &= \frac{\overline{\varphi}^1_m}{16}\Big(\frac{\varepsilon}{u}\Big)\end{aligned} \tag{A.16}$$

Now we calculate the perturbation to n'th Fourier mode, where $n \neq \pm m$:

$$
\begin{aligned}
C_m^n(I) &= \varepsilon \int_0^L \frac{dy}{L}\frac{m\pi}{L}\cos\Big(\frac{n\pi y}{L}\Big)\sin\Big(\frac{n\pi y}{L}\Big)\sum_{m'=1}^{\infty}\frac{\overline{\varphi}^1_{m'}}{2u}\frac{L}{2\pi m'}\sin\Big[2\pi m'\frac{y}{L}\Big] \\
&= \varepsilon m\int_0^L \frac{\pi dy}{L}\frac{1}{2}\Big(\sin\Big[(n+m)\frac{\pi y}{L}\Big]+\sin\Big[(m-n)\frac{\pi y}{L}\Big]\Big)\sum_{m'=1}^{\infty}\frac{\overline{\varphi}^1_{m'}}{4\pi m' u}\sin\Big[2\pi m'\frac{y}{L}\Big] \\
&= \varepsilon\sum_{m'=1}^{\infty} m\int_0^L \frac{\pi dy}{L}\frac{1}{4}\Big(\cos\Big[(n+m-2m')\frac{\pi y}{L}\Big]-\cos\Big[(n+m+2m')\frac{\pi y}{L}\Big] \\
&+ \cos\Big[(m-n-2m')\frac{\pi y}{L}\Big]-\cos\Big[(m-n+2m')\frac{\pi y}{L}\Big]\Big)\frac{\varphi^1_{m'}}{4\pi m' u} \qquad \text{(A.17)}
\end{aligned}
$$

Finally, the above integral simplifies to

$$
C_m^n(I) = \varepsilon\sum_{m'=1}^{\infty}\big(\delta_{n,-m+2m'}-\delta_{n,-m-2m'}+\delta_{n,m-2m'}-\delta_{n,m+2m'}\big)\frac{m\overline{\varphi}^1_{m'}}{4\pi m' u} \qquad \text{(A.18)}
$$

In the above Kronecker delta functions, if m is odd, n must be odd and if m is even, n must be even in order to get a nonzero result. Since $m' > 0$, we can further simplify Eq. (A.18) to obtain:

$$
C_m^n(I) = \frac{m}{8}\left(\frac{\overline{\varphi}^1_{|m-n|/2}}{m-n}+\frac{\overline{\varphi}^1_{|m+n|/2}}{m+n}\right)\Big(\frac{\varepsilon}{u}\Big), \quad n \neq \pm m \qquad \text{(A.19)}
$$

For both n and m odd or both even. In summary we have:

$$
\begin{aligned}
C_m^n(I) &= [C_m^m(I)]^{(0)} + \alpha_m^n \varepsilon/u, && \text{(A.20)} \\
\big[C_m^m(I)\big]^{(0)} &= \frac{1}{2}\delta_{|n|,m}, && \text{(A.21)} \\
\alpha_m^n &= \frac{m}{8}\left[\frac{\overline{\varphi}^1_{|m-n|/2}}{m-n}+\frac{\overline{\varphi}^1_{|m+n|/2}}{m+n}\right], n \neq m && \text{(A.22)} \\
&= \frac{\overline{\varphi}^1_m}{16}, \quad n = \pm m.
\end{aligned}
$$

For the $r\,z$ system, the Fourier series expansion for the scaled Debye shielded squeeze potential $\overline{\varphi}_1(r,z)$, defined in Eq. (1.156), is given by:

$$\overline{\varphi}_1(r,z) \;=\; \left\langle \overline{\varphi}_1(r,z)\right\rangle_z + \sum_{m=1}^{\infty} \overline{\varphi}^1_m(r)\cos\left[2\pi\frac{m}{L}(z+L/2)\right].$$

We can perform similar calculations, starting from Eqs. (1.159) through (1.163). Fourier coefficients of the squeezed $r\,z$ system, to the first order in ε are given by:

$$C^n_m(r,\tfrac{\varepsilon}{u}) = \frac{1}{2}\delta_{|n|,m} + \alpha^n_m(r)\frac{\varepsilon}{u}, \tag{A.23}$$

where coefficients $\alpha^n_m(r)$ are functions of radius given by:

$$\begin{aligned}\alpha^n_m(r) \quad &= \frac{m}{8}\left[\frac{\overline{\varphi}^1_{|m-n|/2}(r)}{m-n} + \frac{\overline{\varphi}^1_{|m+n|/2}(r)}{m+n}\right], n\neq m \\ &= \frac{\overline{\varphi}^1_m(r)}{16}, \quad n=\pm m.\end{aligned} \tag{A.24}$$

Appendix B

Matrix calculation

In order to obtain expressions for the zeroth, first and second order dispersion matrices $\mathbf{M}_0, \mathbf{M}_1$ and $\mathbf{M}_2$ from Eq. (1.51), we need the functional form of $u_n(\varepsilon)$ for $\varepsilon \ll 1$, where $u_n(\varepsilon)$ is the scaled energy at which $\omega_b(u_n) = \omega/n$. In dimensionless form this relation is:

$$\overline{\omega}_b(u_n, \varepsilon) = \overline{\omega}/n\,. \tag{B.1}$$

We first expand $\overline{\omega}_b(u, \varepsilon)$ to second order in ε, obtaining, from Eq. (A.1),

$$\overline{\omega}_b = 1/\int_{-L/2}^{L/2} dz/L \frac{1}{\sqrt{2u}}\left(1 + \frac{\varepsilon\overline{\varphi}_1(z)}{u} + \frac{3}{8}\varepsilon^2\frac{\overline{\varphi}_1^2(z)}{u^2}\right) \tag{B.2}$$

which implies

$$\overline{\omega}_b(u, \varepsilon) = \sqrt{2u}\left[1 - \frac{\varepsilon}{2u}\langle\overline{\varphi}_1\rangle + \frac{\varepsilon^2}{4u^2}\left(\langle\overline{\varphi}_1\rangle^2 - \frac{3}{2}\langle\overline{\varphi}_1^2\rangle\right) + \ldots\right]. \tag{B.3}$$

We can then invert this expression to solve Eq. (B.1) for u_n, writing $u_n = u_{n0} + \varepsilon u_{n1} + \ldots$ and collecting terms of the same order in ε. The result is

$$u_n = \frac{\overline{\omega}^2}{2n^2} + \left\langle\overline{\varphi}_1\right\rangle\varepsilon + \frac{3}{2}\left(\frac{n}{\overline{\omega}}\right)^2(\left\langle\overline{\varphi}_1^2\right\rangle - \left\langle\overline{\varphi}_1\right\rangle^2)\varepsilon^2 + \ldots \tag{B.4}$$

As a result we have to second order in ε:

$$e^{-u_n} = e^{-\frac{\overline{\omega}^2}{2n^2}}\left(1-\left\langle\overline{\varphi}_1\right\rangle\varepsilon-\frac{3}{2}\left(\frac{n}{\overline{\omega}}\right)^2(\left\langle\overline{\varphi}_1^2\right\rangle-\left\langle\overline{\varphi}_1\right\rangle^2)\varepsilon^2+\frac{1}{2}\left\langle\overline{\varphi}_1\right\rangle^2\varepsilon^2+\ldots\right). \tag{B.5}$$

Furthermore, we expand $1/\left\langle e^{-\varepsilon\overline{\varphi}_1}\right\rangle$:

$$\begin{aligned} 1/\left\langle e^{-\varepsilon\overline{\varphi}_1}\right\rangle &= 1/\left(1-\left\langle\overline{\varphi}_1\right\rangle\varepsilon+\frac{1}{2}\left\langle\overline{\varphi}_1^2\right\rangle\varepsilon^2+\ldots\right) \\ &= 1+\left\langle\overline{\varphi}_1\right\rangle\varepsilon-\frac{1}{2}\left\langle\overline{\varphi}_1^2\right\rangle\varepsilon^2+\left\langle\overline{\varphi}_1\right\rangle^2\varepsilon^2\ldots \end{aligned} \tag{B.6}$$

Thus, we have:

$$\frac{e^{-u_n}}{\left\langle e^{-\varepsilon\overline{\varphi}_1}\right\rangle} = e^{-\frac{\overline{\omega}^2}{2n^2}}\left(1-\left(\frac{3}{2}\left(\frac{n}{\overline{\omega}}\right)^2+\frac{1}{2}\right)\left[\left\langle\overline{\varphi}_1^2\right\rangle-\left\langle\overline{\varphi}_1\right\rangle^2\right]\varepsilon^2+\ldots\right). \tag{B.7}$$

We also need $d\overline{\omega}_b(u_n,\varepsilon)/du$. Taking the derivative of Eq. (B.3) and using Eq. (B.4) implies:

$$\frac{d\overline{\omega}_b(u_n,\varepsilon)}{du} = \frac{n}{\overline{\omega}}\left(1+3\left(\frac{n}{\overline{\omega}}\right)^4(\left\langle\overline{\varphi}_1^2\right\rangle-\left\langle\overline{\varphi}_1\right\rangle^2)\varepsilon^2+\ldots\right). \tag{B.8}$$

We now use these results to expand the dispersion matrix $\mathbf{M}(\overline{\omega},\varepsilon)$ in powers of ε. To zeroth order we use the lowest order forms in Eq. (1.45), $\overline{\omega}_b=\sqrt{2u}$ (from Eq. (B.3)), and $C_{m,n}=\delta_{m,|n|}/2$ from Eq. (A.21). This implies

$$M_0^{mn}(\overline{\omega}) = \delta_{mn}\left[1+\frac{1}{K_m^2\lambda_D^2}\mathrm{W}(\overline{\omega}/m)\right]. \tag{B.9}$$

The first order correction is found using the first-order expansions of $1/\langle e^{-\varepsilon\overline{\varphi}_1}\rangle$, $\overline{\omega}_b$ and $C_{m,n}$ in Eq. (1.45). This results in the expression

$$M_1^{mp}(\overline{\omega}) = -\frac{8(K_m\lambda_D)^{-2}}{\sqrt{2\pi}}\sum_{n=1}^{\infty}\Bigg\{-\overline{\varphi}_s\frac{\overline{\omega}_b(0,0)}{(\overline{\omega}/n)^2-\overline{\omega}_b(0,0)^2}C_p^n(0)C_m^n(0)$$
$$+\left[\left\langle\overline{\varphi}_1\right\rangle\int_0^{\infty}du\,\frac{\overline{\omega}_b(u,0)e^{-u}}{(\overline{\omega}/n)^2-\overline{\omega}_b(u,0)^2}+\int_0^{\infty}du\,\partial_\varepsilon\overline{\omega}_b(u,0)\frac{(\overline{\omega}/n)^2+\overline{\omega}_b(u,0)^2}{((\overline{\omega}/n)^2-\overline{\omega}_b(u,0)^2)^2}e^{-u}\right]C_p^n(0)C_m^n(0)$$
$$+\int_0^{\infty}du\,\frac{\overline{\omega}_b(u,0)e^{-u}}{(\overline{\omega}/n)^2-\overline{\omega}_b(u,0)^2}\left(\partial_\varepsilon C_p^n(0)C_m^n(0)+\partial_\varepsilon C_m^n(0)C_p^n(0)\right)\Bigg\}. \tag{B.10}$$

The first term on the right hand side arises from expansion in ε of the lower bound in the u-integral in Eq. (1.43). This is zero since from Eq. (B.3) we have $w(0,0)=0$. The second term arises from expansion of $1/\langle\mathbf{e}^{-\varepsilon\overline{\varphi}_1}\rangle$ using Eq. (B.6), and the last two terms arise from expansion of $\overline{\omega}_b$ and C_m^n respectively. From Eq. (B.3) we have:

$$\overline{\omega}_b(u,0)=\sqrt{2u},\quad \partial_\varepsilon\overline{\omega}_b(u,0)=-\left\langle\overline{\varphi}_1\right\rangle/\sqrt{2u}. \tag{B.11}$$

Using Eq. (B.11) and Eq. (A.20) the remaining terms on the right hand side of Eq. (B.10) can be simplified to obtain

$$M_1^{mp}(\overline{\omega}) = -\frac{2(K_m\lambda_D)^{-2}}{\sqrt{2\pi}}\Bigg\{\left\langle\overline{\varphi}_1\right\rangle\int_0^{\infty}du\,\frac{\sqrt{2u}e^{-u}}{(\overline{\omega}/m)^2-2u}\delta_{mp}$$
$$-\left\langle\overline{\varphi}_1\right\rangle\int_0^{\infty}du\,\frac{(\overline{\omega}/m)^2+2u}{\sqrt{2u}((\overline{\omega}/m)^2-2u)^2}e^{-u}\delta_{mp}$$
$$+2\int_0^{\infty}du\,\frac{\sqrt{2u}e^{-u}}{u((\overline{\omega}/m)^2-2u)}\alpha_p^m+2\int_0^{\infty}du\,\frac{\sqrt{2u}e^{-u}}{u((\overline{\omega}/p)^2-2u)}\alpha_m^p\Bigg\}, \tag{B.12}$$

Now, using integration by parts we can show that

$$\langle\overline{\varphi}_1\rangle\int_0^\infty d\,u\,\frac{(\overline{\omega}/m)^2+2u}{\sqrt{2u}((\overline{\omega}/m)^2-2u)^2}e^{-u}=\langle\overline{\varphi}_1\rangle\int_0^\infty d\,u\,e^{-u}\frac{d}{d\,u}\left(\frac{\sqrt{2u}}{(\overline{\omega}/m)^2-2u}\right)$$
$$=\langle\overline{\varphi}_1\rangle\int_0^\infty d\,u\,\frac{\sqrt{2u}}{(\overline{\omega}/m)^2-2u}e^{-u}. \tag{B.13}$$

Thus the first two terms in Eq. (B.12) cancel and we are left with

$$M_1^{mp}(\overline{\omega})= \tag{B.14}$$
$$-\frac{2(K_m\lambda_D)^{-2}}{\sqrt{2\pi}}\left\{2\int_0^\infty d\,u\,\frac{\sqrt{2u}e^{-u}}{u((\overline{\omega}/m)^2-2u)}\alpha_p^m+2\int_0^\infty d\,u\,\frac{\sqrt{2u}e^{-u}}{u((\overline{\omega}/p)^2-2u)}\alpha_m^p\right\}.$$

Using the following relation we further simplify $M_1^{mp}(\overline{\omega})$:

$$\int_0^\infty d\,u\,\frac{\sqrt{2u}e^{-u}}{u((\overline{\omega}/m)^2-2u)}=\int_0^\infty d\,u\,\frac{2\sqrt{2u}}{(\overline{\omega}/m)^2}\left(\frac{1}{2u}+\frac{1}{(\overline{\omega}/m)^2-2u}\right)e^{-u}$$
$$=\frac{\sqrt{2}}{(\overline{\omega}/m)^2}\mathrm{P}\int_0^\infty\frac{e^{-u}}{\sqrt{u}}d\,u+\frac{2}{(\overline{\omega}/m)^2}\mathrm{P}\int_0^\infty\frac{\sqrt{2u}}{(a/m)^2-2u}e^{-u}d\,u$$
$$=\frac{m^2}{\overline{\omega}^2}\sqrt{2\pi}\left[1-\mathrm{W}(\overline{\omega}/m)\right], \tag{B.15}$$

where $\mathrm{W}(x)$ is defined in Eq. (1.56). As a result we obtain

$$M_1^{mp}(\overline{\omega})=$$
$$-\frac{4}{K_m^2\lambda_D^2}\left(\frac{m^2}{\overline{\omega}^2}\left[1-\mathrm{W}(\overline{\omega}/m)\right]\alpha_p^m+\frac{p^2}{\overline{\omega}^2}\left[1-\mathrm{W}(\overline{\omega}/p)\right]\alpha_m^p\right). \tag{B.16}$$

For $\mathbf{M}_2$, we note that we have need only of $\mathrm{Im}\,\mathbf{M}_2$ in our lowest-order expression for the damping rate due to squeeze. Applying Eqs. (B.4), (B.5), (B.7) and (B.8) to

Eq. (1.45) we obtain the following pure series form for $\mathrm{Im}\,\mathbf{M}(\overline{\omega},\varepsilon)$:

$$\begin{aligned}
\mathrm{Im}M^{mp}(\overline{\omega},\varepsilon) &= \frac{4\pi}{\lambda_D^2 K_m^2\sqrt{2\pi}}\sum_{n=1}^{\infty}\frac{\overline{\omega}}{n}e^{-\overline{\omega}^2/2n^2}\left(1-\left(\frac{3}{2}\left(\frac{n}{\overline{\omega}}\right)^2+\frac{1}{2}\right)\left[\left\langle\overline{\varphi}_1^2\right\rangle-\left\langle\overline{\varphi}_1\right\rangle^2\right]\varepsilon^2+\ldots\right)\\
&\times\left(1-3\left(\frac{n}{\overline{\omega}}\right)^4[\left\langle\overline{\varphi}_1^2\right\rangle-\left\langle\overline{\varphi}_1\right\rangle^2]\varepsilon^2+\ldots\right)\\
&\times\left(\delta_{nm}/2+\frac{2n^2}{\overline{\omega}^2}\alpha_m^n\varepsilon+(\beta_m^n-\left\langle\overline{\varphi}_1\right\rangle\alpha_m^n)\left(\frac{2n^2}{\overline{\omega}^2}\right)^2\varepsilon^2+\ldots\right)\\
&\times\left(\delta_{np}/2+\frac{2n^2}{\overline{\omega}^2}\alpha_p^n\varepsilon+(\beta_p^n-\left\langle\overline{\varphi}_1\right\rangle\alpha_p^n)\left(\frac{2n^2}{\overline{\omega}^2}\right)^2\varepsilon^2+\ldots\right),
\end{aligned}\tag{B.17}$$

where we also used the following series expansion, which is obtained in detail in appendix A to the first order(second order coefficients β_m^n are not evaluated since they do not contribute to our results):

$$\begin{aligned}
C_m^n(\varepsilon/u_n) &= \delta_{nm}/2+(\varepsilon/u_n)\alpha_m^n+(\varepsilon/u_n)^2\beta_m^n+\ldots\\
&= \delta_{nm}/2+\varepsilon\frac{2n^2}{\overline{\omega}^2}\alpha_m^n+\varepsilon^2(\beta_m^n-\left\langle\overline{\varphi}_1\right\rangle\alpha_m^n)\left(\frac{2n^2}{\overline{\omega}^2}\right)^2+\ldots
\end{aligned}\tag{B.18}$$

The zeroth, first and second order Im$\mathbf{M}$ are found by collecting terms in Eq. (B.17):

$$\mathrm{Im}M_0^{mp}(\overline{\omega}) = \frac{4\pi}{\lambda_D^2 K_m^2\sqrt{2\pi}}\frac{\overline{\omega}}{m}e^{-\overline{\omega}^2/2m^2}\delta_{m,p}/4,\tag{B.19}$$

$$\mathrm{Im}M_1^{mp}(\overline{\omega}) = \frac{4\pi}{\lambda_D^2 K_m^2\sqrt{2\pi}}\left[e^{-\overline{\omega}^2/2p^2}\frac{p}{\overline{\omega}}\alpha_m^p+e^{-\overline{\omega}^2/2m^2}\frac{m}{\overline{\omega}}\alpha_p^m\right],\tag{B.20}$$

$$\begin{aligned}
\mathrm{Im}M_2^{mp}(\overline{\omega}) &= \frac{4\pi}{\lambda_D^2 K_m^2\sqrt{2\pi}}\left[-\frac{\overline{\omega}}{m}e^{-\overline{\omega}^2/2m^2}\left(3\left(\frac{m}{\overline{\omega}}\right)^4+\frac{3}{2}\left(\frac{m}{\overline{\omega}}\right)^2+\frac{1}{2}\right)\left[\left\langle\overline{\varphi}_1^2\right\rangle-\left\langle\overline{\varphi}_1\right\rangle^2\right]\delta_{m,p}/4\right.\\
&+2e^{-\overline{\omega}^2/2p^2}(\beta_m^p-\left\langle\overline{\varphi}_1\right\rangle\alpha_m^p)\left(\frac{p}{\overline{\omega}}\right)^3+2e^{-\overline{\omega}^2/2m^2}(\beta_p^m-\left\langle\overline{\varphi}_1\right\rangle\alpha_p^m)\left(\frac{m}{\overline{\omega}}\right)^3\\
&\left.+\sum_{n=1}^{\infty}4\left(\frac{n}{\overline{\omega}}\right)^3e^{-\overline{\omega}^2/2n^2}\alpha_m^n\alpha_p^n\right].
\end{aligned}\tag{B.21}$$

Note that the expression for $\mathrm{Im}\,\mathbf{M}_1$ agrees with the imaginary part of Eq. (B.16).

Appendix C

Matrix calculation for the RZ system

In order to carry out a perturbation expansion of the dispersion relation of the $r\,z$ system given by Eq. (1.178), in terms of ε as the smallness parameter, we need the series expansion of $M^{\bar{l}l\overline{m}m}$ given by Eq. (1.180) in terms of ε. We write this matrix as:

$$M^{\bar{l}l\overline{m}m} = \delta_{\bar{l}l}\delta_{\overline{m}m} + \frac{\int_0^{r_w} r\,d\,r\,\mathrm{J}_0(\frac{x_l}{r_w}r)\mathrm{J}_0(\frac{x_{\bar{l}}}{r_w}r)\overline{n}_0(r)b(r,\varepsilon)\mathscr{M}^{\overline{m}m}(r,\overline{\omega},\varepsilon)}{\left[\left(\frac{x_{\bar{l}}}{r_w}\right)^2 + k_{\overline{m}}^2\right]\frac{r_w^2}{2}\mathrm{J}_1^2(x_{\bar{l}})}, \tag{C.1}$$

where

$$b(r,\varepsilon) = \frac{\left\langle \mathbf{e}^{-\varepsilon\varphi_1(r,z)/T}\right\rangle_z}{\left\langle \overline{n}_0(r)e^{-\varepsilon\varphi_1(r,z)/T}/\left\langle \overline{n}_0(r)\right\rangle_r\right\rangle_{rz}} \tag{C.2}$$

is a Boltzmann prefactor due to variation of the squeeze potential with radius, and

$$\mathscr{M}^{\overline{m}m}(r,\overline{\omega},\varepsilon) = -\frac{8}{\sqrt{2\pi}\,\lambda_D^2\left\langle e^{-\epsilon\overline{\varphi}_1(r,z)}\right\rangle_z}\sum_{n=1}^{\infty}\int_{\varepsilon\overline{\varphi}_1(r,0)}^{\infty} d\,u\,\frac{\overline{\omega}_b\,e^{-u}}{(\overline{\omega}/n)^2-\overline{\omega}_b^2}\,C_m^n\left(r,\tfrac{\varepsilon}{u}\right)C_{\overline{m}}^n\left(r,\tfrac{\varepsilon}{u}\right) \tag{C.3}$$

is the same matrix as appeared in the 1D calculation (the second term in Eq. (1.45)) (aside from multiplicative constant K_m^{-2} that does not appear in Eq. (C.3)). We expanded this matrix in ε in Appendix B and can use those results to obtain the re-

quired ε expansion here. The zeroth order matrix is (see Eq. (B.9))

$$\mathscr{M}_0^{\overline{m}m} = \delta_{\overline{m}m} \mathrm{W}(\overline{\omega}/m)/\lambda_D^2 \,, \tag{C.4}$$

and the first-order correction $\mathscr{M}_1^{\overline{m}m}$ is given by Eq. (B.16) (multiplied by K_m^2):

$$\mathscr{M}_1^{\overline{m}m} = -\frac{4}{\lambda_D^2}\left\{\frac{\overline{m}^2}{\overline{\omega}^2}\left[1-\mathrm{W}(\overline{\omega}/\overline{m})\right]\alpha_{\overline{m}}^m + \frac{m^2}{\overline{\omega}^2}\left[1-\mathrm{W}(\overline{\omega}/m)\right]\alpha_m^{\overline{m}}\right\}. \tag{C.5}$$

Let us call the second-order correction $\mathscr{M}_2^{\overline{m}m}$; the imaginary part of this matrix was evaluated in Eq. (B.21). Now, expanding $b(r,\varepsilon)$ to second-order yields $b(r,\varepsilon) = 1+\varepsilon\, b_1(r)+\varepsilon^2 b_2(r)$ where

$$b_1(r) = \frac{\varepsilon}{T}\left(\langle \overline{n}_0(r)\varphi_1\rangle_{rz}/\langle \overline{n}_0(r)\rangle_r - \langle\varphi_1\rangle_z\right) \tag{C.6}$$

and

$$b_2(r) = \frac{1}{T^2}\left(\frac{1}{2}\langle\varphi_1^2\rangle_z + \left(\langle \overline{n}_0\varphi_1/\langle\overline{n}_0\rangle_z\rangle_{rz}\right)^2 - \frac{1}{2}\langle \overline{n}_0\varphi_1^2/\langle\overline{n}_0\rangle_r\rangle_{rz} - \langle\varphi_1\rangle_z\langle \overline{n}_0\varphi_1/\langle\overline{n}_0\varphi_1/\langle\overline{n}_0\rangle_r\rangle_{rz}\right) \tag{C.7}$$

and thus the combination $b(r,\varepsilon)\mathscr{M}^{\overline{m}m}(r,\overline{\omega},\varepsilon)$ has the following expansion, up to second order:

$$\begin{aligned} b(r,\varepsilon)\mathscr{M}^{\overline{m}m}(r,\overline{\omega},\varepsilon) &= \mathscr{M}_0^{\overline{m}m}(r,\overline{\omega}) + \varepsilon\left(\mathscr{M}_1^{\overline{m}m}(r,\overline{\omega}) + \mathscr{M}_0^{\overline{m}m}(r,\overline{\omega})b_1(r)\right) \\ &+\varepsilon^2\left(\mathscr{M}_2^{\overline{m}m}(r,\overline{\omega}) + \mathscr{M}_1^{\overline{m}m}(r,\overline{\omega})b_1(r) + \mathscr{M}_0^{\overline{m}m}(r,\overline{\omega})b_2(r)\right). \end{aligned} \tag{C.8}$$

Using Eqs. (C.1), (C.4) and (C.8) we obtain the following explicit form for the zeroth order matrix $M_0^{\bar{l}\,l\,\overline{m}m}$,

$$M_0^{\bar{l}\,l\,\overline{m}m} = \delta_{\overline{m}m}\left(\delta_{\bar{l}\,l} + 2\mathrm{W}(\overline{\omega}/m)\frac{\int_0^{r_w} r\,d\,r\,\overline{n}_0(r)\mathrm{J}_0(x_{\bar{l}}\,r/r_w)\mathrm{J}_0(x_l\,r/r_w)}{\lambda_D^2\left[x_{\bar{l}}^2 + k_{\overline{m}}^2 r_w^2\right]\mathrm{J}_1^2(x_{\bar{l}})}\right) \tag{C.9}$$

and using Eq. (C.5) we obtain the first order matrix $M_1^{\bar{l}\,l\,\overline{m}m}$,

$$M_1^{\bar{l}\,l\,\overline{m}m} = \frac{\int_0^{r_w} r\,d\,r\,\overline{n}_0(r)\mathrm{J}_0(x_{\bar{l}}r/r_w)\mathrm{J}_0(x_l r/r_w)\left[\mathscr{M}_1^{\overline{m}m}(r,\overline{\omega}) + \mathscr{M}_0^{\overline{m}m}(r,\overline{\omega})b_1(r)\right]}{\lambda_D^2\left[x_{\bar{l}}^2 + k_{\overline{m}}^2 r_w^2\right]\mathrm{J}_1^2(x_{\bar{l}})}. \quad \text{(C.10)}$$

For the second order matrix, we only require the imaginary part, given by

$$\mathrm{Im}\,M_2^{\bar{l}\,l\,\overline{m}m} = \quad \text{(C.11)}$$
$$-\frac{\int_0^{r_w} r\,d\,r\,\overline{n}_0(r)\mathrm{J}_0(x_{\bar{l}}r/r_w)\mathrm{J}_0(x_l r/r_w)\left[\mathrm{Im}\,\mathscr{M}_2^{\overline{m}m}(r,\overline{\omega}) + \mathrm{Im}\,\mathscr{M}_1^{\overline{m}m}(r,\overline{\omega})b_1(r) + \mathrm{Im}\,\mathscr{M}_0^{\overline{m}m}(r,\overline{\omega})b_2(r)\right]}{\lambda_D^2\left[x_{\bar{l}}^2 + k_{\overline{m}}^2 r_w^2\right]\mathrm{J}_1^2(x_{\bar{l}})}$$

where $\mathrm{Im}\,\mathscr{M}_2^{\overline{m}m}(r,\overline{\omega})$ is given by Eq. (B.21) (except for the factor of K_m^{-2}).

Appendix D

Collisionless heating for $v_{ph}/v_T \gg 1$

In the large frequency limit the heating due to passing particle resonance is exponentially small, thus the plasma heating is due to the trapped resonances:

$$\frac{dE}{dt} = \pi L n_0 \frac{|\delta\overline{\phi}|^2}{T} \sum_{n'=n_{\min}}^{\infty} k_{2n'} |C^l_{n'}|^2 v^2 \mathrm{F}_0(v)|_{v=\frac{\omega}{k_{2n'}}}, \quad n_{\min} = \lceil \tfrac{\omega}{k_2 v_s} \rceil \tag{D.1}$$

For $n_{\min} \gg 1$, from Eq. (2.26) we can approximate:

$$C^l_n \approx -\frac{m}{4n^2} \tag{D.2}$$

Defining the drive frequency $f = \omega/2\pi$, the trapped heating in the large frequency limit, substituting for F_0 from Eq. (1.8), in the limit $\omega/k_m v_T \gg 1$ can be written as

$$\frac{dE}{dt} = \sqrt{\frac{2}{\pi}} \frac{n_0}{m_q} |\delta\overline{\phi}|^2 \sum_{n'=\lceil \frac{Lf}{v_s} \rceil}^{\infty} \frac{L^2 f^2}{v_T^3} \frac{m^2}{4(n')^5} \exp\left(-\frac{f^2 L^2}{2(n')^2 v_T^2} \right) \tag{D.3}$$

We perform the change of dummy variable n' to $n + \lceil \frac{Lf}{v_s} \rceil$, and since $\frac{Lf}{v_s}$ is large, in the argument of the sum we substitute $\lceil \frac{Lf}{v_s} \rceil$ with $\frac{Lf}{v_s}$ to obtain:

$$\begin{aligned} \frac{dE}{dt} &= \sqrt{\frac{2}{\pi}} \frac{n_0}{m_q} |\delta\overline{\phi}|^2 \frac{m^2}{4v_T^3} \sum_{n=0}^{\infty} \frac{L^2 f^2}{(n + \frac{Lf}{v_s})^5} \exp\left(-\frac{f^2 L^2}{2(n + \frac{Lf}{v_s})^2 v_T^2} \right) \\ &= \sqrt{\frac{2}{\pi}} \frac{n_0}{m_q} |\delta\overline{\phi}|^2 \frac{m^2}{4v_T^3} \frac{v_s^4}{L^2 f^2} S(v_s/v_T), \end{aligned} \tag{D.4}$$

where we defined

$$S(v_s/v_T) = \sum_{n=0}^{\infty} \frac{1}{(1+t_n)^5} e^{-\frac{(v_s/v_T)^2}{2(1+t_n)^2}} (t_{n+1}-t_n) \tag{D.5}$$

$$t_n = \frac{n v_s}{Lf} \tag{D.6}$$

In the limit $\frac{Lf}{v_s} \to \infty$ we have $t_{n+1}-t_n = 1/\frac{Lf}{v_s} \to 0$, the above sum can be approximated by the Riemann integral as follows [7]

$$\begin{aligned} S(f) &= \int_0^{\infty} \frac{1}{(1+t)^5} e^{-\frac{(v_s/v_T)^2}{2(1+t)^2}} dt = \int_0^1 u^3 e^{-(\frac{v_s}{v_T})^2 \frac{u^2}{2}} du \\ &= 2\left(\frac{v_T}{v_s}\right)^4 \left[1-\left(1+\frac{1}{2}\left(\frac{v_s}{v_T}\right)^2\right) e^{-\frac{1}{2}\left(\frac{v_s}{v_T}\right)^2}\right] \end{aligned} \tag{D.7}$$

Thus, in the limit of large frequencies in which $v_{ph} = \omega/k_m \gg v_T$, we have

$$\frac{dE}{dt} = 2\sqrt{\frac{2}{\pi}} \frac{n_0}{m_q} |\delta\overline{\phi}|^2 \frac{v_T}{v_{ph}^2} \left[1-\left(1+\frac{1}{2}\left(\frac{v_s}{v_T}\right)^2\right) e^{-\frac{1}{2}\left(\frac{v_s}{v_T}\right)^2}\right], \quad \omega/k_m v_T \gg 1 \tag{D.8}$$

In the limit where $v_s/v_T \gg 1$, the exponential term in (D.8) will tend to zero. Therefore the heating will be of the form

$$\frac{dE}{dt} = \frac{2n_0|\delta\overline{\phi}|^2}{m_q} \sqrt{\frac{2}{\pi}} \frac{v_T}{v_{ph}^2} \tag{D.9}$$

In the limit where $v_s/v_T \ll 1$, we expand the exponential in D.8 to obtain

$$\begin{aligned} \frac{dE}{dt} &= \frac{2n_0|\delta\overline{\phi}|^2}{m_q} \sqrt{\frac{2}{\pi}} \frac{v_T}{v_{ph}^2} \left[1-\left(1+\frac{v_s^2}{2v_T^2}\right)\left(1-\frac{v_s^2}{2v_T^2}+\frac{v_s^4}{8v_T^4}+\ldots\right)\right] \\ &\approx \frac{n_0|\delta\overline{\phi}|^2}{m_q} \sqrt{\frac{2}{\pi}} \frac{v_s^4}{4v_{ph}^2 v_T^3} \end{aligned} \tag{D.10}$$

In summary, we have:

$$\frac{dE}{dt} = \frac{2n_0|\delta\overline{\phi}|^2}{m_q}\sqrt{\frac{2}{\pi}}\frac{v_T}{v_{ph}^2}, \quad v_{ph} \gg v_s \gg v_T \tag{D.11}$$

$$= \frac{n_0|\delta\overline{\phi}|^2}{m_q}\sqrt{\frac{2}{\pi}}\frac{v_s^4}{4v_{ph}^2 v_T^3}, \quad v_{ph} \gg v_T \gg v_s \tag{D.12}$$

Appendix E

Numerical grids method

We use the grids method to numerically solve for the linear distribution of finite length plasma with weak collisions and an applied squeeze which is infinitesimally narrow. We solve the following linearized Boltzmann equation to obtain the time independent part of the linear distribution function $\delta f(z,v)$ define in Eq. (2.10)

$$-i\omega\delta f + v\frac{\partial \delta f}{\partial v} + \frac{v}{T}\delta\varphi(z)\mathrm{F}_0(v) = D\frac{\partial}{\partial v}\left(\frac{\partial \delta f}{\partial v} + \frac{v}{T}\delta f\right) \tag{E.1}$$

where $\delta\varphi(z)$ is given by Eq. (2.6) and the diffusion coefficient D is taken to be a constant in all phase-space. The above equation is a PDE in z and v. We can descretize these independent variables in the above equation and solve for δf on a coarse-grained (z,v) phase-space. Grid point position coordinates in phase-space are given by

$$\begin{aligned} z_n &= n\Delta z - z_0, \quad n = -N+1,\ldots,N \\ v_m &= m\Delta v - v_0, \quad m = -M+1,\ldots,M \end{aligned} \tag{E.2}$$

where $\Delta z = L/(2N)$ and $\Delta v = V_{max}/M$ are the step sizes between grid points in position and velocity space, $z_0 = \Delta z/2$ and $v_0 = \Delta v/2$. At a constant velocity v_m, there are equal number of grid points $N/2$ on the left and right side of $z = 0$. The leftmost of which is $z_{-N+1} = -L + \Delta z/2$, which is the closest part of plasma near the left wall, and the right-most of which is $z_N = L - \Delta z/2$, closest the plasma gets to

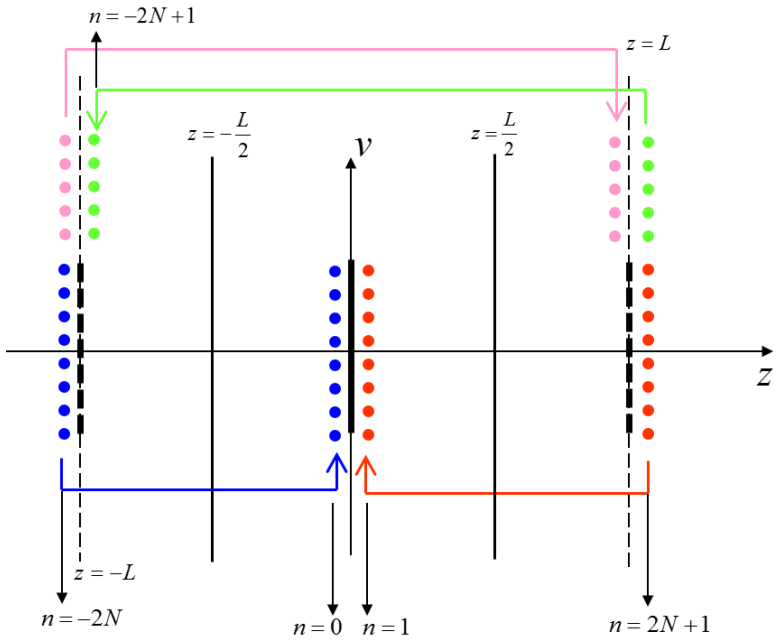

Figure E.1: Enforcing the periodic boundary condition on the grid point solutions outside the extended phase-space.

the right wall. V_{max} is an arbitrary velocity magnitude at which we approximate the value of δf to be given by the collisionless solution in Eq. (2.33), which must be far enough from the separatrix or resonances such that the boundary solution does not affect the solutions in the aforementioned regions.

Axial boundary conditions on the left and right wall and on the squeeze are all specular, given by Eqs. (2.4) and (2.41) Since trapped particles specularly reflect off of squeeze, back to their trap. Based on these boundary condition we construct the extended coarse-grained phase-space. Figure (E.1) describes the grid boundary positions and enforcing the boundary conditions which relate the value of δf at different grid points.

The linear PDE in equation (E.1) must become descretized by replacing all the partial derivatives with their descrete form, which we choose to be centered dif-

ference:

$$\begin{aligned}
\frac{\partial \delta f(z_n, v_m)}{\partial z} &= \frac{\delta f(z_n + \Delta z, v_m) - \delta f(z_n - \Delta z, v_m)}{2\Delta z} \\
&= \frac{\delta f(z_{n+1}, v_m) - \delta f(z_{n-1}, v_m)}{2\Delta z} \\
\frac{\partial \delta f(z_n, v_m)}{\partial v} &= \frac{\delta f(z_n, v_m + \Delta v) - \delta f(z_n, v_m - \Delta v)}{2\Delta v} \\
&= \frac{\delta f(z_{n+1}, v_{m+1}) - \delta f(z_n, v_{m-1})}{2\Delta v} \\
\frac{\partial^2 \delta f(z_n, v_m)}{\partial v^2} &= \frac{\delta f(z_n, v_{m+1}) - 2\delta f(z_n, v_m) + \delta f(z_n, v_{m-1})}{\Delta v^2}
\end{aligned} \tag{E.3}$$

Replacing the discrete derivatives in Eq. (E.1), this equation is transformed into a series of coupled, linear equations for $\delta f(x_n, v_m)$. There is an equation for each point inside the (extended) phase-space. We solve these equations over the constructed phase-space and its related boundary conditions. In the next step, the discrete solution is interpolated over the 2D phase-space to get a smooth and continuous solution. Furthermore, using Eq. (2.41) we can use the obtained $\delta f(z, v)$ to calculate the heating per unit time.

Appendix F

Numerical simulations of the fluid plasma

For our numerical simulation of cold fluid plasma we used the Mathematica software. We expand the density and velocity in terms of Fourier serier:

$$N(t) = 1 + \sum_{m=-M}^{M} \mathrm{n}_m(t) e^{i k_m z}, \quad v(t) = \sum_{m=-M}^{M} \mathrm{v}_m(t) e^{i k_m z} \tag{F.1}$$
$$\mathrm{n}_{-m}(t) = \mathrm{n}_m^*(t) \quad \mathrm{v}_{-m}(t) = \mathrm{v}_m^*(t)$$

Using the Fourier series expansions above we write the continuity and momentum equations as follows:

$$\frac{d}{dt}\mathrm{n}_m(t) = -i k_m \mathrm{v}_m(t) - i k_m \sum_{l=-M}^{M} \mathrm{n}_l(t)\mathrm{v}_{m-l}(t), \quad m = 1,2,\ldots,M \tag{F.2}$$

$$\frac{d}{dt}\mathrm{v}_m(t) = -i \sum_{l=-M}^{M} k_l \mathrm{v}_l(t)\mathrm{v}_{m-l}(t) - i\frac{\omega_m^2}{k_m}\mathrm{n}_m(t) + F_m(t), \quad m = 1,2,\ldots,M \tag{F.3}$$

with time scaled to ω_p^{-1}, mode ω_m are the linear mode frequencies:

$$\omega_m = \frac{k_m}{\sqrt{k_\perp^2 + k_m^2}}, \tag{F.4}$$

$F_m(t)$'s are the external forces coming from the external potential:

$$\begin{aligned} V^{\text{ext}}(z,t) &= \sum_{m=-M}^{M} V_m(t) e^{ik_m z} \\ F_m(t) &= -ik_m V_m(t), \end{aligned} \tag{F.5}$$

which we use to drive the system and excite waves. With initial conditions $n_m(t)=0$ and $v_m(t)=0$, we use the following functional form in time for the external potential:

$$V_m(t) = \overline{V}_m g^{\text{slow}}(t) g_m^{\text{fast}}(t)$$

$\overline{V}_m$ is the drive potential amplitude for mth spatial Fourier term. Slow variation of the drive potential over the forcing time T_F is given by

$$\begin{aligned} g^{\text{slow}}(t) &= \sin^2[2\pi t/T_F], \quad t < T_F/4 \\ &= 1, \quad T_F/4 < t < 3T_F/4 \\ &= \sin^2[2\pi t/T_F], \quad 3/4\,T_F < t < T_F \\ &= 0, \quad t > T_F \end{aligned}$$

Fast time variation of the drive potential is given by the following time functions, depending on the type of the wave desired, traveling or standing with zero force at the plasma ends $d\phi/dz=0$:

$$\begin{aligned} g_m^{\text{fast}}(t) &= \cos[\omega_m t] \quad \text{standing waves} \\ g_m^{\text{fast}}(t) &= e^{-i\omega_m t} \quad \text{traveling waves} \end{aligned}$$

We were specifically interested in the wave wave interaction of TG modes 1 and 2. Therefore, in accordance with the experiments, we choose our drive potential amplitudes to be

$$V_2 = b, \quad V_1 = \epsilon b, \quad V_m = 0, m \neq 12 \tag{F.6}$$

Above choice of amplitudes includes mode 2 with amplitude b, and mode 1 with its amplitude being a small fraction of mode 2 ($10^{-7} \leq \epsilon \leq 10^{-2}$) as a seed.

Appendix G

Details of mode frequency calculation for section 3.3

We will evaluate the last two terms of Eq. (3.122):

$$
\begin{aligned}
&[v^{(2)}v^{(1)}]_l = \sum_m v_m^{(2)} v_{l-m}^{(1)} \\
&= \sum_m \Bigg(\sum_q Y_{m,q} \Big[n_q n_{m-q} e^{-i(\omega_q+\omega_{m-q})\tau_0} - n_q^* n_{m-q}^* e^{i(\omega_q+\omega_{m-q})\tau_0} \Big] \\
&- \sum_q Z_{m,q} \Big[n_q n_{m-q}^* e^{i(\omega_{m-q}-\omega_q)\tau_0} - n_q^* n_{m-q} e^{-i(\omega_{m-q}-\omega_q)\tau_0} \Big] \Bigg) \\
&\times \Big(\tfrac{\omega_{l-m}}{k_{l-m}} n_{l-m} e^{-i\omega_{l-m}\tau_0} - \tfrac{\omega_{l-m}}{k_{l-m}} n_{l-m}^* e^{i\omega_{l-m}\tau_0} \Big) \\
&= \sum_{m,q} \tfrac{\omega_{l-m}}{k_{l-m}} Y_{m,q} [n_q n_{m-q} n_{l-m} e^{-i(\omega_q+\omega_{m-q}+\omega_{l-m})\tau_0} - n_q n_{m-q} n_{l-m}^* e^{-i(\omega_q+\omega_{m-q}-\omega_{l-m})\tau_0} \\
&- n_q^* n_{m-q}^* n_{l-m} e^{i(\omega_q+\omega_{m-q}-\omega_{l-m})\tau_0} + n_q^* n_{m-q}^* n_{l-m}^* e^{i(\omega_q+\omega_{m-q}+\omega_{l-m})\tau_0}] \\
&- \sum_{m,q} \tfrac{\omega_{l-m}}{k_{l-m}} Z_{m,q} [n_q n_{m-q}^* n_{l-m} e^{-i(\omega_q-\omega_{m-q}+\omega_{l-m})\tau_0} - n_q^* n_{m-q} n_{l-m} e^{i(\omega_q-\omega_{m-q}-\omega_{l-m})\tau_0} \\
&- n_q n_{m-q}^* n_{l-m}^* e^{-i(\omega_q-\omega_{m-q}+\omega_{l-m})\tau_0} + n_q^* n_{m-q} n_{l-m}^* e^{i(\omega_q-\omega_{m-q}+\omega_{l-m})\tau_0}]
\end{aligned}
\tag{G.1}
$$

Index change:

$$
\begin{aligned}
&-\sum_{m,q}\frac{\omega_{l-m}}{k_{l-m}}Z_{m,q}[n_q n^*_{m-q} n_{l-m} e^{-i(\omega_q-\omega_{m-q}+\omega_{l-m})\tau_0} + n^*_q n_{m-q} n^*_{l-m} e^{i(\omega_q-\omega_{m-q}+\omega_{l-m})\tau_0}] \\
&=-\sum_{m,q}\frac{\omega_{l-m}}{k_{l-m}}Z_{m,m-q}[n^*_q n_{m-q} n_{l-m} e^{-i(-\omega_q+\omega_{m-q}+\omega_{l-m})\tau_0} \\
&+n_q n^*_{m-q} n^*_{l-m} e^{i(-\omega_q+\omega_{m-q}+\omega_{l-m})\tau_0}], \quad (q\to m-q)
\end{aligned}
$$

Index change:

$$
\begin{aligned}
&\sum_{m,q}\frac{\omega_{l-m}}{k_{l-m}}Y_{m,q}[-n_q n_{m-q} n^*_{l-m} e^{-i(\omega_q+\omega_{m-q}-\omega_{l-m})\tau_0} - n^*_q n^*_{m-q} n_{l-m} e^{i(\omega_q+\omega_{m-q}-\omega_{l-m})\tau_0}] \\
&=\sum_{m,q}\frac{\omega_q}{k_q}Y_{l-q,l-m}[-n_{l-m} n_{m-q} n^*_q e^{-i(\omega_{l-m}+\omega_{m-q}-\omega_q)\tau_0} - n^*_{l-m} n^*_{m-q} n_q e^{i(\omega_{l-m}+\omega_{m-q}-\omega_q)\tau_0}] \\
&\quad (q\to l-m, m\to l-q)
\end{aligned}
$$

Finally

$$
\begin{aligned}
&[v^{(2)}v^{(1)}]_l = \sum_{m,q}\frac{\omega_{l-m}}{k_{l-m}}Y_{m,q}[n_q n_{m-q} n_{l-m} e^{-i(\omega_q+\omega_{m-q}+\omega_{l-m})\tau_0} + n^*_q n^*_{m-q} n^*_{l-m} e^{i(\omega_q+\omega_{m-q}+\omega_{l-m})\tau_0}] \\
&+\sum_{m,q}[\frac{\omega_{l-m}}{k_{l-m}}Z_{m,q} - \frac{\omega_{l-m}}{k_{l-m}}Z_{m,m-q} - \frac{\omega_q}{k_q}Y_{l-q,l-m}] \\
&\times\left(n_{l-m} n_{m-q} n^*_q e^{-i(\omega_{l-m}+\omega_{m-q}-\omega_q)\tau_0} + n^*_{l-m} n^*_{m-q} n_q e^{i(\omega_{l-m}+\omega_{m-q}-\omega_q)\tau_0}\right) \qquad \text{(G.2)}
\end{aligned}
$$

Next term:

$$
\begin{aligned}
&[v^{(2)}n^{(1)}]_l = \sum_m v_m^{(2)} n_{l-m}^{(1)} \\
&= \sum_m \Bigg(\sum_q Y_{m,q} \Big[n_q n_{m-q} e^{-i(\omega_q+\omega_{m-q})\tau_0} - n_q^* n_{m-q}^* e^{i(\omega_q+\omega_{m-q})\tau_0} \Big] \\
&- \sum_q Z_{m,q} \Big[n_q n_{m-q}^* e^{i(\omega_{m-q}-\omega_q)\tau_0} - n_q^* n_{m-q} e^{-i(\omega_{m-q}-\omega_q)\tau_0} \Big] \Bigg) \Big(n_{l-m} e^{-i\omega_{l-m}\tau_0} + n_{l-m}^* e^{i\omega_{l-m}\tau_0} \Big) \\
&= \sum_{m,q} Y_{m,q} [n_q n_{m-q} n_{l-m} e^{-i(\omega_q+\omega_{m-q}+\omega_{l-m})\tau_0} + n_q n_{m-q} n_{l-m}^* e^{-i(\omega_q+\omega_{m-q}-\omega_{l-m})\tau_0} \\
&- n_q^* n_{m-q}^* n_{l-m} e^{i(\omega_q+\omega_{m-q}-\omega_{l-m})\tau_0} - n_q^* n_{m-q}^* n_{l-m}^* e^{i(\omega_q+\omega_{m-q}+\omega_{l-m})\tau_0}] \\
&- \sum_{m,q} Z_{m,q} [n_q n_{m-q}^* n_{l-m} e^{-i(\omega_q-\omega_{m-q}+\omega_{l-m})\tau_0} - n_q^* n_{m-q} n_{l-m} e^{i(\omega_q-\omega_{m-q}-\omega_{l-m})\tau_0} \\
&n_q n_{m-q}^* n_{l-m}^* e^{-i(\omega_q-\omega_{m-q}+\omega_{l-m})\tau_0} - n_q^* n_{m-q} n_{l-m}^* e^{i(\omega_q-\omega_{m-q}+\omega_{l-m})\tau_0}]
\end{aligned}
\tag{G.3}
$$

We do an index change:

$$
\begin{aligned}
&\sum_{m,q} Y_{m,q} [n_q n_{m-q} n_{l-m}^* e^{-i(\omega_q+\omega_{m-q}-\omega_{l-m})\tau_0} - n_q^* n_{m-q}^* n_{l-m} e^{i(\omega_q+\omega_{m-q}-\omega_{l-m})\tau_0}] \\
&= \sum_{u,v} Y_{l-u,l-v} [n_{l-v} n_{v-u} n_u^* e^{-i(\omega_{l-v}+\omega_{v-u}-\omega_u)\tau_0} - n_{l-v}^* n_{v-u}^* n_u e^{i(\omega_{l-v}+\omega_{v-u}-\omega_u)\tau_0}] \\
&, \quad (m \to l-u, q \to l-v) \\
&= \sum_{m,q} Y_{l-q,l-m} [n_{l-m} n_{m-q} n_q^* e^{-i(\omega_{l-m}+\omega_{m-q}-\omega_q)\tau_0} - n_{l-m}^* n_{m-q}^* n_q e^{i(\omega_{l-m}+\omega_{m-q}-\omega_q)\tau_0}] \\
&, \quad (u \to q, v \to m)
\end{aligned}
$$

We do an index change:

$$
\begin{aligned}
&\sum_{m,q} Z_{m,q} [n_q n_{m-q}^* n_{l-m} e^{-i(\omega_q-\omega_{m-q}+\omega_{l-m})\tau_0} - n_q^* n_{m-q} n_{l-m}^* e^{i(\omega_q-\omega_{m-q}+\omega_{l-m})\tau_0}] \\
&= \sum_{m,q} Z_{m,m-q} [n_{m-q} n_q^* n_{l-m} e^{-i(\omega_{m-q}-\omega_q+\omega_{l-m})\tau_0} - n_{m-q}^* n_q n_{l-m}^* e^{i(\omega_{m-q}-\omega_q+\omega_{l-m})\tau_0}] \\
&, \quad (q \to m-q)
\end{aligned}
$$

Finally:

$$
\begin{aligned}
&[v^{(2)}n^{(1)}]_l = \sum_{m,q} Y_{m,q}[n_q n_{m-q} n_{l-m} e^{-i(\omega_q+\omega_{m-q}+\omega_{l-m})\tau_0} \\
&-n_q^* n_{m-q}^* n_{l-m}^* e^{i(\omega_q+\omega_{m-q}+\omega_{l-m})\tau_0} \\
&+\sum_{m,q}(Y_{l-q,l-m}+Z_{m,q}-Z_{m,m-q})[n_{m-q} n_{l-m} n_q^* e^{-i(\omega_{m-q}-\omega_q+\omega_{l-m})\tau_0} \\
&-n_{m-q}^* n_{l-m}^* n_q e^{i(\omega_{m-q}-\omega_q+\omega_{l-m})\tau_0}]
\end{aligned}
\tag{G.4}
$$

Next term:

$$
\begin{aligned}
&[n^{(2)}v^{(1)}]_l = \sum_m n_m^{(2)} v_{l-m}^{(1)} \\
&= \sum_m \Bigg(\sum_q W_{m,q}\left[n_q n_{m-q} e^{-i(\omega_q+\omega_{m-q})\tau_0} + n_q^* n_{m-q}^* e^{i(\omega_q+\omega_{m-q})\tau_0}\right] \\
&+\sum_q V_{m,q}\left[n_q n_{m-q}^* e^{i(\omega_{m-q}-\omega_q)\tau_0} + n_q^* n_{m-q} e^{-i(\omega_{m-q}-\omega_q)\tau_0}\right]\Bigg) \\
&\times\left(\tfrac{\omega_{l-m}}{k_{l-m}} n_{l-m} e^{-i\omega_{l-m}\tau_0} - \tfrac{\omega_{l-m}}{k_{l-m}} n_{l-m}^* e^{i\omega_{l-m}\tau_0}\right) \\
&= \sum_{m,q} \tfrac{\omega_{l-m}}{k_{l-m}} W_{m,q}[n_q n_{m-q} n_{l-m} e^{-i(\omega_q+\omega_{m-q}+\omega_{l-m})\tau_0} - n_q n_{m-q} n_{l-m}^* e^{-i(\omega_q+\omega_{m-q}-\omega_{l-m})\tau_0} \\
&+n_q^* n_{m-q}^* n_{l-m} e^{i(\omega_q+\omega_{m-q}-\omega_{l-m})\tau_0} - n_q^* n_{m-q}^* n_{l-m}^* e^{i(\omega_q+\omega_{m-q}+\omega_{l-m})\tau_0}] \\
&+\sum_{m,q} \tfrac{\omega_{l-m}}{k_{l-m}} V_{m,q}[n_q n_{m-q}^* n_{l-m} e^{-i(\omega_q-\omega_{m-q}+\omega_{l-m})\tau_0} + n_q^* n_{m-q} n_{l-m} e^{i(\omega_q-\omega_{m-q}-\omega_{l-m})\tau_0} \\
&-n_q n_{m-q}^* n_{l-m}^* e^{-i(\omega_q-\omega_{m-q}+\omega_{l-m})\tau_0} - n_q^* n_{m-q} n_{l-m}^* e^{i(\omega_q-\omega_{m-q}+\omega_{l-m})\tau_0}]
\end{aligned}
\tag{G.5}
$$

We do an index change:

$$
\begin{aligned}
&\sum_{m,q} \tfrac{\omega_{l-m}}{k_{l-m}} V_{m,q}[n_q n_{m-q}^* n_{l-m} e^{-i(\omega_q-\omega_{m-q}+\omega_{l-m})\tau_0} - n_q^* n_{m-q} n_{l-m}^* e^{i(\omega_q-\omega_{m-q}+\omega_{l-m})\tau_0}] \\
&= \sum_{m,q} \tfrac{\omega_{l-m}}{k_{l-m}} V_{m,m-q}[n_q^* n_{m-q} n_{l-m} e^{-i(-\omega_q+\omega_{m-q}+\omega_{l-m})\tau_0} - n_q n_{m-q}^* n_{l-m}^* e^{i(-\omega_q+\omega_{m-q}+\omega_{l-m})\tau_0}] \\
&, \quad (q \to m-q)
\end{aligned}
$$

We do an index change:

$$\sum_{m,q} \frac{\omega_{l-m}}{k_{l-m}} W_{m,q}[n_q n_{m-q} n^*_{l-m} e^{-i(\omega_q+\omega_{m-q}-\omega_{l-m})\tau_0} - n^*_q n^*_{m-q} n_{l-m} e^{i(\omega_q+\omega_{m-q}-\omega_{l-m})\tau_0}]$$
$$= \sum_{m,q} \frac{\omega_q}{k_q} W_{l-q,l-m}[n_{l-m} n_{m-q} n^*_q e^{-i(\omega_{l-m}+\omega_{m-q}-\omega_q)\tau_0} - n^*_{l-m} n^*_{m-q} n_q e^{i(\omega_{l-m}+\omega_{m-q}-\omega_q)\tau_0}]$$
$$, \quad (q \to l-m, m \to l-q)$$

Finally

$$[n^{(2)} v^{(1)}]_l = \sum_{m,q} \frac{\omega_{l-m}}{k_{l-m}} W_{m,q}[n_q n_{m-q} n_{l-m} e^{-i(\omega_q+\omega_{m-q}+\omega_{l-m})\tau_0} - n^*_q n^*_{m-q} n^*_{l-m} e^{i(\omega_q+\omega_{m-q}+\omega_{l-m})\tau_0}]$$
$$+ \sum_{m,q} [\frac{\omega_{l-m}}{k_{l-m}} V_{m,q} + \frac{\omega_{l-m}}{k_{l-m}} V_{m,m-q} - \frac{\omega_q}{k_q} W_{l-q,l-m}]$$
$$\times \left(n_{l-m} n_{m-q} n^*_q e^{-i(\omega_{l-m}+\omega_{m-q}-\omega_q)\tau_0} - n^*_{l-m} n^*_{m-q} n_q e^{i(\omega_{l-m}+\omega_{m-q}-\omega_q)\tau_0} \right) \tag{G.6}$$

Using (G.6), (G.4) we write:

$$[n^{(2)} v^{(1)} + v^{(2)} n^{(1)}]_l \tag{G.7}$$
$$= \sum_{m,q} \left(\frac{\omega_{l-m}}{k_{l-m}} (V_{m,q} + V_{m,m-q}) - \frac{\omega_q}{k_q} W_{l-q,l-m} + (Y_{l-q,l-m} + Z_{m,q} - Z_{m,m-q}) \right)$$
$$\times [n_{l-m} n_{m-q} n^*_q e^{i(\omega_q-\omega_{l-m}-\omega_{m-q})\tau_0} - n^*_{l-m} n^*_{m-q} n_q e^{-i(\omega_q-\omega_{l-m}-\omega_{m-q})\tau_0}]$$
$$+ \sum_{m,q} \left(Y_{m,q} + \frac{\omega_{l-m}}{k_{l-m}} W_{m,q} \right) [n_q n_{m-q} n_{l-m} e^{-i(\omega_q+\omega_{m-q}+\omega_{l-m})\tau_0} - n^*_q n^*_{m-q} n^*_{l-m} e^{i(\omega_q+\omega_{m-q}+\omega_{l-m})\tau_0}]$$

In (G.7) and (G.2) there are two types of terms. For the first type which have the form:

$$n_{l-m} n_{m-q} n_q e^{-i(\omega_q+\omega_{m-q}+\omega_{l-m})\tau_0}, \tag{G.8}$$

the secular terms for which $\omega_q + \omega_{l-m} + \omega_{m-q} = \pm\omega_l$ happen if:

$$q = l, m-l \Rightarrow$$
$$n_{l-m} n_{m-q} n_q e^{-i(\omega_q+\omega_{l-m}+\omega_{m-q})\tau_0} = |n_{m-l}|^2 n_l e^{-i\omega_l\tau_0}$$
$$n^*_{l-m} n^*_{m-q} n^*_q e^{i(\omega_q+\omega_{l-m}+\omega_{m-q})\tau_0} = |n_{m-l}|^2 n^*_l e^{i\omega_l\tau_0}$$

The second type of terms have the form $n_{l-m}n_{m-q}n_q^* e^{i(\omega_q-\omega_{l-m}-\omega_{m-q})\tau_0}$ and its complex conjugate. The only secular terms for which $\omega_q-\omega_{l-m}-\omega_{m-q}=\pm\omega_l$, comes from the $q=l$ term

$$
\begin{aligned}
&q=l\Rightarrow\\
&n_{l-m}n_{m-q}n_q^* e^{i(\omega_q-\omega_{l-m}-\omega_{m-q})\tau_0}=|n_{m-l}|^2 n_l^* e^{i\omega_l\tau_0}\\
&n_{l-m}^* n_{m-q}^* n_q e^{-i(\omega_q-\omega_{l-m}-\omega_{m-q})\tau_0}=|n_{m-l}|^2 n_l e^{-i\omega_l\tau_0}
\end{aligned}
$$

The non-secular terms for which $\omega_q-\omega_{l-m}-\omega_{m-q}\neq\pm\omega_l$ contribute to third order oscillations. Keeping only the secular terms in Eq. (G.7) we get:

$$
\begin{aligned}
&[n^{(2)}v^{(1)}+v^{(2)}n^{(1)}]_l \qquad\qquad (G.9)\\
&=\sum_m\Bigg(\tfrac{\omega_{l-m}}{k_{l-m}}[V_{m,l}+V_{m,m-l}]+Z_{m,l}-Z_{m,m-l}\\
&-\tfrac{\omega_{l-m}}{k_{l-m}}[W_{m,l}+\overline{\delta}_{m,2l}W_{m,m-l}]-Y_{m,l}-\overline{\delta}_{m,2l}Y_{m,m-l}\Bigg)\left[|n_{l-m}|^2 n_l^* e^{i\omega_l\tau_0}-|n_{l-m}|^2 n_l e^{-i\omega_l\tau_0}\right]
\end{aligned}
$$

We defined the function $\overline{\delta}_{i,j}$ to avoid double counting:

$$
\overline{\delta}_{i,j}=1-\delta_{i,j}, \qquad\qquad (G.10)
$$

where $\delta_{i,j}$ is the Kronecker delta. Keeping only the secular terms in Eq. (G.2) we get:

$$
\begin{aligned}
&[v^{(2)}v^{(1)}]_l \qquad\qquad (G.11)\\
&=\sum_m\tfrac{\omega_{l-m}}{k_{l-m}}(Z_{m,l}-Z_{m,m-l}+Y_{m,l}+\overline{\delta}_{m,2l}Y_{m,m-l})\left[|n_{l-m}|^2 n_l^* e^{i\omega_l\tau_0}+|n_{l-m}|^2 n_l e^{-i\omega_l\tau_0}\right]
\end{aligned}
$$

We substitute (G.9) and (G.11) in (3.122) and setting the secular terms to zero results in the following relation and its complex conjugate:

$$
\begin{aligned}
&-\partial_{\tau_2}n_l+i\tfrac{k_l}{2}\sum_m\Bigg\{\tfrac{\omega_{l-m}}{k_{l-m}}(V_{m,l}+V_{m,m-l}-W_{m,l}-\overline{\delta}_{m,2l}W_{m,m-l})\\
&+(Z_{m,l}-Z_{m,m-l}-Y_{m,l}-\overline{\delta}_{m,2l}Y_{m,m-l})\\
&-\tfrac{k_l}{\omega_l}\tfrac{\omega_{l-m}}{k_{l-m}}[Z_{m,l}-Z_{m,m-l}+Y_{m,l}+\overline{\delta}_{m,2l}Y_{m,m-l}]\Bigg\}|n_{l-m}|^2 n_l=0
\end{aligned}
$$

which can be rearanged as:

$$-\partial_{\tau_2} n_l + i\frac{k_l}{2}\sum_m \Big\{ \frac{\omega_{l-m}}{k_{l-m}}(V_{m,l} + V_{m,m-l} - W_{m,l} - \overline{\delta}_{m,2l}\, W_{m,m-l}) + [1 - \frac{k_l}{\omega_l}\frac{\omega_{l-m}}{k_{l-m}}](Z_{m,l} - Z_{m,m-l})]$$
$$-[1 + \frac{k_l}{\omega_l}\frac{\omega_{l-m}}{k_{l-m}}](Y_{m,l} + \overline{\delta}_{m,2l}\, Y_{m,m-l})\Big\} |n_{l-m}|^2 n_l = 0$$

Appendix H

Wave-wave interaction in the RZ fluid model

We start from 2D, r, z fluid equations coupled with Poisson equation:

$$\partial_t N + \partial_z (N v) = 0 \text{(continuity)}, \tag{H.1}$$

$$\partial_t v + v \partial_z v = -\partial_z \phi - T \frac{\partial_z N}{N}, \text{ (momentum)} \tag{H.2}$$

$$(\frac{1}{r}\partial_r r \partial_r + \partial_z^2)\phi = -N \text{ (Poisson)}. \tag{H.3}$$

We only use the pressure force term (second term on the right-hand side of Eq. (H.2)) for obtaining the equilibrium density profile and for the rest of our calculation we neglect this term due to coldness of plasma. In the above equations:

$$v = v(r, z, t), \quad N = N(r, z, t), \quad \phi = \phi(r, z, t). \tag{H.4}$$

Time is scaled to plasma frequency $\omega_p^2 = 4\pi q^2 n_0 / m_q$ and plasma density has been scaled to the maximum equilibrium density n_0, which is the density on the axis of cylinder, at $r = 0$. We expand the spatial dependence of the variables in terms of

Fourier series:

$$
\begin{aligned}
v(r,z,t) &= \sum_{m=-\infty}^{\infty} \mathrm{v}_m(r,t) e^{ik_m z}, \\
N(r,z,t) &= N_0(r)\left[1 + \sum_{m=-\infty}^{\infty} \mathrm{n}_m(r,t) e^{ik_m z}\right], \\
\phi(r,z,t) &= \phi_0(r) + \sum_{m=-\infty}^{\infty} \phi_m(r,t) e^{ik_m z}.
\end{aligned}
\tag{H.5}
$$

$\phi_0(r)$ is the equilibrium potential, we assume $v_0(r) = 0$ and $N_0(r)$ is the equilibrium density, scaled to its maximum at $r = 0$. The equilibrium density and potential profile for the system is obtained through solving the following equations:

$$
-\partial_z \phi - T(r)\frac{\partial_z N_0}{N_0} = 0, \tag{H.6}
$$

$$
\frac{1}{r}\partial_r r \partial_r \phi_0(r) = -N_0(r). \tag{H.7}
$$

We multiply Eq. (H.1) through Eq. (H.3) by $\frac{1}{L}e^{-ik_l z}$ and integrate over the length of the plasma L and use the Fourier expansions given in Eq.'s (H.5). From the Poisson equation Eq. (H.3) we obtain:

$$
[k_\perp^2 + k_l^2]\phi_l = \mathrm{n}_l. \tag{H.8}
$$

We use the following relation in the continuity equation (H.1):

$$
\begin{aligned}
&\frac{1}{L}\int_0^L \partial_z[(N(r,z,t)-1)\mathrm{v}(r,z,t)]e^{-ik_l z}\,dz \\
&= ik_l \sum_{m=-\infty}^{\infty}\sum_{m'=-\infty}^{\infty} \frac{1}{L}\int_0^L \mathrm{n}_m \mathrm{v}_{m'} e^{i(k_m + k_{m'} - k_l)z}\,dz = ik_l \sum_{m=-\infty}^{\infty} \mathrm{n}_m \mathrm{v}_{l-m},
\end{aligned}
$$

We use the following relation in the momentum equation (H.2):

$$
\begin{aligned}
&\frac{1}{L}\int_0^L [\mathrm{v}(r,z,t)\partial_z \mathrm{v}(r,z,t)]e^{-ik_l z}\,dz \\
&= \sum_{m=-\infty}^{\infty}\sum_{m'=-\infty}^{\infty} \frac{1}{L}\int_0^L \mathrm{v}_m e^{ik_m z} ik_m \mathrm{v}_{m'} e^{i(k_m + k_{m'} - k_l)z}\,dz = i\sum_{m=-\infty}^{\infty} k_m \mathrm{v}_m \mathrm{v}_{l-m},
\end{aligned}
$$

As a result we obtain the exact equations

$$\frac{d}{dt}\mathrm{n}_l + ik_l\mathrm{v}_l + ik_l\sum_{m=-\infty}^{\infty}\mathrm{n}_m\mathrm{v}_{l-m} = 0, \tag{H.9}$$

$$\frac{d}{dt}\mathrm{v}_l + i\sum_{m=-\infty}^{\infty}k_m\mathrm{v}_m\mathrm{v}_{l-m} = -ik_l\phi_l, \tag{H.10}$$

where we used Eq. (H.8) on the right hand side of Eq. (H.10). Using multiple time-scale expansion, we assume weak nonlinearity and propose the following solution forms for all m:

$$\begin{aligned}\mathrm{v}_m &= \varepsilon v_m^{(1)} + \varepsilon^2 v_m^{(2)} + \varepsilon^3 v_m^{(3)} + \ldots, \\ \mathrm{n}_m &= \varepsilon n_m^{(1)} + \varepsilon^2 n_m^{(2)} + \varepsilon^3 n_m^{(3)} + \ldots, \\ \phi_m &= \varepsilon \phi_m^{(1)} + \varepsilon^2 \phi_m^{(2)} + \varepsilon^3 \phi_m^{(3)} + \ldots.\end{aligned} \tag{H.11}$$

Multiple timescales have the following hierarchy:

$$\tau_0 = t, \quad \tau_1 = \varepsilon t, \quad \tau_2 = \varepsilon^2 t, \ldots \tag{H.12}$$

$$\frac{d}{dt} = \frac{\partial}{\partial\tau_0} + \varepsilon\frac{\partial}{\partial\tau_1} + \varepsilon^2\frac{\partial}{\partial\tau_2} + \ldots. \tag{H.13}$$

To the first order in ε, Eqs. (H.1) through (H.3) give:

$$\partial_{\tau_0} n_m^{(1)} + ik_m v_m^{(1)} = 0, \tag{H.14}$$

$$\partial_{\tau_0} v_m^{(1)} = -ik_m\phi_m^{(1)}, \tag{H.15}$$

$$\left[-\nabla_r^2 + k_l^2\right]\phi_l^{(1)} = N_0(r)n_l^{(1)}. \tag{H.16}$$

From Eqs. (H.14) and (H.15) we get

$$\partial_{\tau_0}^2 n_m^{(1)} + k_m^2\phi_m^{(1)} = 0. \tag{H.17}$$

For traveling modes, the linear solutions with axial Fourier number m is of the form:

$$n_m^{(1)}(r;\tau_0,\tau_1) = n_m(r;\tau_1)e^{-i\omega_m\tau_0}, \tag{H.18}$$

$$\phi_m^{(1)}(r;\tau_0,\tau_1) = \phi_m(r;\tau_1)e^{-i\omega_m\tau_0}, \tag{H.19}$$

with ω_m, the mode frequency to be determined. The amplitude of the linear traveling mode in the laboratory is defined by:

$$\begin{aligned} n_m^t(r,z;t) &= A_m^t(r;t)\cos[k_m z - \omega_m t + \alpha_m(t)] \\ &= \frac{A_m^t(r;t)}{2}\left[e^{-i(k_m z-\omega_m\tau_0+\alpha_m(t))} + e^{i(k_m z-\omega_m\tau_0+\alpha_m(t))}\right] \\ &= n_m(r;\tau_1)e^{i(k_m z-\omega_m\tau_0)} + n_m^*(r;\tau_1)e^{-i(k_m z-\omega_m\tau_0)}. \end{aligned} \tag{H.20}$$

Thus we have:

$$n_m(r;\tau_1) = \frac{A_m^t(r;t)}{2}e^{i\alpha_m(t)}. \tag{H.21}$$

From (H.14) and (H.18) we obtain $v_m^{(1)}$:

$$v_m^{(1)} = \frac{\omega_m}{k_m}n_m(r;\tau_1)e^{-i\omega_m\tau_0}. \tag{H.22}$$

which gives:

$$v_m^t(r,z,t) = v_m^{(1)}e^{ik_m z} + v_{-m}^{(1)}e^{-ik_m z} = \frac{\omega_m}{k_m}A_m^t(r;t)\cos[k_m z - \omega_m t + \alpha_m(t)]. \tag{H.23}$$

For standing modes, the linear solutions with axial Fourier number m is of the form:

$$n_m^{(1)}(r;\tau_0,\tau_1) = n_m(r;\tau_1)e^{-i\omega_m\tau_0} + n_m^*(r;\tau_1)e^{i\omega_m\tau_0}, \tag{H.24}$$

$$\phi_m^{(1)}(r;\tau_0,\tau_1) = \phi_m(r;\tau_1)e^{-i\omega_m\tau_0} + \phi_m^*(r;\tau_1)e^{i\omega_m\tau_0}, \tag{H.25}$$

with ω_m, the mode frequency to be determined. The amplitude of the linear standing mode in the laboratory is defined by:

$$\begin{aligned} n_m^s(r,z;t) &= A_m^s(r;t)\cos[\omega_m t-\alpha_m(t)]\cos[k_m z] \\ &= \frac{A_m^s(r;t)}{4}\left[e^{-i(\omega_m\tau_0-\alpha_m(t))}+e^{i(\omega_m\tau_0-\alpha_m(t))}\right]\left[e^{ik_m z}+e^{-ik_m z}\right] \\ &= [n_m(r;\tau_1)e^{-i\omega_m\tau_0}+n_m^*(r;\tau_1)e^{i\omega_m\tau_0}]\left[e^{ik_m z}+e^{-ik_m z}\right]. \end{aligned} \tag{H.26}$$

Thus we have:

$$n_m(r;\tau_1)=\frac{A_m^s(r;t)}{4}e^{i\alpha_m(t)}. \tag{H.27}$$

From Eqs. (H.14) and (H.24) we obtain $v_m^{(1)}$:

$$v_m^{(1)}=\frac{\omega_m}{k_m}n_m(r;\tau_1)e^{-i\omega_m\tau_0}-\frac{\omega_m}{k_m}n_m^*(r;\tau_1)e^{i\omega\tau_0}, \tag{H.28}$$

which gives:

$$v_m^s(r,z,t)=v_m^{(1)}e^{ik_m z}+v_{-m}^{(1)}e^{-ik_m z}=\frac{\omega_m}{k_m}A_m^s(r;t)\sin[\omega_m t-\alpha_m(t)]\sin[k_m z]. \tag{H.29}$$

From (H.16) and (H.17) we obtain the dispersion relation:

$$\left[-\nabla_r^2+k_m^2-\left(\frac{k_m}{\omega}\right)^2 N_0(r)\right]\phi_m(r;\tau_1)=0. \tag{H.30}$$

Solving the above eigenvalue equation determines mode frequency and radial profile of the eigenmodes. Solution to the above equation is of the form:

$$\phi_m(r;\tau_1)=\overline{\phi}_{m,q}(\tau_1)R_{m,q}(r),\quad q=1,2,\ldots. \tag{H.31}$$

In the above equation, subscripts q and m respectively correspond to different radial and axial mode numbers of the mode $\mu=(m,q)$ with eigenfrequency $\omega_{m,l}$. $\overline{\phi}_{m,l}(\tau_1)$ is the complex linear mode amplitude which evolves in slow timescale τ_1.

We can show that $R_{m,q}(r)$'s are orthonormal. Starting from:

$$\left[-\nabla_r^2 + k_m^2 - \left(\frac{k_m}{\omega_{m,l}}\right)^2 N_0(r)\right] R_{m,q}(r) = 0, \tag{H.32}$$

$$\left[-\nabla_r^2 + k_m^2 - \left(\frac{k_m}{\omega_{m,n}}\right)^2 N_0(r)\right] R_{m,\overline{q}}(r) = 0. \tag{H.33}$$

Multiplying Eq. (H.32) by $r R_{m,\overline{q}}(r)$ and Eq. (H.33) by $r R_{m,q}(r)$, subtracting Eq. (H.33) from Eq. (H.32) and integrating from 0 to r_w we get:

$$\begin{aligned} &k_l^2 \left[\frac{1}{\omega_{m,\overline{q}}^2} - \frac{1}{\omega_{m,q}^2}\right] \int_0^{r_w} N_0(r) R_{m,q}(r) R_{m,\overline{q}}(r) r\, dr \\ &= \int_0^{r_w} dr\, \partial_r \left(R_{m,q}(r) \partial_r R_{m,\overline{q}}(r) - R_{m,\overline{q}}(r) \partial_r R_{m,q}(r)\right) = 0. \end{aligned} \tag{H.34}$$

The right hand side is zero, since $R_{l,q}(r)$ and $R_{l,\overline{q}}(r)$ are zero at the wall. Thus we arrive at the following orthogonality condition:

$$\int_0^{r_w} N_0(r) R_{m,q}(r) R_{m,\overline{q}}(r) r\, dr = \delta_{q,\overline{q}}. \tag{H.35}$$

For cold plasmas, modes with radial mode number $q = 1$ are undamped while modes with $q > 1$ have lower frequencies and are heavily damped(see Ref. 5). Thus for longer times, we ignore the linear modes with $q > 1$ and we only keep the linear modes $\mu = (m, 1)$:

$$\phi_m(r;\tau_1) = \overline{\phi}_{m,1}(\tau_1) R_{m,1}(r), \tag{H.36}$$

$$n_m(r;\tau_1) = \overline{n}_{m,1}(\tau_1) R_{m,1}(r), \tag{H.37}$$

$$n_m^{(1)} = n_m(r;\tau_1) e^{-i\omega_{m,1}\tau_0} + n_m^*(r;\tau_1) e^{i\omega_{m,1}\tau_0}, \tag{H.38}$$

$$v_m^{(1)} = \frac{\omega_m}{k_m} n_m(r;\tau_1) e^{-i\omega_{m,1}\tau_0} - \frac{\omega_m}{k_m} n_m^*(r;\tau_1) e^{i\omega_{m,1}\tau_0}. \tag{H.39}$$

For long, thin plasmas i.e. $L \gg r_p$, which is our interest, the frequency mis-match (detuning), between linear modes m, $l-m$, and l is small as well as the mode am-

plitudes:

$$(\omega_{m,1}+\omega_{l-m,1}-\omega_{l,1})/\omega_{m,1}\sim|n_m|\ll 1. \tag{H.40}$$

Thus we define the detuning $\Delta_{m,l}$ as:

$$\omega_{m,1}+\omega_{l-m,1}-\omega_{l,1}=\varepsilon\Delta_{m,l}, \tag{H.41}$$

$$\tau_0(\omega_{m,1}+\omega_{l-m,1}-\omega_{l,1})=\varepsilon\tau_0\Delta_{m,l}=\tau_1\Delta_{m,l}, \tag{H.42}$$

where we used Eq. (H.12) in Eq. (H.42).

To the second order in ε we have:

$$\partial_{\tau_0}n_l^{(2)}+\partial_{\tau_1}n_l^{(1)}+ik_l\sum_{m=-\infty}^{\infty}n_m^{(1)}v_{l-m}^{(1)}+ik_lv_l^{(2)}=0, \tag{H.43}$$

$$\partial_{\tau_0}v_l^{(2)}+\partial_{\tau_1}v_l^{(1)}+i\sum_{m=-\infty}^{\infty}k_mv_m^{(1)}v_{l-m}^{(1)}=-ik_l\phi_l^{(2)}, \tag{H.44}$$

$$\left[-\nabla_r^2+k_l^2\right]\phi_l^{(2)}=N_0(r)n_l^{(2)}. \tag{H.45}$$

Using Eqs. (H.24) and (H.28), we use the following in Eq. (H.43):

$$\begin{aligned}
&ik_l\sum_{m=-\infty}^{\infty}n_m^{(1)}v_{l-m}^{(1)} \\
&=ik_l\sum_{m=-\infty}^{\infty}\frac{\omega_{l-m,1}}{k_{l-m}}\left(n_m(r;\tau_1)e^{-i\omega_{m,1}\tau_0}+n_m^*(r;\tau_1)e^{i\omega_{m,1}\tau_0}\right) \\
&\left(n_{l-m}(r;\tau_1)e^{-i\omega_{l-m,1}\tau_0}-n_{l-m}^*(r;\tau_1)e^{i\omega_{l-m,1}\tau_0}\right) \\
&=ik_l\sum_{m=-\infty}^{\infty}\frac{\omega_{l-m,1}}{k_{l-m}}\Big(n_m(r;\tau_1)n_{l-m}(r;\tau_1)e^{-i\Delta_{m,l}\tau_1-i\omega_{l,1}\tau_0} \\
&+n_m^*(r;\tau_1)n_{l-m}(r;\tau_1)e^{i(\omega_{m,1}-\omega_{l-m,1})\tau_0}\Big)+c.c..
\end{aligned} \tag{H.46}$$

Furthermore using Eq. (H.28), we use the following in Eq. (H.45):

$$
\begin{aligned}
& i \sum_{m=-\infty}^{\infty} k_m v_m^{(1)} v_{l-m}^{(1)} \qquad \text{(H.47)} \\
& = i \sum_{m=-\infty}^{\infty} \omega_{m,1} \frac{\omega_{l-m,1}}{k_{l-m}} \left(n_m(r;\tau_1) e^{-i\omega_{m,1}\tau_0} - n_m^*(r;\tau_1) e^{i\omega_{m,1}\tau_0} \right) \\
& \left(n_{l-m}(r;\tau_1) e^{-i\omega_{l-m,1}\tau_0} - n_{l-m}^*(r;\tau_1) e^{i\omega_{l-m,1}\tau_0} \right) \\
& = i \sum_{m=-\infty}^{\infty} \omega_{m,1} \frac{\omega_{l-m,1}}{k_{l-m}} \Big(n_m(r;\tau_1) n_{l-m}(r;\tau_1) e^{-i\Delta_{m,l}\tau_1 - i\omega_{l,1}\tau_0} \\
& - n_m^*(r;\tau_1) n_{l-m}(r;\tau_1) e^{i(\omega_{m,1}-\omega_{l-m,1})\tau_0} + c.c. \Big).
\end{aligned}
$$

We used Eq. (H.42) to write $e^{-i(\omega_{m,1}+\omega_{l-m,1})\tau_0}$ as $e^{-i\Delta_{m,l}\tau_1 - i\omega_{l,1}\tau_0}$ in Eqs. (H.46) and (H.47).

Laplace transform is performend on equations Eqs. (H.43) through (H.45) w.r.t. fast time variable τ_0, using:

$$
\begin{aligned}
\tilde{\phi}_k^{(2)}(r;s,\tau_1) &= \int_0^{\infty} d\tau_0 \phi_k^{(2)}(r;\tau_0,\tau_1) e^{-s\tau_0}, \qquad \text{(H.48)} \\
\phi_k^{(2)}(r;\tau_0,\tau_1) &= \frac{1}{2\pi i} \int_C d\tau_0 \tilde{\phi}_k^{(2)}(r;s,\tau_1) e^{s\tau_0}.
\end{aligned}
$$

Similarly Laplace transform of $v^{(2)}$ and $n^{(2)}$ are respectively given by $\tilde{v}^{(2)}$ and $\tilde{n}^{(2)}$ .With initial conditions:

$$
\begin{aligned}
\phi_k^{(2)}(r;\tau_0=0,\tau_1) &= 0, \\
v_k^{(2)}(r;\tau_0=0,\tau_1) &= 0, \\
n_k^{(2)}(r;\tau_0=0,\tau_1) &= 0.
\end{aligned}
$$

From performing Laplace transform on Eq. (H.43) we obtain:

$$
\begin{aligned}
& s\tilde{n}_l^{(2)} + \frac{\partial_{\tau_1} n_l}{s+i\omega_{l,1}} + \frac{\partial_{\tau_1} n_l^*}{s-i\omega_{l,1}} \\
& + i k_l \sum_{m=-\infty}^{\infty} \frac{\omega_{l-m,1}}{k_{l-m}} \Big[\frac{n_m n_{l-m} e^{-i\Delta_{m,l}\tau_1}}{s+i\omega_{l,1}} - \frac{n_m^* n_{l-m}^* e^{i\Delta_{m,l}\tau_1}}{s-i\omega_{l,1}} + \frac{n_m^* n_{l-m}}{s-i\omega_{m,1}+i\omega_{l-m,1}} \\
& - \frac{n_m n_{l-m}^*}{s+i\omega_{m,1}-i\omega_{l-m,1}} \Big] + i k_l \tilde{v}_l^{(2)} = 0. \qquad \text{(H.49)}
\end{aligned}
$$

From performing Laplace transform on Eq. (H.44) and using Eq. (H.29) we get:

$$
\begin{aligned}
&s\tilde{v}_l^{(2)} + \frac{\omega_l}{k_l}\frac{\partial_{\tau_1} n_l}{s+i\omega_{l,1}} - \frac{\omega_l}{k_l}\frac{\partial_{\tau_1} n_l^*}{s-i\omega_{l,1}} \\
&+i\sum_{m=-\infty}^{\infty}\omega_{m,1}\frac{\omega_{l-m,1}}{k_{l-m}}\Bigg[\frac{n_m n_{l-m}e^{-i\Delta_{m,l}\tau_1}}{s+i\omega_{l,1}} + \frac{n_m^* n_{l-m}^* e^{i\Delta_{m,l}\tau_1}}{s-i\omega_{l,1}} - \frac{n_m^* n_{l-m}}{s-i\omega_{m,1}+i\omega_{l-m,1}} \\
&-\frac{n_m n_{l-m}^*}{s+i\omega_{m,1}-i\omega_{l-m,1}}\Bigg] = -ik_l\tilde{\phi}_l^{(2)}.
\end{aligned}
\tag{H.50}
$$

From performing Laplace transform on Eq. (H.45) we get:

$$
\left[-\nabla_r^2 + k_l^2\right]\tilde{\phi}_l^{(2)} = N_0(r)\tilde{n}_l^{(2)}. \tag{H.51}
$$

From Eqs. (H.49) and (H.50) we eliminate $\tilde{v}_l^{(2)}$, solve for $\tilde{n}_l^{(2)}$ and substitute in Poisson equation (H.51) to obtian:

$$
\begin{aligned}
&D(r;k_l,s)\tilde{\phi}_l^{(2)} \\
&= N_0(r)\Bigg[-\frac{(s-i\omega_{l,1})\partial_{\tau_1} n_l}{s^2(s+i\omega_{l,1})} - \frac{(s+i\omega_{l,1})\partial_{\tau_1} n_l^*}{s^2(s-i\omega_{l,1})} + ik_l\sum_{m=-\infty}^{\infty}\frac{\omega_{l-m,1}}{k_{l-m}}\Bigg\{ \\
&\frac{(i\omega_{m,1}-s)n_m n_{l-m}}{s^2(s+i\omega_{l,1})}e^{-i\Delta_{m,l}\tau_1} + \frac{(i\omega_{m,1}+s)n_m^* n_{l-m}^*}{s^2(s-i\omega_{l,1})}e^{i\Delta_{m,l}\tau_1} \\
&-\frac{(i\omega_{m,1}+s)n_m^* n_{l-m}}{s^2(s-i\omega_{m,1}+i\omega_{l-m,1})} - \frac{(i\omega_{l,1}-s)n_m n_{l-m}^*}{s^2(s+i\omega_{m,1}-i\omega_{l-m,1})}\Bigg\}\Bigg],
\end{aligned}
\tag{H.52}
$$

where $D(r;k_l,s)$ is the dispersion operator given by

$$
D(r;k_l,s) = -\nabla_r^2 + k_l^2 + \left(\frac{k_l}{s}\right)^2 N_0(r). \tag{H.53}
$$

Solving the equation Eq. (H.52) for $\tilde{\phi}_l^{(2)}$ and performing inverse Laplace will lead to secular solutions, which have a $\tau_0 e^{-i\omega_{l,1}\tau_0}$ time behavior, as well as non-secular solutions, for large τ_0. Left hand side of equation Eq. (H.52) is similar to linear dispersion relation Eq. (H.30), i.e. if $\tilde{\phi}_l^{(2)}(r;s,\tau_1) = \tilde{\bar{\phi}}_{l,1}^{(2)}(s,\tau_1)R_{l,1}(r)$ will be an eigenmode of $D(r;k_l,s)$ for $s=-i\omega_{l,1}$. We wish to remove the secular terms related to this fre-

quency. We write Eq. (H.53) as follows

$$D(r;k_l,s)=D(r;k_l,-i\omega_{l,1})+k_l^2N_0(r)\left(\frac{1}{\omega_{l,1}^2}+\frac{1}{s^2}\right). \tag{H.54}$$

Substituting from Eq. (H.54), and using the expansion form of $\phi_l^{(2)}(r,s)$ in terms of the complete series of radial eigenfunctions $R_{l,\mu}$ given by

$$\phi_l^{(2)}(r,s)=\sum_{q'}\tilde{\overline{\phi}}_{l,q'}^{(2)}(s)R_{l,q'}(r), \tag{H.55}$$

the left hand side of Eq. (H.52) is written as

$$\begin{aligned}&D(r;k_l,s)\tilde{\phi}_l^{(2)}\\&=\left\{D(r;k_l,-i\omega_{l,1})+k_l^2N_0(r)\left(\frac{1}{\omega_{l,1}^2}+\frac{1}{s^2}\right)\right\}\left[\sum_{q'}\tilde{\overline{\phi}}_{l,q'}^{(2)}(s)R_{l,q'}(r)\right].\end{aligned} \tag{H.56}$$

Operating $\int_0^{r_w}R_{l,1}(r)r\,dr$ on both sides of equation Eq. (H.52), we use Eqs. (H.35) (orthogonality), (H.30) (linear disperision) and the Hermitian property of D, which implies that

$$\int_0^{r_w}R_{l,1}(r)D(r;k_l,-i\omega_{l,1})R_{l,q'}(r)r\,dr=0, \tag{H.57}$$

to obtain:

$$\begin{aligned}&k_l^2\left(\frac{1}{\omega_{l,1}^2}+\frac{1}{s^2}\right)\tilde{\overline{\phi}}_{l,1}^{(2)}(s,\tau_1)\\&=-\frac{(s-i\omega_{l,1})\partial_{\tau_1}\overline{n}_l}{s^2(s+i\omega_{l,1})}-\frac{(s+i\omega_{l,1})\partial_{\tau_1}\overline{n}_l^*}{s^2(s-i\omega_{l,1})}+ik_l\sum_{m=-\infty}^{\infty}\Xi(l,m)\frac{\omega_{l-m,1}}{k_{l-m}}\Bigg\{\\&\frac{(i\omega_{m,1}-s)\overline{n}_m\overline{n}_{l-m}}{s^2(s+i\omega_{l,1})}e^{-i\Delta_{m,l}\tau_1}+\frac{(i\omega_{m,1}+s)\overline{n}_m^*\overline{n}_{l-m}^*}{s^2(s-i\omega_{l,1})}e^{i\Delta_{m,l}\tau_1}\\&-\frac{(i\omega_{m,1}+s)\overline{n}_m^*\overline{n}_{l-m}}{s^2(s-i\omega_{m,1}+i\omega_{l-m,1})}-\frac{(i\omega_{m,1}-s)\overline{n}_m\overline{n}_{l-m}^*}{s^2(s+i\omega_{m,1}-i\omega_{l-m,1})}\Bigg\},\end{aligned} \tag{H.58}$$

where the radial coupling coefficient $\Xi(l,m)$ is defined as

$$\Xi(l,m)=\int_0^{r_w} R_{m,1}(r)R_{l-m,1}(r)R_{l,1}(r)N_0(r)r\,dr. \tag{H.59}$$

Simplifying equation Eq. (H.58), we obtain:

$$\begin{aligned}
&\tilde{\overline{\phi}}^{(2)}_{l,1}(s,\tau_1)\\
&=\frac{\omega_{l,1}^2}{k_l^2}\Bigg(-\frac{\partial_{\tau_1}\overline{n}_l}{(s+i\omega_{l,1})^2}+ik_l\sum_{m=-\infty}^{\infty}\Xi(l,m)\frac{\omega_{l-m,1}}{k_{l-m}}\Bigg\{-\frac{(s-i\omega_{m,1})\overline{n}_m\overline{n}_{l-m}}{(s-i\omega_{l,1})(s+i\omega_{l,1})^2}e^{-i\Delta_{m,l}\tau_1}\\
&+\frac{(s-i\omega_{m,1})\overline{n}_m\overline{n}^*_{l-m}}{(s^2+\omega_{l,1}^2)(s+i\omega_{m,1}-i\omega_{l-m,1})}\Bigg\}\Bigg)+c.c.
\end{aligned} \tag{H.60}$$

We perform inverse Laplace transform on Eq. (H.60) and set the secular part (terms proportional to τ_0) equal to zero. On the right hand side of Eq. (H.60), the following integral will appear, as a result of inverse Laplace transform:

$$\begin{aligned}
&\frac{1}{2\pi i}\int_C ds\frac{g(s)e^{s\tau_0}}{(s+i\omega_{l,1})^2}=-\frac{1}{2\pi i}\frac{g(s)}{(s+i\omega_{l,1})}e^{s\tau_0}|_C+\frac{1}{2\pi i}\int ds\frac{g(s)\tau_0 e^{s\tau_0}}{(s+i\omega_{l,1})}\\
&+\frac{1}{2\pi i}\int ds\frac{dg/ds e^{s\tau_0}}{(s+i\omega_{l,1})}=dg/ds|_{s=-i\omega_{l,1}}e^{-i\omega_{l,1}\tau_0}+g(-i\omega_{l,1})\tau_0 e^{-i\omega_{l,1}\tau_0},
\end{aligned} \tag{H.61}$$

where $g(s)$ is an arbitrary analytical function. The first term on the right hand side of Eq. (H.61) is a trivial homogeneous solution to the linear dispersion relation and the second term is a resonant term growing linearly in fast time τ_0. These resonant terms on the right hand side of Eq. (H.61) must cancel each other to avoid the secular growth of $\overline{\phi}^{(2)}_{l,1}$. To this purpose, we set:

$$\partial_{\tau_1}\overline{n}_l+ik_l\sum_{m=-\infty}^{\infty}\Xi(l,m)\tfrac{\omega_{l-m,1}}{2k_{l-m}}\left(1+\tfrac{\omega_{m,1}}{\omega_{l,1}}\right)\overline{n}_m\overline{n}_{l-m}e^{-i\Delta_{m,l}\tau_1}=0. \tag{H.62}$$

Above equation expresses the time evolution of the linear modes, due to nonlinear coupling to the other linear modes.

Bibliography

[1] R.E. Aamodt. *Phys. Rev. A*, 138:45, 1965.

[2] M. Abramowitz and I. A. Stegun. *Handbook of mathematical functions*, page 446. Dover Publications, New York, 1964.

[3] L. M. Al'tshul' and V. I. Karpman. *Sov. Phys. JETP*, 20:1043, 1965.

[4] M. W. Anderson, T. M. O'Neil, D. H. E. Dubin, and R. W. Gould. *Phys. Plasmas*, 18:102113, 2011.

[5] Arash Ashourvan and Daniel H. E. Dubin. *Phys. Plasmas*, 21:052109, 2014.

[6] C. M. Bender and S. A. Orszag. *Advanced mathematical methods for scientists and engineers*, chapter 9. Applied Mathematical Sciences. McGraw-Hill, 1978.

[7] C. M. Bender and S. A. Orszag. *Advanced mathematical methods for scientists and engineers*, chapter 6, pages 302–304. Applied Mathematical Sciences. McGraw-Hill, 1978.

[8] C. Benedetti, C. B. Schroeder, E. Esarey, and W. P. Leemans. *Phys. Plasmas*, 21:056706, 2014.

[9] John P. Boyd. *J. Comput Phys.*, 110:360, 1994.

[10] M. Camac, A. R. Kantrowitz, and M. Litvak. *Nucl. Fusion Suppl.*, 2:423, 1962.

[11] B. Coppi, M. N. Rosenbluth, and R.N. Sudan. *Ann. Phys. (New York)*, 55:207, 1969.

[12] R. C. Davidson. *J. Plasma Phys.*, 1:341, 1967.

[13] R. C. Davidson. *Phys. Rev.*, 176:344, 1968.

[14] R. C. Davidson. *Phys. Fluids*, 12:149, 1969.

[15] C. F. Driscoll, A. A. Kabantsev, and D. H. E. Dubin. Transport, damping, and wave-couplings from chaotic and collisional neoclassical transport. In *Non-Neutral Plasma Physics VIII; AIP Conf. Proc. 1521*, number 15, 2013.

[16] D. H. E. Dubin. *Numerical and Analytical Methods for Scientists and Engineers Using Mathematica*, chapter 2, page 151. Applied Mathematical Sciences. Wiley-Interscience, Hoboken, New Jersey, 2003.

[17] D. H. E. Dubin. *Phys. Plasmas*, 12:042107, 2005.

[18] D. H. E. Dubin and T. M. O'Neil. *Rev. Mod. Phys.*, 71(1):87, January 1999.

[19] D. H. E. Dubin and Yu. A. Tsidulko. *Phys. Plasmas*, 18:062114, 2011.

[20] D. F. DuBois and M. V. Goldman. *Phys. Rev. Lett.*, 14:544, 1965.

[21] C. Joshi, W. B. Mori, T. Katsouleas, J. M. Dawson, J. M. Kindel and D. W. Forslund. *Nature*, 311:525, 1984.

[22] R. Assman, P. Chen, F. J. Decker, R. Iverson, P. Raimondi, T. Raubenheimer, S. Rockni, R. Siemann, D. Walz, D. Whittum, S. Chattopadhyay, W. Leemans, T. Katsouleas, S. Lee, C. Clayton, C. Joshi, K. Marsh, W. Mori, G. Wang. *Stanford Linear Accelerator Center Proposal*, 1997.

[23] A. A. Galeev and V. I. Karpman. *Sov. Phys. JETP*, 17:403, 1963.

[24] A. A. Galeev, V. I. Karpman, and R. Z. Sagdeev. *Nucl. Fusion*, 5:20, 1965.

[25] A. A. Galeev and R. N. Sudan, editors. *Basic Plasma Physics*, volume 1 of *Handbook of Plasma Physics*, pages 704–705. North-Holland Publishing Company, Amsterdam.New York.Oxford, 1983.

[26] T. J. Hilsabeck and T. M. O'Neil. *Phys. Plasmas*, 10:3492, 2003.

[27] B. B. Kadomtsev. *Plasma Turbulence*. Handbook of Plasma Physics. Academic Press, New York, 1965.

[28] Igor D. Kaganovich, Edward A. Startsev, and Ronald C. Davidson. *Phys. Plasmas*, 11:3546, 2004.

[29] N. A. Krall and A. W. Trivelpiece. *Principles of Plasma Physics*, chapter 8, pages 375–383. San Francisco Press Inc., San Francisco, 1986.

[30] A. H. Nayfeh and D. T. Mook. *Nonlinear Oscillations*. Wiley Classics Library. Wiley, New York, 1995.

[31] K. Nishikawa. *Phys. Soc. Jpn.*, 24:916, 1968.

[32] V. N. Oraevskii and R. Z. Sagdeev. *Sov. Phys. Tech. Phys.*, 7:955, 1963.

[33] S. A. Prasad and T. M. O'Neil. *Phys. Fluids*, 26:665, 1983.

[34] S. A. Prasad and T. M. O'Neil. *Phys. Fluids*, 27:206, 1984.

[35] W. H. Press, B. P. Flannery, S. A. Teukolsky, and W. T. Vetterling. *Numerical Recipes: The Art of Scientific Computing*, chapter 11, page 564. Applied Mathematical Sciences. Cambridge University Press, Cambridge, England, 3 edition, 2007.

[36] W. E. Schiesser. *The Numerical Method of Lines*. Academic Press, 1991.

[37] V. P. Silin. *Zh. Eksp. Teor. Fiz.*, 48:1676, 1965.

[38] S. H. Strogatz. *Nonlinear Dynamics and Chaos, with Applications to Physics, Biology, Chemistry and Engineering*, chapter 5. Studies in Nonlinearity. Persus Books, Massachusetts, 1994.

[39] P. A. Sturrock. *Proc. Int. Sch. Phys. Enrico Fermi*, 25:180, 1964.

[40] A. W. Trivelpiece and R. W. Gould. *J. Appl. Phys.*, 30:1784, 1959.

[41] C. J. Walsh, D. M. Villeneuve, and H. A. Baldis. *Phys. Rev. Lett.*, 53:1445, 1965.

[42] G. M. Walters and E. G. Harris. *Phys. Fluids*, 11:112, 1968.

[43] V. E. Zakhorov. *Sov. Phys. JETP*, 35:908, 1972.